FLIGHT TEST OF ADVANCED-GEOMETRY BORON BLADES

BOEING COMPANY, VERTOL DIVISION

PREPARED FOR
ARMY AIR MOBILITY RESEARCH AND DEVELOPMENT LABORATORY

FEBRUARY 1973

AD

USAAMRDL TECHNICAL REPORT 72-65

FLIGHT TEST OF ADVANCED-GEOMETRY BORON BLADES

By

Donald J. Hoffstedt
Harold E. Bishop
Herbert H. Steinmann

February 1973

EUSTIS DIRECTORATE
U. S. ARMY AIR MOBILITY RESEARCH AND DEVELOPMENT LABORATORY
FORT EUSTIS, VIRGINIA

CONTRACT DAAJ02-72-C-0010
THE BOEING COMPANY, VERTOL DIVISION
PHILADELPHIA, PENNSYLVANIA

DISCLAIMERS

The findings in this report are not to be construed as an official Department of the Army position unless so designated by other authorized documents.

When Government drawings, specifications, or other data are used for any purpose other than in connection with a definitely related Government procurement operation, the US Government thereby incurs no responsibility nor any obligation whatsoever; and the fact that the Government may have formulated, furnished, or in any way supplied the said drawings, specifications, or other data is not to be regarded by implication or otherwise as in any manner licensing the holder or any other person or corporation, or conveying any rights or permission, to manufacture, use, or sell any patented invention that may in any way be related thereto.

Trade names cited in this report do not constitute an official endorsement or approval of the use of such commercial hardware or software.

DISPOSITION INSTRUCTIONS

Destory this report when no longer needed. Do not return it to the originator.

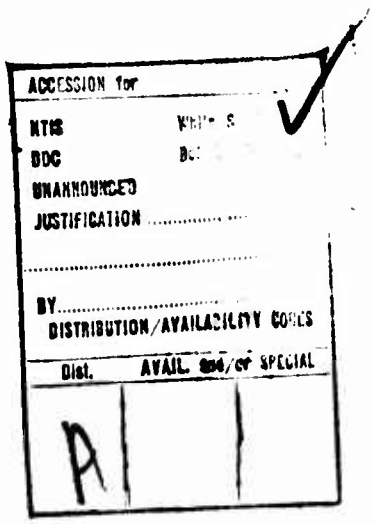

Unclassified
Security Classification

DOCUMENT CONTROL DATA - R & D

(Security classification of title, body of abstract and indexing annotation must be entered when the overall report is classified)

1. ORIGINATING ACTIVITY (Corporate author) THE BOEING COMPANY, Vertol Division Boeing Center, P.O. Box 16858 Philadelphia, Pennsylvania 19142	2a. REPORT SECURITY CLASSIFICATION Unclassified 2b. GROUP

3. REPORT TITLE

Flight Test of Advanced-Geometry Boron Blades

4. DESCRIPTIVE NOTES (Type of report and inclusive dates)

Final Technical Report

5. AUTHOR(S) (First name, middle initial, last name)

Donald J. Hoffstedt
Harold E. Bishop
Herbert H. Steinmann

6. REPORT DATE	7a. TOTAL NO. OF PAGES	7b. NO. OF REFS
February 1973	~~211~~ 213	8

8a. CONTRACT OR GRANT NO.	9a. ORIGINATOR'S REPORT NUMBER(S)
DAAJ02-72-C-0010	USAAMRDL Technical Report 72-65
b. PROJECT NO. 1F163204D15713	
c.	9b. OTHER REPORT NO(S) (Any other numbers that may be assigned this report) D210-10486-1
d.	

10. DISTRIBUTION STATEMENT

Approved for public release; distribution unlimited.

11. SUPPLEMENTARY NOTES	12. SPONSORING MILITARY ACTIVITY
	Eustis Directorate U.S. Army Air Mobility Research and Development Laboratory, Ft Eustis, Va.

13. ABSTRACT

This report presents the results of an exploratory flight test program conducted on a CH-47C Army helicopter for the purpose of investigating the structural performance of boron-reinforced epoxy aft rotor blades and the associated effects on the helicopter system.

This program has demonstrated the flightworthiness of boron-reinforced epoxy main rotor blades in the demanding environment of the aft rotor on a tandem-rotor helicopter. No structural problems were encountered. There were no restrictive 3/rev vibrations despite a first-elastic-mode, flap-bending natural frequency of 3.21 times rotor speed. The torsional stiffness of the boron blade provided excellent blade-to-blade track conformance throughout the program after minimal initial adjustment.

DD FORM 1 NOV 68 1473 REPLACES DD FORM 1473, 1 JAN 64, WHICH IS OBSOLETE FOR ARMY USE.

Unclassified
Security Classification

14. KEY WORDS	LINK A		LINK B		LINK C	
	ROLE	WT	ROLE	WT	ROLE	WT
Boron-Reinforced Rotor Blades Advanced Geometry Boron Blades						

DEPARTMENT OF THE ARMY
U. S. ARMY AIR MOBILITY RESEARCH & DEVELOPMENT LABORATORY
EUSTIS DIRECTORATE
FORT EUSTIS, VIRGINIA 23604

This study was performed under Contract DAAJ02-72-C-0010 with the Vertol Division, The Boeing Company, Philadelphia, Pennsylvania. The technical monitor for this contract was Mr. James P. Waller, Technology Applications Division.

The report contains the results of data collection and analysis from limited flight testing of the boron advanced-geometry rotor blade.

This report has been reviewed by the Eustis Directorate, U. S. Army Air Mobility Research and Development Laboratory and is considered to be technically sound. It is published for the exchange of information and the stimulation of future research.

Task 1F163204D15713
Contract DAAJ02-72-C-0010
USAAMRDL Technical Report 72-65
February 1973

FLIGHT TEST OF ADVANCED-GEOMETRY BORON BLADES

Final Report

D210-10486-1

By

Donald J. Hoffstedt
Harold E. Bishop
Herbert H. Steinmann

Prepared by

THE BOEING COMPANY, Vertol Division
Philadelphia, Pennsylvania

for

EUSTIS DIRECTORATE
U.S. ARMY AIR MOBILITY RESEARCH AND DEVELOPMENT LABORATORY
FORT EUSTIS, VIRGINIA

SUMMARY

This report presents the results of an exploratory flight test program conducted on a CH-47C Army helicopter for the purpose of investigating the structural performance of boron-reinforced epoxy aft rotor blades and the associated effects on the helicopter system.

The boron-reinforced epoxy aft rotor blades were developed under an Air Force contract and are currently the property of the U.S. Army. The forward rotor was equipped with S-glass-reinforced epoxy rotor blades and are the same aerodynamic configuration as the boron blades.

On-board instrumentation was used to provide real-time telemetric monitoring and magnetic tape recording of 132 data parameters on the CH-47C. Data were obtained at nominal gross weights of 33,000, 40,000, 46,000, and 50,000 pounds gross weight at altitudes from sea level through 15,000 feet density altitude and were recorded on level-flight airspeed sweeps, rpm sweeps, climbs, turns, autorotation, partial-power descent, and mild flare maneuvers.

The inception of rotor blade moment stall was not delayed over that of the similar glass blade configuration evaluated and reported in USAAMRDL Technical Report 71-42. Pitch link alternating control loads did not build up abruptly after inception of moment stall, as is typical of the conventional CH-47 rotor system; hence, significant expansion of the CH-47C structural envelope was demonstrated.

This program has demonstrated the flightworthiness of boron-reinforced epoxy main rotor blades in the demanding environment of the aft rotor on a tandem-rotor helicopter. No structural problems were encountered. There were no restrictive 3/rev vibrations despite a first-elastic-mode, flap-bending natural frequency of 3.21 times rotor speed. Track adjustments were required on the forward rotor throughout the program (S-glass blades). The increase in torsional stiffness of the boron blade over the glass blade provided excellent blade-to-blade track conformance throughtout the program after minimal initial adjustment.

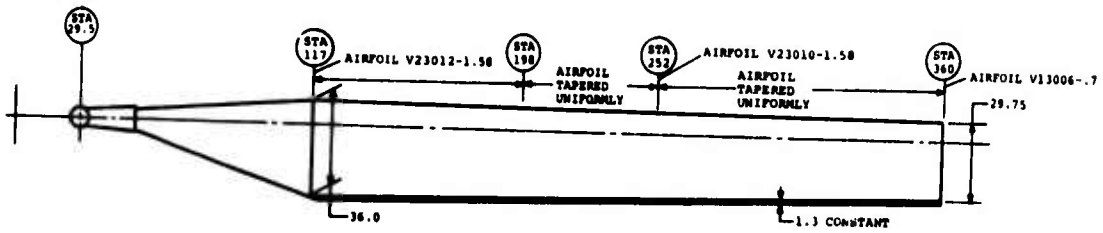

ADVANCED-GEOMETRY BLADE

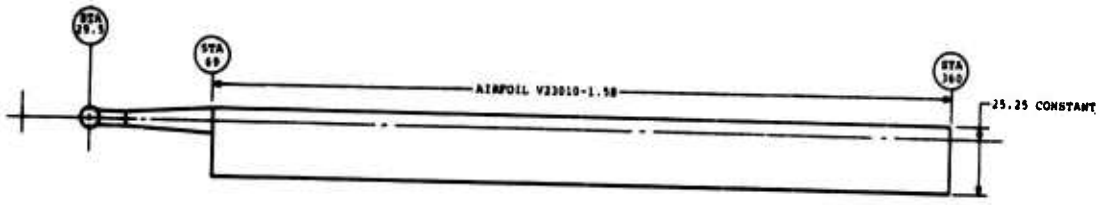

CH-47C BLADE

FOREWORD

This report was prepared by The Boeing Company's Vertol Division under Contract DAAJ02-72-C-0010, DA Project 1F163204D157, for the Eustis Directorate, U.S. Army Air Mobility Research and Development Laboratory, Fort Eustis, Virginia. Mr. James Waller, Structures Division, was the Contracting Officer's Technical Representative.

Principal contributors to this program are listed below:

Program Manager	D. J. Hoffstedt
Flight Test Operations	P. A. Farnschlader H. S. Groh K. Lunn J. C. Kutkuhn
Flight Test Instrumentation	E. T. Winchester R. D. Wolbach
Experimental Test Pilots	R. C. Gangwish E. C. Nelson A. J. Hutto P. Camerano
Flight Test Data Analysis	F. Pearson
Flight Test Ground Operations	B. D. Carpenter
Flight Test Manufacturing Division	E. T. Williams
Rotor Development Technology	H. E. Bishop C. S. Beshore
Structures Technology	H. H. Steinmann J. R. Hoover
Dynamics Technology	M. Kumpel
Flying Qualities Technology	H. J. Neeb
Quality Assurance	W. Roettger

TABLE OF CONTENTS

LIST OF ILLUSTRATIONS

LIST OF TABLES

LIST OF SYMBOLS

AGB	advanced-geometry blade
BL	buttline, distance left or right from aircraft centerline, inches
C	chord, feet
$\mathbb{C}_L$	centerline
C_T/σ	thrust coefficient divided by rotor solidity, a proportionality related to sensity altitude
EAS	equivalent airspeed, knots
FLT	flight
f	function, a function of
g	acceleration of gravity, 32.2 feet per second per second at sea level
H_D	density altitude, feet
Hz	Hertz, cycles per second
I_θ	polar mass moment of inertia
LBL	left buttline
PPD	partial-power descent
R	length of rotor blade from root to tip, unity
RBL	right buttline
r	fractional length of rotor blade from root to tip, expressed as r/R, decimal fraction

STA	station, distance along the length of the fuselage or of the rotor blade from some arbitrary zero point, inches
TAS	true airspeed, knots
TOGW	takeoff gross weight, pounds
TOS	(from) top of shaft, location of strain gages on aft rotor shaft, inches
V_T	tip velocity, feet per second
α	angle of attack, degrees
θ_t	blade twist, degrees
μ	advance ratio
ρ	density of air, slugs per cubic foot
ψ	location around the blade azimuth from 0 to 360 degrees in direction of rotation, degrees
ω_θ	revolutions per minute presented in radians per second
1/rev, 3/rev, etc.	frequency of vibration related to revolutions of the helicopter rotor

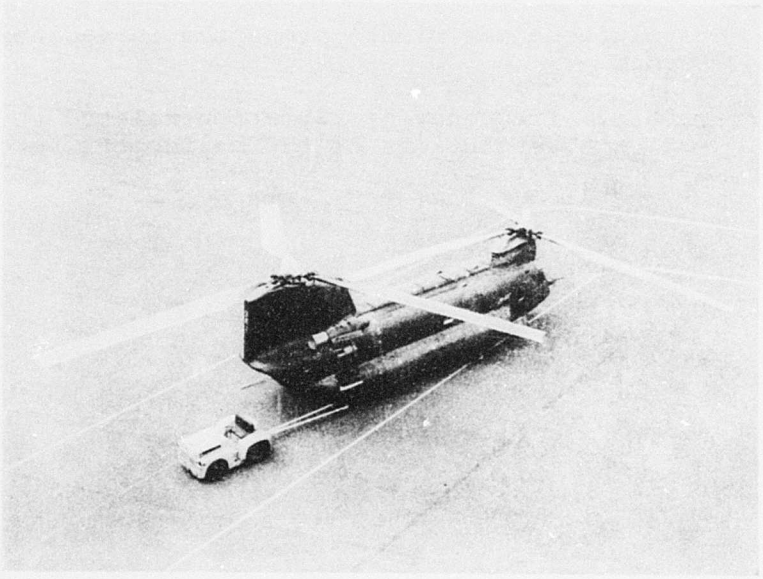

Figure 1. NCH-47C Helicopter With Boron Advanced-Geometry Blades on Aft Rotor and Fiberglass Advanced-Geometry Blades on Forward Rotor.

INTRODUCTION

The exploratory flight test program conducted under Contract DAAJ02-72-C-0010 represents a significant milestone in the demonstration and evaluation of advanced-composite materials in primary structural applications.

The design, material characterization testing, fabrication, quality assurance, and preflight test program on the boron-reinforced epoxy aft rotor blades were reported in Reference 1. The development and test of these blades, in conjunction with the development and test of a boron horizontal stabilizer for the F-111, represented significant technological development objectives. The rotor blades were bench-tested and whirl-tested under an Air Force contract. The U.S. Army confirmed the flightworthiness of the rotor blades by implementing this program which included a safety-of-flight review, assignment of a CH-47 aircraft (Figure 1), aircraft modification, instrumentation and calibration of blades and aircraft systems, blade tracking, ground mechanical instability tests, approximately 15 hours of flight test and data accumulation at four gross weights throughout the altitude and speed capability of the CH-47 aircraft, and analysis and reporting of the data.

The flight testing was accomplished between 1 March and 30 April 1972 at the Vertol Division Flight Test facility in Philadelphia, Pennsylvania.

FLIGHT TEST

Flight testing was performed on an NCH-47C aircraft, Army serial no. 66-19103, between 25 February and 28 April 1972 at the Vertol Division Flight Test Facility in Philadelphia, Pennsylvania, and at the Vertol Division's auxiliary test site at Millville Municipal Airport, New Jersey.

The detailed flight test requirements for the program are described in Reference 2; the methods and procedures for conducting stress and motion and performance tests are presented in Reference 3. Table I is a summary of the flight test conditions and associated data flight runs conducted to comply with the requirements of Reference 2.

The program encompassed a broad spectrum of test conditions at configurations from design gross weight of the CH-47C (33,000 pounds) to maximum gross weight (50,000 pounds). The latter weight is not currently approved by the Army for service operation; however, Boeing has conducted considerable testing at this gross weight. The program and gross weight/center-of-gravity envelope shown in Figure 2 were approved following a safety-of-flight review based on data contained in Reference 4.

The flight test program on the advanced-geometry boron blade accumulated 14 hours 41 minutes of flying time.

AIRCRAFT CONFIGURATION

The aircraft used for the flight test was an NCH-47C helicopter as stated. The N designation indicates that the aircraft is in a special test configuration.

The following changes were made to the aircraft for this program:

NOTE: Helicopter rotor blades are commonly color coded in some manner for easy identification after installation. Throughout this report the blade color cited refers to the color band on the corresponding arm of the pitch varying housing. Such red, yellow, and green coding marks are placed on all CH-47 rotor heads.

- Advanced-geometry fiberglass-reinforced epoxy rotor blades were installed on the forward rotor hub:
  - * No. BCW-1-104, green
  - * No. BCW-1-105, yellow (instrumented)
  - * No. BCW-1-106, red

TABLE I. PROGRAM DATA FLIGHT SUMMARY

Data Category	Gross Weight (lb)	CG Location	Rotor Speed (rpm)	Altitude, H_D (ft)	Flight No.	Remarks
Mechanical Instability	35,000	7 in. aft	235	N/A	325	-
Mechanical Instability	44,000	2.3 in. aft	235	N/A	326	-
Stress and Motion	33,000	7 in. aft	235	3,000	327	Abort (telemetry)
Stress and Motion	33,000	7 in. aft	235	4,000	328	-
Stress and Motion	46,000	4 in. aft	235, 245	3,000, 6,000	330	-
Stress and Motion	46,000	4 in. aft	235, 245	Climb to service ceiling, 6,000, 7,500, and 10,000	332	-
Stress and Motion	50,000	0	235, 245	2,500, 7,500, 6,000	333	-
Performance	32,000	1 in. fwd	-	-	334	Abort (no data)
Stress and Motion	46,000	4 in. aft	235, 245	2,500	336	-
Stress and Motion	46,000	4 in. aft	235, 245	Climb to service ceiling, 6,500	339	-
Stress and Motion	50,000	4 in. fwd	245	2,500, 3,500, Climb to service ceiling	340	-
Stress and Motion	40,000	4 in. aft		Service ceiling, 1,000, 8,000, 7,500, 6,000		

- Advanced-geometry boron-reinforced epoxy rotor blades were installed on the aft rotor hub:

  * A-2-104, green
  * A-2-101, yellow (instrumented)
  * A-2-103, red

- Modifications were made to the control kinematics to maintain similarity to the production cambered-airfoil, steel-spar rotor blades of the sensitivity of the controls to pilot longitudinal inputs and to the stability augmentation system (SAS).

- Standard production CH-47C self-tuning vibration absorbers were installed in the nose and cockpit, tuned for rotor speeds of 232 to 251 rpm. The 90-pound-mass, fixed-tuned absorber installed at the station 575 in the aft pylon was in the standard production configuration (tuned to 243 rpm rotor speed).

- A water ballast tank system of 8,000-pound capacity with an emergency dump capability was installed.

- A cruise guide indicator (CGI) was installed in the pilot's instrument panel to monitor loads in the upper flight controls.

- An on-board data-recording system was included as discussed under INSTRUMENTATION.

See Figure 3 for the orientation of the rotor blades on the helicopter.

EQUIPMENT

Special equipment used during the program was as follows:

- A Strobex blade tracker for in-flight blade tracking.

- A tethered hover rig consisting of the necessary cables, fixed ground attachment points, and load cell-cable angle instrumentation. Used unsuccessfully to record hover performance.

INSTRUMENTATION

All data were recorded on a narrow-band frequency-modulation (NBFM), 14-track Ampex tape recorder, Model AR-200, fitted with 250-kilocycle recording heads.

Table II lists all parameters which were recorded during the program. NBFM data signals from each of the 14 banks of limited-frequency-range oscillators were mixed into a composite signal and recorded on tape. Data were recovered by passing the composite signal through a bank of frequency discriminators to obtain the individual analog signals.

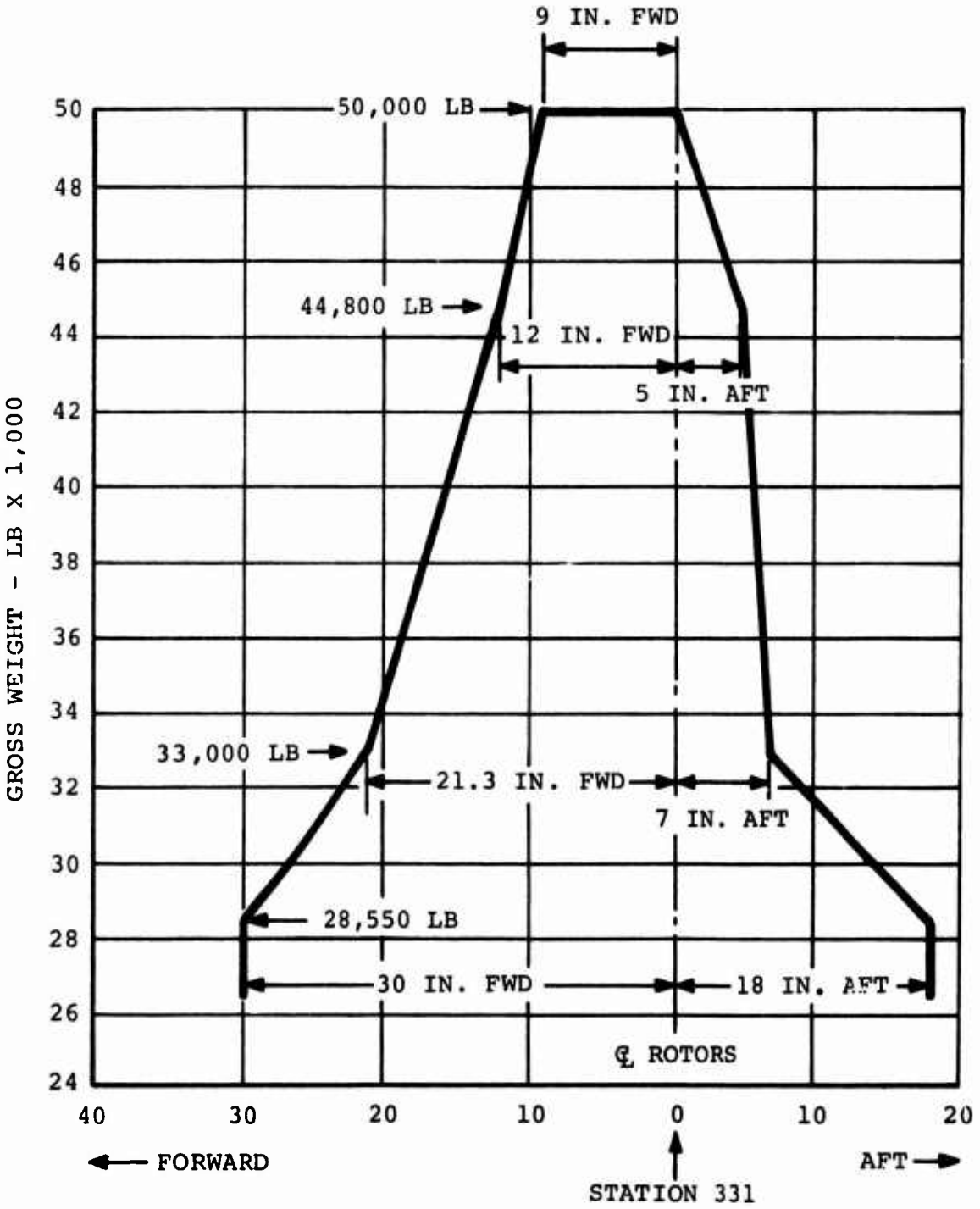

Figure 2. Center-of-Gravity Envelope for the CH-47C Helicopter.

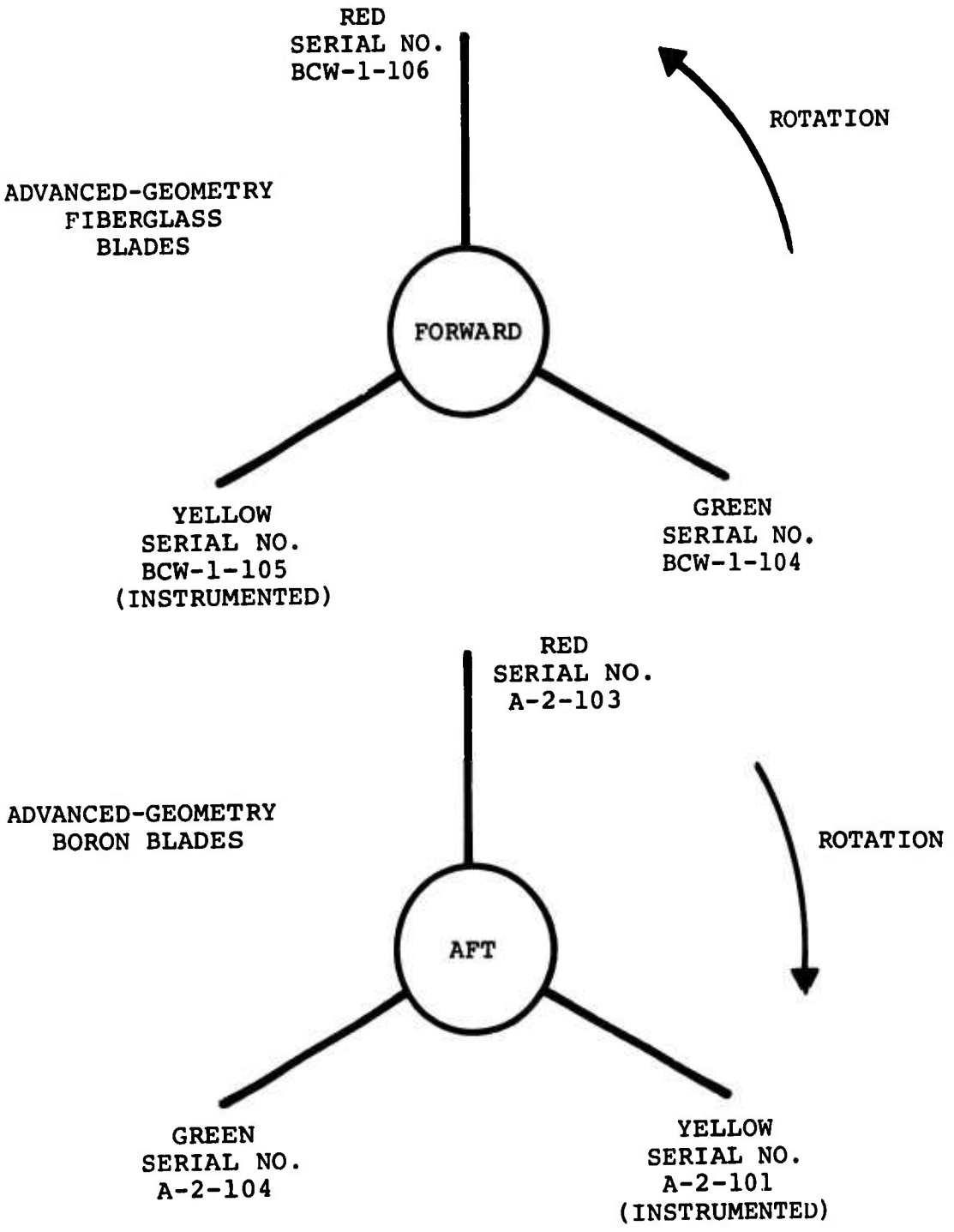

Figure 3. Orientation of Advanced-Geometry Blades on CH-47C Helicopter.

TABLE II. AVAILABILITY OF INSTRUMENTATION AND DATA RECORDING

Code No.	Parameter	Location	Unit	Flight GR78	325	326	327	328	329	330	GR79	331	332	333	334	GR80	GR81	335	336	337	338	339	340
	Basic Aircraft																						
6240	Airspeed	Ship(prod.)system	in. H_2O	O	O	O	O	O		O			O	O	O			O				O	O
6130	Altitude	Ship(prod.)system	in. Hg	O	O	O	O	O		O			(1)	O	O			O				O	(1)
7301	Outside Air Temperature		°C	O	O	O	O	O		O			O	O	O			O				O	O
3601	Rotor Speed	Forward	1/rev	O	O	O	O	O		O			O	O	O			O				O	O
3604	Rotor Speed	Aft	1/rev	O	O	O	O	O		O			O	O	O			O				O	O
1501	Rotor Speed (Analog)		rpm	O	O	O	O	O		O			O	O	O			O				O	O
3608	Event Marker			O	O	O	O	O		O			O	O	O			O				O	O
2124	Cyclic Trim Position	Forward	deg	O	O	O	O	O		O			O	O	O			O				O	O
2125	Cyclic Trim Position	Aft	deg	O	O	O	O	O		O			O	O	O			O				O	O
3162	Time Code (Slow)			O	O	O	O	O		O			O	O	O			O				O	O
3160	Time Code (Fast			O	O	O	O	O		O			O	O	O			O				O	O
8202	Fuel Total	No. 1(left)engine	lb	O	O	O	O	O		O			O	O	O			O				O	O
8204	Fuel Total	No. 2(right)engine	lb	B	O	O	O	O		O			O	O	O			O				O	O
	Droop Stop Light	Forward		O	O	O	O	O		O			O	O	O			O				O	O
	Droop Stop Light	Aft		O	O	O	O	O		O			O	O	O			O				O	O
	Performance																						
7201	Fuel Temperature	No. 1(left)engine	°C	O	O	O	O	O		O			O	O	O			O				O	O
7203	Fuel Temperature	No. 2(right)engine	°c	X	X	X	X	O		O			O	O	O			O				O	O
8201	Fuel Flow Rate	No. 1(left)engine	gal/min	O	O	O	O	O		O			O	O	O			O				O	O
8203	Fuel Flow Rate	No. 2(right)engine	gal/min	O	O	O	O	O		O			O	O	O			O				O	O
1503	Compressor Speed N_1	No. 1(left)engine	Hz	O	O	O	O	O		O			O	O	O			O				O	O
1504	Compressor Speed N_1	No. 2(right)engine	Hz	O	O	O	O	O		O			O	O	O			O				O	O
3606	Engine Torque	No. 1(left)engine	pct	O	O	O	O	O		O			O	O	O			O				O	O
3607	Engine Torque	No. 2(right)engine	pct	X	X	X	R	O		O			O	O	O			O				O	O
2224	Tethered Hover Long. Cable	Cargo hook													O								
2225	Tethered Hover Lat Cable	Cargo hook													O								
5485	Tethered Hover Cable Load	Cargo hook	lb												X								
	Rotor Blade Position																						
2202	Flap Angle	Fwd yellow blade	deg	O	O	O	O	O		O			O	O	O			O				O	O
2204	Lead-Lag Angle	Fwd yellow blade	deg	O	O	O	O	O		O			O	O	O			O				O	O
2203	Lead-Lag Angle	Aft yellow blade	deg	O	O	O	B	O		O			O	O	O			O				O	O
2201	Flap Angle	Aft yellow blade	deg	O	O	O	O	O		O			O	O	O			O				O	O
2226	Delta Flap Angle	Aft yellow blade	deg				O	O		O			O	O	O			O				O	O
	Acceleration																						
1318	Vertical	Pilot seat	g	O	O	O	O	O		O				O	O			O				O	O
1373	Vertical Cockpit	Sta 50 LH	g	O	O	O	O	O		O				O	O			O				O	O
1375	Vertical Cockpit	Sta 50 RH	g	O	O	O	B	O		O				O	O			O				O	O
1329	Lateral Cockpit	Sta 95 BL 0	g	O	O	O	O	O		O				O	O			O				O	O
1330	Longitudinal Cockpit	Sta 95 BL 0	g	O	O	O	O	O		O				O	O			O				O	O
1350	Vertical Cabin	Sta 320 LBL 49	g	O	O	O	O	O		O				O	O			O				O	O
1351	Lateral Cabin	Sta 320 LBL 49	g	O	O	O	O	O		O				O	O			O				O	O
1246	Vertical Cabin	Sta 320 RBL 49	g	O	O	O	O	O		O				O	O			O				O	O
1357	Vertical Cabin	Sta 350 LBL 25	g	O	O	O	O	O		O			O	O	O			O				O	O
1360	Vertical Cabin	Sta 482 LBL 49	g	O	O	O	O	O		O			O	O	O			O				O	O
1361	Vertical Cabin	Sta 482 RBL 49	g	O	O	O	O	O		O			O	O	O			O				O	O
1363	Lateral Cabin	Sta 482 LBL 49	g	O	O	O	O	O		O			O	O	O			O				O	O

TABLE II - Continued

Code No.	Parameter	Location	Unit	Flight																
				GR78	325	326	327	328	329	330	GR79	331	332	333	334	GR80	GR81	335	336	337	338	339	340
	Rotor Blade Loads																						
4110	Flap Bending Moment	Aft sta 49.5	in.-lb	O	O	O	O	O		O			O	O	O			O				O	O
4112	Flap Bending Moment	Aft sta 49.5	in.-lb																				
4122	Flap Bending Moment	Aft sta 117.0	in.-lb	O	Ø	O	O	O		Ø			O	O	O			O				O	O
4124	Flap Bending Moment	Aft sta 160.0	in.-lb	O	Ø	O	O	O		O			O	O	O			O				O	O
4126	Flap Bending Moment	Aft sta 198.0	in.-lb	O	Ø	O	O	O		O			O	O	O			O				O	O
4128	Flap Bending Moment	Aft sta 252.0	in.-lb	O	Ø	O	O	O		Ø			O	O	O			O				O	O
4130	Flap Bending Moment	Aft sta 288.0	in.-lb	Ø	Ø	O	O	O		X													
4114	Chord Bending Moment	Aft sta 49.5	in.-lb	Ø	Ø																		
4142	Trailing-Edge Tension	Aft sta 198.0	in.-lb	Ø	O	O	O	O		O			X	X									
4146	Spar Torsion	Aft sta 285.6	in.-lb	O	O	O	O	B		X													
4148	Spar Torsion	Aft sta 286.4	in.-lb	O	O	O	O	O		O			O	O	O			O				O	O
4150	Absolute Stress	Aft sta 288, upper 90°	in./in.		O	O	O	O		O			O	O	O			O				O	O
4152	Absolute Stress	Aft sta 288, lower 0°	in./in.		O	O	O	O		O			O	O	O			O				O	O
4154	Absolute Stress	Aft sta 290, upper 225°	in./in.																				
4156	Absolute Stress	Aft sta 288, upper 315°	in./in.		O	O	O	O		O			O	O	O			O				O	O
4106	Lag Damper Load	Aft	lb	O	O	O	O	O		O			O	O	O			O				O	O
4109	Flap Bending Moment	Fwd sta 49.5	in.-lb	B	B	X	X																
4111	Flap Bending Moment	Fwd sta 49.5	in.-lb				O	O		O			O	O	O			O				O	O
4113	Chord Bending Moment	Fwd sta 49.5	in.-lb	O	O	O	O	O		O			O	O	O			O				O	O
4115	Chord Bending Moment	Fwd sta 49.5	in.-lb																				
4141	Trailing-Edge Tension	Fwd sta 198.0	in.-lb	O	O	O	O	X															
4143	Trailing-Edge Tension	Fwd sta 198.0	in.-lb					B		X													
4105	Lag Damper Load	Forward	lb	O	O	O	O	O		O			O	O	O			O				O	O
	Control Position																						
2107	Longitudinal Stick	Pilot controls	in.	O	O	O	O	O		O			O	O	O			O				O	O
2108	Lateral Stick	Pilot controls	in.	O	O	O	O	O		O			O	O	O			O				O	O
2109	Directional Pedal	Pilot controls	in.	O	O	O	O	O		O			O	O	O			O				O	O
2110	Collective Thrust Lever	Pilot controls	in.	O	O	O	O	O		O				O	O			O				O	O
2112	SAS Pitch Actuator	No. 1 system	in.	O	O	O	O	O		O			O	O	O			O				O	O
2113	SAS Pitch Actuator	No. 2 system	in.	O	O	O	O	O		O			O	O	O			O				O	O
2114	SAS Roll Actuator	No. 1 system	in.	O	O	O	O	O		O			O	O	O								
2115	SAS Roll Actuator	No. 2 system	in.	O	O	O	O	O		O			O	O	O			O				O	O
2116	SAS Yaw Actuator	No. 1 system	in.	O	O	O	O	O		O			O	O	O			O				O	O
2117	SAS Yaw Actuator	No. 2 system	in.	O	O	O	O	O		O			O	O	O			O				O	O
2122	Pivoting Actuator	Forward	in.	O	O	O	O	O		O			O	O	O			O				O	O
2120	Swiveling Actuator	Forward	in.	O	O	O	O	O		X			O	O	O			O				O	O
2123	Pivoting Actuator	Aft	in.	O	O	O	O	O		O			O	O	O			O				O	O
2121	Swiveling Actuator	Aft	in.	O	O	O	O	O		O			O	O	O			O				O	O
	Aircraft Motion																						
2250	Pitch Attitude		deg	O	O	O	O	O		O				O	O			O				O	O
2251	Roll Attitude		deg	O	O	O	O	O		O			O	O	O			O				O	O
2252	Yaw Attitude		deg	O	O	O	O	O		O			O	O	O			O				O	O
2208	Sideslip Angle	Fwd rotor	deg	O	O	O	O	O		O			O	O	O			O				O	O
1601	Pitch Rate		deg/sec	O	O	O	O	O		O				O	O			O				O	O
1602	Roll Rate		deg/sec	O	O	O	O	O		O			O	O	O			O				O	O
1603	Yaw Rate		deg/sec	O	O	O	O	O		O			O	O	O			O				O	O

TABLE II - Continued

Code No.	Parameter	Location	Unit	Flight GR78	325	326	327	328	329	330	GR79	331	332	333	334	GR80	GR81	335	336	337	338	339	340
	Upper Controls Loads																						
5464	Pivot Actuator Tension	Forward	lb		O	O	O	O	O		O			O	O	O			O			O	O
5465	Pivot Actuator Tension	Forward	lb																				
5460	Pivot Actuator Tension	Aft	lb		O	O	S	O	O		O			O	O	O			O			O	O
5462	Pivot Actuator Tension	Aft	lb																				
5465	Swiv Actuator Tension	Forward	lb		O	O	O	O	O		O			O	O	O			O			O	O
5467	Swiv Actuator Tension	Forward	lb																				
5461	Swiv Actuator Tension	Aft	lb																				
5463	Swiv Actuator Tension	Aft	lb		O	O	O	O	O		O			O	O	O			O			O	O
5482	Fixed Link Tension	Forward	lb		Ø	Ø	Ø	O	O		O			O	O	O			O			O	O
5484	Fixed Link Tension	Forward	lb																				
5481	Fixed Link	Aft	lb		O	O	O	O	O		O			O	O	O			O			O	O
5483	Fixed Link	Aft	lb																				
5935	Lower Drive Arm	Aft	lb		O	O	O	O	O		O			O	O	O			O			O	O
5937	Lower Drive Arm	Aft	lb																				
5442	Red Pitch Link	Forward	lb		O	O	O	O	O		O			O	O	O			O			O	O
5444	Red Pitch Link	Forward	lb																				
5441	Red Pitch Link	Aft	lb		O	O	O	O	O		Ø			O	O	O			O			O	O
5443	Red Pitch Link	Aft	lb																				
5431	Yellow Pitch Link	Aft	lb		O	O	O	O	O		Ø			O	O	O			O			O	O
5433	Yellow Pitch Link	Aft	lb																				
5451	Green Pitch Link	Aft	lb		O	O	O																
5453	Green Pitch Link	Aft	lb																				
	Rotor Shaft Loads																						
5260	Bending 0-180°	Fwd sta 23.5	in.-lb		O	O	O	O	O		O			O	O	O			O			S	S
5262	Bending 0-180°	Fwd sta 23.5	in.-lb					O	O		O			O	O	O			O			O	O
5268	Bending 0-180°	Fwd sta 32.8	in.-lb																				
5270	Bending 0-180°	Fwd sta 32.8	in.-lb		O	O	O	O	O		X												
5272	Bending 90-270°	Fwd sta 32.8	in.-lb								O			O	O	O			O			O	O
5274	Bending 90-270°	Fwd sta 32.8	in.-lb																				
5251	Bending 0-180°	Aft sta 23.1	in.-lb																				
5253	Bending 0-180°	Aft sta 23.1	in.-lb		O	O	O		O		O			O	O	O			O			O	O
5259	Bending 0-180°	Aft sta 37.0	in.-lb		O	Ø																	
5261	Bending 0-180°	Aft sta 37.0	in.-lb				O	O	O		S			S	S	O			S			S	S
	Rotor Shaft Torque																						
5501	Torque 45-135°	Fwd sta 22.4	in.-lb																				
5504	Torque 0-90°	Fwd sta 22.4	in.-lb		O	O	O	O	O		O			O	O	O			O			O	O
5506	Torque 45-135°	Fwd sta 22.4	in.-lb		O	O	O	O	O		O			O	O	O			O			O	O
5510	Torque 45-135°	Fwd sta 23.5	in.-lb		O	O	O	O	O		O			O	O	O			O			O	O
5501	Torque 45-135°	Aft sta 64.3	in.-lb		O	O	O	O	O		O			O	O	O			O			O	O
5505	Torque 0-90°	Aft sta 66.0	in.-lb		O	O	O	X	O		O			O	O	O			O			O	O
5509	Torque 0-90°	Aft sta 66.0	in.-lb		O	O	O	O	O		O			O	O	O			O			O	O

TABLE II - Continued

Code No.	Parameter	Location	Unit	Flight GR78	325	326	327	328	329	330	GR79	331	332	333	334	GR80	GR81	335	336	337	338	339	340
	Additional Parameters																						
1746	Vert Accel Anti-Ice Valve	No. 1 engine	g											X	X		X		0			0	0
1766	Vert Accel Difsr Inbd 100° Clockwise	No. 1 engine	g											0	0		0		0			0	0
7347	Drag Link Temp	No. 1 engine fwd end	°C														0		0			0	0
2118	DCP Speed Trim Actr Position	Forward closet, lower controls	in.																			0	0
6130	Low-Sensitivity Altitude, Ship	Pitot-static system	ft																				0

NOTES:
1. Blank space - Data intentionally not recorded
2. O - Operational parameter
3. Ø - Parameter operational but data questionable due to calibration error, sensitivity, or voltage drift
4. B - Parameter operational on preflight calibration but data trace went to band edge intermittently or completely during flight
5. R - Reverse polarity
6. S - Parameter operational on preflight calibration but data trace had light to moderate spiking (not to band edge) during flight; spiking affected analog to digital data recovery
7. X - Parameter operational on preflight calibration but failed during preflight or flight or channel was turned off due to operational difficulty
8. ① - Altitude sensitivity restricted on tape from -1,458 feet to +9,565 feet for full bandwidth based on standard day

All data parameters were monitored before each flight, and their electrical signals were adjusted to a standard base line of zero or other predetermined constant. Because of static preloads on certain dynamic components, the rotor blades were positioned at the same azimuth for each preflight calibration.

Preflight requirements were:

- Lag damper blocks installed so that the rotor blades were maintained in full-lead position throughout the calibration sequence
- Forward yellow (instrumented) blade pitch arm 90 degrees to the fuselage centerline on the right side

FLIGHT ENVELOPE AND LIMITATIONS

The gross-weight/center-of-gravity envelope for the CH-47C helicopter is shown in Figure 2. The estimated flight envelopes for 33,000-, 40,000-, and 46,000-pound gross weights are shown in Figures 4, 5, and 6 respectively.

Level-flight speeds were to be terminated in flight when load levels on any telemetry parameter reached 150 percent of endurance limit values; maneuvers were to be terminated when these load levels reached 200 percent of endurance limit values. The aircraft fuselage q-limit airspeed of 201 knots EAS was to be observed. All maneuvers were limited to 1.5g.

The maximum rotor speed was restricted to 247 rpm (power on or power off) due to the heavier weight of the advanced-geometry blade versus the standard metal blade. The test program was to be conducted using the CH-47C programmed cyclic trim on the forward and aft rotor heads.

Transmission and engine limitations were as follows:

Transmission Torque (1300 ft-lb = 100%)

Dual Engine	- Continuous	1235 ft-lb/eng
	Transient (10 sec)	1300 ft-lb/eng
Single Engine	- Continuous	1300 ft-lb
	Transient (10 sec)	1950 ft-lb

Engine Rating, T55-L-11A

NRP - Continuous	3000 hp (1040 ft-lb at 235 rpm)
MRP - 30 Min	3400 hp (1180 ft-lb at 235 rpm)
Max - 10 Min	3750 hp (1300 ft-lb at 235 rpm)

MECHANICAL INSTABILITY TESTS

Qualitative mechanical instability tests were performed in the testing described in Table I at 35,000 pounds gross weight, 235 rotor rpm, and at 44,000 pounds gross weight, 235 rotor rpm.

At each gross weight and associated rotor speed setting, testing consisted of a hover in ground effect and hover-to-landing tests encompassing touchdown collective positions of 1 degree to 5 degrees in 1-degree increments, with the landing gear swivels both locked and unlocked. At each gross weight, rpm, and touchdown collective pitch setting, the pilot excited the aircraft with lateral stick and directional pedal motion at a medium and a fast frequency, with a minimum of 25 percent of

control travel and 5 cycles of input. All tests were performed with SAS off.

A qualitative evaluation of the stability characteristics of the helicopter was performed by the test pilot. Stability assessments were made at each test point according to the standard pilot numerical rating of aircraft response shown below:

1. Unable to induce oscillation
2. Oscillation damps rapidly
3. Oscillation damps slowly
4. Neutral oscillation
5. Oscillation slowly divergent
6. Oscillation rapidly divergent

At no time at either weight was the pilot's assessment greater than 2.

GROUND RUNS AND BLADE TRACKING

The helicopter was positioned on the ramp away from other aircraft and buildings. With fire equipment, telemetry equipment, and photographers standing by, the auxiliary power unit was started and blocks were removed. The engines were then started and aircraft characteristics were noted at the GROUND IDLE condition. The engine speeds were slowly advanced to FLY and again the aircraft characteristics were noted. The pilot then shut down the engines and restarted them, going from GROUND IDLE to FLY in a normal-to-fast rate.

During these ground runs, a track was performed which showed the aft boron blades to be in track. Several pitch link adjustments were required to bring the forward fiberglass blades into proper track.

At no time during the initial run were any aircraft handling problems encountered.

Table III gives the results of all tracking and adjustments made to the boron blades. No details are provided for the forward blades since they are not the subject of this test program.

All tracking was conducted with the Strobex tracking system, with the equipment tracking the blade at the 10 o'clock

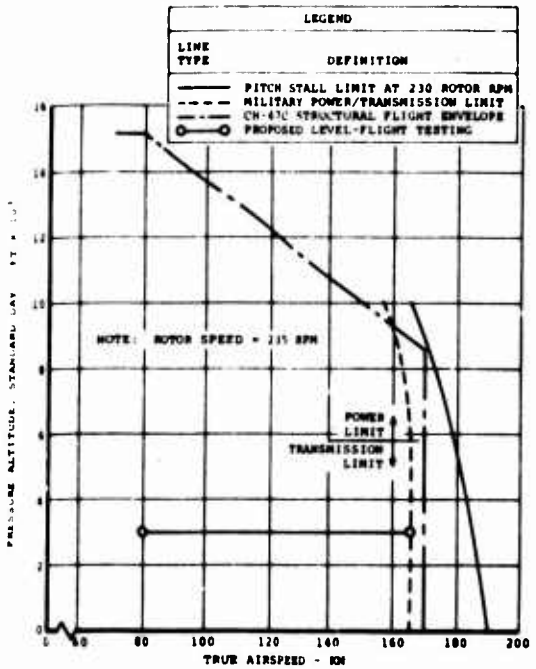

Figure 4. Predicted Airspeed Capability for the CH-47C Helicopter with Advanced-Geometry Blades at 33,000 Pounds Gross Weight.

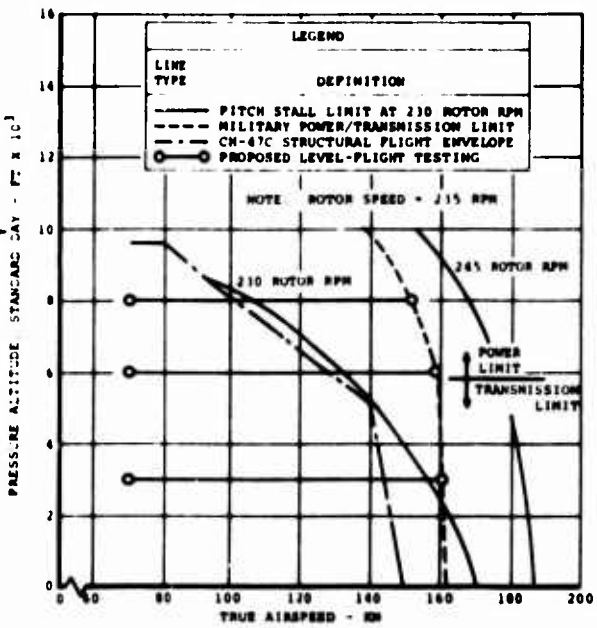

Figure 5. Predicted Airspeed Capability for the CH-47C Helicopter with Advanced-Geometry Blades at 40,000 Pounds Gross Weight.

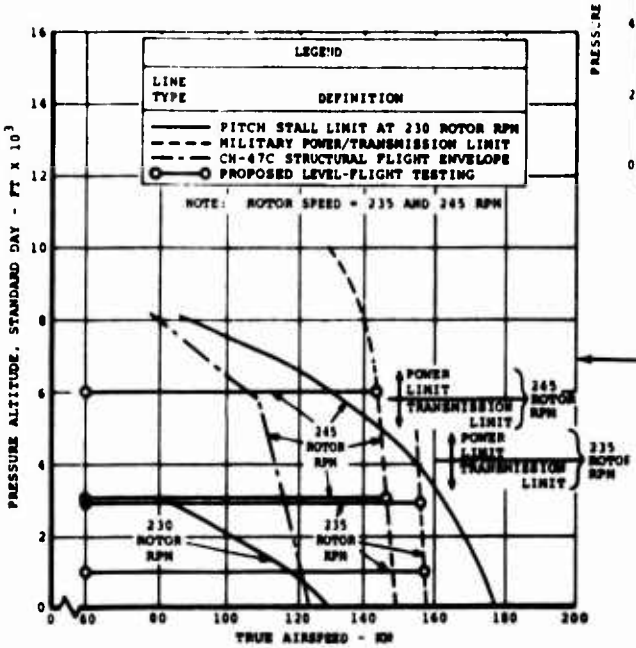

Figure 6. Predicted Airspeed Capability for the CH-47C Helicopter with Advanced-Geometry Blades at 46,000 Pounds Gross Weight.

TABLE III. BLADE TRACKING RESULTS AND CORRESPONDING PITCH LINK ADJUSTMENTS FOR BORON BLADES ON AFT ROTOR

Test No.	Track No.	Rotor Speed (rpm)/ Airspeed (kn)	Tracking Results	Pitch Link Adjustment (marks)
GR78	1	220/ -	G 1/4 in. high	Green, decrease 20
	2	235/ -	G 1/4 in. high	Red, increase 5
325	1	235/ -	Y 3/8 in. low	-
	2	235/hover	Y 3/4 in. low	Yellow, increase 3
326	1	235/ -	Y 3/8 in. low	-
	2	235/hover	Y 3/8 in. low	Yellow, increase 3
327	1	235/ -	in track	-
	2	235/hover	in track	-
	3	235/130	Y 1/2 in. low	nil
333	1	235/ -	in track	-
	2	235/80	in track	-
	3	235/130	in track	nil

position. The 12 o'clock reference point would be the blade tip located at the forward centerline of the aircraft.

The following blade color code has been used in presenting the blade tracking results and the corresponding pitch link adjustments:

- Y, yellow
- G, green
- R, red

All out-of-track conditions are relative to the red blade.

After the initial tracking results shown in Table III, the boron blade maintained a consistent track throughout the test program.

ANALYSIS OF FLIGHT TEST DATA

ROTOR MOMENT STALL CHARACTERISTICS

This section presents studies of the flight loads of the CH-47C helicopter equipped with boron advanced-geometry rotor blades. The boron blades have the same aerodynamic shape as the fiberglass advanced-geometry blades reported in Reference 5. The primary purpose of this study is to establish the boron rotor blade moment stall characteristics, with emphasis on comparison of the pitch link loads and waveforms with those of the CH-47C equipped with metal-spar blades and with fiberglass/epoxy advanced-geometry blades.

The following information is given in this section:

1. Definition of moment stall for the boron advanced-geometry rotor blade
2. Illustration of pitch link load growth rate in stall
3. Display of flights of the boron blade encountering moment stall
4. Effects of rpm on moment stall
5. Effect of altitude on moment stall, including growth rate with altitude
6. Comparison of pitch link loads and waveforms for the three different blades under similar flight conditions and at equivalent C_T/σ
7. Comparison of flight test pitch link load data on basis of a flutter parameter
8. Blade structural properties and damping

Definition of Moment Stall

As stated in Reference 5, moment stall recognizes the increase in blade alternating pitching moments resulting from stall occurring along portions of the blade span. The blade pitching moments are reflected in the pitch link loads; examination of the pitch link load waveforms is necessary to define the inception and development of moment stall on the boron advanced-geometry blade.

The definition of moment stall inception for the boron blade is the same as that defined for the fiberglass blade; namely, that inception occurs at the point at which the first full cycle of moment stall is discernible. This is indicated by

the second compression spike (nose-down pitching moment) in the pitch link load waveform. The second compression spike by definition must also occur in at least 50 percent of the level-flight cycles to be called moment stall. Figures 7B and 7C display examples of this definition in the fiberglass and boron blades, respectively. CH-47C metal blade waveforms are shown in Figure 7A, where inception is defined as that point where the peak-to-peak loading occurring during the moment stall cycle equals the peak-to-peak loading of the basic pitch link waveform and occurs in at least 50 percent of the level-flight cycles analyzed.

Load Growth Rate

In Figure 174 of Reference 5, it was noted that the fiberglass blade pitch link load growth rate followed a V^2 trend in stall, while the CH-47C metal blade growth rate was much more abrupt. The boron blade pitch link load trends also follow essentially a V^2 trend after stall, very similar to that of the fiberglass blade. Figures 8 and 9 illustrate this comparison.

It should be noted that the boron blade load trend for comparison is at a 51,200-pound gross weight and 2,200-foot density altitude, rather than the approximately 46,000-pound gross weight and 6,000-foot altitude for the fiberglass and metal blades. The flight at 51,200 pounds was used for comparison because the boron blade was stalled continuously at 46,000 pounds and 6,000 feet.

There is no explanation at present for the differences in load growth rates between the metal blade and the composite blades. Considerations such as structural damping differences, thin tips versus thick tips, and pitch axis location have been related to load growth rates. There is a limited amount of stall data available on the BO-105 rotor that displays load growth rates significantly higher than V^2. Inasmuch as the BO-105 blade is a composite (fiberglass) blade and has a 25-percent pitch axis, one might conclude that the low load growth rates on the advanced-geometry blades are due to the thin tip construction. Although there is some wind tunnel model data available for the comparison of thin tips and the 23010 airfoil, unfortunately it is beyond the scope of this program to pursue the problem in depth.

Summary of Flight Conditions Analyzed

Table I of this report summarizes the flight conditions tested during the boron blade program. Table IV identifies those flight conditions in which evidence of moment stall was encountered. Figure 10 presents the same information on an

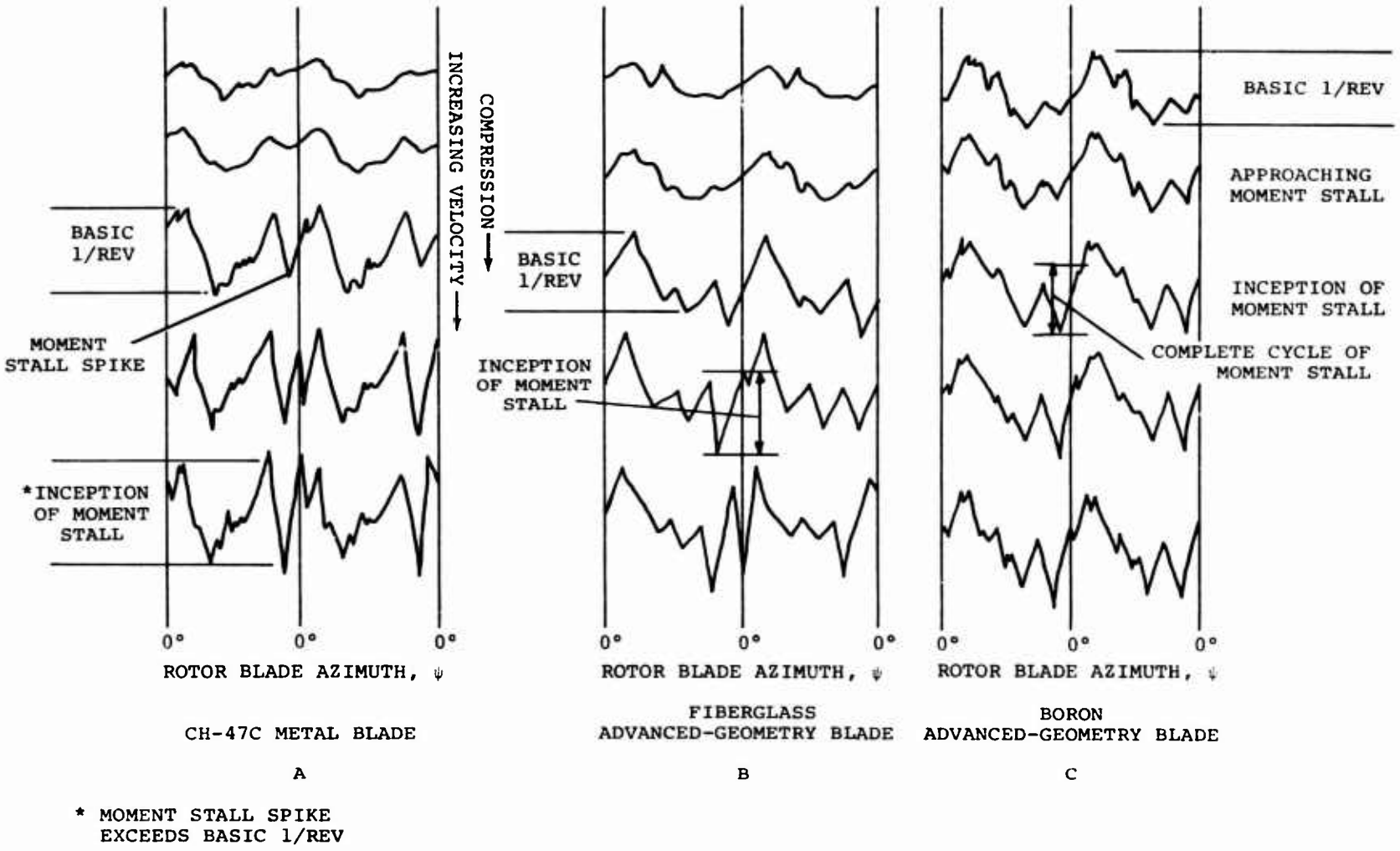

* MOMENT STALL SPIKE EXCEEDS BASIC 1/REV

Figure 7. Comparison of Pitch Link Load Waveforms.

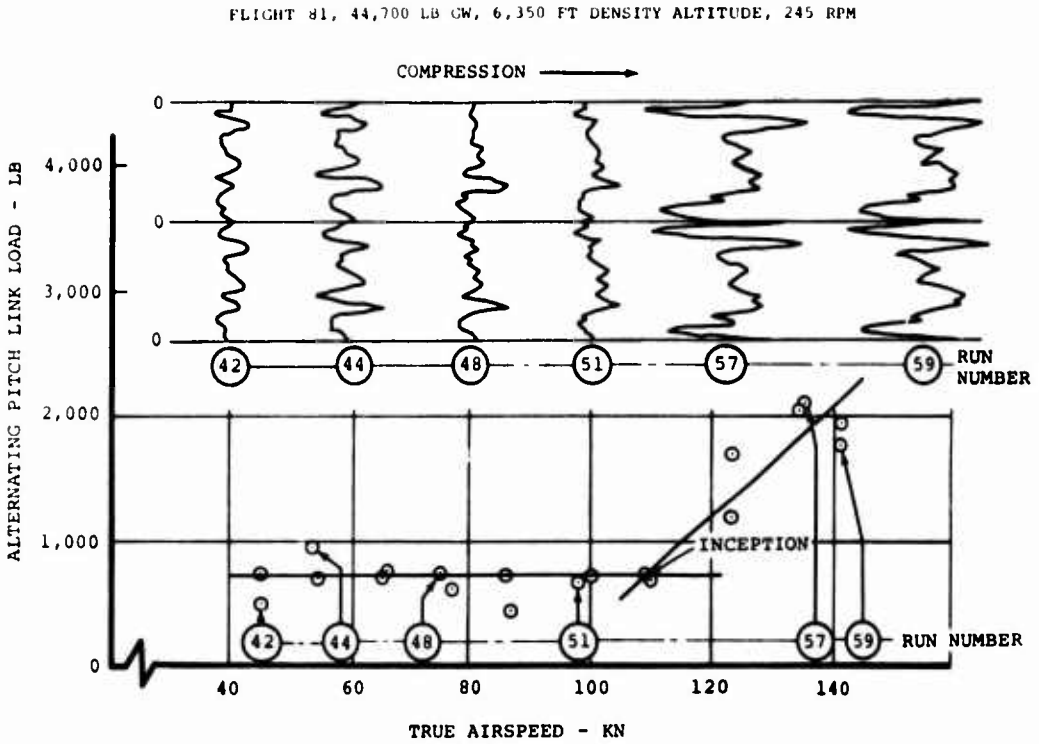

CH-47C METAL BLADES

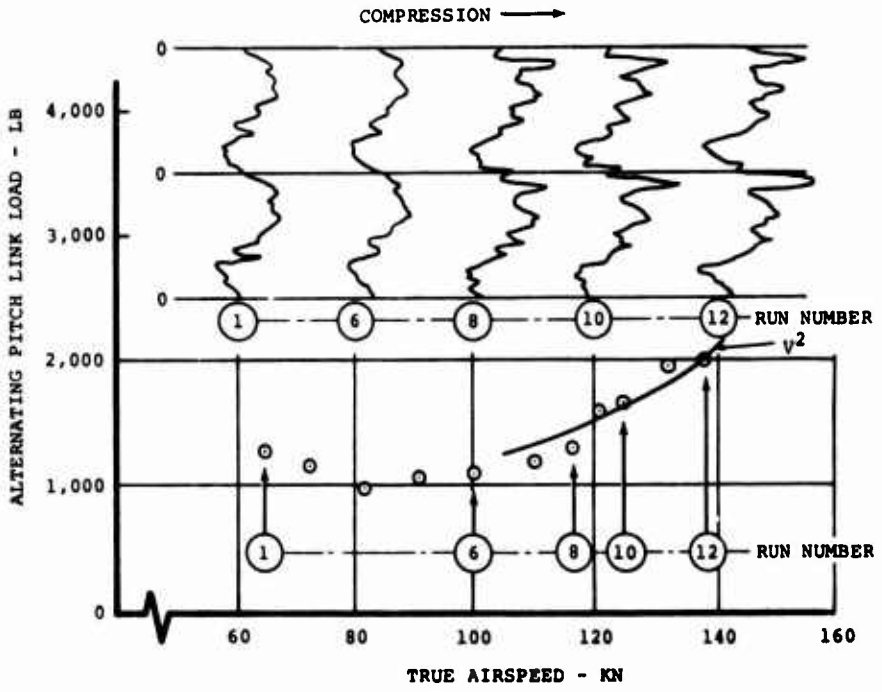

FIBERGLASS ADVANCED-GEOMETRY BLADES

Figure 8. Pitch Link Load Growth With CH-47C Metal Blades and Fiberglass Advanced-Geometry Blades.

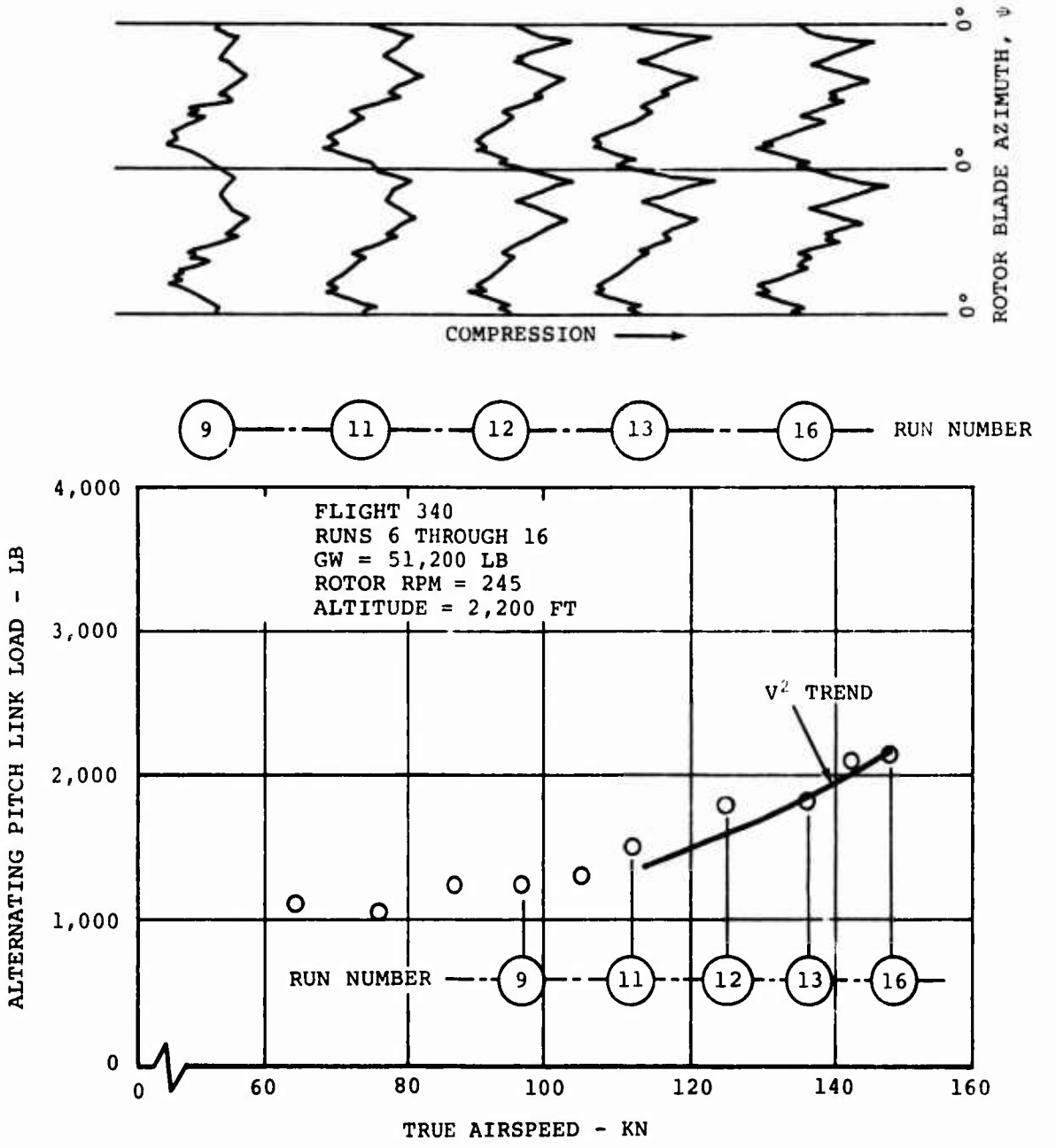

Figure 9. Pitch Link Load Growth With Boron Advanced-Geometry Blades.

TABLE IV. SUMMARY OF LEVEL-FLIGHT RUNS HAVING MOMENT STALL BASED ON WAVEFORM ANALYSIS

Flight	Runs	GW (lb)	Density Altitude (ft)	TAS (kn)	Rotor RPM
332	21 through 26	46,500	6,300	50-143	245
332	27 through 34	46,100	6,000	50-142	235
332	35 through 39	45,800	6,100	69-110	245
332	45 through 55	45,000	6,700	39-139	235
332	57 through 62	44,600	7,400	42-142	245
332	63 through 66	44,300	9,100	96-117	245
332	68 through 73	44,000	8,800	61-121	235
333	7 through 13	51,000	2,000	51-132	245
333	30 through 34	49,700	5,900	60-112	245
333	41 through 46	48,800	5,000	54-132	245
333	48 through 52	48,500	5,300	93-125	235
333	55 through 60	48,000	1,700	68-139	235
339	15 through 20	46,650	5,000	70-120	245
339	21 through 23	46,300	4,300	128-146	245
340	6 through 16	51,200	2,200	66-147	245
340	17 through 24	50,850	3,300	69-135	245
340	48 through 53	41,150	11,200	88-136	245
340	56 through 64	40,800	7,300	70-144	245
340	65 through 70	40,500	6,400	88-140	235
340	73 through 79	40,200	5,200	87-147	235

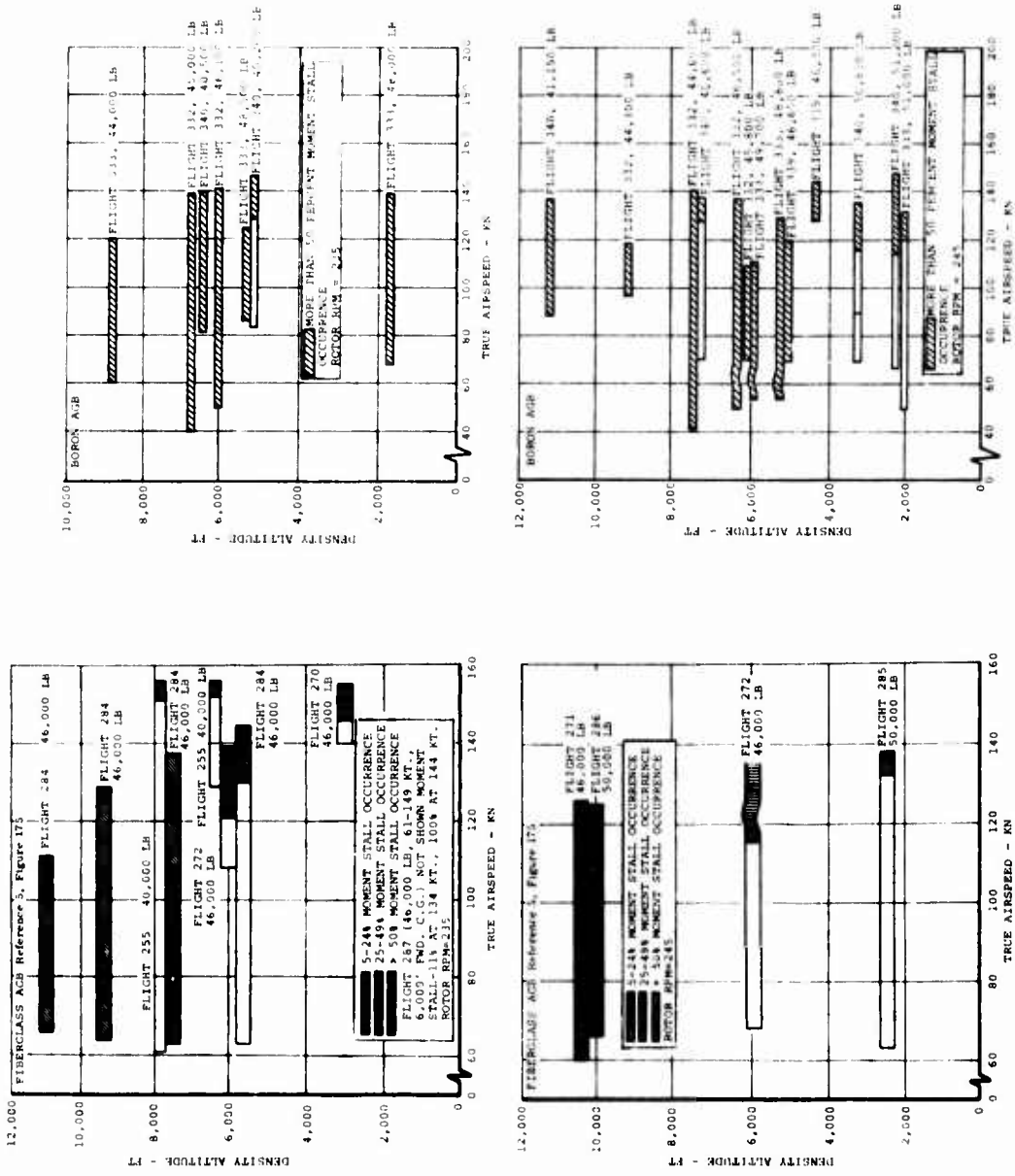

Figure 10. Summary of Flights Having Moment Stall.

airspeed/altitude plot to obtain a better perspective of where moment stall was encountered. A comparison to Figure 175 of Reference 5 clearly displays the evidence of moment stall occurring earlier on the boron advanced-geometry blade than on the fiberglass advanced-geometry blade. For every combination of gross weight, altitude, and rpm where comparative flight conditions are available, the boron blade stalls earlier than the fiberglass blade.

Effect of RPM on Moment Stall

The effect of rotor rpm is illustrated in Figure 11 and shows the same trend as seen on the fiberglass advanced-geometry blades and the CH-47C metal blades. As rpm increases, the stall spike becomes progressively smaller until it disappears altogether.

Effect of Altitude on Moment Stall

Figure 12 displays a comparison of the pitch link waveforms for the fiberglass and boron advanced-geometry blades as a function of altitude. The test data were obtained by stabilizing the aircraft in a military power climb at 90 knots and recording data at various altitudes. In order to more clearly display the relative moment stall inception points, the alternating pitch link loads were plotted versus density altitude in Figure 13 and versus C_T/σ in Figure 14. From these plots it can be seen that stall inception occurs earlier on the boron blade by 2,000 feet in altitude or by a C_T/σ increment of 0.005. The test conditions were comparable for both blades except for outside air temperatures and the difference in rate of climb resulting from the temperature differential. These differences were accounted for in the trim analysis used to convert density altitude to C_T/σ.

Pitch Link Load Comparison

Comparisons have been made for similar flight conditions (equal thrust) and equivalent C_T/σ (equal unit blade loading). The comparison of pitch link load waveforms is shown in Figures 15 and 16 respectively for the CH-47C metal and the fiberglass and boron advanced-geometry blades. The waveforms for the boron blade are similar in character and magnitude to those of the fiberglass blade except that moment stall occurs earlier with the boron blade (in the cases compared, stall is continuous on the boron blade). Figures 17 through 21 compare alternating aft pitch link loads for similar flight conditions for each of the three blades over a gross weight range from 33,000 to 50,000 pounds. The unstalled pitch link loads for

the boron blade are almost identical in magnitude to those of the fiberglass blade as evidenced by Figures 17, 18, and 20. The only conflict with these conclusions occurs at the 50,000-pound-gross-weight test condition (Figure 21). The boron blade loads are consistently higher than the glass blade loads even in the unstalled regions of flight. However, as discussed earlier, the boron blade stalls earlier than the fiberglass blade; and as one would expect, the stalled loads are higher than the comparable glass blade loads.

A comparison of the boron blade pitch link loads on an equivalent C_T/σ basis, as shown in Figure 22, was necessarily made at the same blade loadings used for the fiberglass blade as shown in Figure 184 of Reference 5. The boron blade, however, is stalled continuously at those conditions, thus accounting for the higher loads. A nondimensional comparison of pitch link loads serves to confirm only that pitch link load coefficients are substantially higher in stall than for unstalled conditions (see Figure 23). Pages 188 through 192 of Reference 5 present the equations used to nondimensionalize pitch link loads.

Comparison Based on Moment Stall Parameters

A comparison of the boron advanced-geometry blade with the fiberglass and metal blades by using the nondimensional moment stall inception parameter described on page 195 of Reference 5 shows that stall inception occurs earlier on the boron blade. Figure 24 shows approximately 1 degree lower angle-of-attack capability with the boron blade. It is interesting to note that flexible blade theory predicts that the boron blade operates in forward flight at tip angles of attack on the order of 1/2 degree higher than the fiberglass blade (Figure 25). The moment stall parameter curve, however, was developed using rigid-blade trim analyses to obtain $\alpha_{1,270}$ values and does not account for live twist differences between blades.

Those symbols in Figure 24 with arrows pointing upward and to the left indicate that stall occurred during the entire flight at that altitude and gross weight. The data point represents the lowest airspeed for which stall was recorded.

Summary of Pitch Link Waveforms

Appendix I contains a display of many of the pitch link waveforms examined in the process of establishing waveform characteristics and moment stall inception.

Blade Structural Properties and Effect of Damping

Table V presents a summary of the natural frequencies and critical aerodynamic damping ratios for the three rotor blades under study for the flap, chord, and torsion modes. Table VI summarizes the important design parameters of each blade.

No structural damping measurements were taken on the boron advanced-geometry blade. The only data that remain available are from the fiberglass blade program, wherein the first torsional mode critical structural damping ratios were found to be approximately 1-1/2 percent and 2-1/2 percent for the metal and fiberglass blades, respectively (Reference 5, page 197).

Theoretical calculations predict a critical aerodynamic damping ratio of 27 percent for the boron blade, which falls between 24 percent for the metal blade and 29 percent for the fiberglass blade.

Principal Results and Observations

1. Unstalled pitch link loads for the boron advanced-geometry blade are essentially the same as those for the fiberglass advanced-geometry blade, which in turn are higher than those of the CH-47C metal blade due to the increased blade chord.

2. For the same gross weight, altitude, rpm, cg, and trim, moment stall inception occurs earlier on the boron blade than on the fiberglass blade.

3. The pitch link load waveforms for the boron blade are very similar to those for the fiberglass blade. Moment stall inception for the boron blade is determined in an identical manner as for the glass blade.

4. The pitch link load growth rates after stall on the boron blade are similar to the growth rates on the fiberglass blade, both following approximately a V^2 trend.

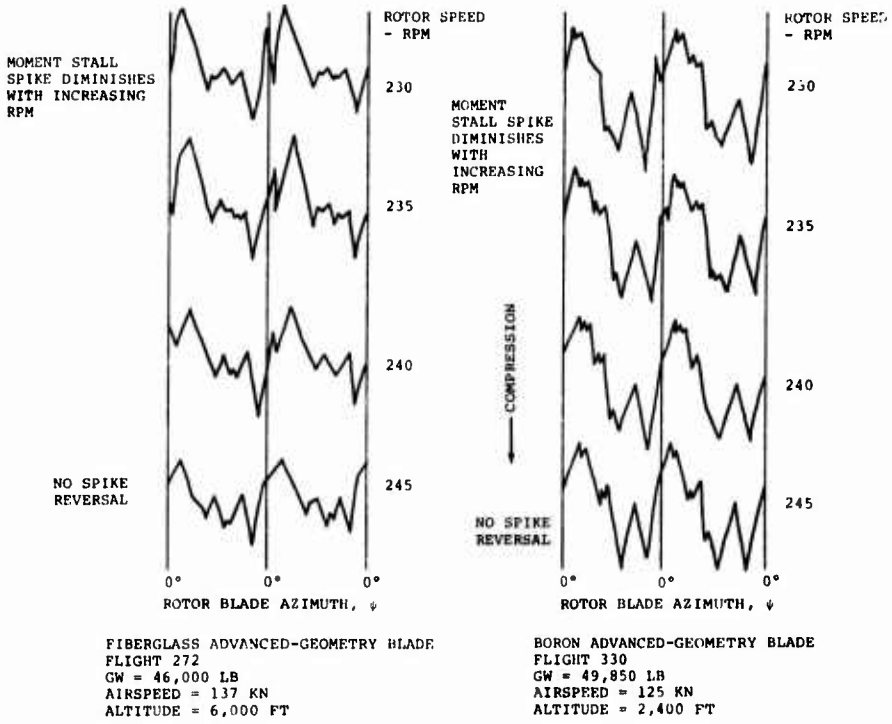

Figure 11. Effect of Rotor Speed on Pitch Link Load Waveform.

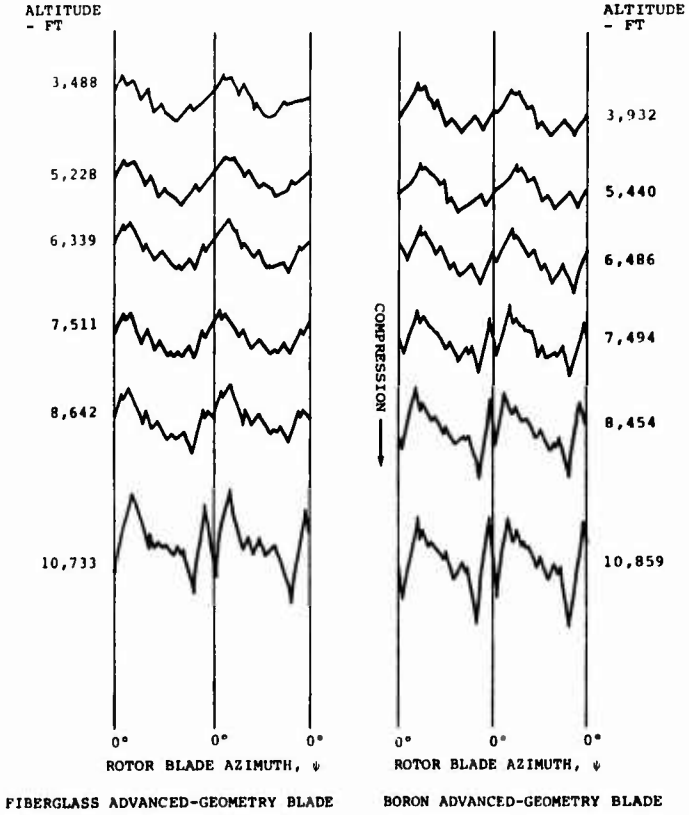

Figure 12. Effect of Altitude on Pitch Link Load Waveform.

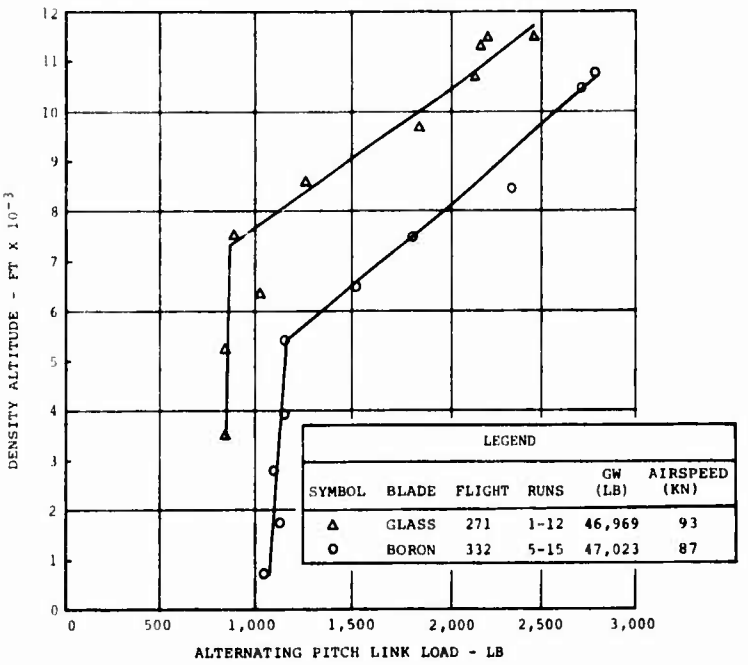

Figure 13. Comparison of Effect of Altitude on Pitch Link Loads During Flight Test of Fiberglass and Boron Advanced-Geometry Blades.

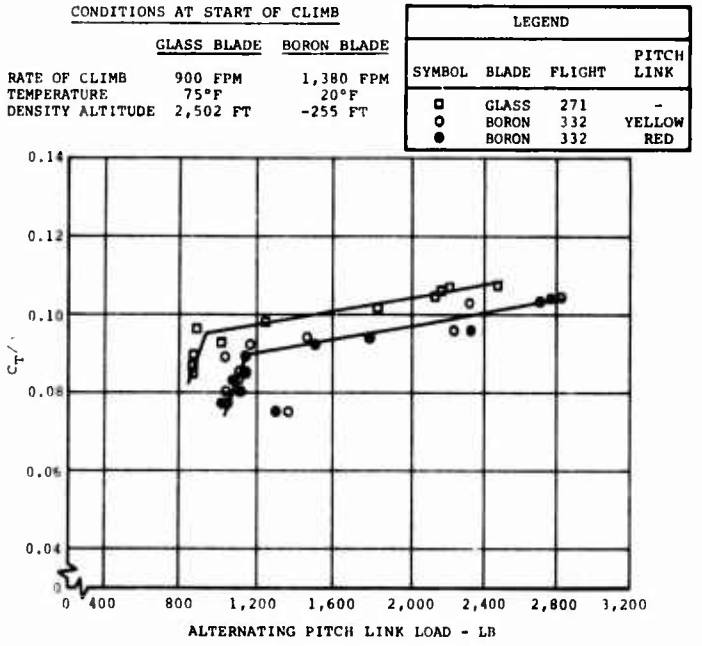

Figure 14. Comparison of Moment Stall Inception on a Non-dimensional Basic C_T/σ During Flight Test of Fiberglass and Boron Advanced-Geometry Blades.

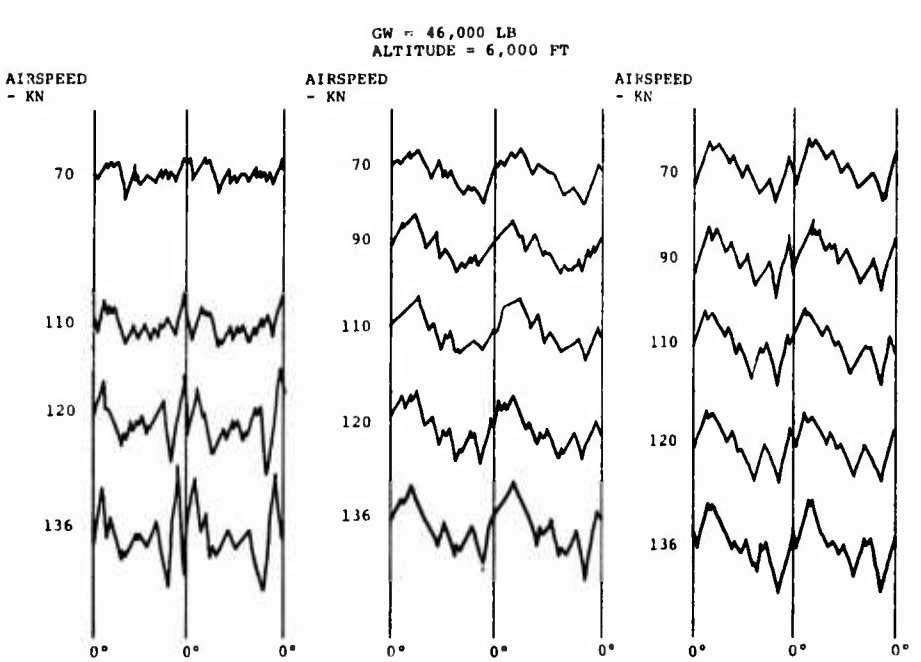

Figure 15. Comparison of Pitch Link Load Waveforms for Three Different Blades Under Similar Flight Conditions.

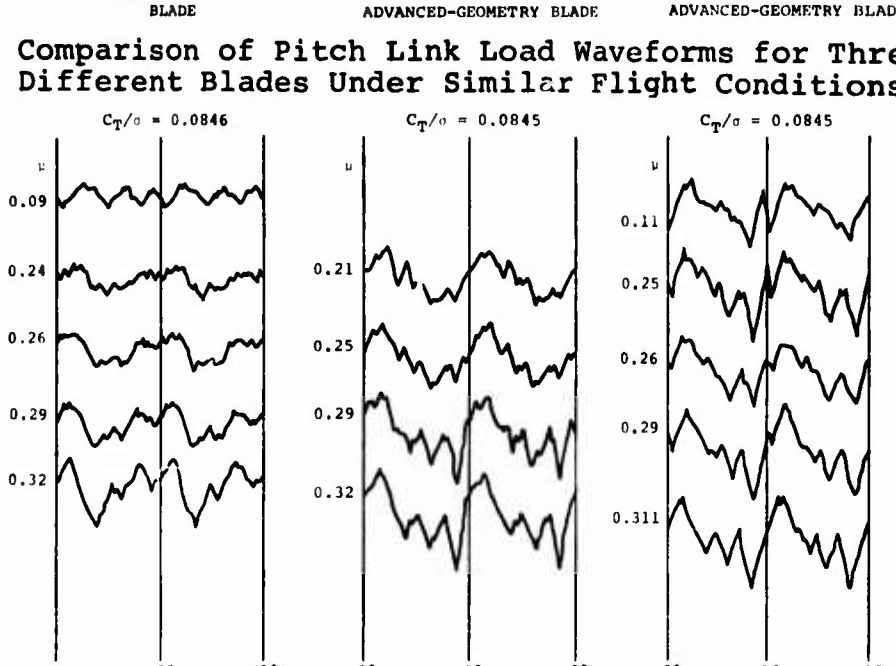

Figure 16. Comparison of Pitch Link Load Waveforms for Three Different Blades at Equivalent C_T/σ.

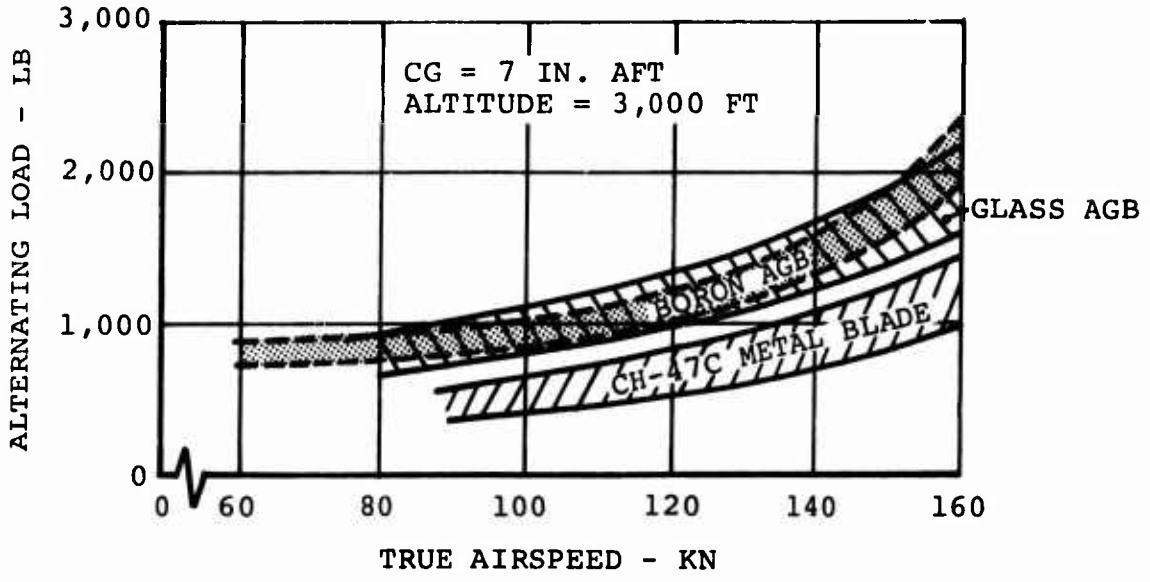

Figure 17. Comparison of Aft Pitch Link Alternating Loads for Three Different Blades at 33,000 Pounds Gross Weight and 235 Rotor RPM.

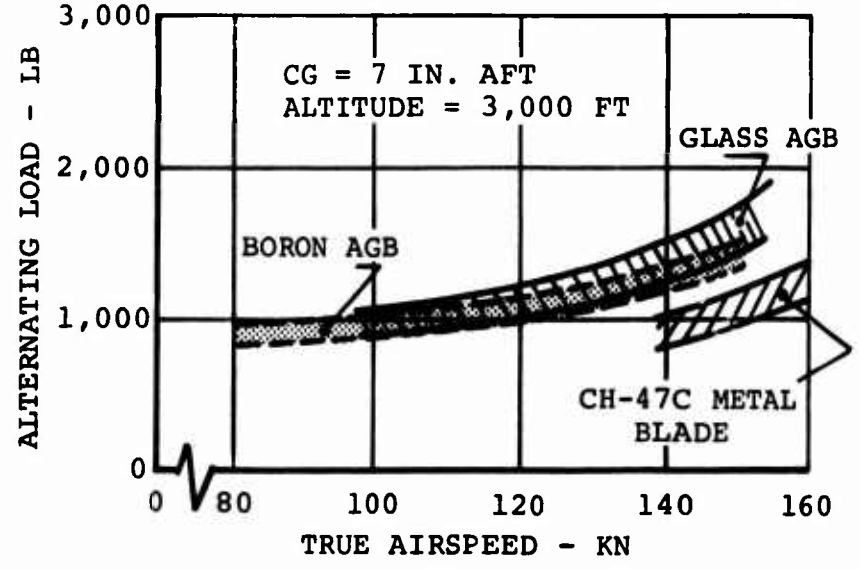

Figure 18. Comparison of Aft Pitch Link Alternating Loads for Three Different Blades at 33,000 Pounds Gross Weight and 245 Rotor RPM.

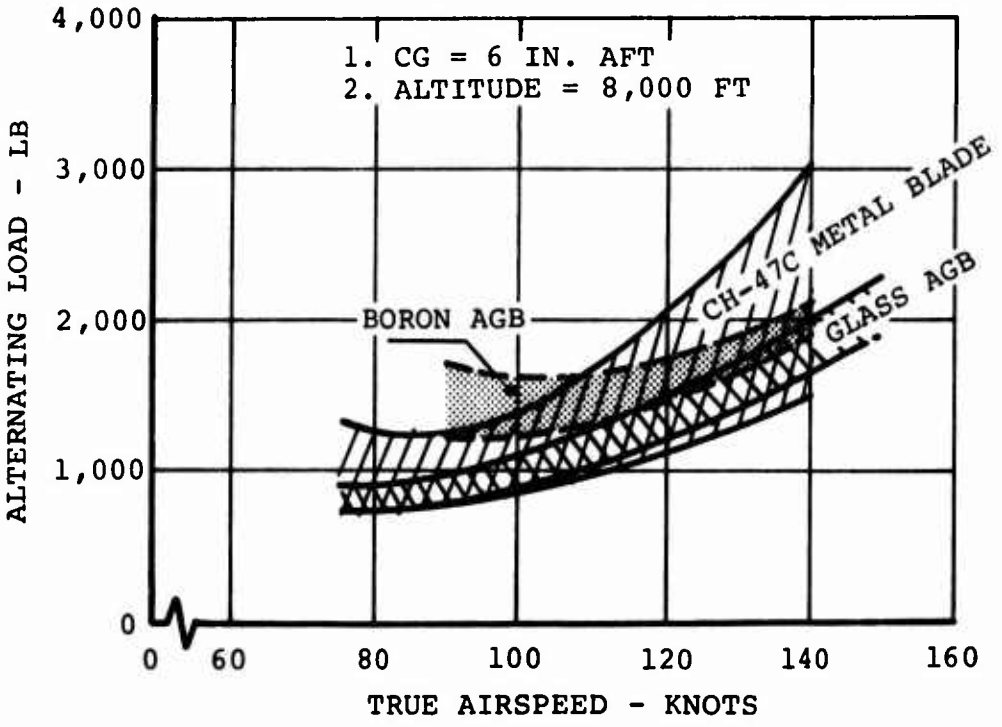

Figure 19. Comparison of Aft Pitch Link Alternating Loads for Three Different Blades at 40,000 Pounds Gross Weight and 235 Rotor RPM.

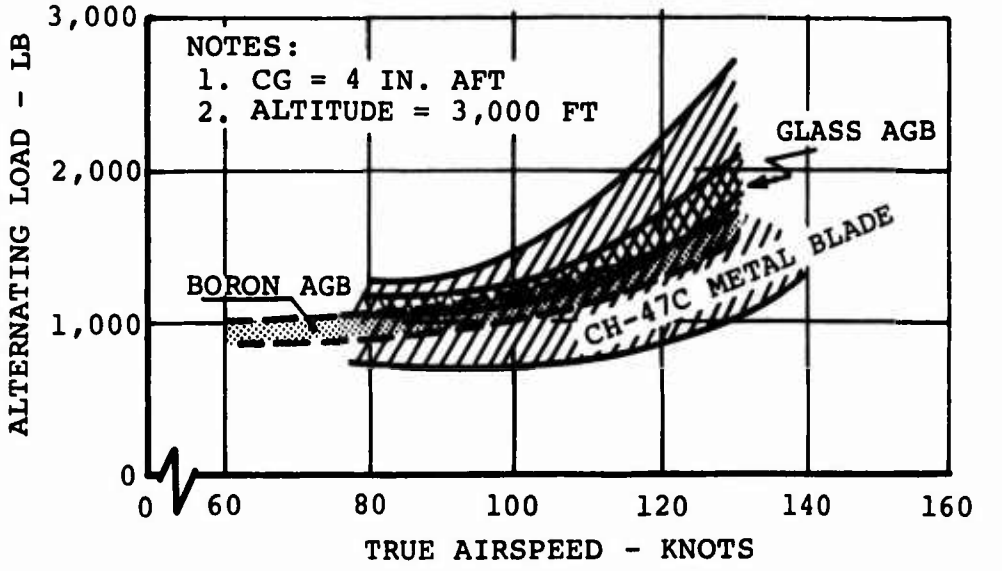

Figure 20. Comparison of Aft Pitch Link Alternating Loads for Three Different Blades at 46,000 Pounds Gross Weight and 245 Rotor RPM.

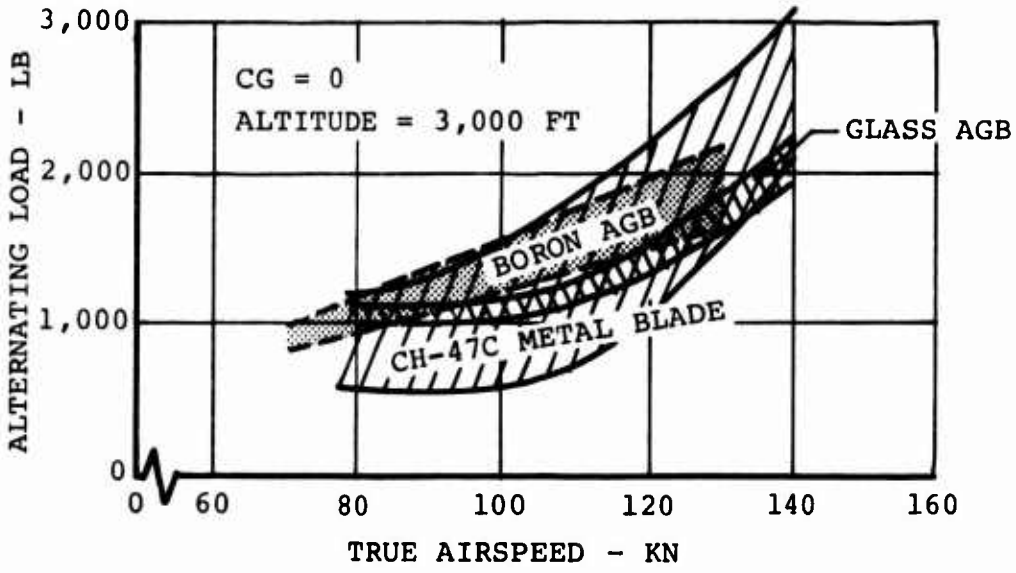

Figure 21. Comparison of Aft Pitch Link Alternating Loads for Three Different Blades at 50,000 Pounds Gross Weight and 245 Rotor RPM.

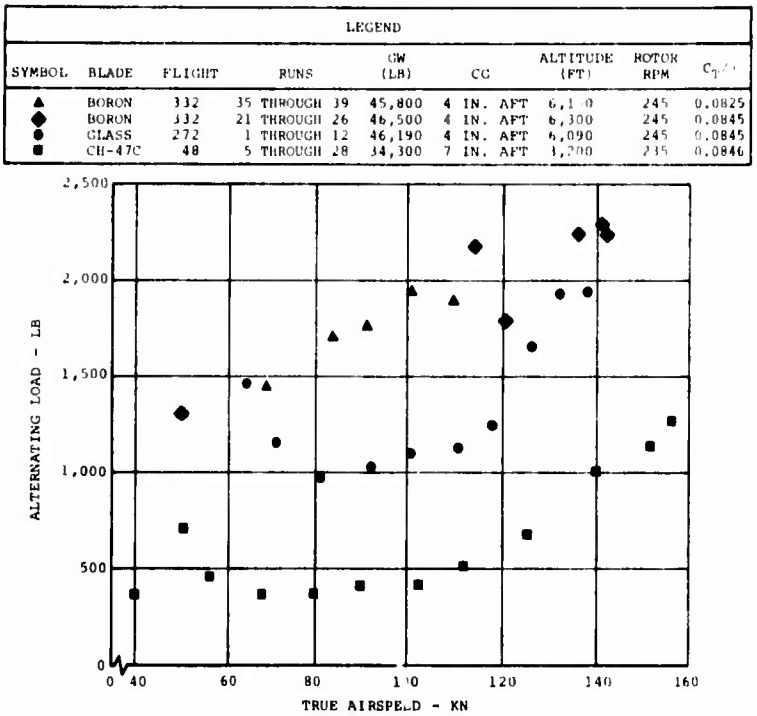

Figure 22. Comparison of Aft Pitch Link Alternating Loads for Three Different Blades at Equivalent C_T/σ.

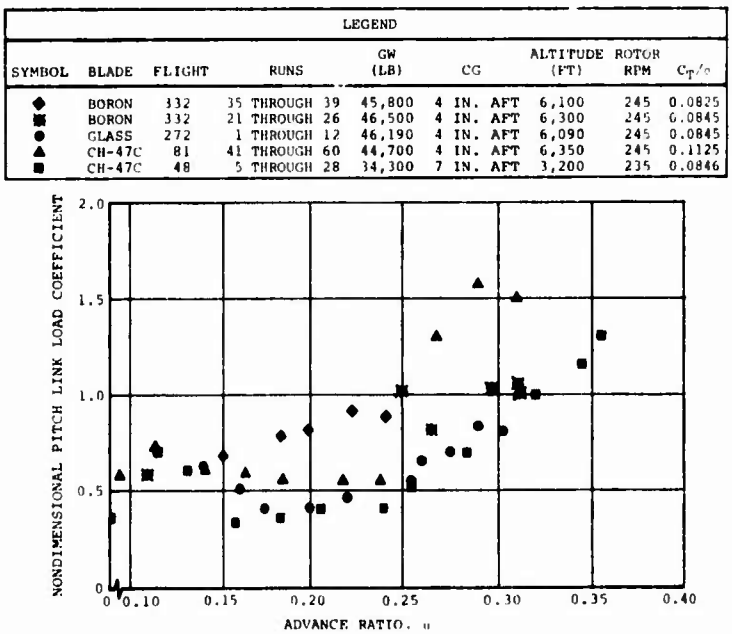

Figure 23. Nondimensional Comparison of Aft Pitch Link Loads for Three Different Blades for Similar Flight Conditions and Equivalent C_T/σ.

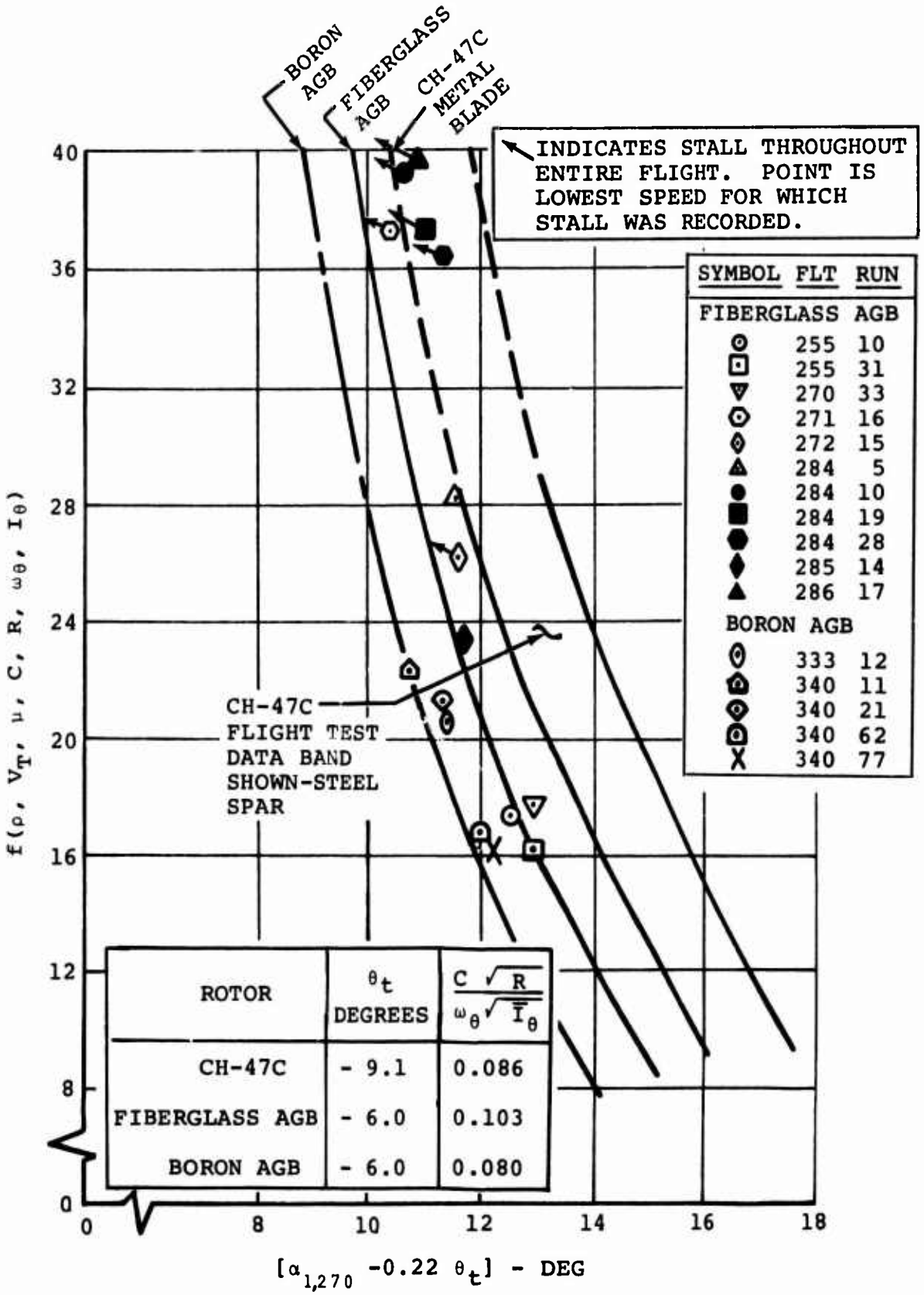

Figure 24. Summary of Boeing-Vertol Experience With Moment Stall Inception.

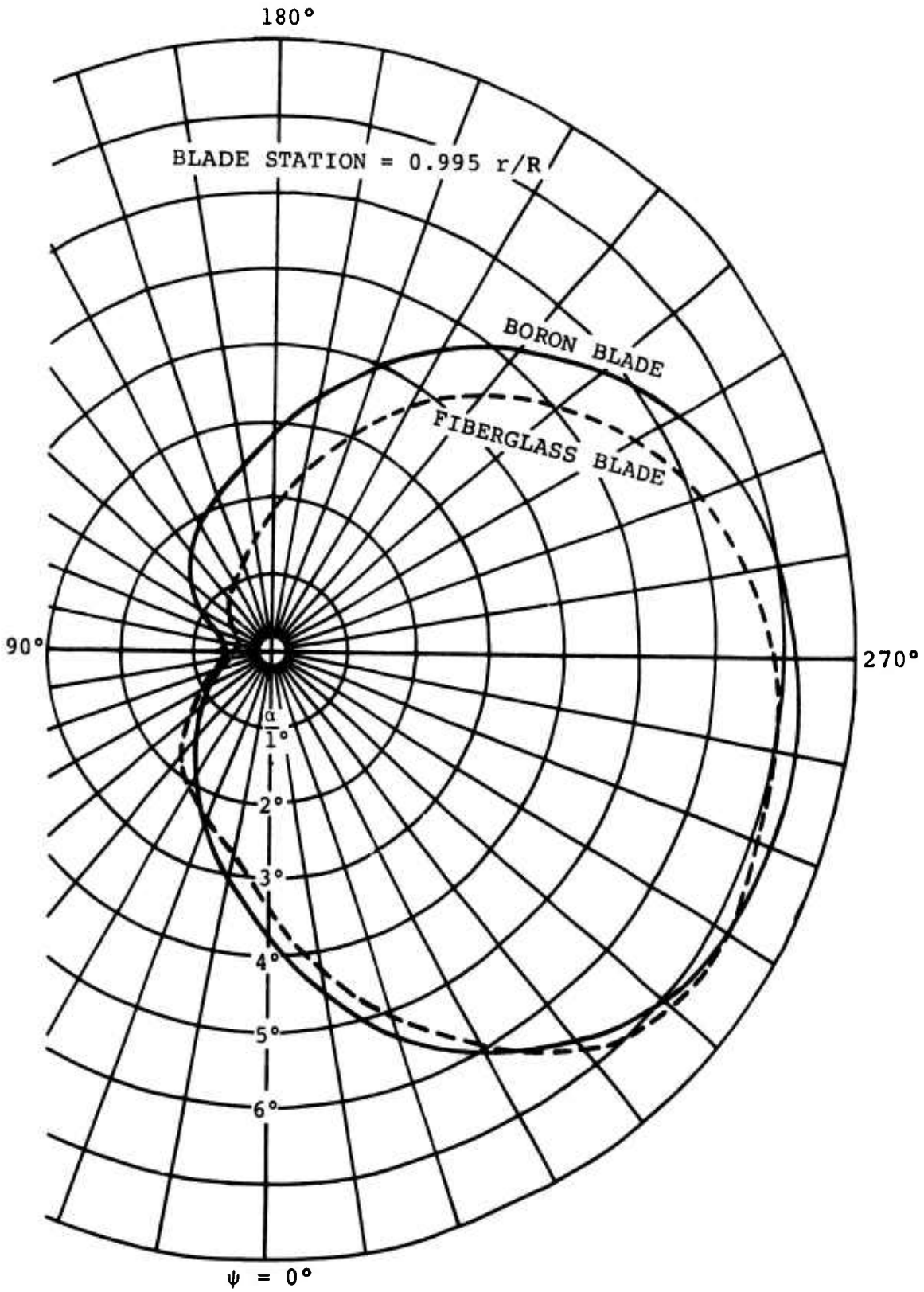

Figure 25. Unstalled Comparison of Tip Angle of Attack at a True Airspeed of 107 Knots.

TABLE V. UNCOUPLED NATURAL FREQUENCIES AND CRITICAL DAMPING RATIOS OF THE CH-47B/C METAL AND FIBERGLASS AND BORON ADVANCED-GEOMETRY BLADES AT 230 RPM

Flap Modes		CH-47B/C	Glass AGB	Boron AGB
Zero	ω_0	1.018	1.018	1.016
	ζ_0	0.5439	0.6449	0.5607
First	ω_1	2.569	2.479	3.230
	ζ_1	0.1531	0.1883	0.1282
Second	ω_2	4.748	4.685	7.126
	ζ_2	0.07559	0.09711	0.05777
Third	ω_3	7.899	7.863	13.333
	ζ_3	0.04495	0.06651	0.02904
Fourth	ω_4	12.19	11.88	-
	ζ_4	0.03047	0.04129	-
Chord Modes		**CH-47B/C**	**Glass AGB**	**Boron AGB**
Zero	ω_0	0.3656	0.3719	0.3389
First	ω_1	5.225	4.256	6.848
Second	ω_2	14.70	11.51	-
Torsion Modes		**CH-47B/C**	**Glass AGB**	**Boron AGB**
First	ω_1	6.416	5.449	6.536
	ζ_1	0.2421	0.2903	0.2666
Second	ω_2	14.74	10.88	14.53
	ζ_2	0.07140	0.1314	0.1015

ω_n : n^{th} mode natural frequency
ζ_n : n^{th} mode critical damping ratio
NOTE: Damping in chord modes based on lag damper only

TABLE VI. DESIGN PARAMETERS OF THE CH-47B/C METAL AND FIBERGLASS AND BORON ADVANCED-GEOMETRY BLADES

Item	CH-47B/C	Glass AGB	Boron AGB
Rotor Radius, ft	30.0	30.0	30.0
Blade Chord 75 Percent R, in.	25.25	33.38	33.38
Number of Blades/Rotor	3	3	3
Rotor Solidity Ratio	0.0669	0.0848	0.0848
Rotor RPM	230	230	230
Rotor Tip Speed, fps	723	723	723
Flapping Weight, lb	491.7	492.7	482.2
Flapping Weight Moment, in.-lb	5.527×10^4	6.125×10^4	6.421×10^4
Flapping Inertia, lb-in.^{2}	1.239×10^7	1.351×10^7	1.520×10^7
Lagging Weight, lb	331.8	371.4	360.9
Lagging Weight Moment, in.-lb	4.635×10^4	5.207×10^4	5.525×10^4
Lagging Inertia, lb-in.^{2}	1.021×10^7	1.108×10^7	1.264×10^7
Pitching Inertia, lb-in.^{2}	1.109×10^4	2.105×10^4	1.720×10^4
Pitch Axis, Percent Chord	19.53	25.00	25.00
Shear Center, Percent Chord	19.53	21.15	22.07
Static CG, Percent Chord	22.24	23.39	25.59
Dynamic CG, Percent Chord	24.88	24.37	25.44
CF at Hor Pin, lb	88,963	97,955	102,284

CONTROL SYSTEM AND ROTOR SHAFT LOADS

Control system and rotor shaft loads are compared for the boron and fiberglass advanced-geometry blades. The airspeed capability for the boron advanced-geometry blades is compared with the structural flight envelope for the fiberglass AGB configuration.

Level-Flight Data

The summary of Table VII identifies the level-flight test conditions for the 24 stress and motion airspeed sweeps conducted with the boron blades. Scattergrams of load versus airspeed for these 24 test conditions are presented in Appendixes II, III, and IV for the most critical fatigue-loaded control and drive system components; namely, the aft pitch links, the aft fixed link, and the aft rotor shaft. The aft rotor shaft bending moments for the boron AGB are reported for a gage installation closer to the rotor hub (station 23) than that used for the glass AGB report (station 37). This was necessitated by electrical spiking which produced incorrect moment values when reduced by the automatic data processing system. The endurance limit of the aft rotor shaft has been referred to the new gage location on the shaft using the appropriate moment slope versus shaft station. This slope has been verified for flight 328 in which both gage installations were functioning and also for selected hand-reduced data points from flight 332.

Comparative level-flight airspeed data for the aft pitch links and rotor shaft at approximately 46,000 pounds gross weight are shown in Figures 26 and 27 for 235 and 245 rpm, respectively.

At 235 and 245 rpm, the aft pitch link loads are slightly below the endurance limit for the boron AGB. The higher pitch link loads at the lower percentage of V_{ne} obtained on the boron AGB rotor are suspected to reflect the presence of moment stall inception at the blade tip. The load increase with airspeed for the boron blade is very gradual for the tip stall condition. This gradual load buildup has necessitated the approach for the boron blade load-limited airspeed assessment discussed in the following paragraph. It should be noted that the pitch link loads are comparable in the absence of tip stall. The rotor shaft bending moments are comparable as shown in Figures 26 and 27.

The airspeed capability of the boron AGB has been assessed by determination of the forward speed at which the load trends intercept the endurance limit in each load scattergram for the 24 test conditions. The comparative airspeed capability is presented in Table VII and Figures 28 and 29. The structurally limited airspeeds were established by the controls. For all

24 test conditions, the rotor shaft bending airspeed capability exceeds the airspeed limit as determined from control loads. The load-limited airspeed determined by the controls was assessed as follows:

1. If loads did not exceed the endurance limit of 2,500 pounds, the pitch link and fixed link loads were based on a V^2 and V^3 load extrapolation, respectively, from the highest airspeed data point.

2. If loads exceeded the endurance limit of 2,500 pounds, the pitch link and fixed link loads were based on a V^2 and V^3 load extrapolation, respectively, passing through the data point in excess of the endurance limit which produced the lowest airspeed capability.

3. The load scattergrams in Appendixes II, III, and IV indicate several data points which deviate from the data trend. These data points are believed to be in error and have been labeled REQUIRE INVESTIGATION. These data points have not been used in the assessment of airspeed capability.

The five test conditions which indicate a significant reduction in airspeed capability relative to the fiberglass AGB flight envelope will be grouped into two categories for the following discussion.

The 33,000- and 40,000-pound-gross-weight test conditions are believed to reflect an advancing-tip Mach number load buildup. Figures 30 and 31 present the aft fixed link loads for 33,000 and 40,000 pounds gross weight respectively, as a function of both airspeed and advancing-tip Mach number. While the boron blade indicates a lower airspeed capability relative to the glass blade, both configurations indicate the same load buildup as a function of advancing-tip Mach number. This suggests that a degradation of the flight envelope of the fiberglass AGB would occur at conditions of lower ambient temperature.

The 46,000-pound-gross-weight test conditions reflect a degradation of speed capability with increasing altitude. While the design load limit of 2,500 pounds is exceeded for the 6,700-foot-density-altitude test condition, the actual endurance limit of 2,710 pounds is not exceeded; in fact, a significant speed increase would be realized with the higher load limit. The CH-47C mission profile time at 9,000 feet density altitude and 46,000 pounds gross weight is very low. Therefore, it may not be necessary to impose an altitude limit for the boron AGB. The boron blade pitch link loads are slightly in excess of the endurance limit when observing the structural envelope for the fiberglass AGB at this test condition. The impact on fatigue life is such that both an acceptable fatigue life and the fiberglass AGB structural envelope can be

achieved. As previously reported, the fiberglass AGB envelope has been established for demonstration purposes and is not considered to be qualified for fleet usage. In view of the foregoing discussions of airspeed limitations and fiberglass blade envelope limitations, it can be concluded that the airspeed capability of the boron AGB is comparable to that of the glass AGB.

Maneuver Data

Comparative maneuver loads for the boron blade relative to the glass blade and conventional CH-47C blade are presented in Figures 32 and 33. The load ranges shown represent the total spectrum of aircraft configuration during the three stress and motion test programs. Again, the parameters investigated are the aft pitch links for the control system and the aft rotor shaft for the drive system. Figure 32 shows the range of boron blade pitch link loads to be lower or comparable to glass blade pitch link loads, with the exception of the left turn maneuver. The maximum value for the boron AGB in a left turn is 5,760 pounds. The next highest value measured is 3,920 pounds, which compares with the maximum value measured for the right turn maneuver. Relative to the CH-47C, this single left turn load is extremely high. Both the right turn maximum load and the next highest left turn load are significantly lower than CH-47C maximum turn loads. Figure 33 shows the range of boron blade rotor shaft moments to be lower or comparable to glass blade rotor shaft moments, with the exception of the left turn maneuver. Higher load levels for this single maneuver condition (left turn) will not have a significant impact on fatigue lives established for the CH-47C. The maintenance of comparable fatigue lives is significant since both the boron and the fiberglass AGB configurations demonstrate an increased airspeed capability.

Testbed Limitations

The complete advanced-geometry blade flight test program was conducted on a CH-47C helicopter. Due to its configuration, this vehicle imposed certain limitations on the blade investigation. These limitations were as follows:

1. The investigation was restricted to operation within the CH-47C strength and power limits. Blade and control fatigue loads were monitored via telemetry during all flights. The proposed initial safe flight limits with this system were 150 percent of endurance limit for level-flight testing and 200 percent for maneuvering flight. These cutoffs were never attained during the program.

   The testing was frequently restricted by power available from the T55-L-11 engines, as well as the transmission

limit. The aircraft was restricted to the CH-47C growth transmission limit of 7,320 hp at 243 rotor rpm (95 percent torquemeter indication).

The operation of the aircraft was limited to 247 maximum rotor rpm due to the additional centrifugal force of the heavy advanced-geometry blades.

2. The aircraft was restricted to operation within the limitations of the systems installed. For example, the aircraft was equipped with the production CH-47C cyclic trim, which is programmed as a function of altitude and airspeed. The effect on loads of changes to the cyclic trim program was not evaluated, consistent with the interest of reducing program costs.

TABLE VII. SUMMARY OF STRESS AND MOTION SURVEY DURING FLIGHT TEST OF THE BORON ADVANCED-GEOMETRY BLADE

Nominal GW (lb)	CG	Rotor Speed (rpm)	Actual GW (lb)	Actual Density Altitude (ft)	Outside Air Temp (°C)	Flight	Run	Critical Load, Aft Rotor	Maximum True Airspeed Attained (kn)	Load-Limited True Airspeed (kn)[1]	V_{ne}, Glass AGB (kn)	ΔV_{ne}, Boron vs Glass (kn)[2]	Boron Blade: Max Tip Mach No.	Boron Blade: Max Equivalent Airspeed (kn)	Limit True Airspeed at Nominal GW and Altitude (kn)[3]
33,000	7 in. aft	235	34,100	4,100	-2	328	5, 13 through 18	fixed link	159	164	179	-15	0.930	150	165
		245	33,200	5,100	-3	328	24, 26 through 29	fixed link	153	164	180	-15	0.951	142	164
40,000	5 in. aft	235	40,100	5,300	-4	340	73 through 49	fixed link	147	154	149	5	0.915	136	155
			40,400	6,300	-3	340	65 through 71	fixed link	151	156	145	11	0.919	137	158
		245	40,800	7,100	-4	340	56 through 64	fixed link	144	143	165	-22	0.939	129	147
			41,100	11,200	-8	340	47 through 54	fixed link	136	140	139	1	0.933	115	152
46,000	4 in. aft	235	46,200	2,900	+4	330	4, 17 through 21	pitch link	147	142	128	14	0.901	141	143
			46,900	4,300	+2	330	8 through 12	pitch link	138	133	121	12	0.891	127	137
			46,100	6,000	-4	332	2, 27 through 34	fixed link	142	145	114	31	0.907	130	146
			45,000	6,700	-7	332	45 through 55	pitch link	139	83	115	-32	0.907	126	74
			43,800	9,000	-11	332	67 through 71, 73	pitch link	121	71	95	-24	0.886	106	51
		245	45,400	2,300	+4	330	29 through 33	pitch link	151	161	153	8	0.936	146	158
			46,500	3,200	+20	336	6 through 19	pitch link	135	158	145	13	0.886	129	160
			46,500	4,400	-6	339	15 through 23	fixed link	146	144	142	2	0.946	137	146
			46,500	6,300	-5	332	21 through 26, 35 through 39	fixed link	142	145	137	8	0.938	129	148
			44,500	7,500	-6	332	57 through 62	fixed link	142	141	144	-3	0.939	127	133
			44,300	9,000	-10	332	63 through 66, 72	pitch link	127	132	134	-2	0.923	111	114
50,000	0	235	48,100	1,700	-7	333	55 through 60	pitch link	139	145	123	22	0.907	136	136
			48,500	5,600	-6	333	48 through 52	pitch link	125	110	98	12	0.883	115	97
		245	51,100	2,200	-8	333	4, 7 through 13	fixed link	132	140	124	16	0.927	128	145
			51,200	2,300	+3	340	6 through 14	pitch link	136	153	123	30	0.915	131	159
			50,800	3,400	0	340	17 through 26	fixed link	146	141	122	19	0.935	139	145
			48,800	5,100	-6	333	41 through 46	pitch link	132	139	128	11	0.924	122	133
			49,700	5,800	-8	333	30 through 34	pitch link	112	115	119	-4	0.896	103	112

Notes:
1. Endurance limits: aft pitch link, ±2,500 lb; aft fixed link, ±2,500 lb; aft rotor shaft (23.1 inches below top of shaft), 280,000 in.-lb
2. Load-limited airspeed for boron AGB minus V_{ne} for glass AGB
3. V_{ne} for glass AGB at nominal gross weight and altitude plus ΔV_{ne}

LEGEND									
SYMBOL	COMPONENT	BLADE	FLIGHT	RUNS	GW (LB)	CG	ROTOR RPM	ALTITUDE (FT)	C_T/σ
●	RED PITCH LINK	BORON	332	27 THROUGH 34	46,100	5.7 IN. AFT	235	6,100	0.0936
▲	YELLOW PITCH LINK	BORON	332	27 THROUGH 34	46,100	5.7 IN. AFT	235	6,100	0.0936
○	RED PITCH LINK	GLASS	272	15 THROUGH 18	45,500	4 IN. AFT	235	5,970	0.0915
△	YELLOW PITCH LINK	GLASS	272	15 THROUGH 18	45,500	4 IN. AFT	235	5,970	0.0915
□	GREEN PITCH LINK	GLASS	272	15 THROUGH 18	45,500	4 IN. AFT	235	5,970	0.0915
◆	AFT ROTOR SHAFT	BORON	332	27 THROUGH 34	46,100	5.7 IN. AFT	235	6,100	0.0936
◇	AFT ROTOR SHAFT	GLASS	272	15 THROUGH 18	45,500	4 IN. AFT	235	5,970	0.0915

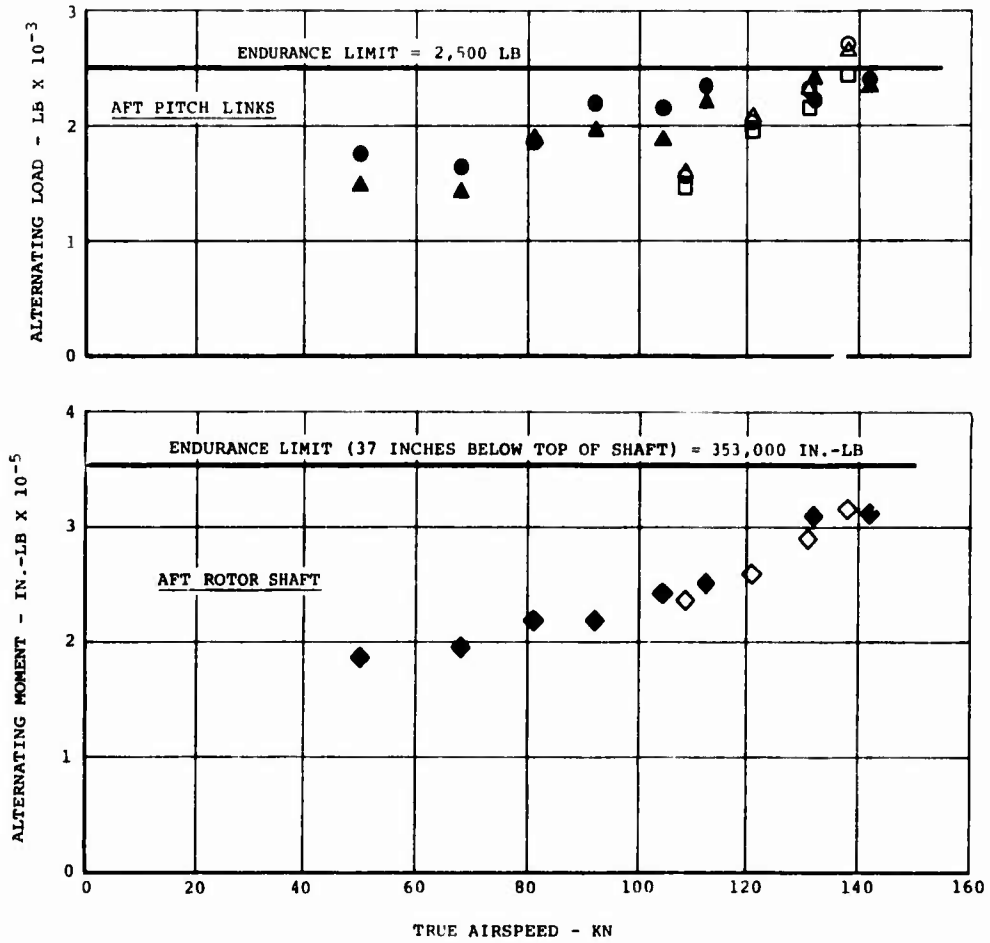

Figure 26. Comparative Aft Pitch Link and Rotor Shaft Loads at 46,000 Pounds Gross Weight and 235 Rotor RPM.

LEGEND									
SYMBOL	COMPONENT	BLADE	FLIGHT	RUNS	GW (LB)	CG	ROTOR RPM	ALTITUDE (FT)	C_T/σ
●	RED PITCH LINK	BORON	332	21 THROUGH 26, 35 THROUGH 39	46,200	5.5 IN. AFT	245	6,200	0.0853
▲	YELLOW PITCH LINK	BORON	332	21 THROUGH 26, 35 THROUGH 39	46,200	5.5 IN. AFT	245	6,200	0.0853
○	RED PITCH LINK	GLASS	272	1 THROUGH 12	46,190	4 IN. AFT	245	6,090	0.0845
△	YELLOW PITCH LINK	GLASS	272	1 THROUGH 12	46,190	4 IN. AFT	245	6,090	0.0845
□	GREEN PITCH LINK	GLASS	272	1 THROUGH 12	46,190	4 IN. AFT	245	6,090	0.0845
◆	AFT ROTOR SHAFT	BORON	332	21 THROUGH 26, 35 THROUGH 39	46,200	5.5 IN. AFT	245	6,200	0.0853
◇	AFT ROTOR SHAFT	GLASS	272	1 THROUGH 12	46,190	4 IN. AFT	245	6,090	0.0845

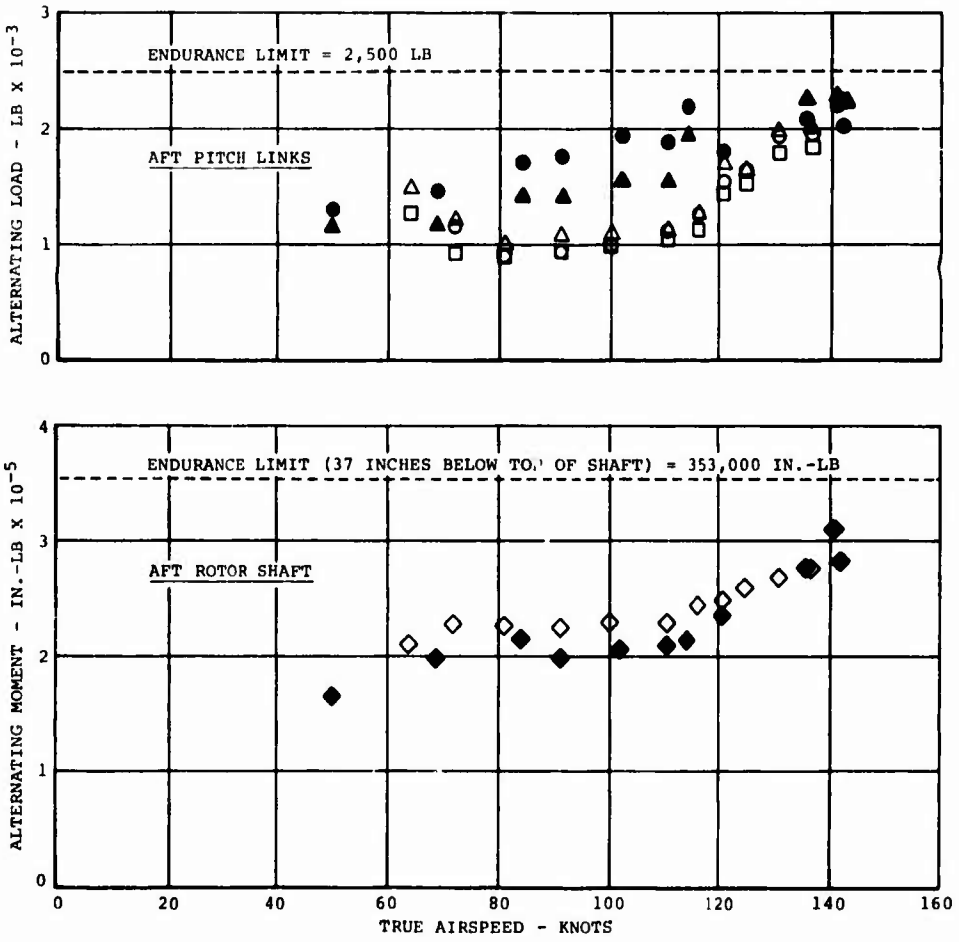

Figure 27. Comparative Aft Pitch Link and Rotor Shaft Loads at 46,000 Pounds Gross Weight and 245 Rotor RPM.

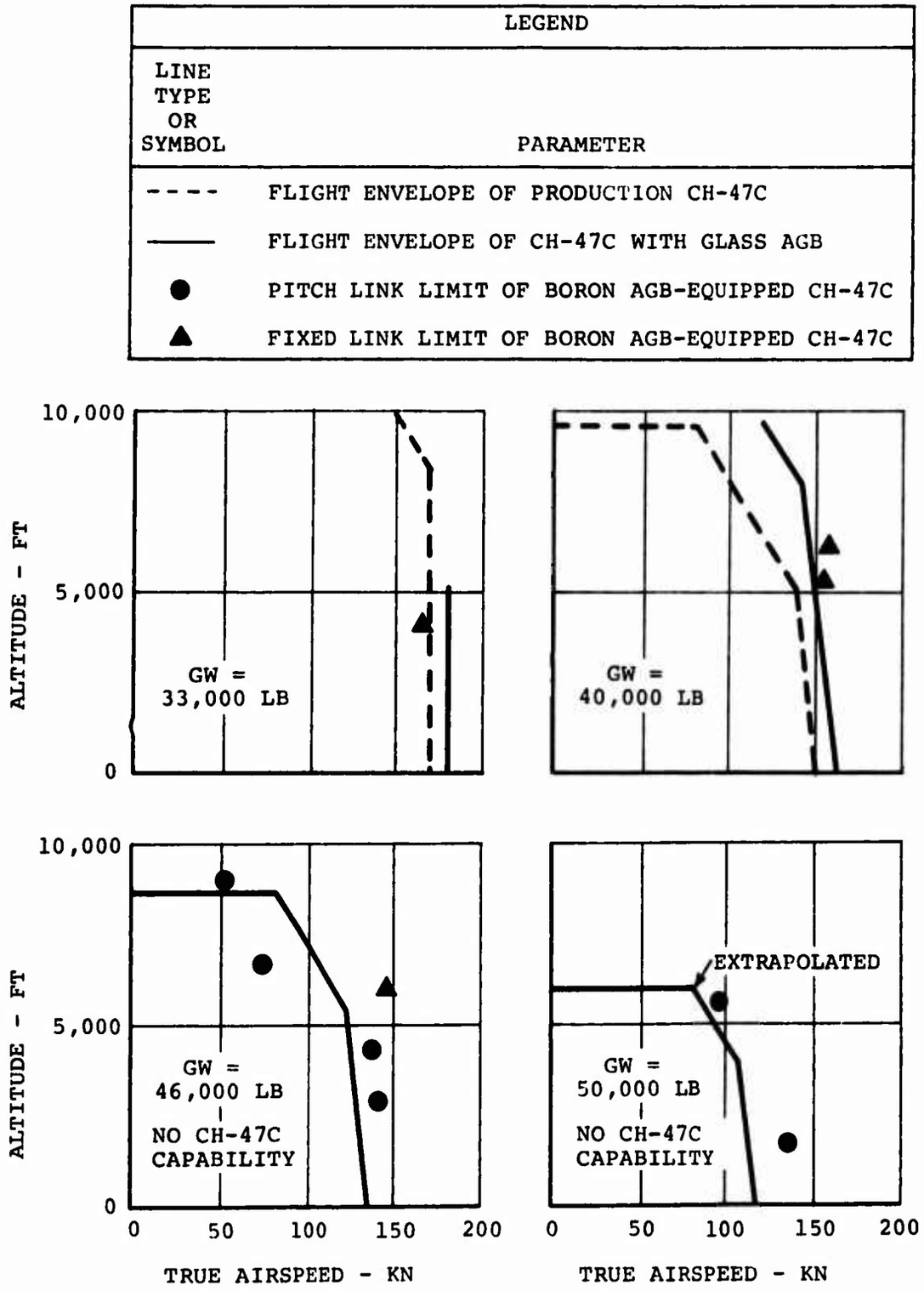

Figure 28. Evaluation of Flight Envelope of CH-47C Helicopter Equipped With Boron Advanced-Geometry Blades at 235 Rotor RPM.

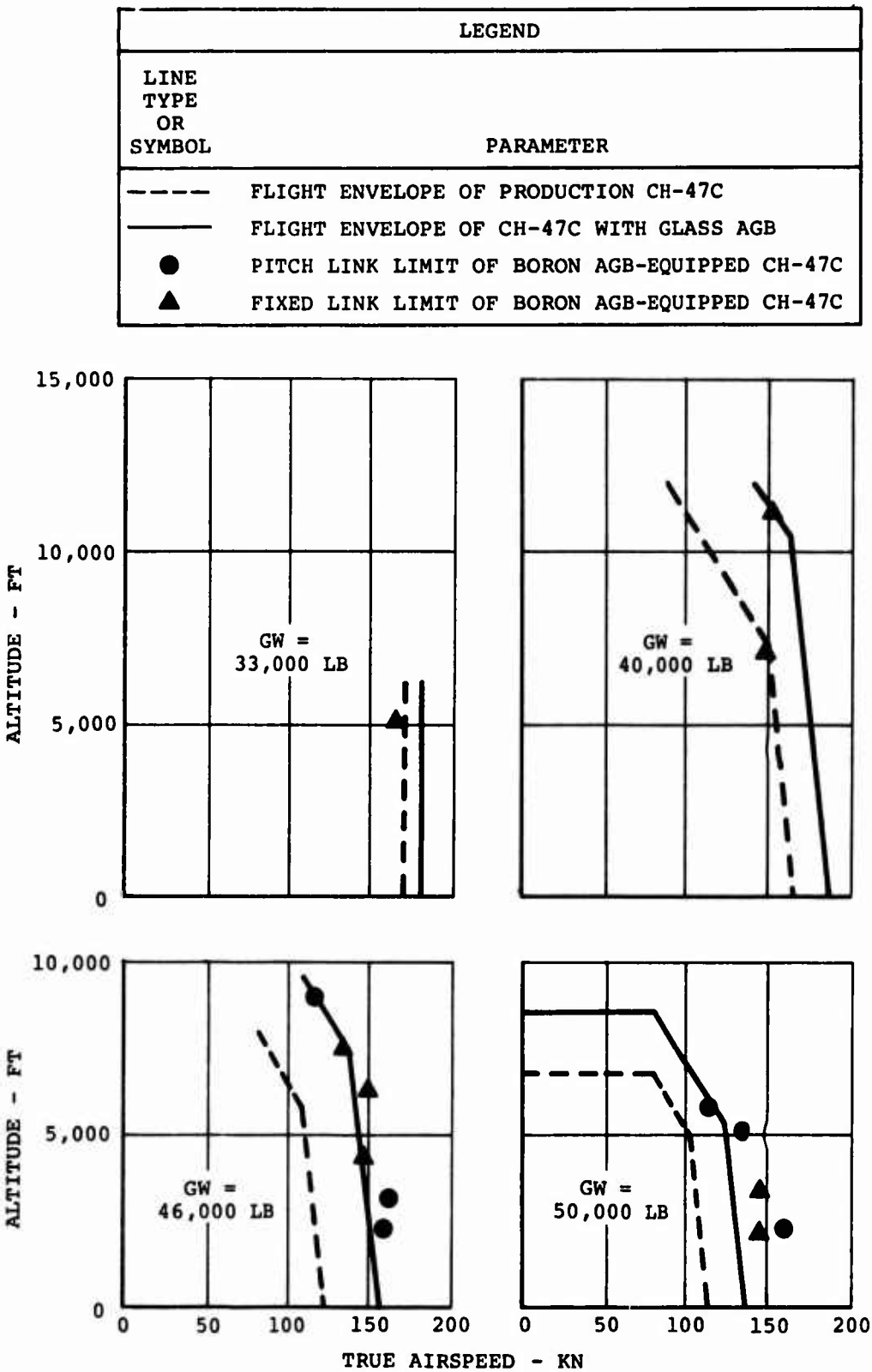

Figure 29. Evaluation of Flight Envelope of CH-47C Helicopter Equipped With Boron Advanced-Geometry Blades at 245 Rotor RPM.

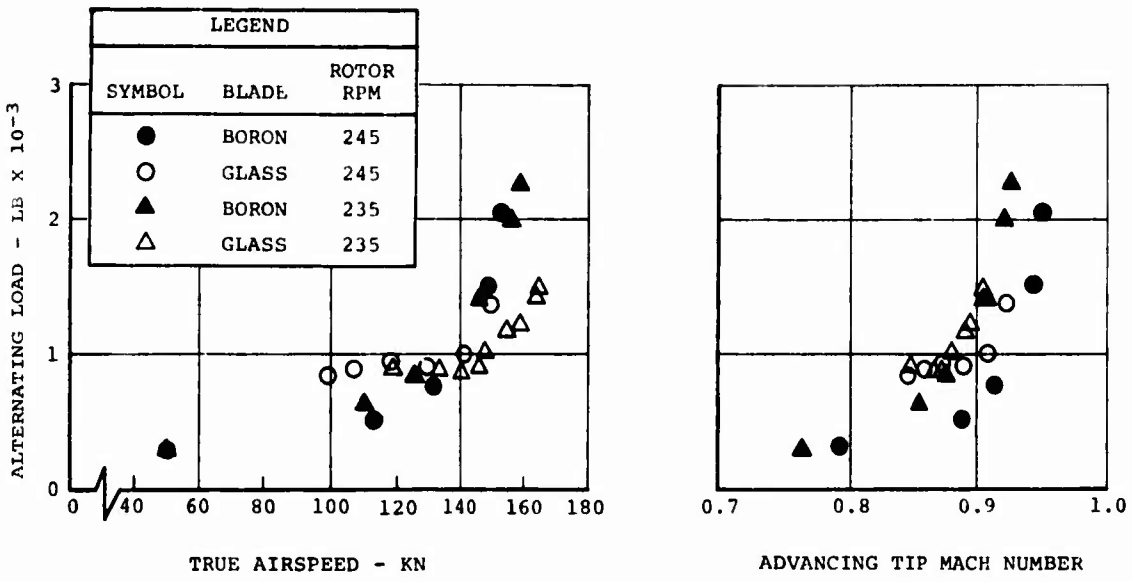

Figure 30. Comparison of Aft Fixed Link Loads for Boron and Glass Advanced-Geometry Blades at 33,000 Pounds Gross Weight.

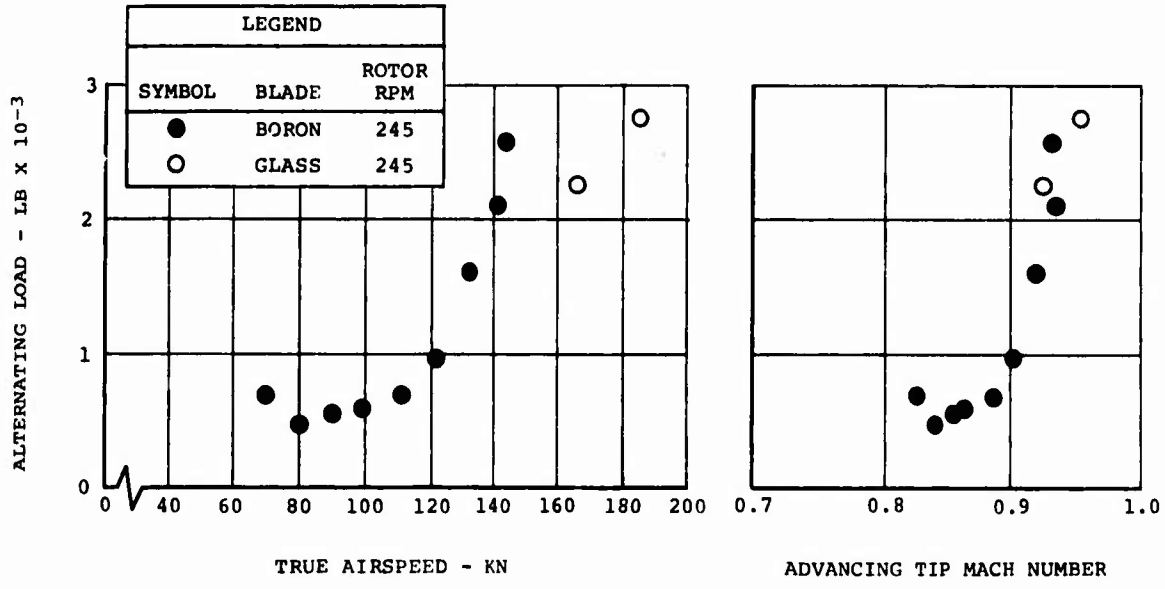

Figure 31. Comparison of Aft Fixed Link Loads for Boron and Glass Advanced-Geometry Blades at 40,000 Pounds Gross Weight.

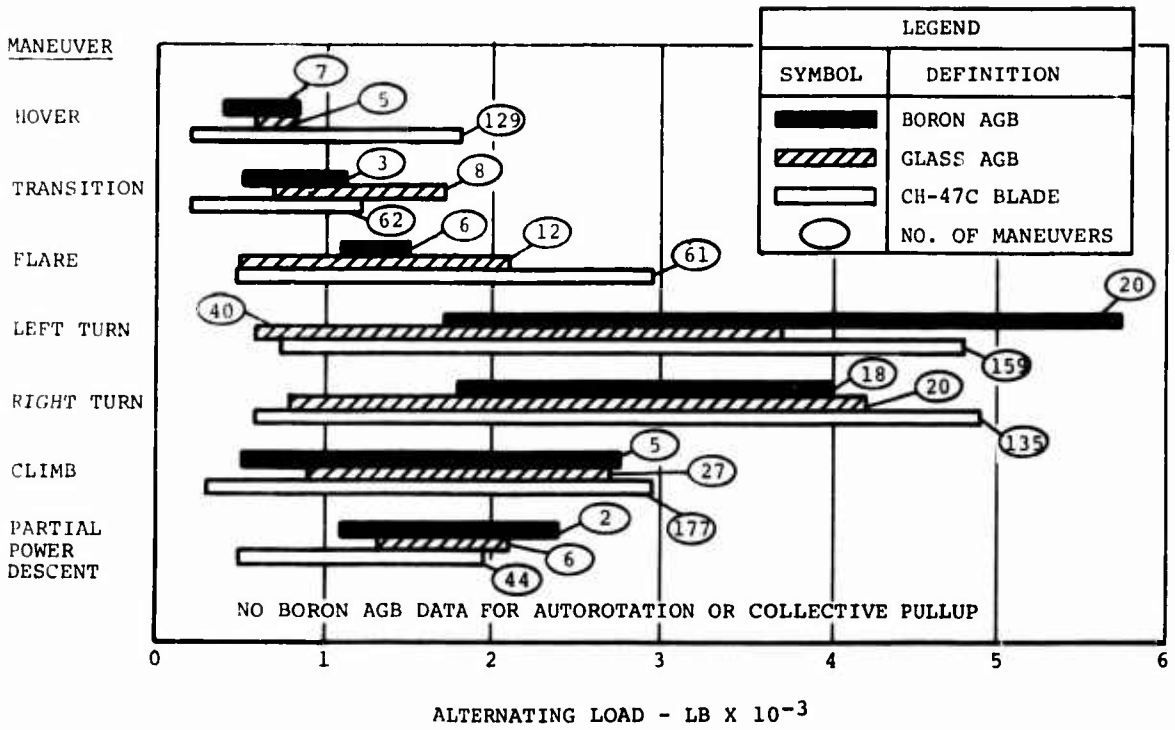

Figure 32. Comparison of Boron and Glass Advanced-Geometry Blades Through Maneuver Loads at Aft Pitch Links.

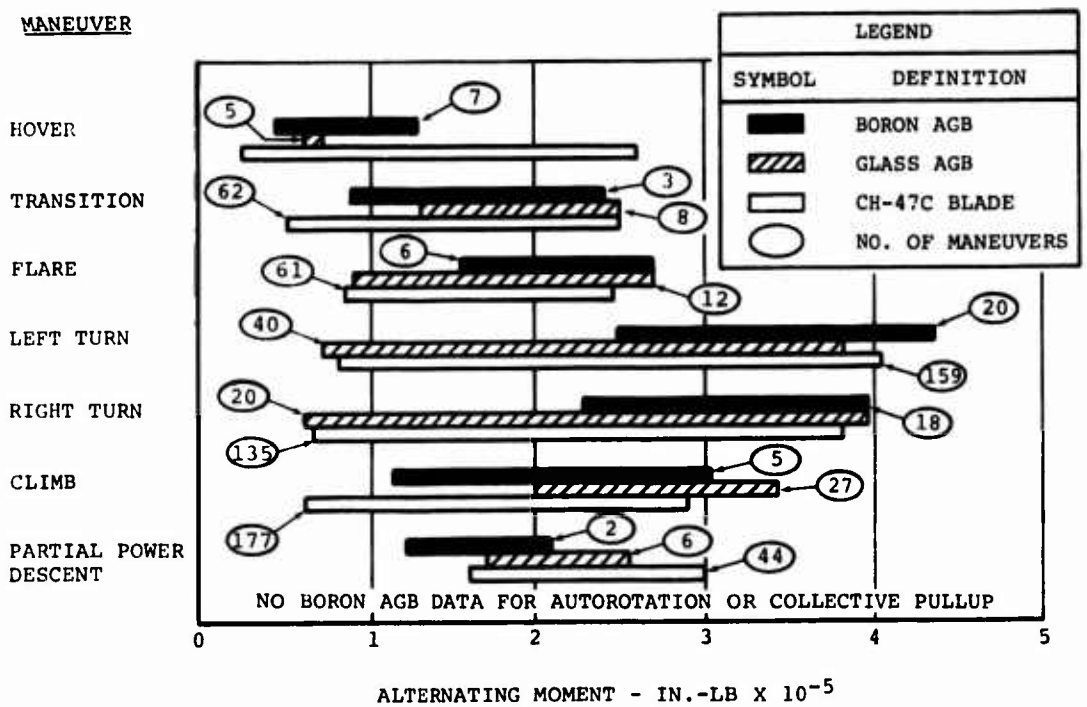

Figure 33. Comparison of Boron and Glass Advanced-Geometry Blades Through Maneuver Loads on Aft Rotor Shaft.

BLADE LOADS

This section contains the following information:

- Comparisons of spanwise distribution of bending moments between the measured boron blade moments and an envelope of the predicted level-flight moment distributions
- Scattergrams of alternating blade moments with airspeed for selected blade parameters
- Component lives established for the socket, spar, and trailing-edge skin for the advanced-geometry blade mission profile
- Measured flight strains and loads compared to material and component allowables

Spanwise Moment Distributions

The spanwise steady and alternating moment distributions are shown in Figures 34 through 44. Flight test data measured throughout the test program for various flight conditions are presented in data bands at the appropriate spanwise location. The flight data are divided into loads for level-flight conditions and maneuvers; a further subdivision is made according to gross weight (33,000, 46,000, and 50,000 pounds). Only aft blade data are presented inasmuch as boron blades were installed on the aft rotor only.

Method of Predicting Blade Loads

The predicted level-flight moment distributions for the aft blade were calculated with Boeing-Vertol computer program L-02 and consist of an envelope of loads determined by airspeeds from 140 knots to V_{max}. The flight conditions for these calculations were:

GW (lb)	Rotor RPM	Altitude	CG
33,000	245	sea level	7 in. aft
46,000	245	sea level	4 in. aft
50,000	245	sea level	0

The trim schedule is shown in Figure 45. The level-flight predictions were used to correlate with both level-flight and maneuver-flight data.

Comparison of Test and Predicted Steady Flapwise Moment Distribution in Level Flight

The level-flight steady flapwise moment distributions exhibit the same trends seen on the fiberglass blade. On the inboard portions of the blade, the measured moments exceed the predicted loads; they generally run lower than predicted on the outboard portions of the blade.

Comparison of Test and Predicted Alternating Flapwise Moment Distribution in Level Flight

Initial predictions for the envelope of level-flight moments were carried out for the same design cyclic trim used on the fiberglass advanced-geometry blade which displayed good correlation with flight data. However, on the boron blade, it was found that better correlation occurred when the actual trims applied during the flight testing were used to predict flap bending loads. Each figure displays the resultant predicted blade bending moment envelope using both approaches to the cyclic trim schedule. There is generally good agreement between measured and predicted moments, although the top-of-scatter data on the outboard gages generally run higher than predicted.

Comparison of Test and Predicted Steady Chordwise Moment Distribution in Level Flight

Figures 37 through 39 display the steady and alternating level-flight chordwise bending moment distributions for predicted and flight test data. The correlation of flight data with predicted steady chord loads remains poor (the fiberglass blade correlation was poor) with no information currently at hand to explain the discrepancies. Reference 5 presents a thorough discussion of the mechanics of predicting steady chord moments and the technique required to obtain flight loads, all of which also apply to the boron blade.

Comparison of Test and Predicted Alternating Chordwise Moment Distribution in Level Flight

The correlation of flight data with predicted data is reasonable, although generally the predictions were conservatively higher than the actual measured data. A comparison of the boron data with fiberglass blade test data (Reference 5, Figure 212) indicates that the top-of-scatter loadings are essentially the same. Unfortunately, the chord bending bridge on the instrumented boron blade was lost before testing was completed, and chord bending data are lacking for the later phases of testing. All data recorded have been included in the correlation study.

Maneuver Loads

The flapwise and chordwise maneuver loads, steady and alternating, are shown in Figures 40 through 44. The maneuver loads were generally higher than the level-flight data, as would be expected, but there were no loads higher than those recorded for the fiberglass blade; they were, in fact, generally lower. Flight loads are compared to the appropriate level-flight predicted moments shown for reference.

Scattergrams of Blade Parameters

Figures 46 through 62 display the scattergrams of measured data for the three critical areas of the boron advanced-geometry blade: the blade socket, the blade spar at station 252, and the blade trailing-edge skin at station 198. The alternating moments for these parameters were top-of-scatter loads for each of the flight conditions noted in each figure. To analyze the blade socket, a ratio of the loads monitored by the bending bridge at blade station 49.5 to station 29.5 (vertical pin) is calculated from the predicted moment distribution of Figure 34,

$$\text{or} \quad M_{Test}(\text{sta } 29.5) = \frac{M_{Pred}(\text{sta } 29.5)}{M_{Pred}(\text{sta } 49.5)} \times M_{Test}(\text{sta } 49.5) \ .$$

Unlike the fiberglass blade data which did not increase significantly at high speeds, the boron blade flap bending loads demonstrate a significant load growth rate (approximately V^2) with airspeed. An examination of the waveforms indicates a strong 3/rev content as might be expected with the first flap natural frequency in proximity to 3/rev. The calculated blade natural frequencies are shown in Figures 63 through 65. This may also account for the significant increase in loads with speed. There was also evidence of a 7/rev loading at transition speeds in the flap bending data, particularly at station 49.5. At higher speeds the 7/rev disappeared from the outboard gages but remained at the station 49.5 gage, indicating a possibility of interaction with chord bending at this station. It is interesting to note that the calculated second flap mode natural frequency is almost on 7/rev in the operating rpm range.

Chordwise moment distributions were conventional in nature and somewhat lower than predicted. In fact, the magnitude of the chord moments was generally about the same as that of the fiberglass blade loads of Reference 5. Examination of the waveforms, however, indicates a predominant 7/rev harmonic content, thereby verifying the predicted natural frequencies

shown in Figure 64. (Note: Static test data predicted a natural frequency near 5/rev.) Unfortunately, the only chord moment gage was not functioning during flight 332 and thereafter, thus accounting for the limited flight data. The subsequent section entitled Blade Life discusses a substitute procedure to enable trailing-edge life calculations to be made.

Comparison of CH-47C Metal and Fiberglass and Boron Advanced-Geometry Blade Loads at Equivalent C_T/σ

In Reference 5, blade loads of the CH-47C metal and the fiberglass advanced-geometry blades were compared for the three critical blade areas at similar flight conditions and equivalent C_T/σ. Such a comparison was not made for the boron blade since there is no significance to blade load differences existing between blades of greatly differing section properties. The more important comparison is between measured data and theoretical predictions as illustrated in Figures 34 through 39.

Blade Life

The fatigue life of the boron advanced-geometry blade was calculated in the same manner as for the glass blade; i.e., Miner's Hypothesis was used. The mission profile (Table VIII) and the flight envelope (Figure 66) for the glass blade were used for the boron blade. A more complete discussion is given on pages 251 through 258 of Reference 5.

The loads used for the life calculations are the maximum moments experienced during flight testing for each gross weight, center of gravity, airspeed, and altitude split. Examination of waveforms indicates that a 1/rev loading condition predominates despite the fact that both 3/rev and 7/rev harmonic contents are substantial.

The trailing-edge tension strain gage at station 198 became erratic after flight 332, thereby creating a shortage of chordwise loads data for the life calculation with no level-flight data at 40,000 pounds gross weight and no maneuver data at 50,000 pounds gross weight. It was necessary to combine data for gross weight, center of gravity, and altitude and to assume that the top-of-scatter loads applied to all gross weights. This was reasonable since the fiberglass blade data of Reference 5 indicate little variation with gross weight.

The strain gage at station 288 (flap bending) also failed for flights subsequent to flight 328, with no data available for 46,000 and 50,000 pounds gross weight. As a result of previous calculations using predicted moments, station 252 was found to be almost as critical as station 288 (within 5 percent); therefore,the spar life calculations were carried out for station 252.

TABLE VIII. GLASS AGB MISSION PROFILE

Gross Weight: 33,000 & 40,000 Lb Percent Time: 70		Gross Weight: 46,000 Lb Percent Time: 25		Gross Weight: 50,000 Lb Percent Time: 5	
Flight Condition	Occurrence	Flight Condition	Occurrence	Flight Condition	Occurrence
Level Flight		Level Flight		Level Flight	
Hover	10 percent	Hover	10 percent	Hover	10 percent
Transition	15 percent	Transition	15 percent	Transition	15 percent
60% V_{NE}	25 percent	70% V_{NE}	25 percent	70% V_{NE}	25 percent
90% V_{NE}	20 percent	90% V_{NE}	20 percent	90% V_{NE}	20 percent
100% V_{NE}	20 percent	100% V_{NE}	20 percent	100% V_{NE}	20 percent
110% V_{NE} or V_{MIL} power	10 percent	110% V_{NE} or V_{MIL} power	10 percent	110% V_{NE} or V_{MIL} power	10 percent
Maneuvers		Maneuvers		Maneuvers	
Landing Flare	4 per hour	Same as 33,000 lb schedule		Same as 33,000 lb schedule	
Maneuver	26 per hour				
RPM Split		RPM Split		RPM Split	
Nominal 235-245rpm	100 percent	Nominal 235-245 rpm	100 percent	Nominal 245 rpm	100 percent
CG Split		CG Split		CG Split	
Aft CG	100 percent	Fwd CG	12.5 percent	Aft CG	100 percent
		Aft CG	87.5 percent		
Altitude Split		Altitude Split		Altitude Split	
6,000 ft and below	50 percent	Fwd CG:		6,000 ft and below	100 percent
6,000 ft and above	50 percent	6,000 ft and below	50 percent		
		6,000 ft and above	50 percent		
		Aft CG:			
		6,000 ft and below	50 percent		
		6,000 ft to 10,000 ft	50 percent		
		10,000 ft and above	10 percent		

In general, loads data were not available out to and beyond the structural envelope as required by the flight profile. To obtain these data, top-of-scatter loads were projected as a function of V^2 consistent with the load trends occurring at the high-speed end of the flight test data.

The fatigue strength of the socket was determined by structural testing of root-end blade sections. The socket fatigue strength at 10^7 cycles at station 29.5 is ±42,000 inch-pounds, as shown in Figure 67. The socket allowable is based on the lowest of 70 percent of mean or 80 percent of bottom of scatter.

Figures 68 through 71 present, in the form of S-N curves and Goodman curves, the allowable alternating strains for the spar and skin materials established from coupon testing.

The fatigue damage summaries for the three critical blade areas are shown in Tables IX through XI. The total fatigue damage, maximum loads, and percentage of damage per hour for the various flight conditions are presented in each table. The blade socket has a limited life, 885 hours for an endurance limit of ±42,000 inch-pounds; the trailing-edge skin at station 198 has a life limited to 855 hours. No damage was incurred on the blade spar at station 252. Consideration should be given to modifications for increased socket and trailing-edge strength or expanded testing of existing structure if and when any extended service flying is envisioned.

Comparison of Design Allowables and Flight Loads

Figure 67 compares maximum measured level-flight and maneuver flap bending moments to the fatigue allowable curve for the blade socket based on the structural testing of two glass blade sockets and two boron blade sockets. For reference purposes, the predicted flap bending moments are also shown. As mentioned previously, the flight data recorded at station 49.5 was ratioed to station 29.5 by use of the theoretical flap bending moment spanwise distribution. The comparison indicates that the flight test data were somewhat higher than predicted; this appears to have been caused by the first mode natural frequency being very close to 3/rev. The flight conditions for the level flight moment of ±44,000 inch-pounds were: flight 340, 51,011 pounds gross weight, neutral center of gravity, 250 rotor rpm, 2,500 feet density altitude, and 147 knots true airspeed. The maximum maneuver load of ±58,900 inch-pounds occurred during a landing flare on flight 336 at 44,800 pounds gross weight, 4 inches aft center of gravity, 234 rotor rpm, 1,000 feet density altitude, and 60 knots true airspeed.

TABLE IX. FATIGUE DAMAGE SUMMARY OF THE BORON BLADE SPAR AT STATION 252

Gross Weight (lb) / Percent Time at GW	33,000 to 44,000 / 70		46,000 / 25		50,000 / 5		Totals / 100	
	Max Load (in.-lb)	Percent Damage	Max Load (in.-lb)	Percent Damage	Max Load (in.-lb)	Percent Damage	Max Load (in.-lb)	Percent Damage
Flight Condition								
Level Flight								
Within Envelope	91,000	0	86,500	0	77,000	0	91,000	0
Beyond Envelope	110,000	0	89,000	0	93,000	0	110,000	0
Maneuvers								
Landing Flare	83,320	0	83,320	0	99,230	0	99,230	0
Other	80,740	0	100,000	0	82,160	0	100,000	0
Total		0		0		0		0

Total Damage = 0
Life of Blade = More than 10,000 hours

TABLE X . FATIGUE DAMAGE SUMMARY OF THE BORON BLADE SOCKET

Gross Weight (lb) / Percent Time at GW	33,000 to 44,000 / 70		46,000 / 25		50,000 / 5		Totals / 100	
	Max Load (in.-lb)	Percent Damage	Max Load (in.-lb)	Percent Damage	Max Load (in.-lb)	Percent Damage	Max Load (in.-lb)	Percent Damage
Flight Condition								
Level Flight								
Within Envelope	37,600	0	36,400	0	36,500	0	37,600	0
Beyond Envelope	38,800	0	41,700	0	43,500	3.3	43,500	3.3
Maneuvers								
Landing Flare	59,000	55.0	59,000	19.6	54,600	2.6	59,000	77.2
Other	42,400	0	66,400	18.2	44,200	1.3	66,400	19.5
Total		55.0		37.8		7.2		100.0

Endurance Limit = 42,000 in.-lb at 10^7 cycles
Total Damage = $1{,}131 \times 10^{-6}$ cycles/hr
Life of Socket = 885 hours

TABLE XI. FATIGUE DAMAGE SUMMARY OF THE BORON BLADE TRAILING-EDGE SKIN AT STATION 198

Cross Weight (lb) / Percent Time at GW	33,000 to 44,000 / 70		46,000 / 25		50,000 / 5		Totals / 100	
	Max Load (in.-lb)	Percent Damage	Max Load (in.-lb)	Percent Damage	Max Load (in.-lb)	Percent Damage	Max Load (in.-lb)	Percent Damage
Flight Condition								
Level Flight								
Within Envelope	60,000	0	42,000	0	32,000	0	60,000	0
Beyond Envelope	74,000	0	50,000	0	38,000	0	74,000	0
Maneuvers								
Landing Flare	106,500	12.5	106,500	4.6	106,500	1	106,500	18.1
Other	107,100	57.5	107,100	20.4	107,100	4	107,100	81.9
Total		70.0		25.0		5		100.0

Total Damage = $1{,}173 \times 10^{-6}$ cycles/hr
Life of Trailing-Edge Skin = 855 hours

Figure 72 illustrates the comparison of measured spar strain allowables at station 252 with the mean minus $3\sigma/1.75$ design allowable of laboratory coupon test data as corrected for Goodman effect to represent the effect of steady stress. The comparison shows that both level-flight and maneuver data never exceed the design allowable. The maximum measured level-flight flapwise bending moment of 98,540 inch-pounds at station 252 occurred during flight 336 at 45,740 pounds gross weight, 4 inches aft center of gravity, 230 rotor rpm, 3,800 feet density altitude, and 48 knots true airspeed. The maximum measured maneuver load of 99,230 inch-pounds occurred during a landing flare on flight 333, 47,800 pounds gross weight, 3.2 inches aft center of gravity, 245 rotor rpm, sea level altitude, and 58 knots true airspeed.

Figure 73 compares the measured flight strains at the trailing edge at station 198 with the mean minus $3\sigma/1.75$ design allowable based on sandwich coupon data and corrected for the applied steady stress. The comparison shows that no fatigue damage occurs during level flight but that the maneuver data are above the design allowable. This accounts for the calculated fatigue life of 855 hours at this blade location. The maximum measured level-flight chord bending moment of 74,520 inch-pounds at station 198 occurred during flight 333 at 51,289 pounds gross weight, 0.5 inch aft center of gravity, 245 rotor rpm, 1,700 feet density altitude, and 51 knots true airspeed. The maximum measured maneuver load of 107,100 inch-pounds occurred during a 35-degree banked left turn on flight 332 at 45,690 pounds gross weight, 6 inches aft center of gravity, 235 rotor rpm, 6,000 feet density altitude, and 129 knots true airspeed.

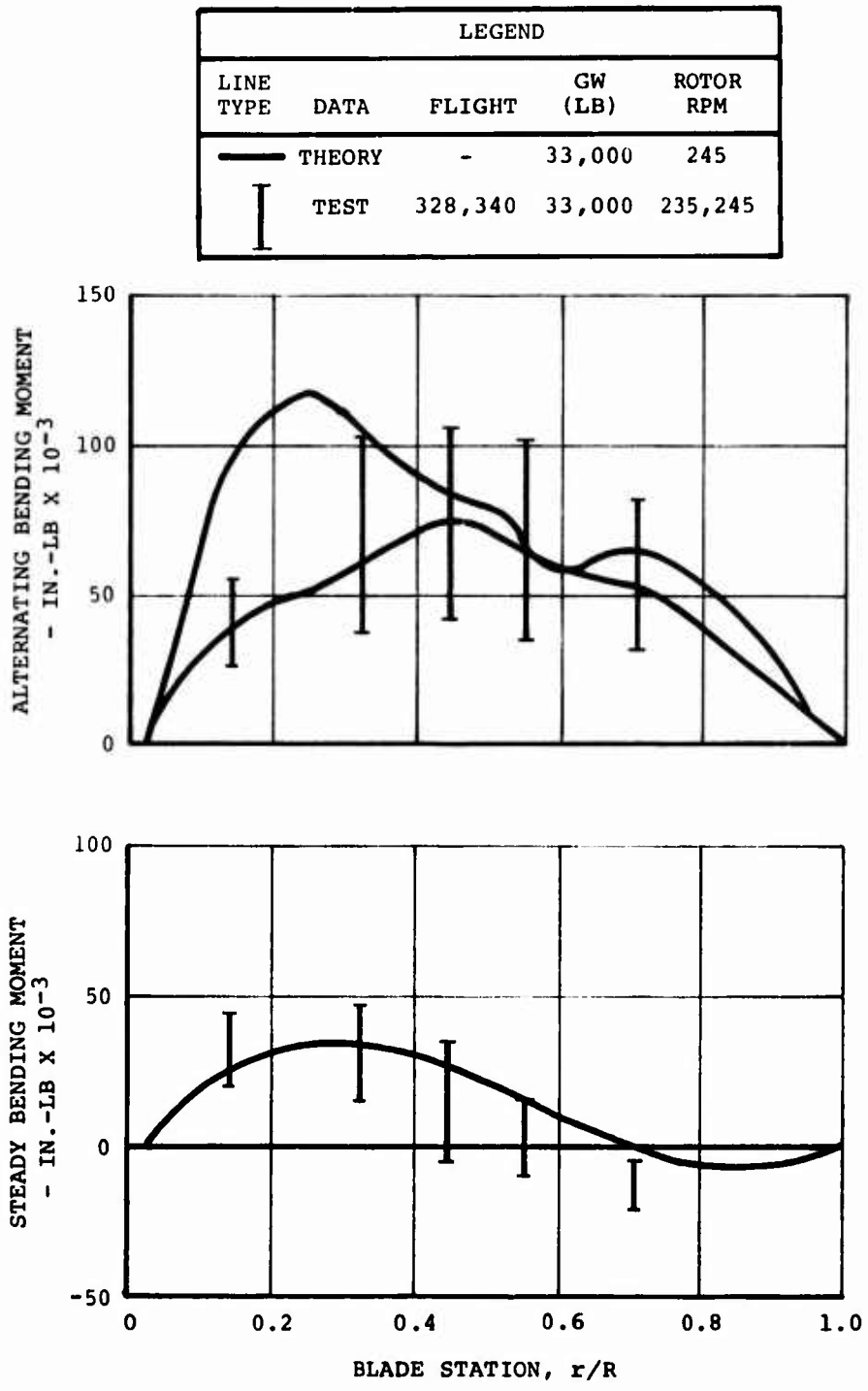

Figure 34. Comparison of Predicted and Flight Test Flapwise Bending Moments in Level Flight.

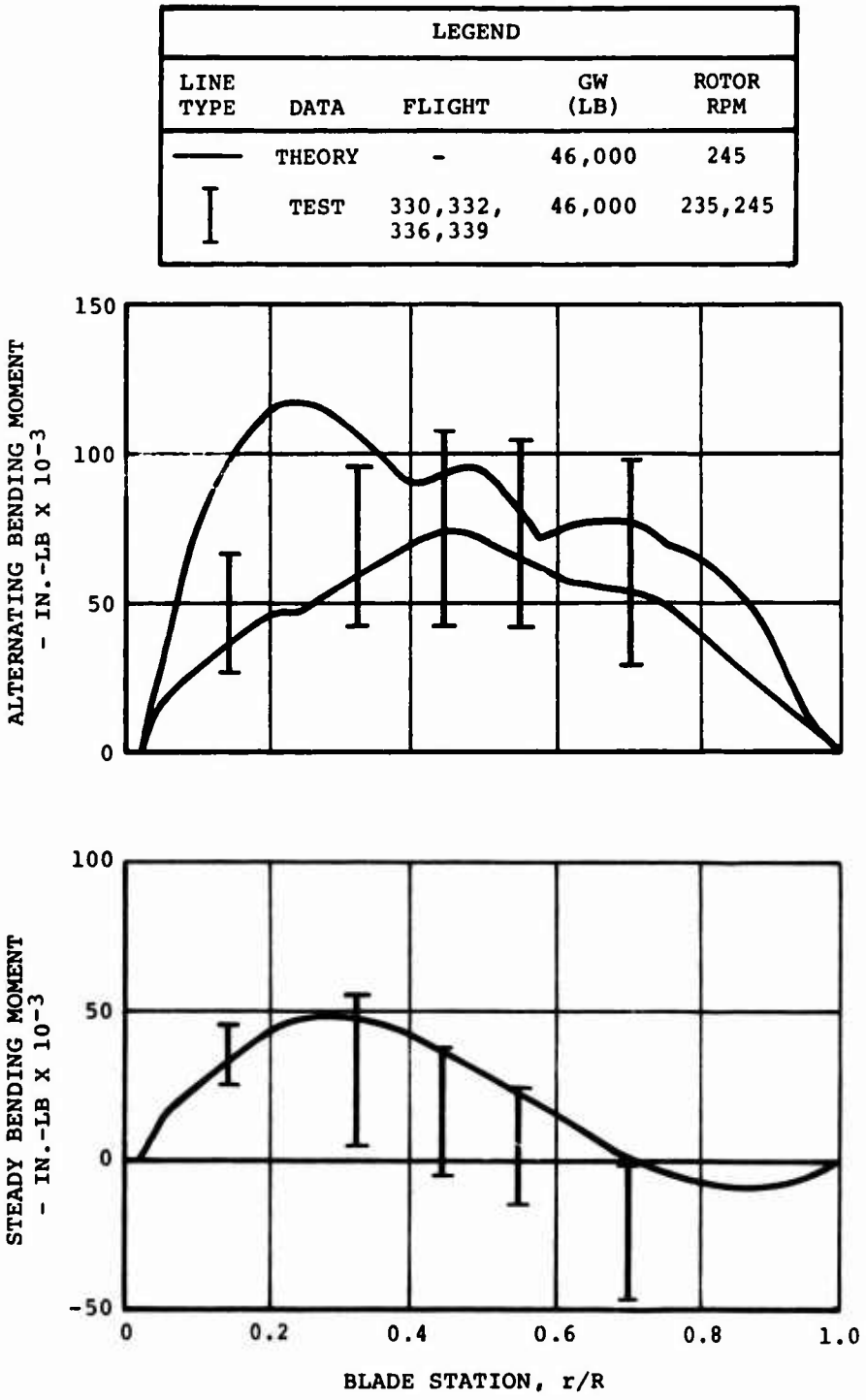

Figure 35. Comparison of Predicted and Flight Test Flapwise Bending Moments in Level Flight.

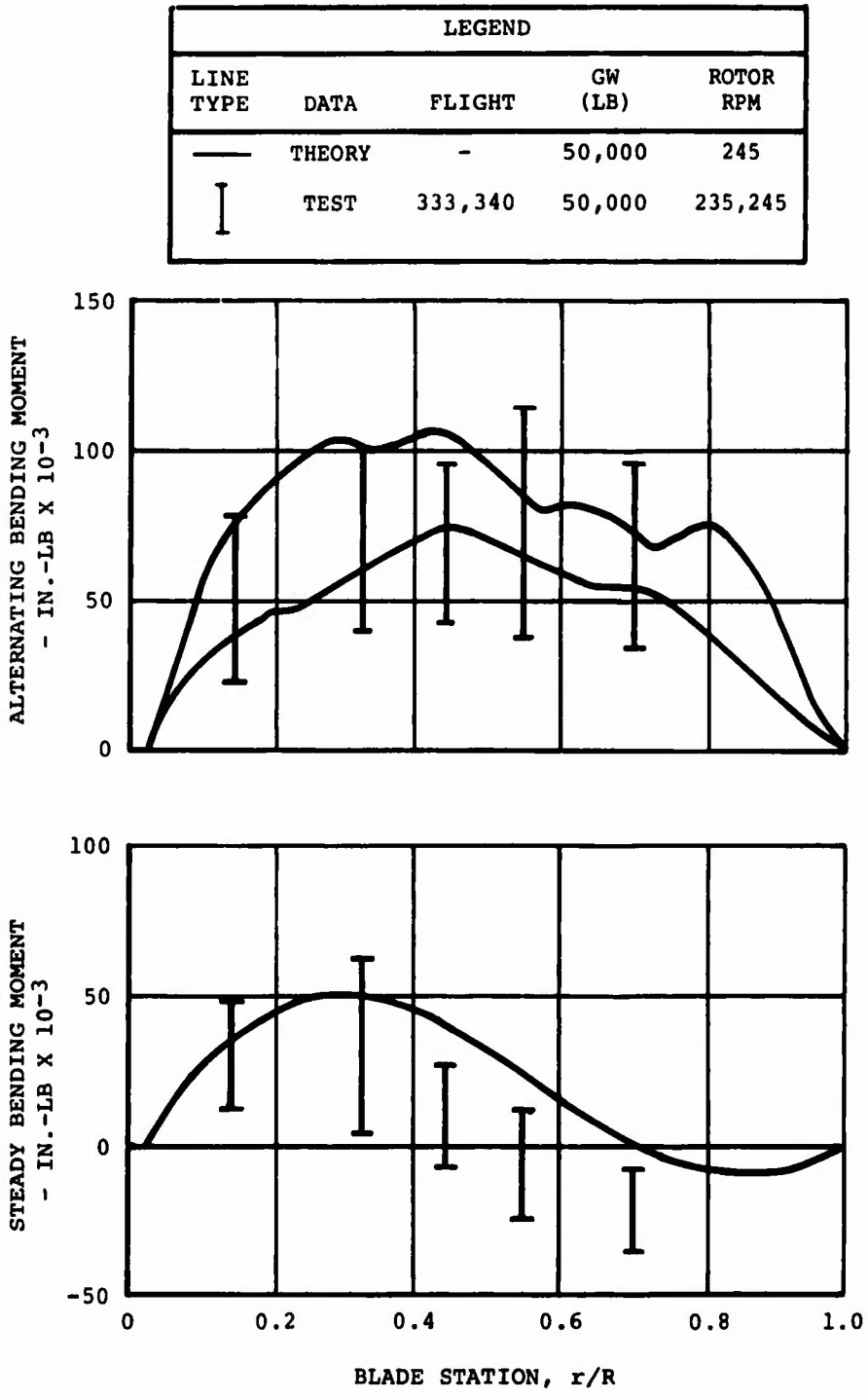

Figure 36. Comparison of Predicted and Flight Test Flapwise Bending Moments in Level Flight.

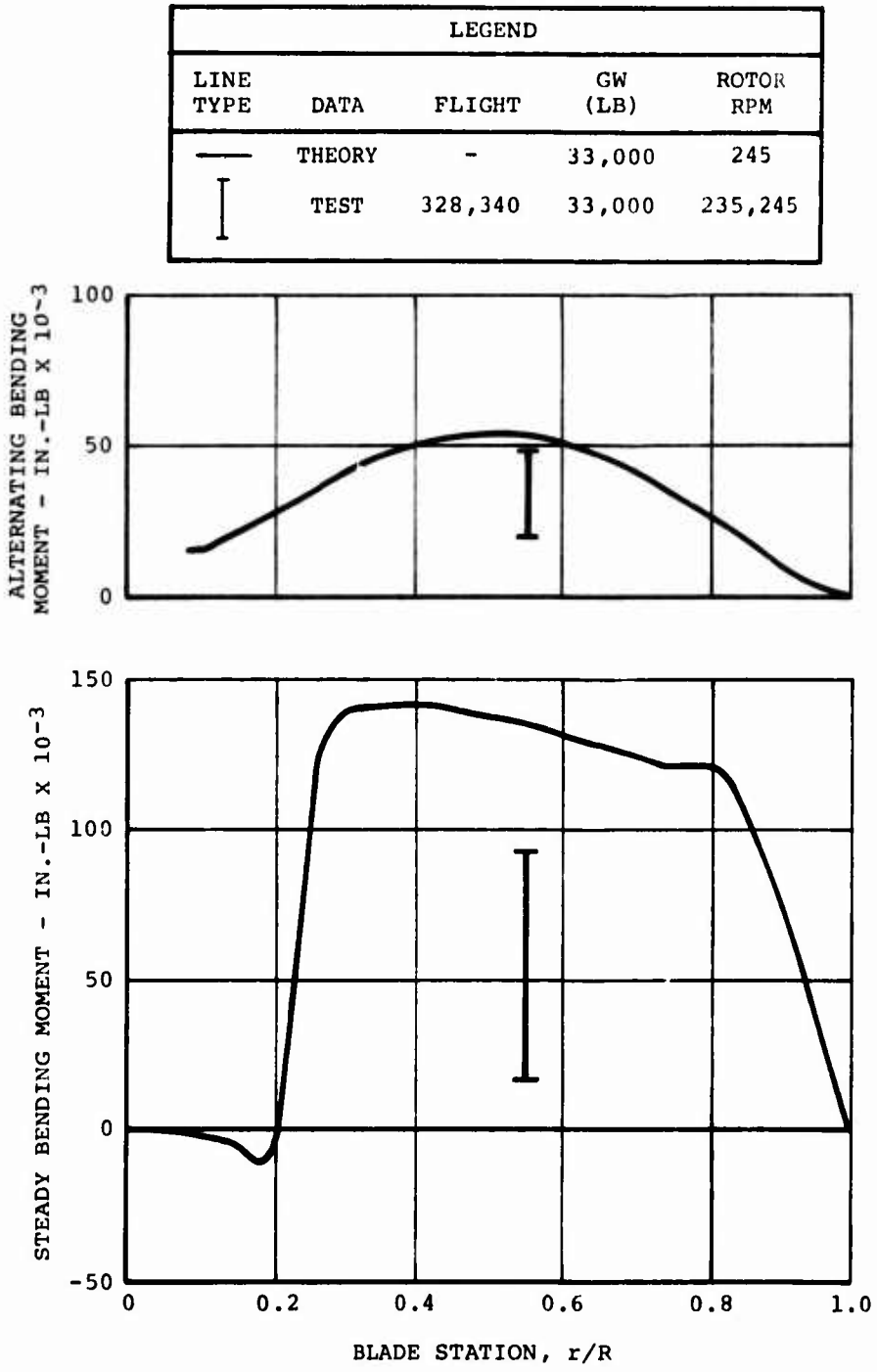

Figure 37. Comparison of Predicted and Flight Test Chordwise Bending Moments in Level Flight.

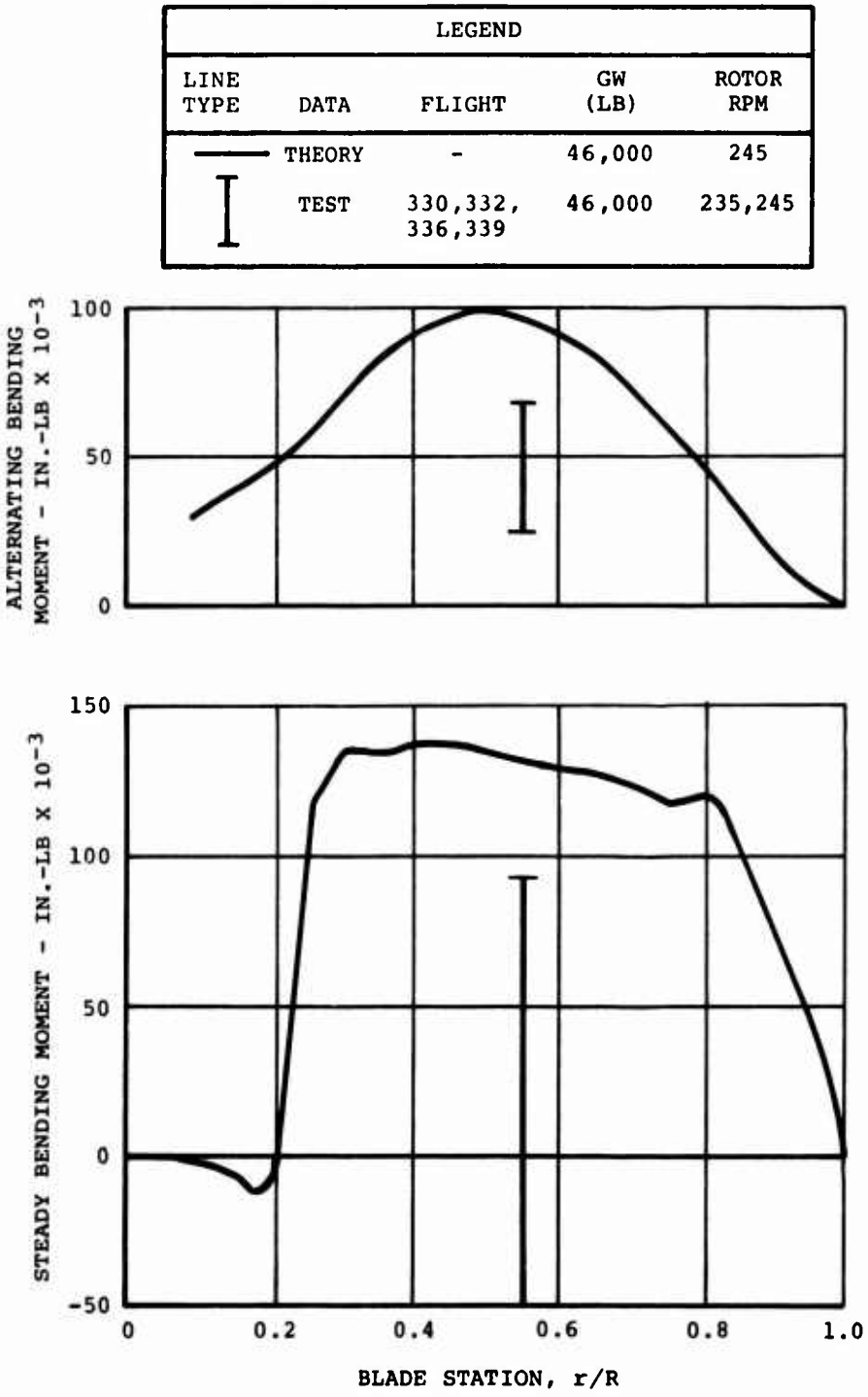

Figure 38. Comparison of Predicted and Flight Test Chordwise Bending Moments in Level Flight.

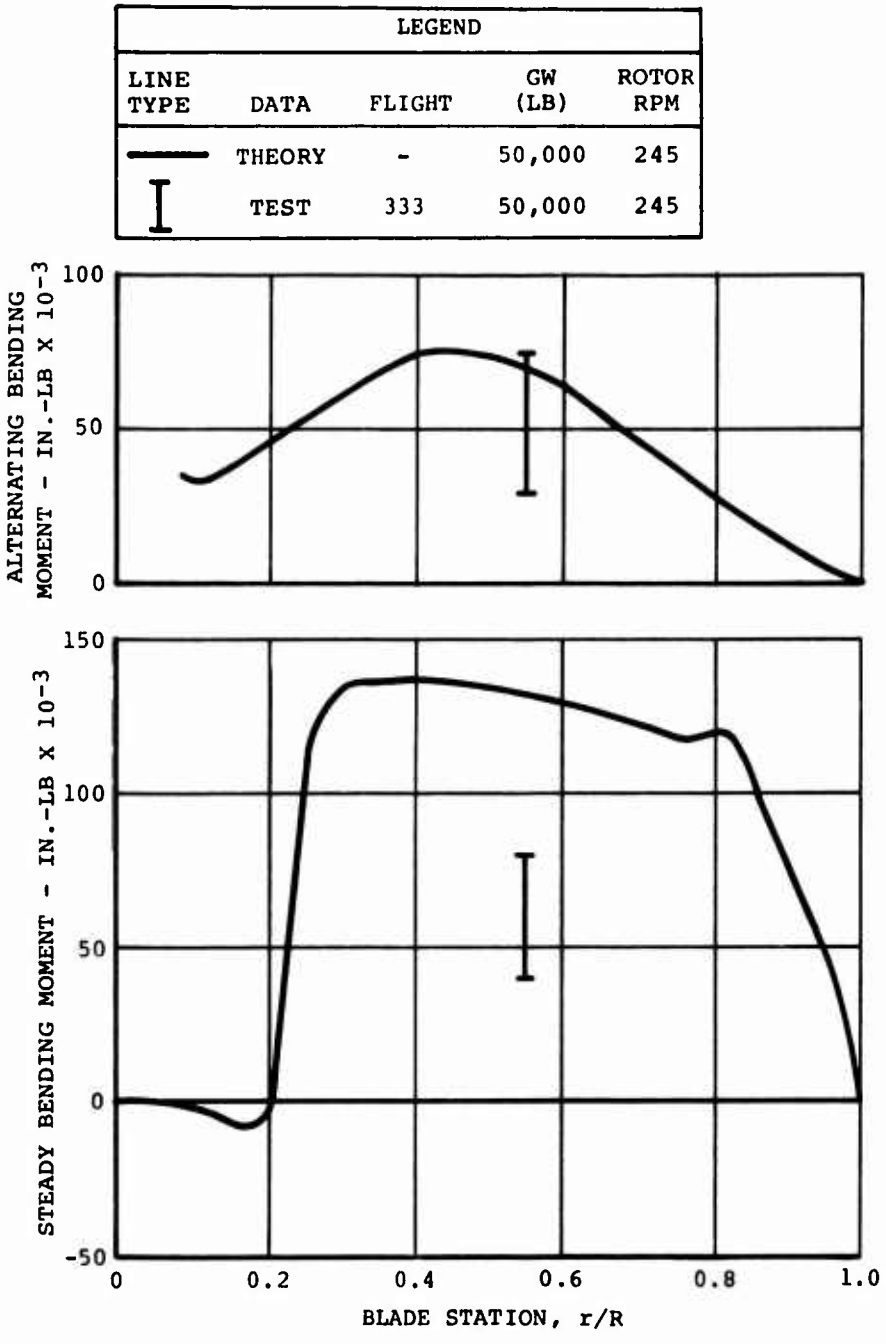

Figure 39. Comparison of Predicted and Flight Test Chordwise Bending Moments in Level Flight.

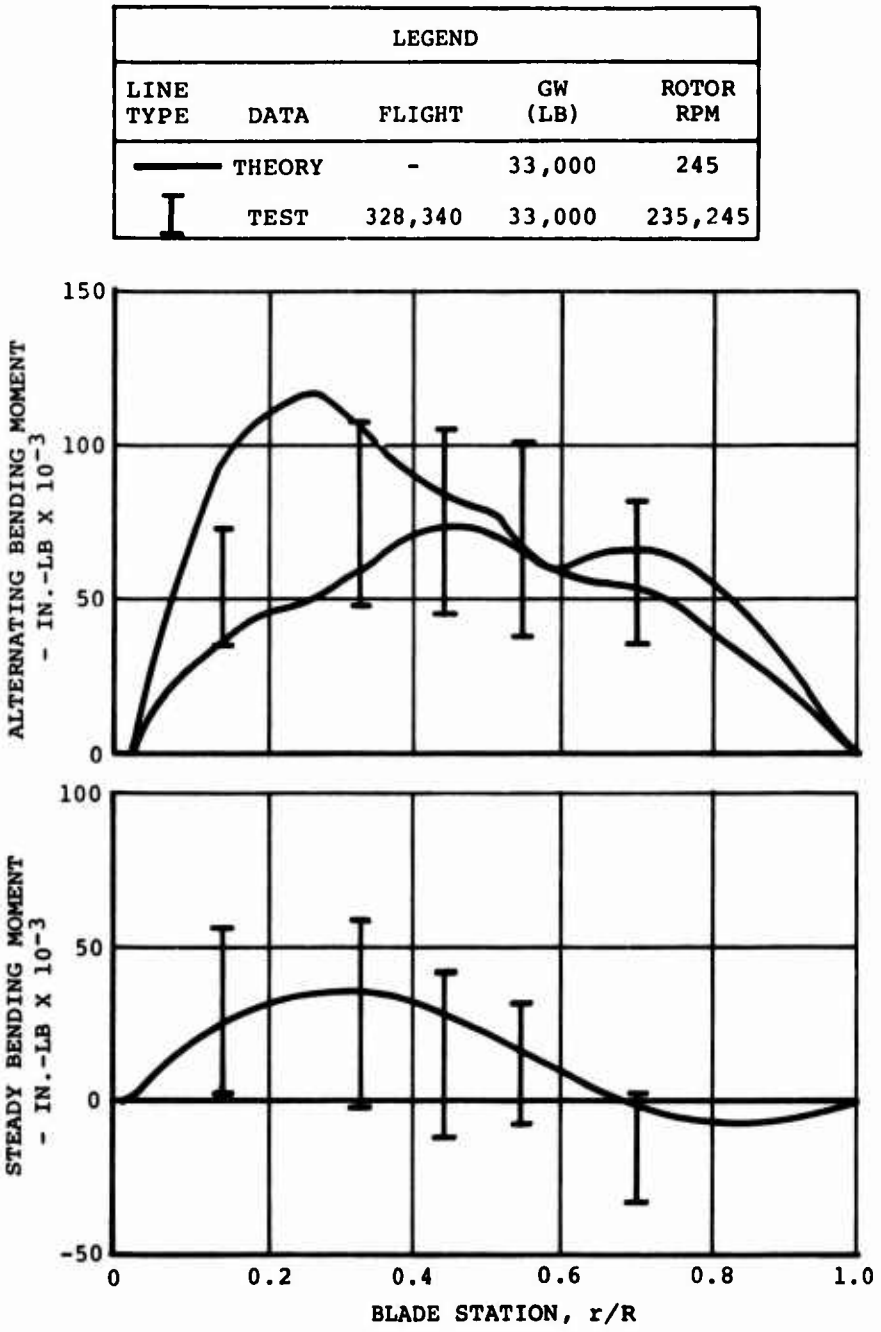

Figure 40. Comparison of Predicted and Flight Test Flapwise Bending Moments in Maneuvering Flight.

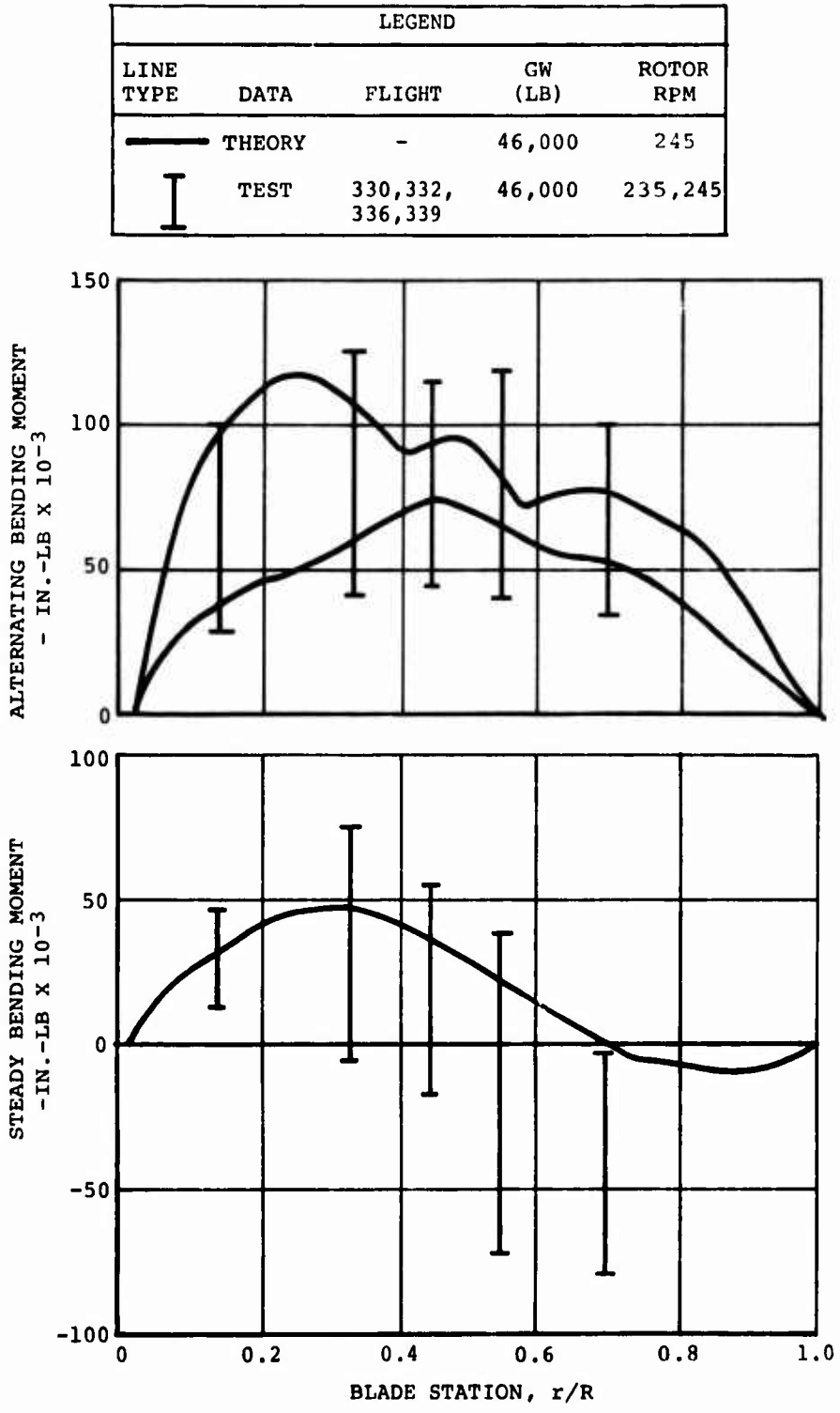

Figure 41. Comparison of Predicted and Flight Test Flapwise Bending Moments in Maneuvering Flight.

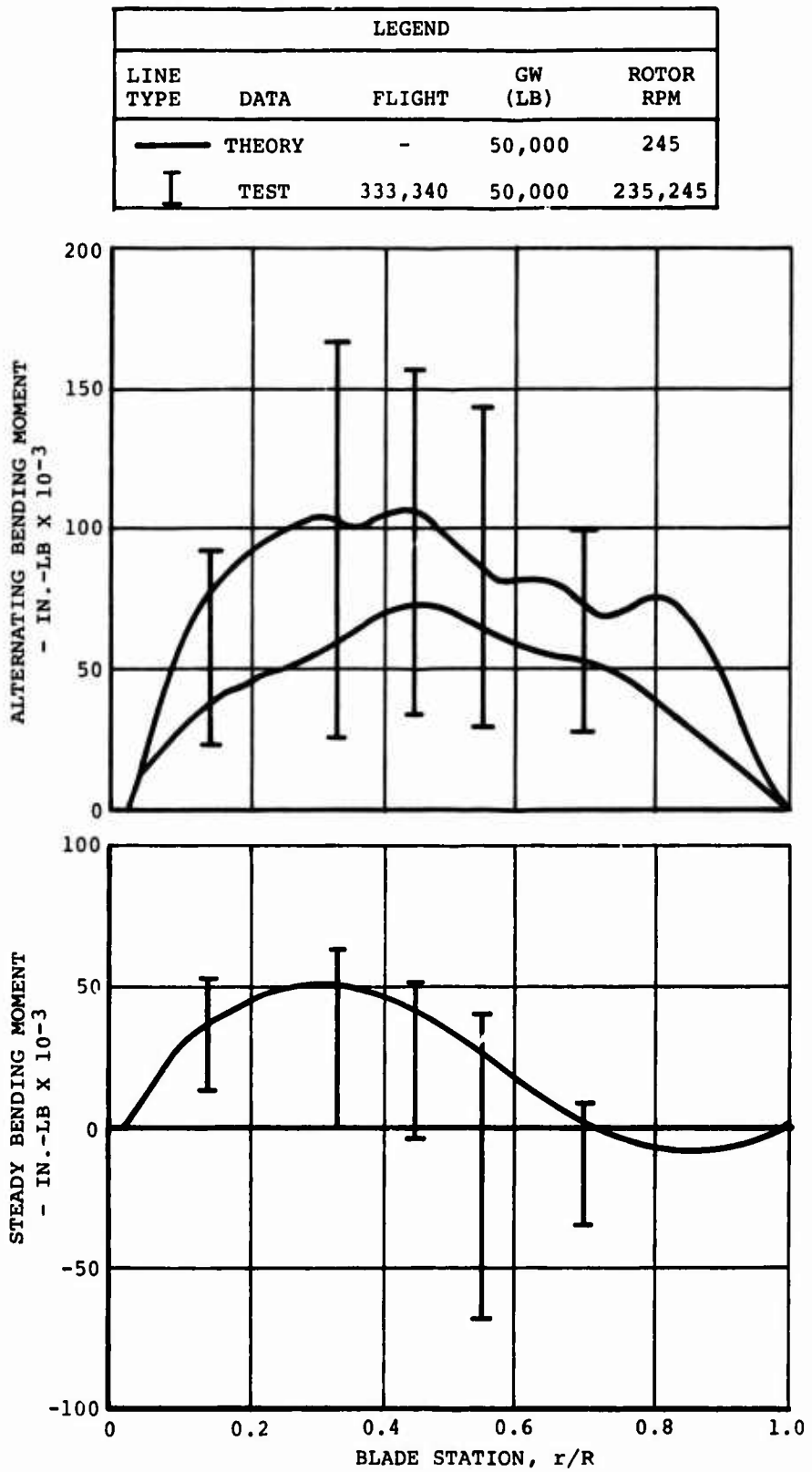

Figure 42. Comparison of Predicted and Flight Test Flapwise Bending Moments in Maneuvering Flight.

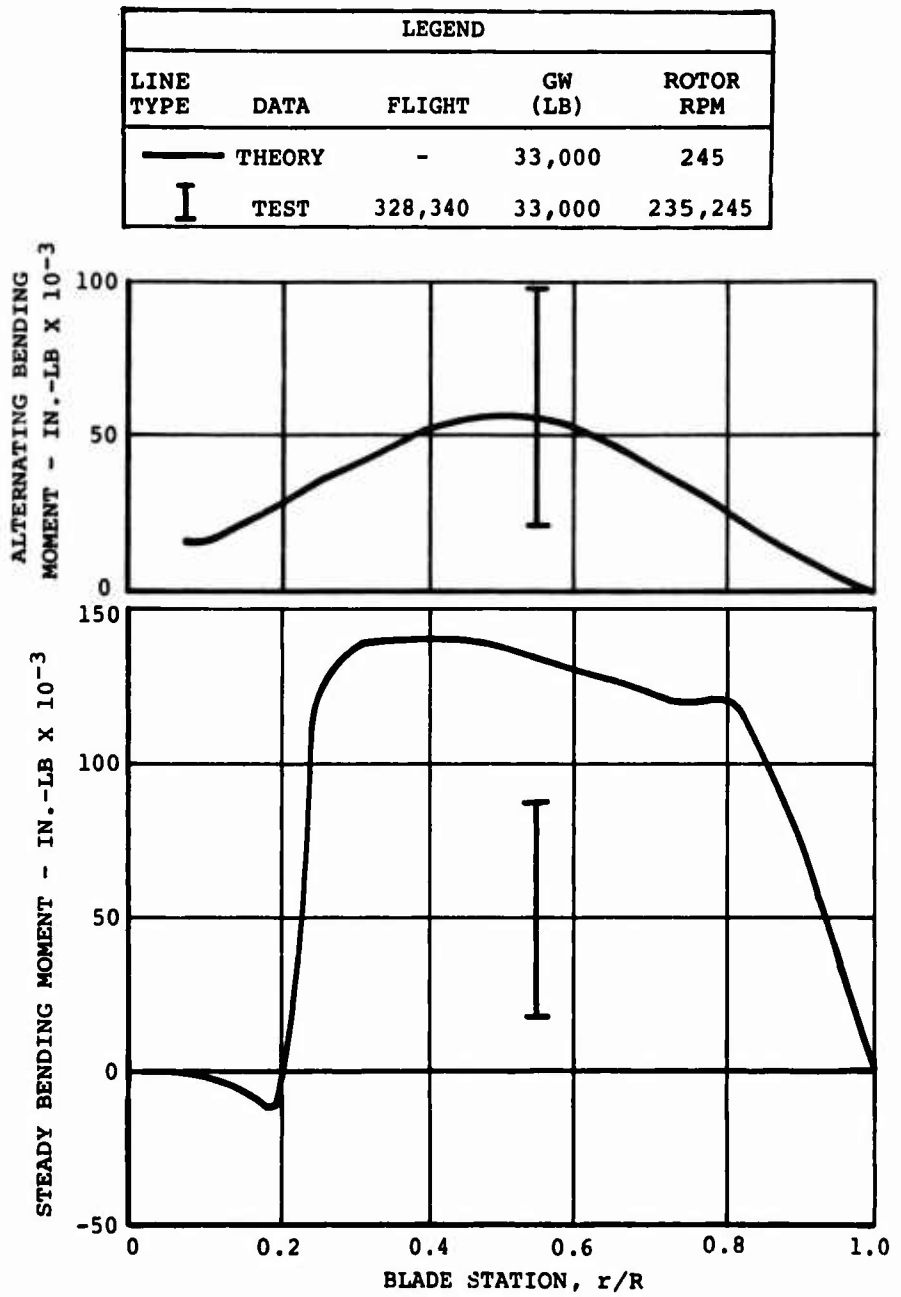

Figure 43. Comparison of Predicted and Flight Test Chordwise Bending Moments in Maneuvering Flight.

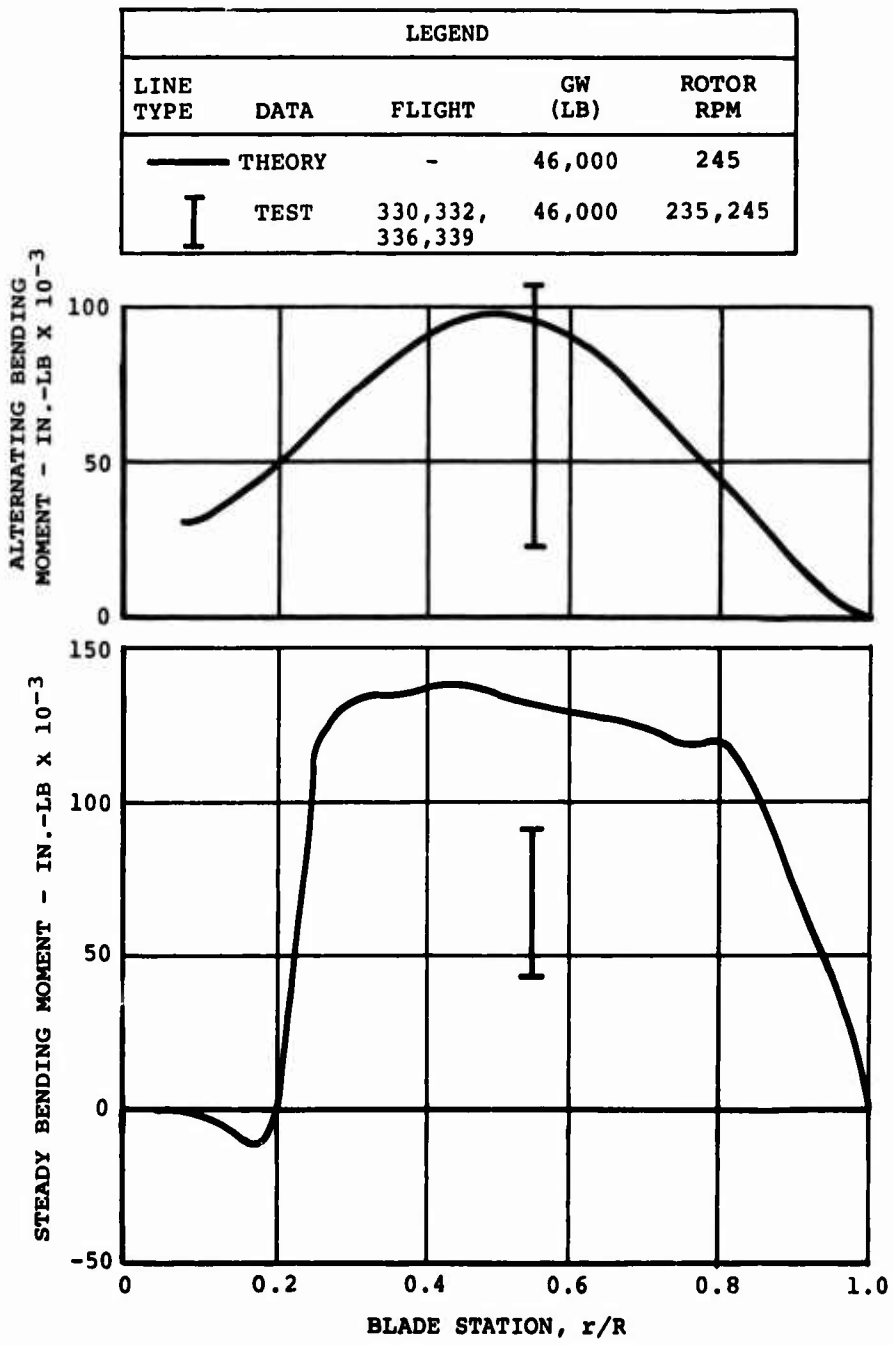

Figure 44. Comparison of Predicted and Flight Test Chordwise Bending Moments in Maneuvering Flight.

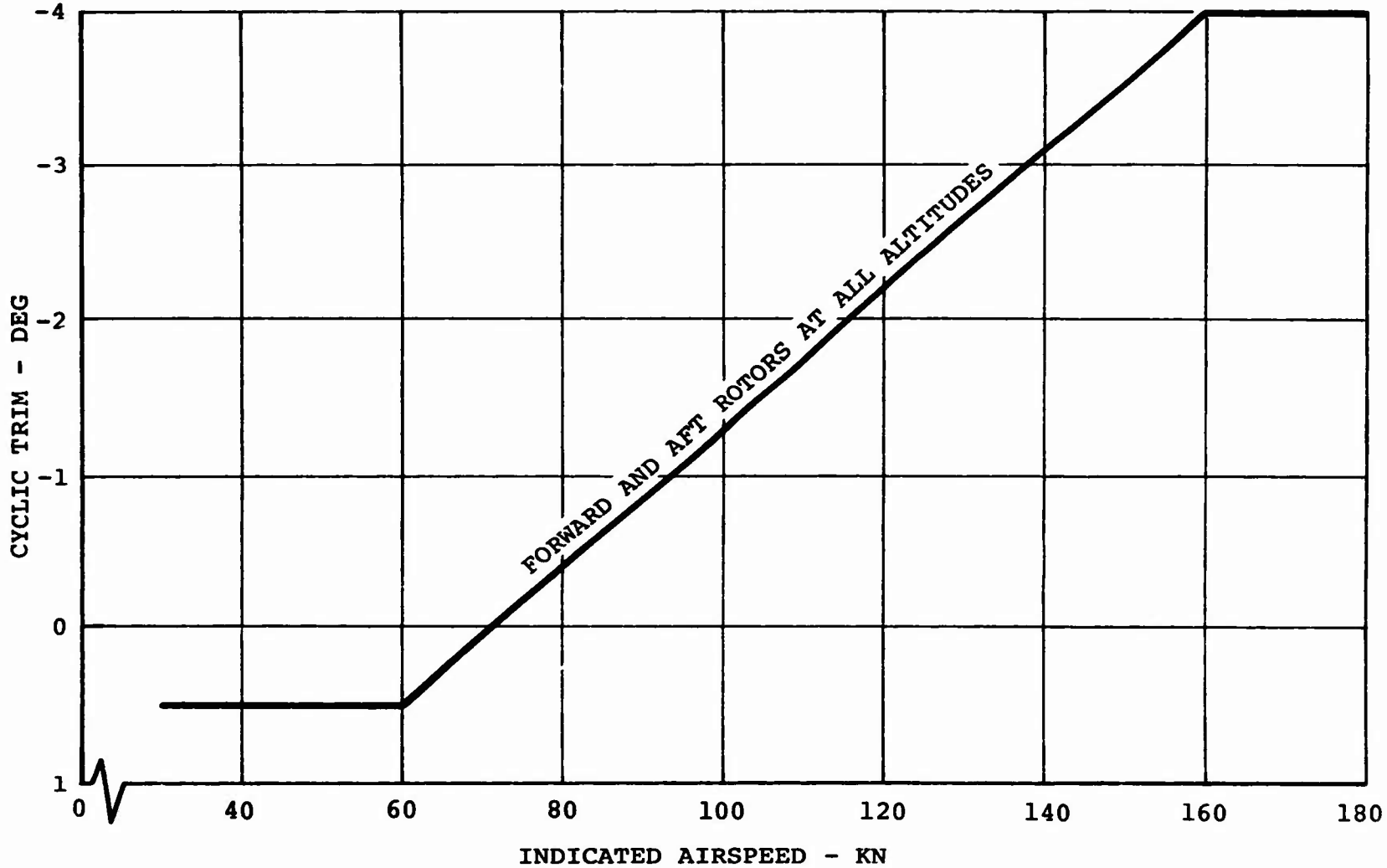

Figure 45. Cyclic Trim Schedule for Flight Test of Boron Advanced-Geometry Blades.

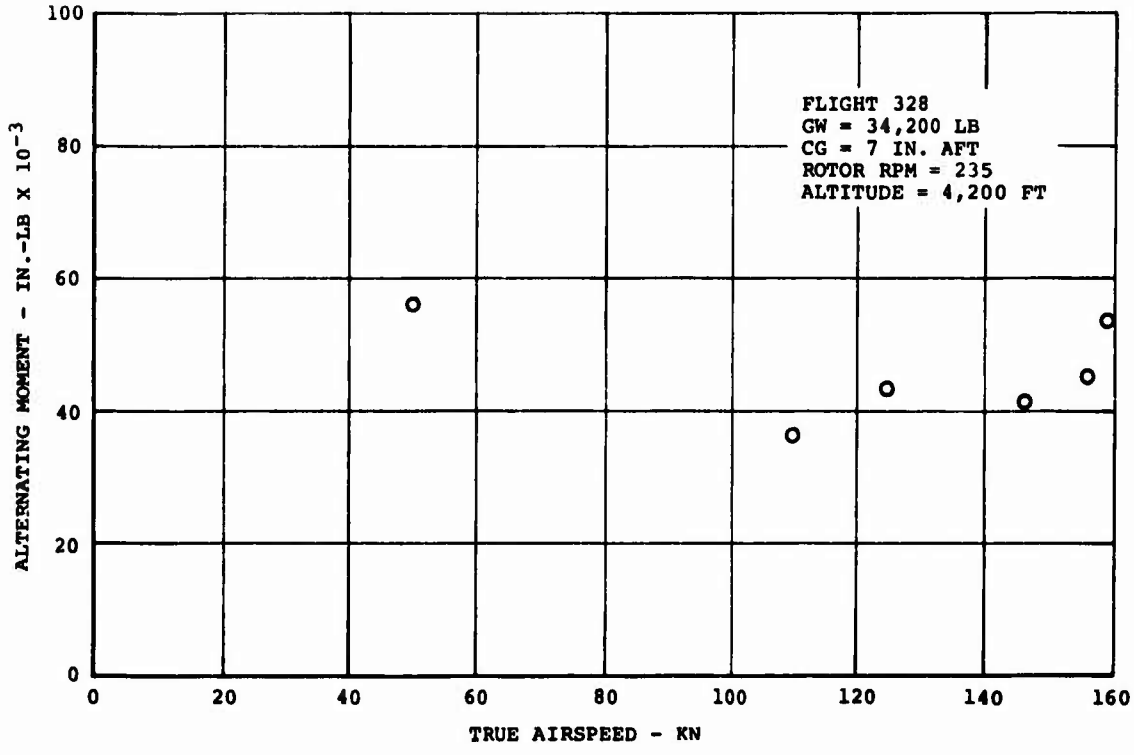

Figure 46. Flapwise Bending of the Blade Socket (Station 49.5).

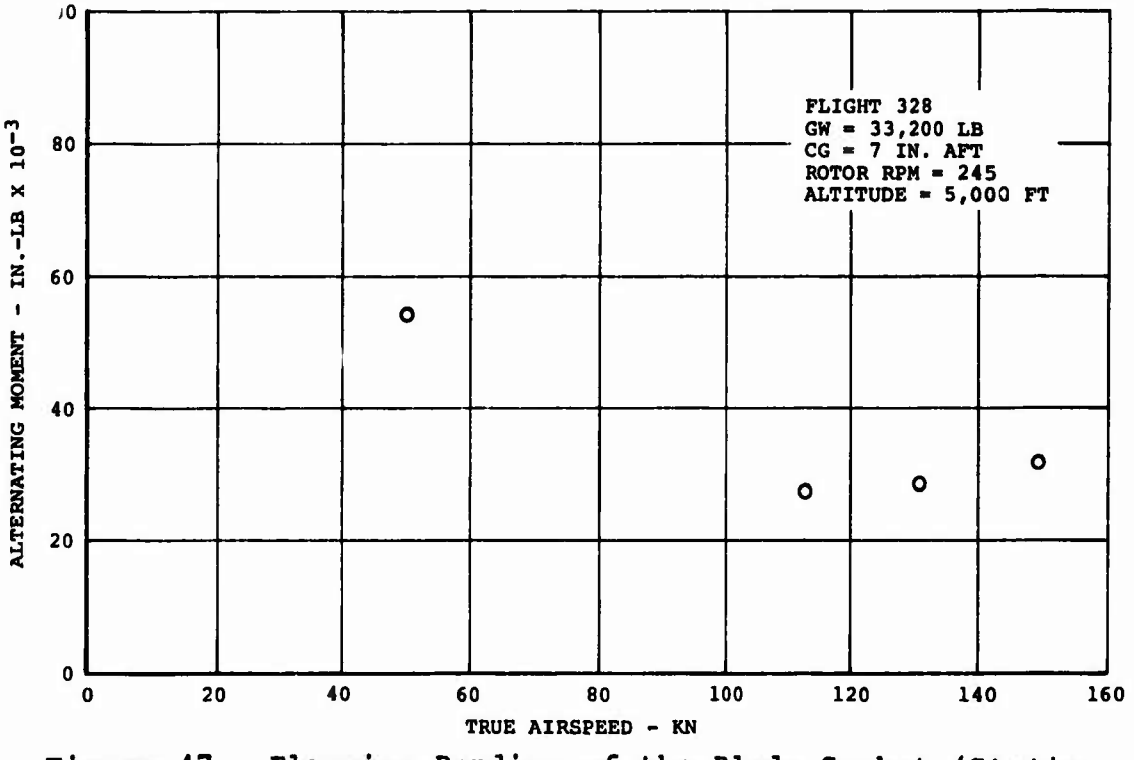

Figure 47. Flapwise Bending of the Blade Socket (Station 49.5).

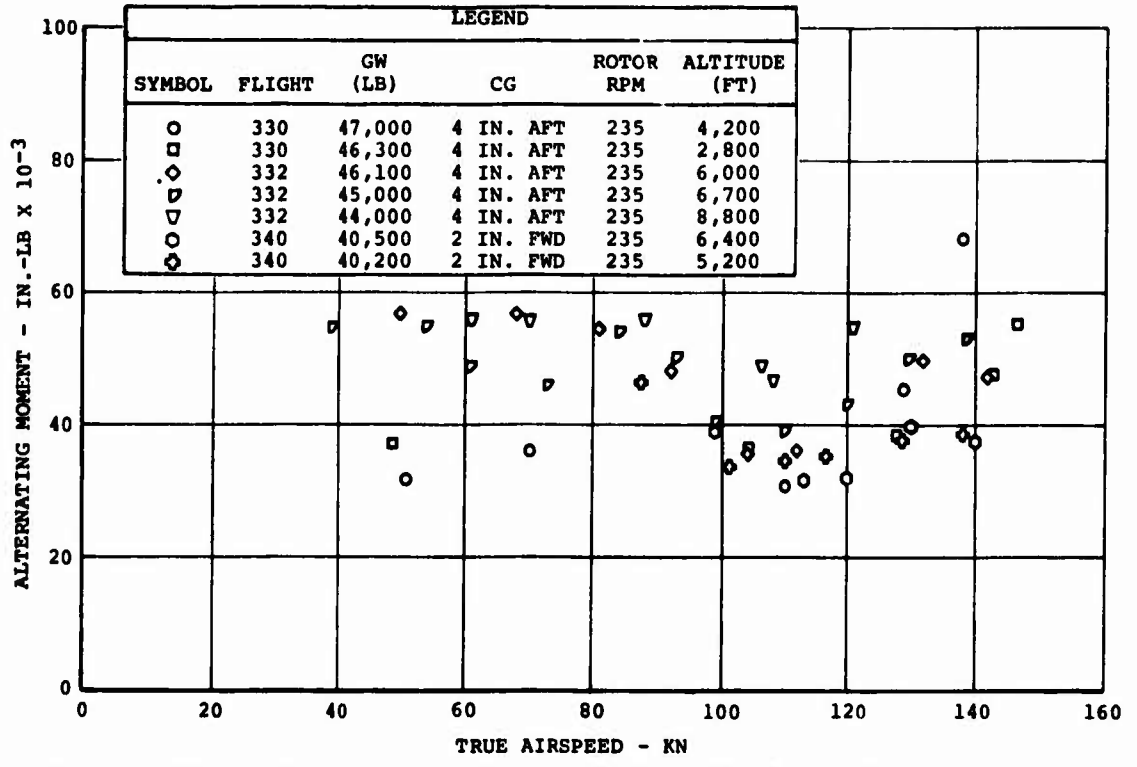

Figure 48. Flapwise Bending of the Blade Socket (Station 49.5).

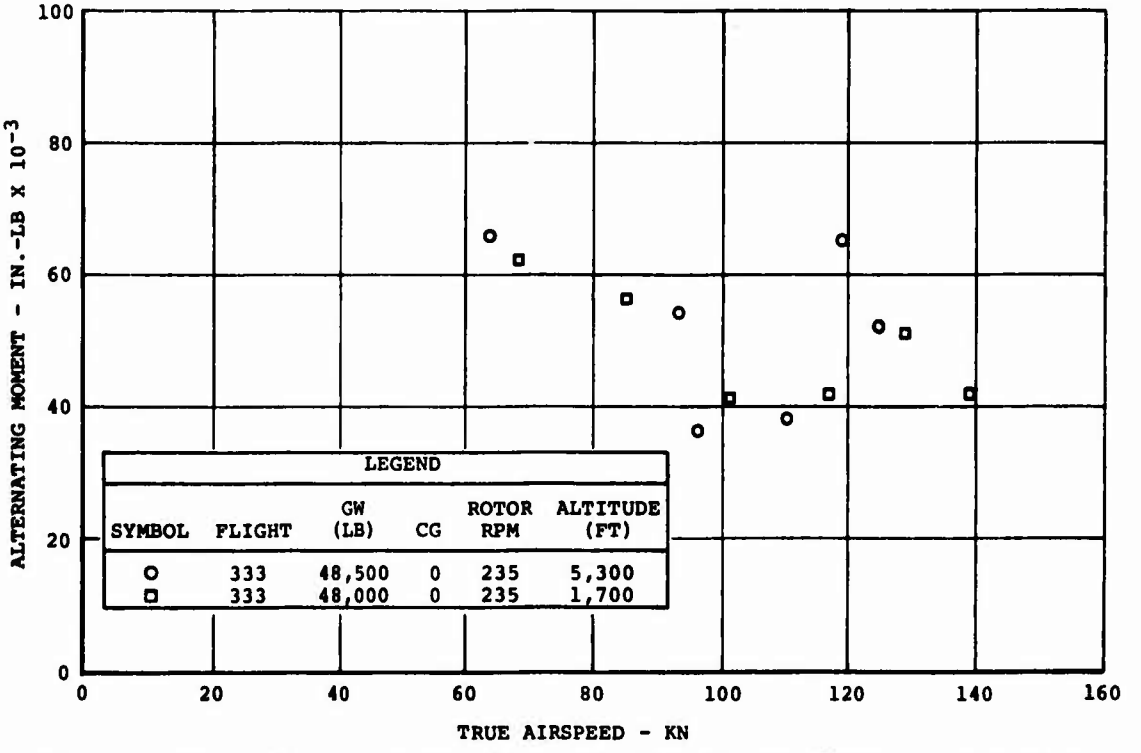

Figure 49. Flapwise Bending of the Blade Socket (Station 49.5).

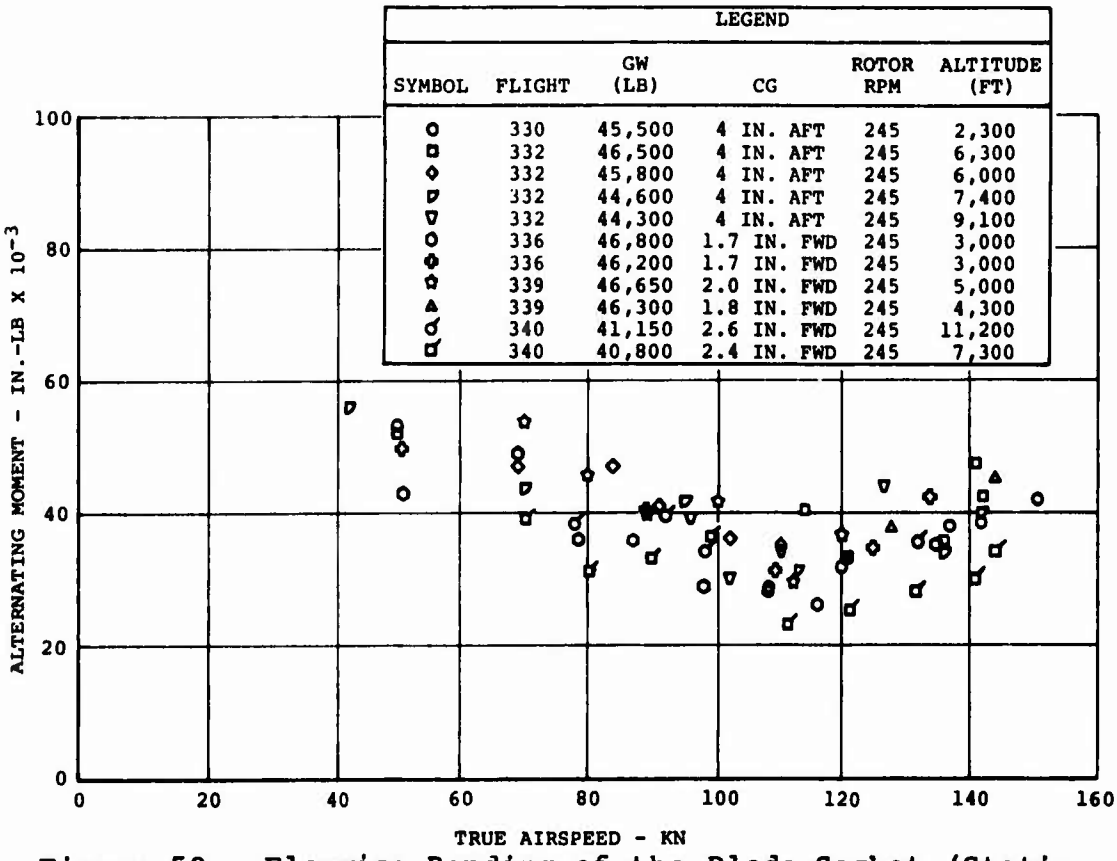

Figure 50. Flapwise Bending of the Blade Socket (Station 49.5).

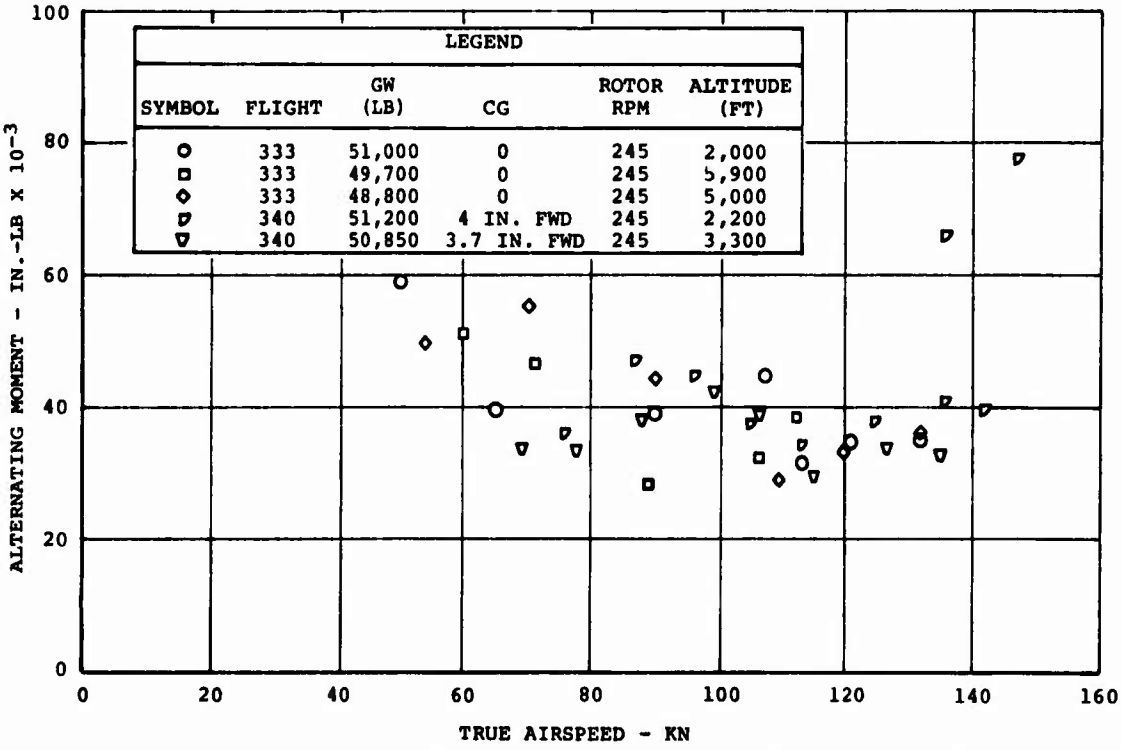

Figure 51. Flapwise Bending of the Blade Socket (Station 49.5).

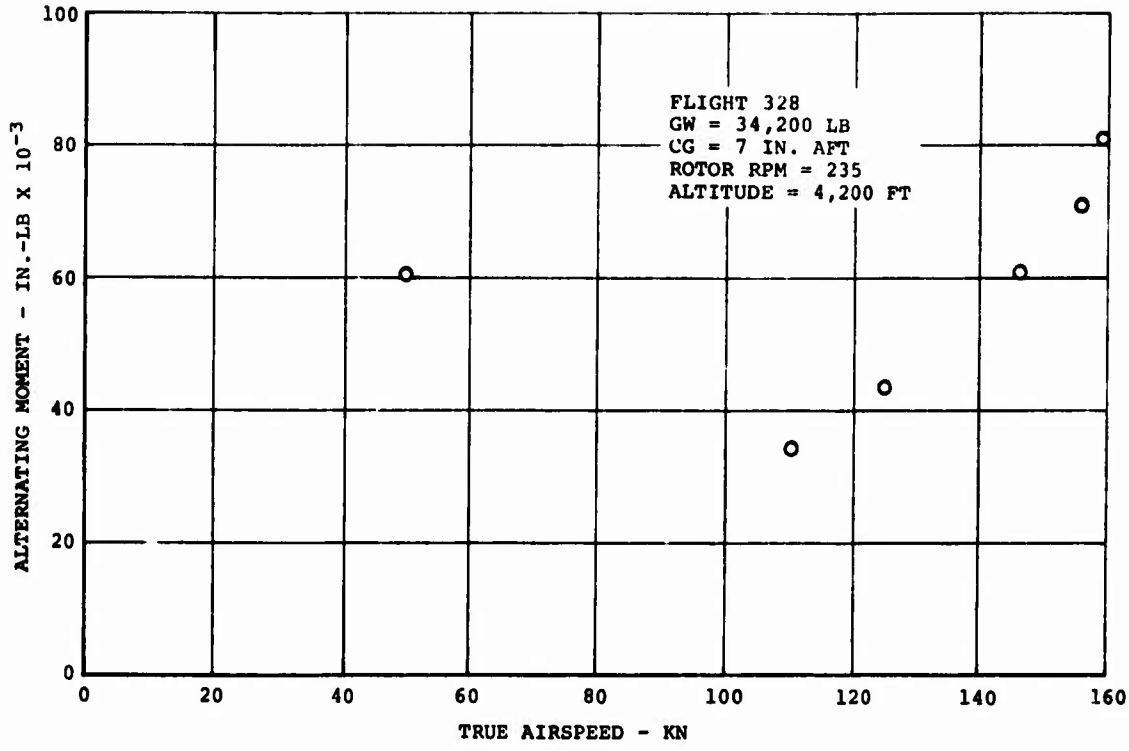

Figure 52. Flapwise Bending of the Blade Spar (Station 252).

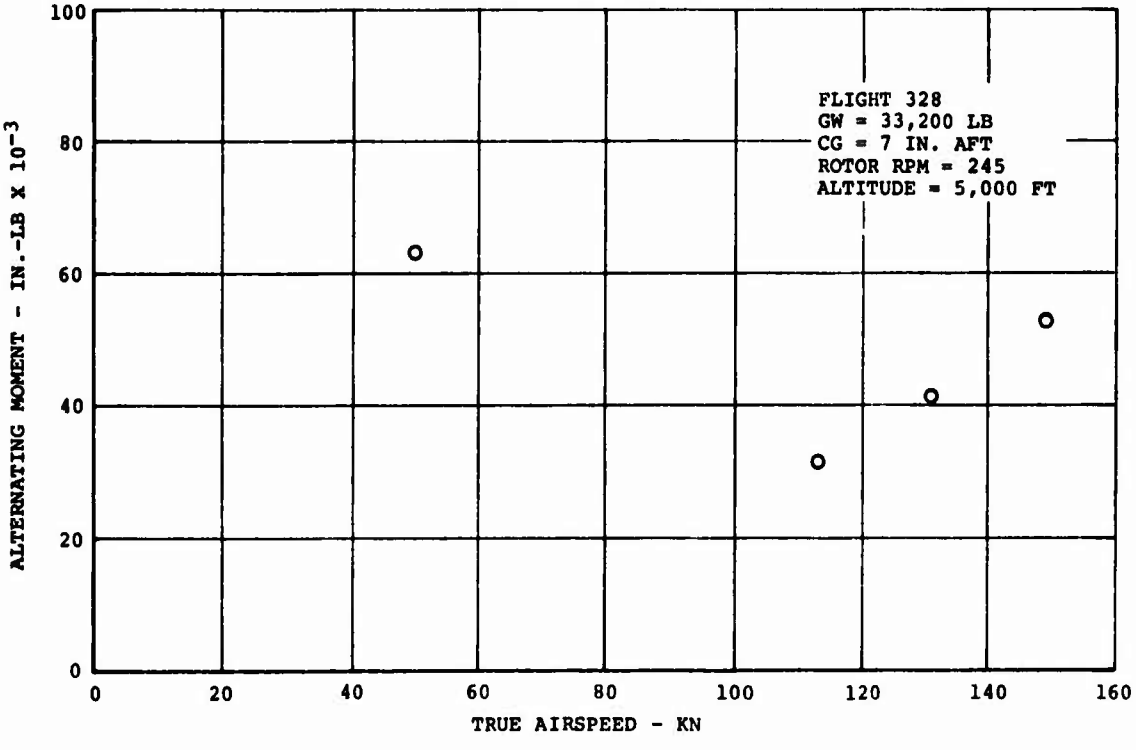

Figure 53. Flapwise Bending of the Blade Spar (Station 252).

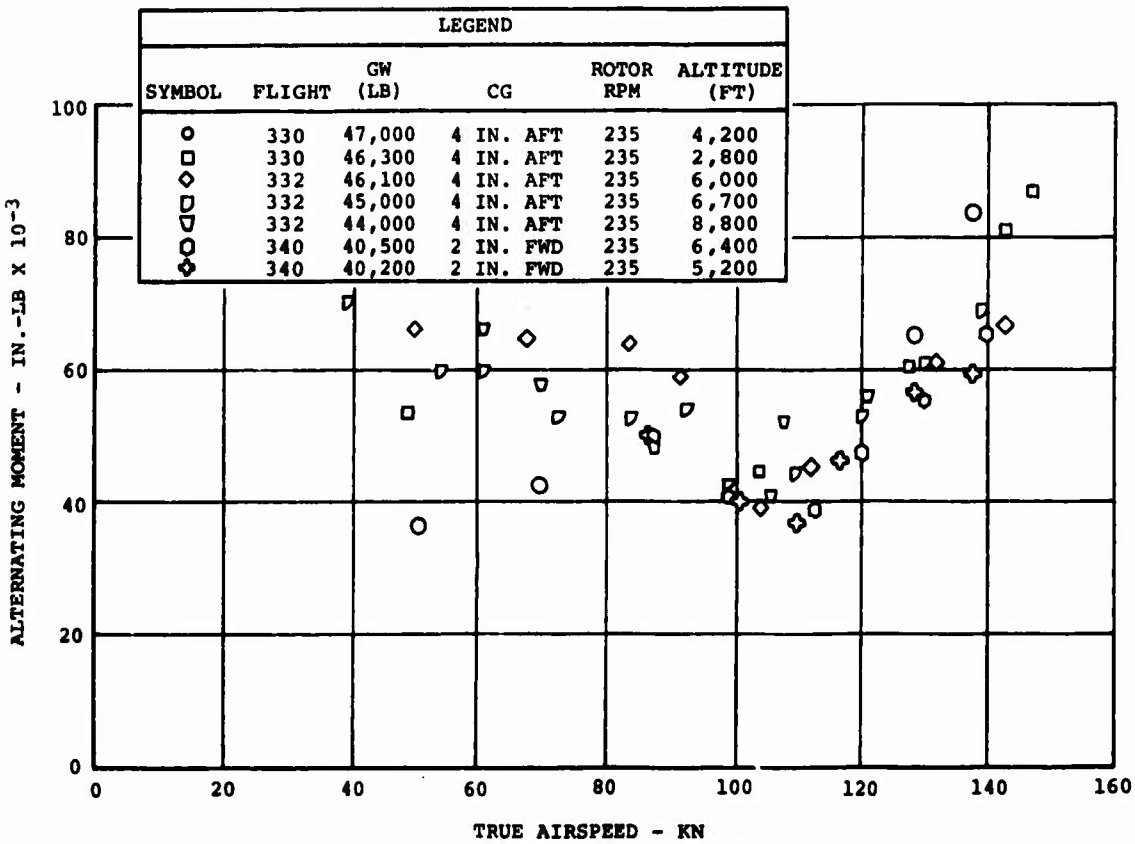

Figure 54. Flapwise Bending of the Blade Spar (Station 252).

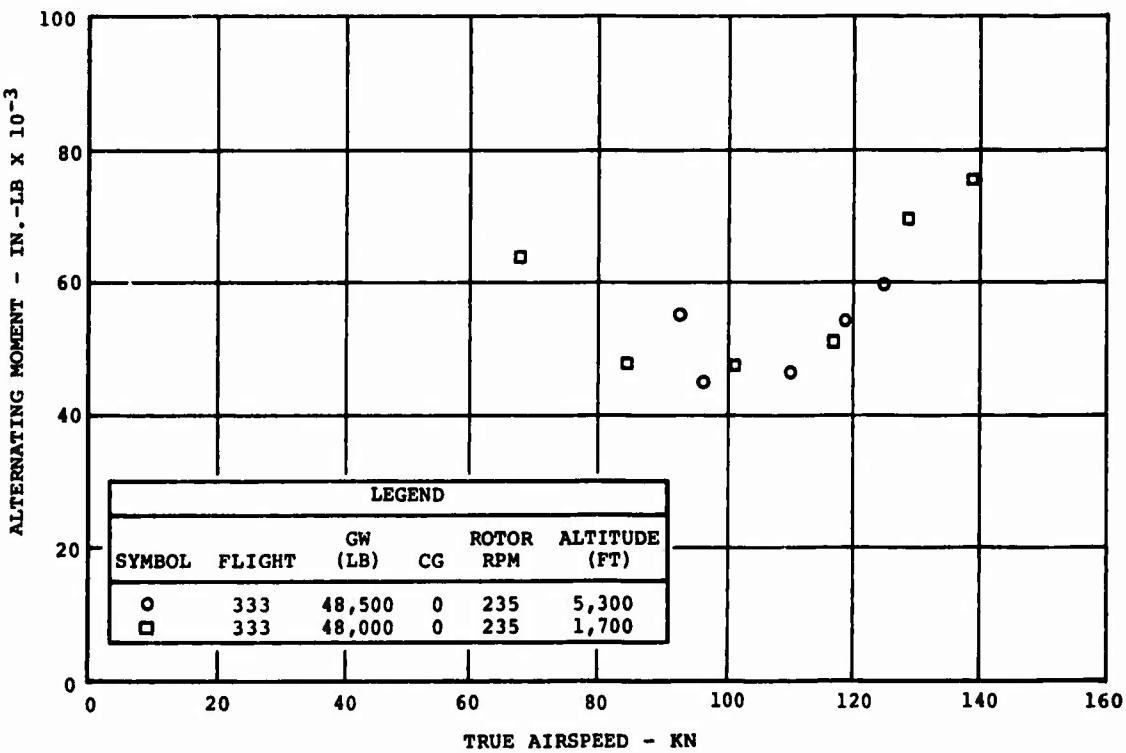

Figure 55. Flapwise Bending of the Blade Spar (Station 252).

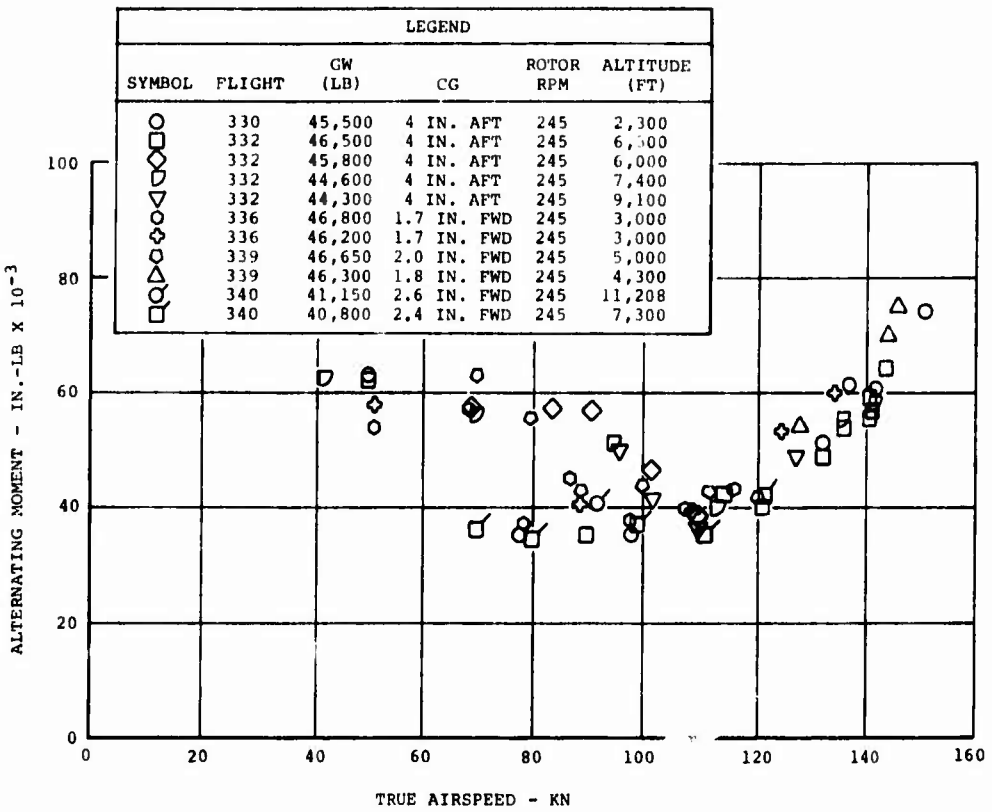

Figure 56. Flapwise Bending of the Blade Spar (Station 252).

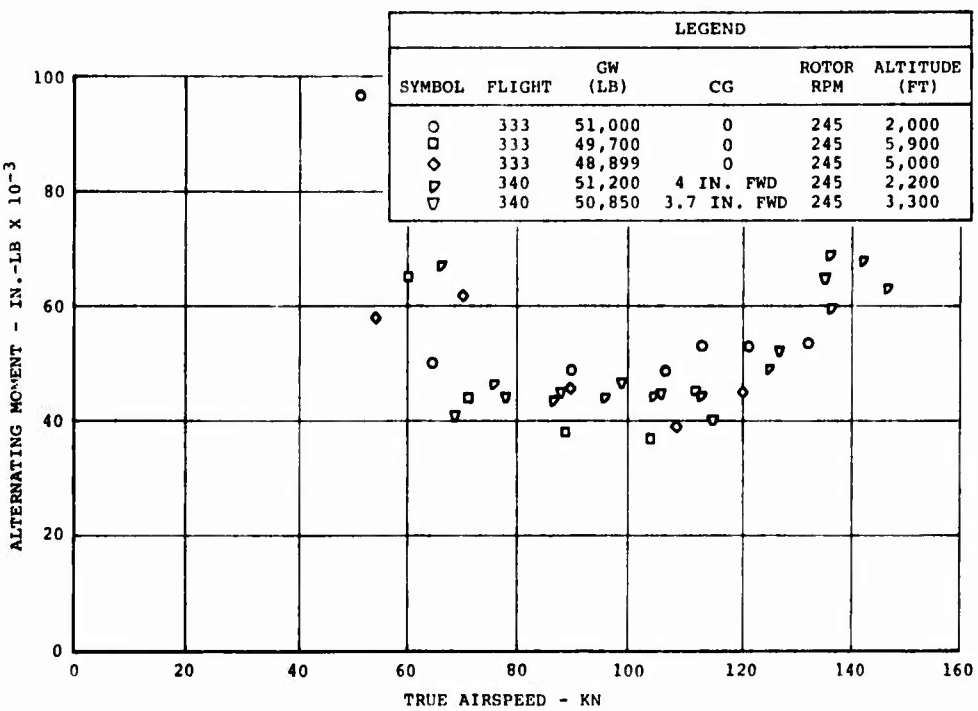

Figure 57. Flapwise Bending of the Blade Spar (Station 252).

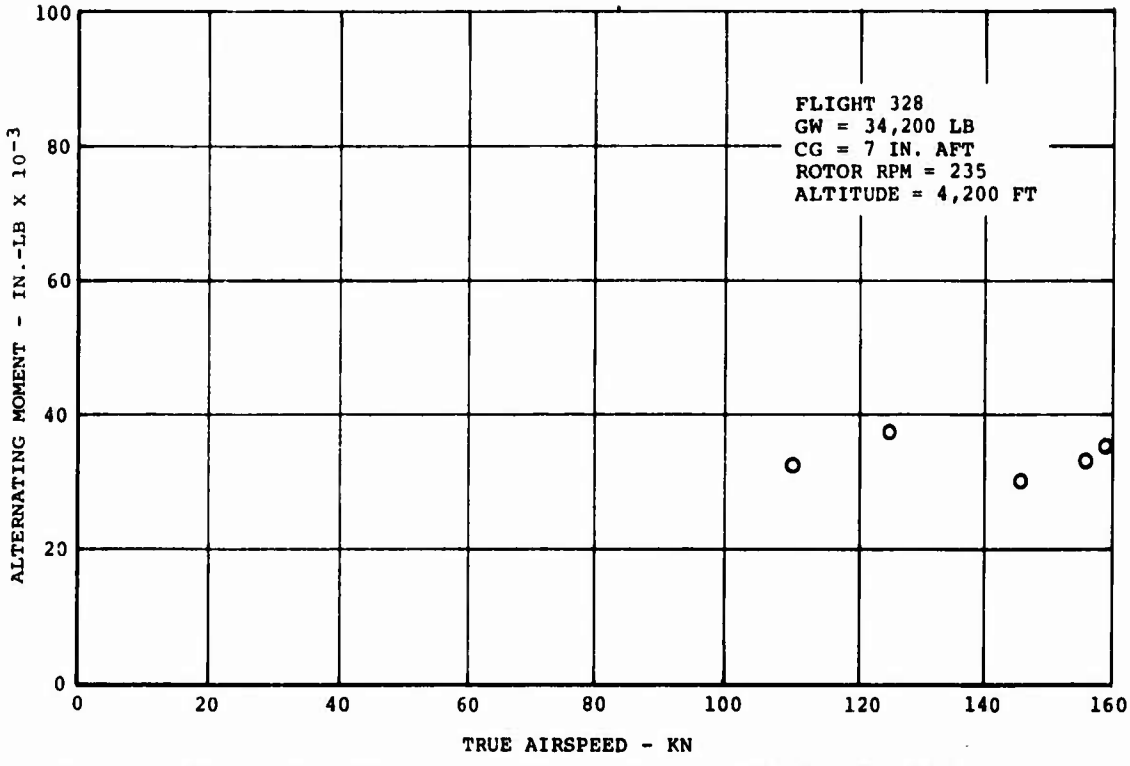

Figure 58. Chordwise Bending of the Blade Trailing Edge (Station 198).

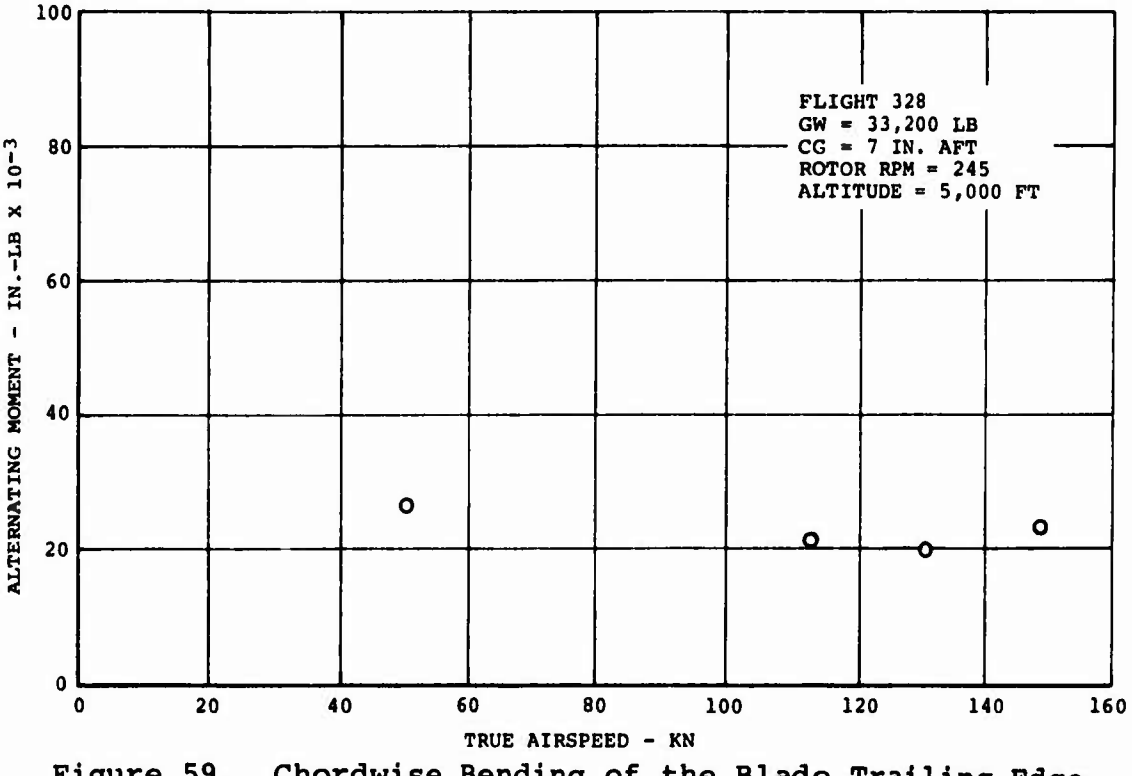

Figure 59. Chordwise Bending of the Blade Trailing Edge (Station 198).

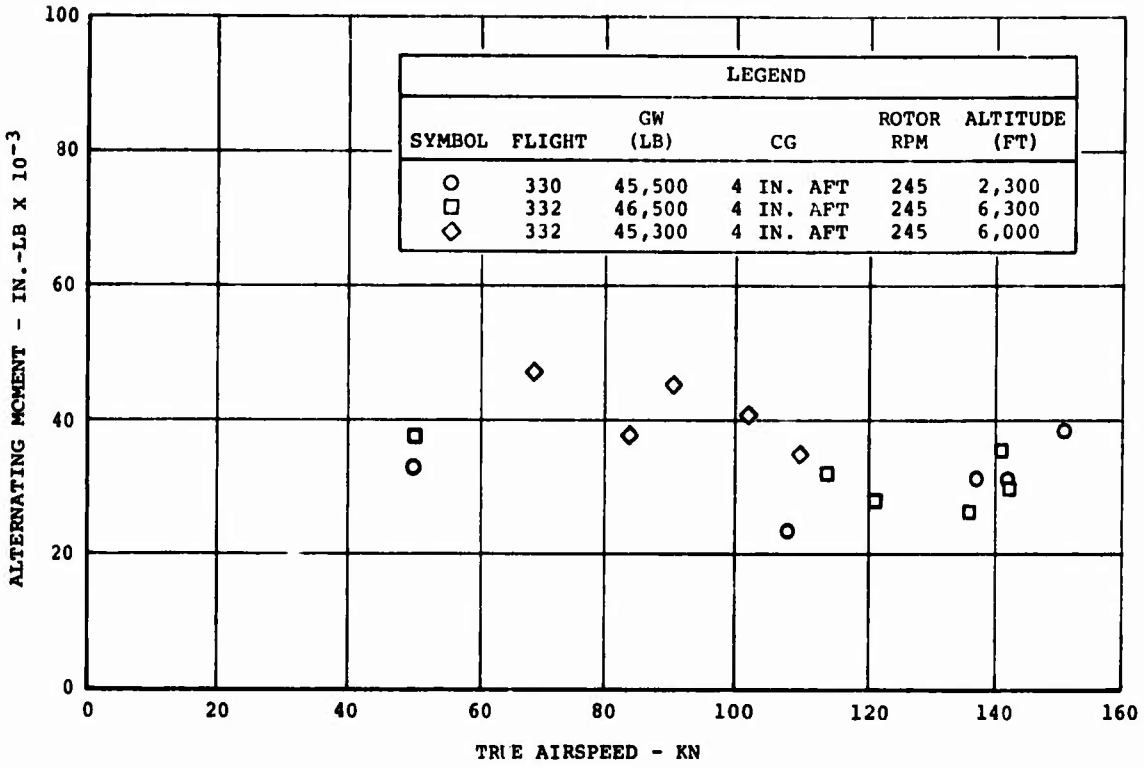

Figure 60. Chordwise Bending of the Blade Trailing Edge (Station 198).

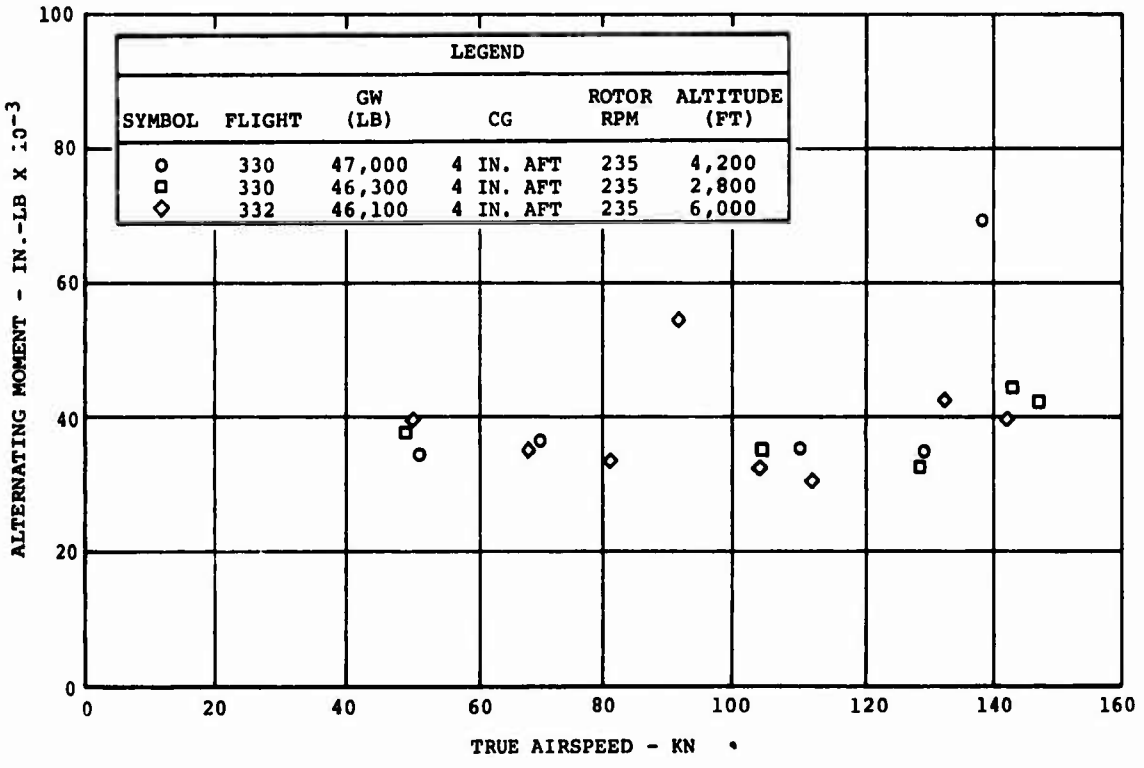

Figure 61. Chordwise Bending of the Blade Trailing Edge (Station 198).

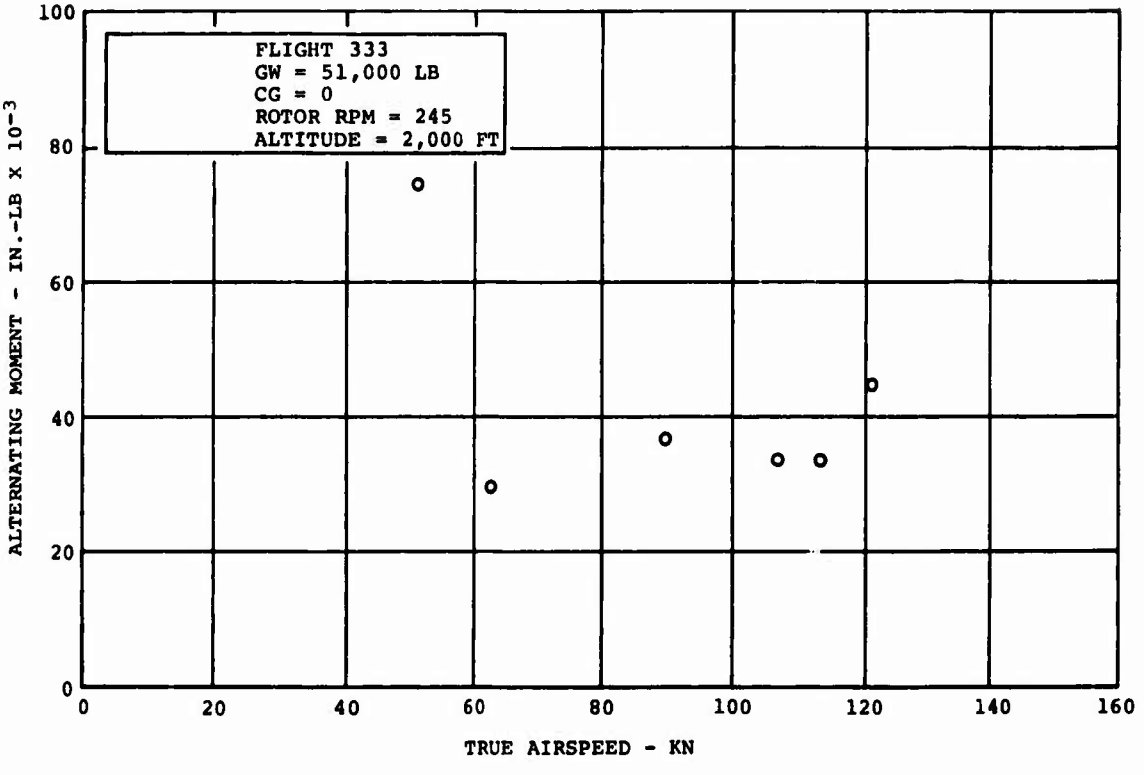

Figure 62. Chordwise Bending of the Blade Trailing Edge (Station 198).

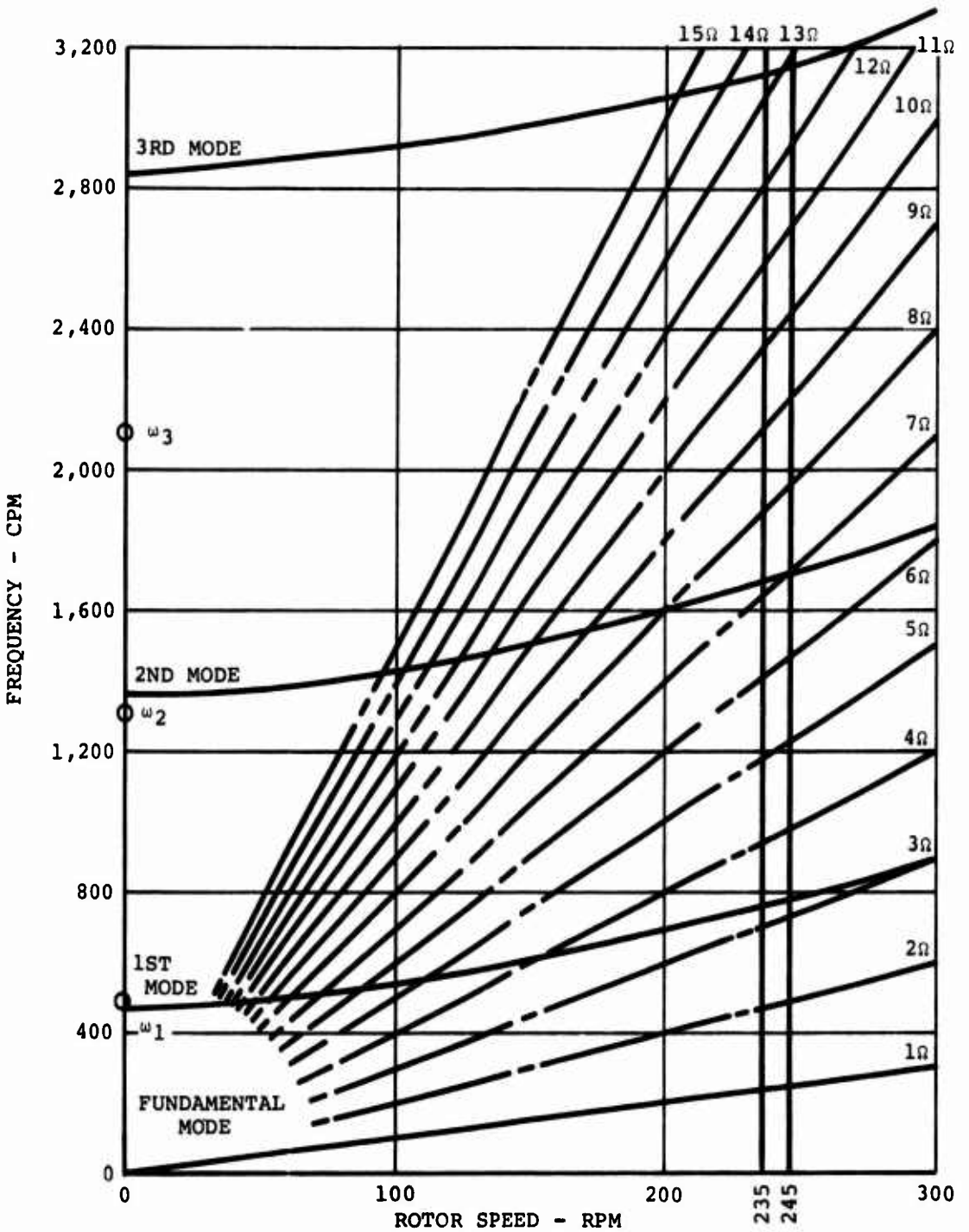

Figure 63. Flapwise Natural Frequency Spectrum of the Boron Advanced-Geometry Blade.

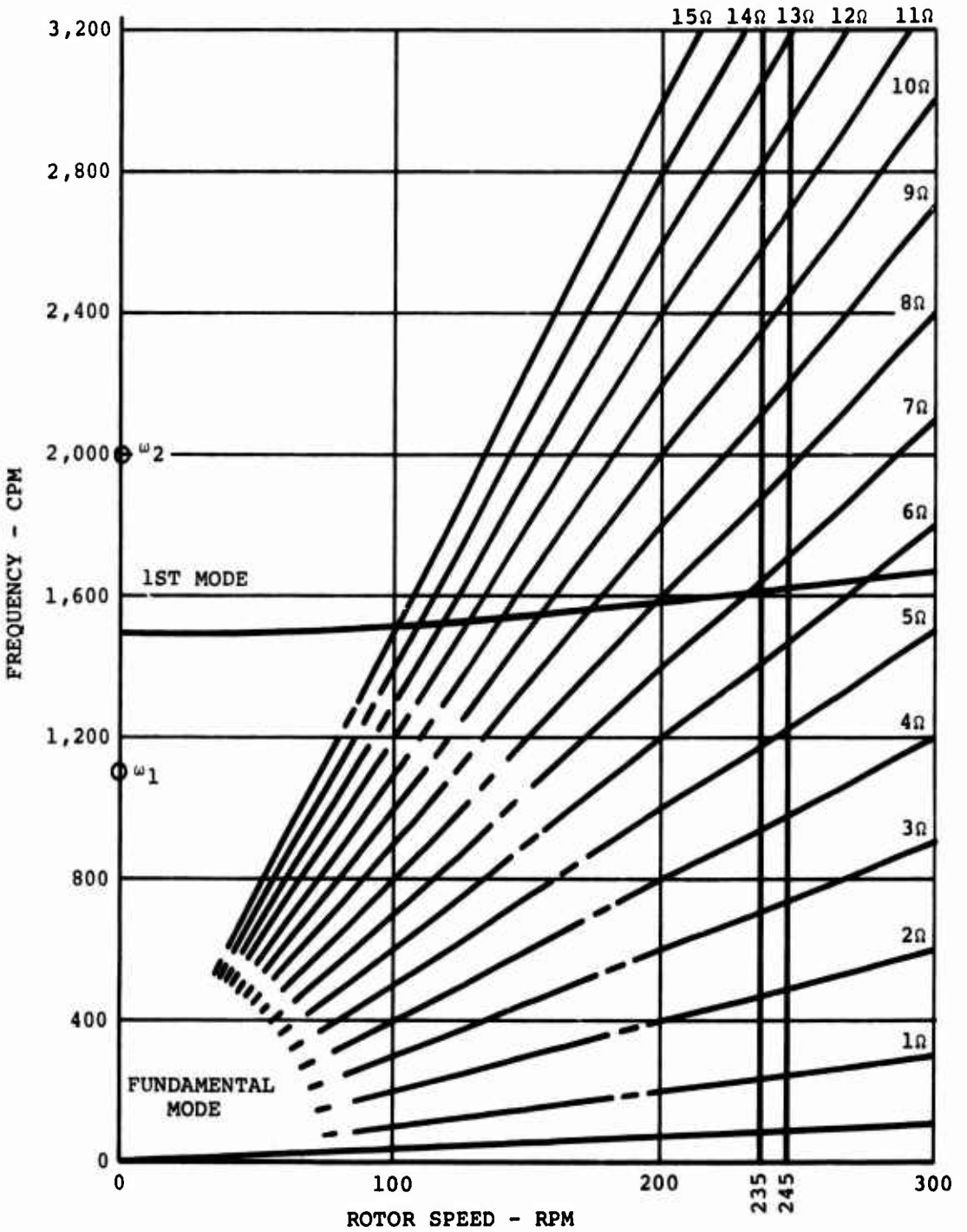

Figure 64. Chordwise Natural Frequency Spectrum of the Boron Advanced-Geometry Blade.

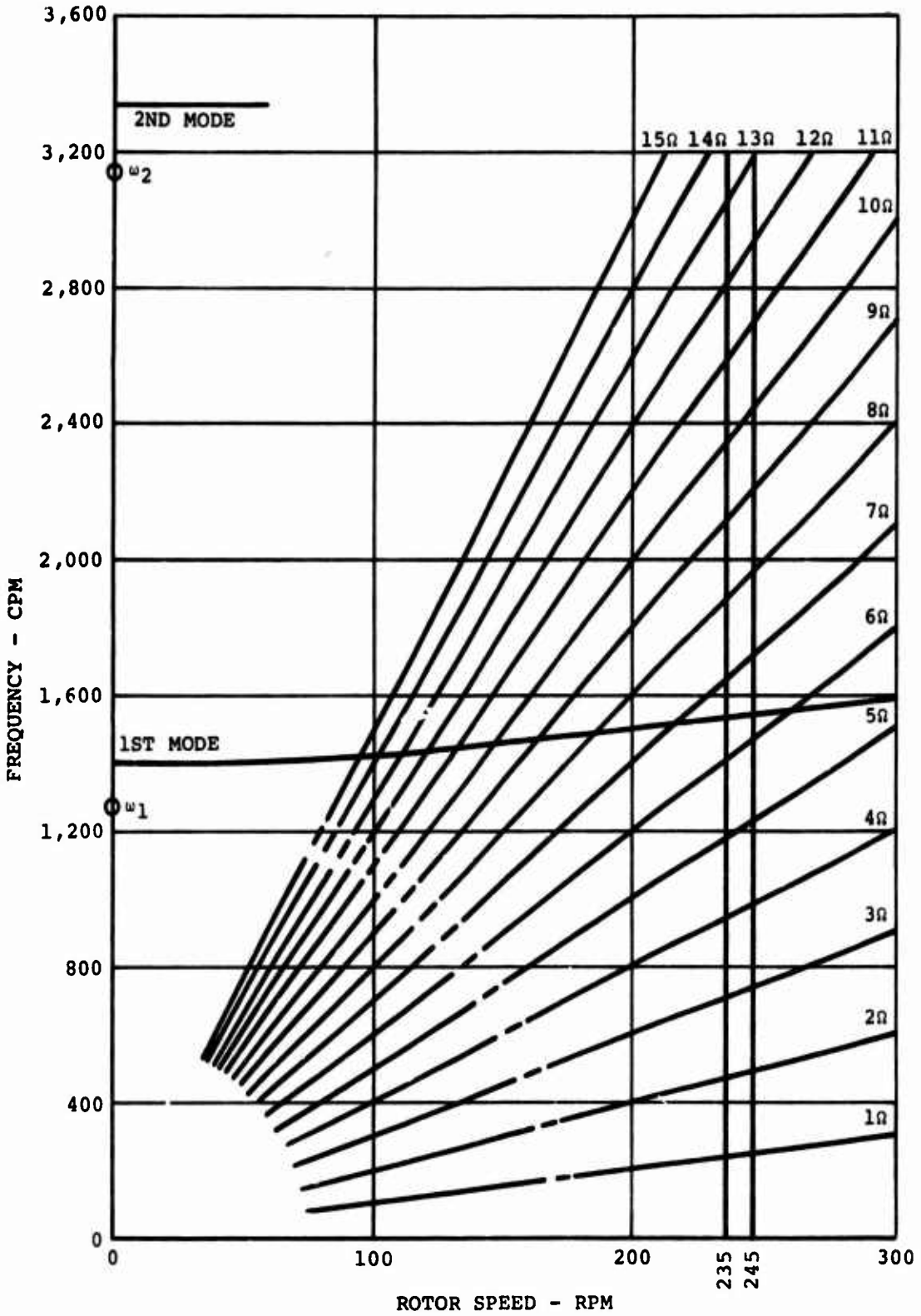

Figure 65. Torsional Natural Frequency Spectrum of the Boron Advanced-Geometry Blade.

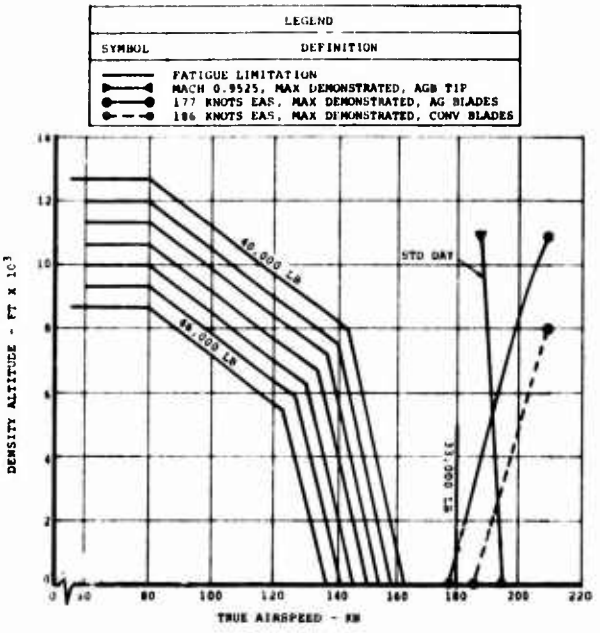

ROTOR RPM = 235

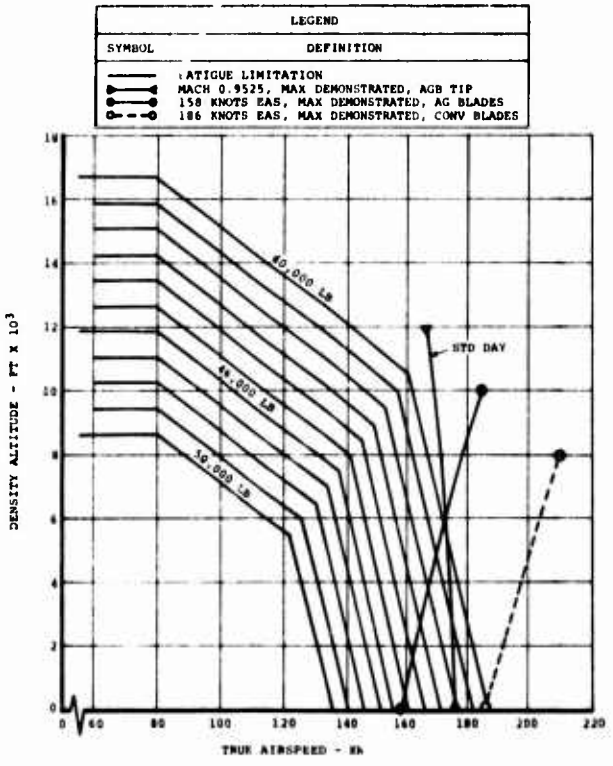

ROTOR RPM = 245

Figure 66. Structural Airspeed Limits of CH-47C Helicopter Equipped With Fiberglass Advanced-Geometry Blades at 235 and 245 Rotor RPM.

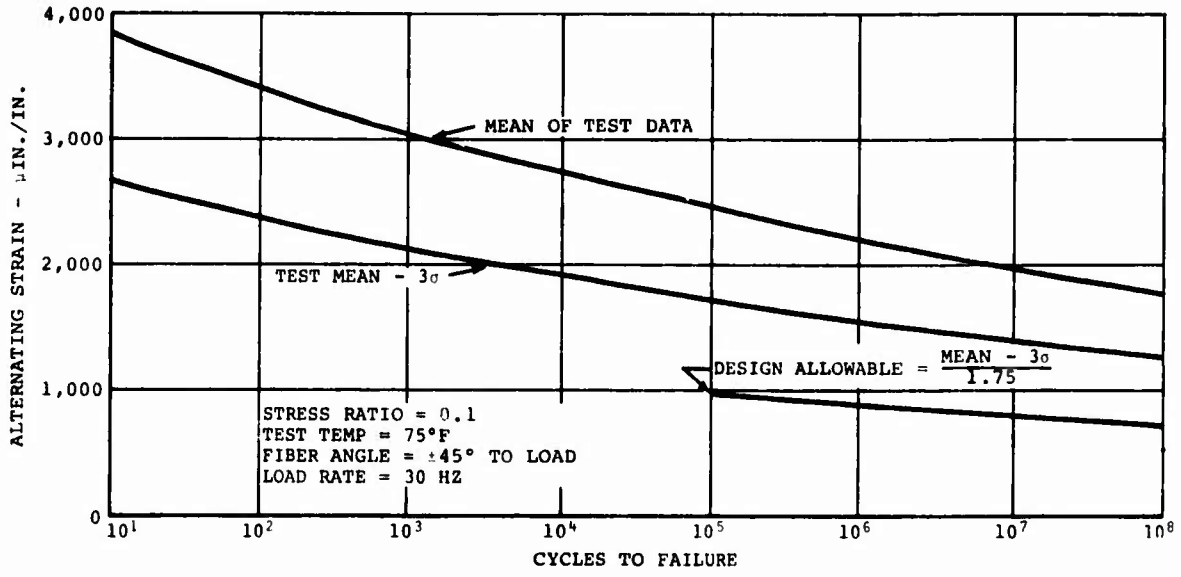

Figure 67. Fatigue Strength of the Blade Socket at Station 29.5.

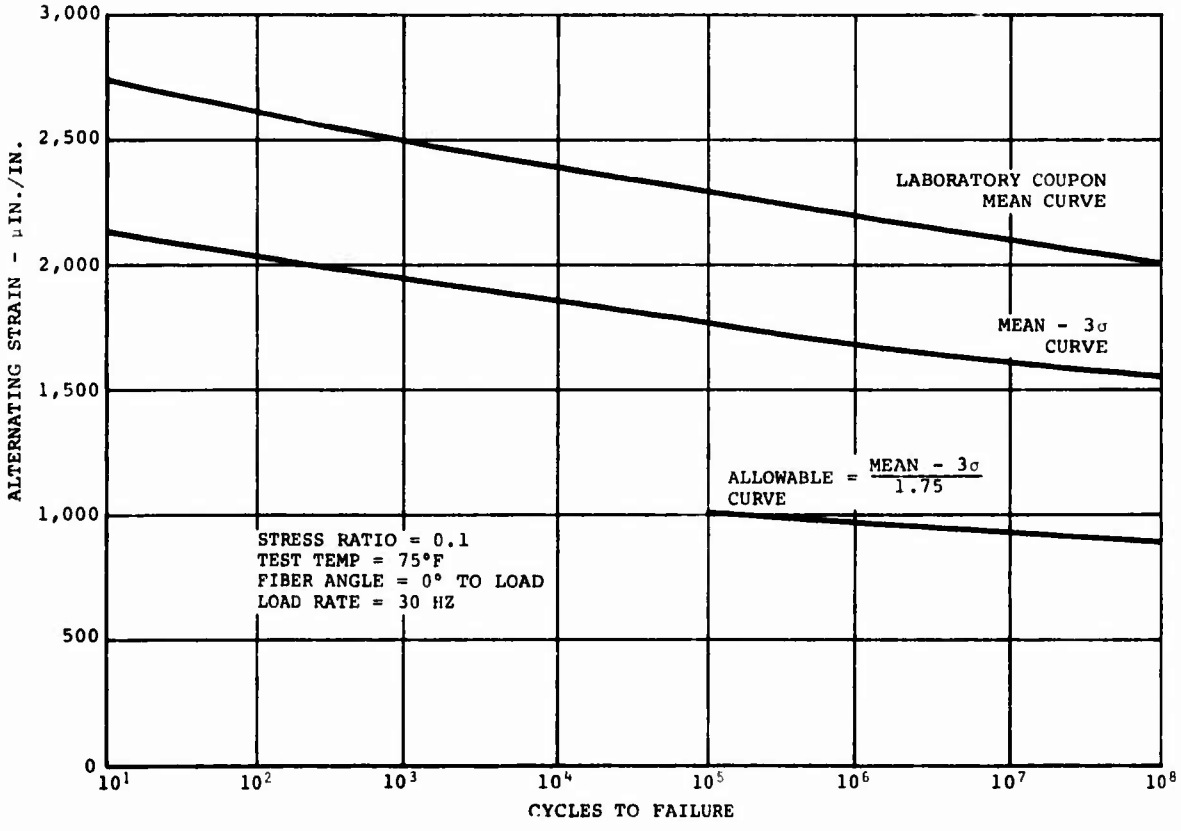

Figure 68. Fatigue Strength of Zero-Degree Type IIB Boron/ Epoxy Loaded in Tension-Tension Fatigue.

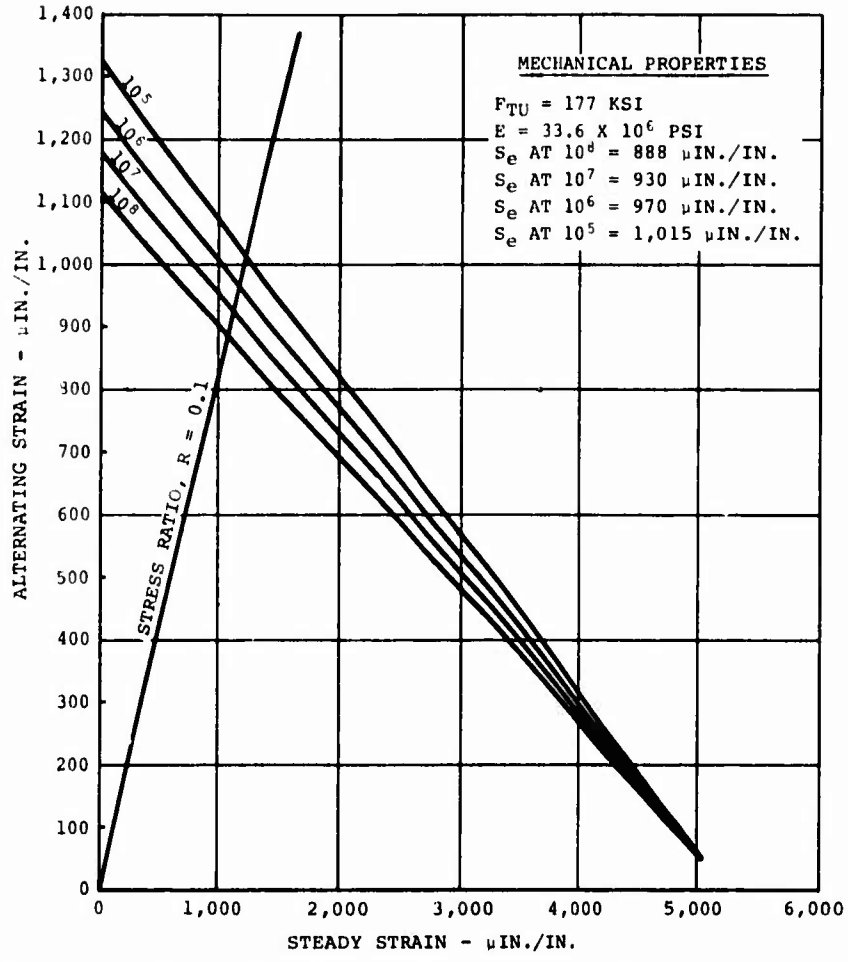

Figure 69. Modified Goodman Diagram for Zero-Degree Type IIB Boron/Epoxy Based on Mean - 3σ/1.75 Values.

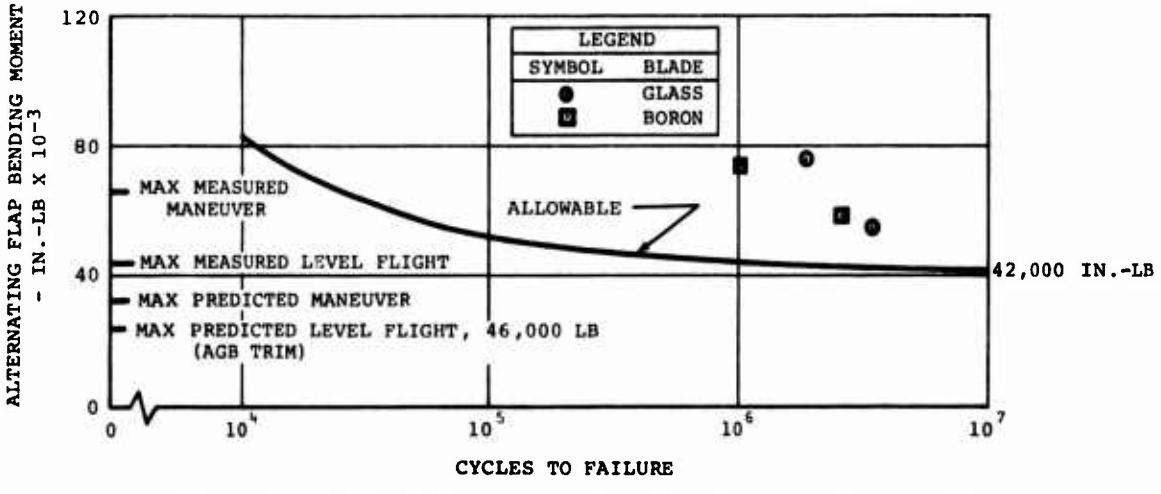

Figure 70. Fatigue Strength of ±45-Degree Type IIB Boron/Epoxy Sandwich Beams Loaded in Flexural Fatigue.

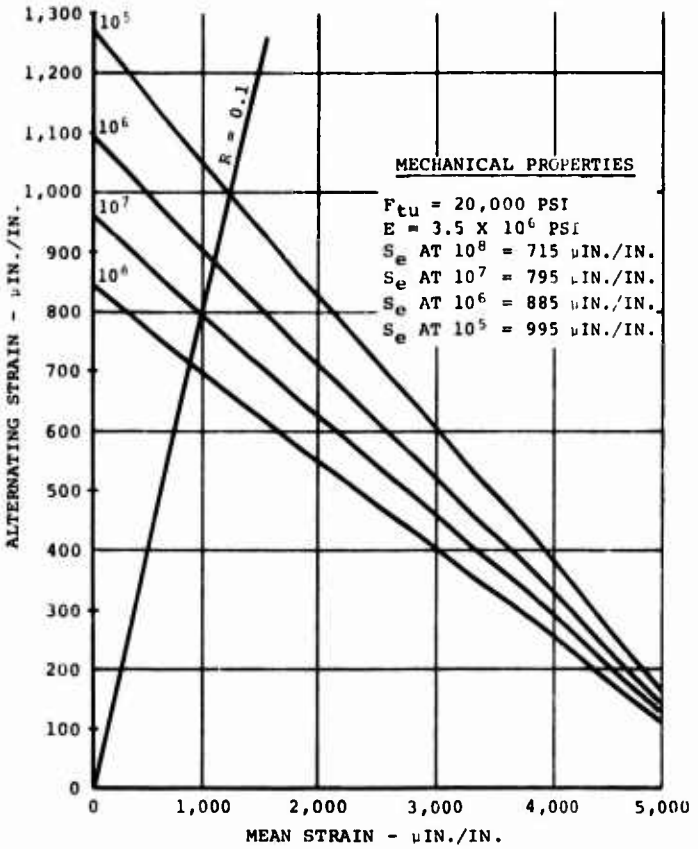

Figure 71. Modified Goodman Diagram for ±45-Degree Boron/ Epoxy Sandwich Beams Based on Mean - 3σ/1.75 Values.

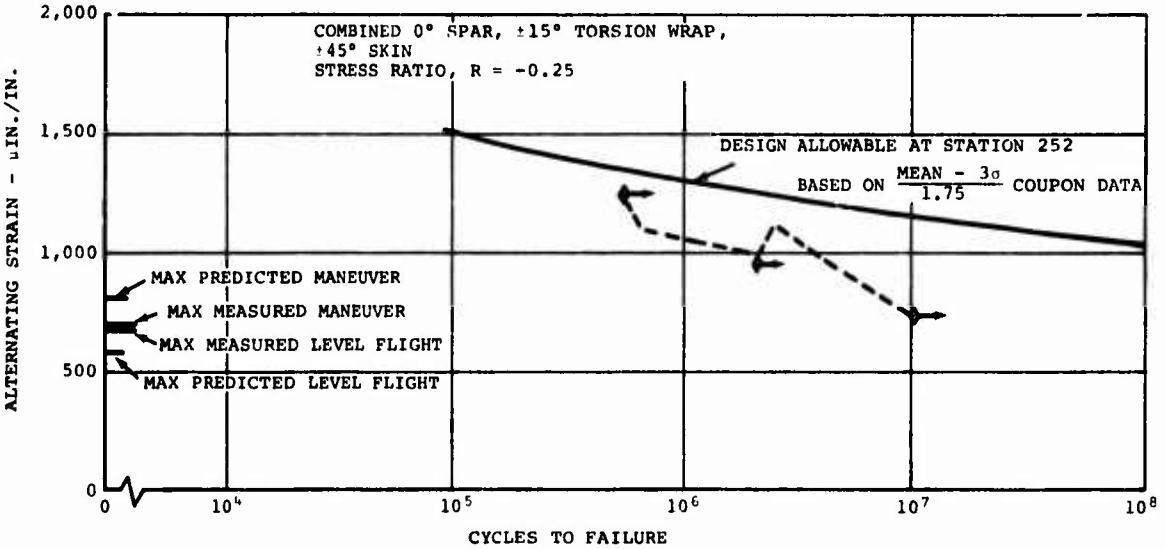

Figure 72. Allowable Fatigue Strain for Flapwise Bending of the Boron Advanced-Geometry Blade at Station 252.

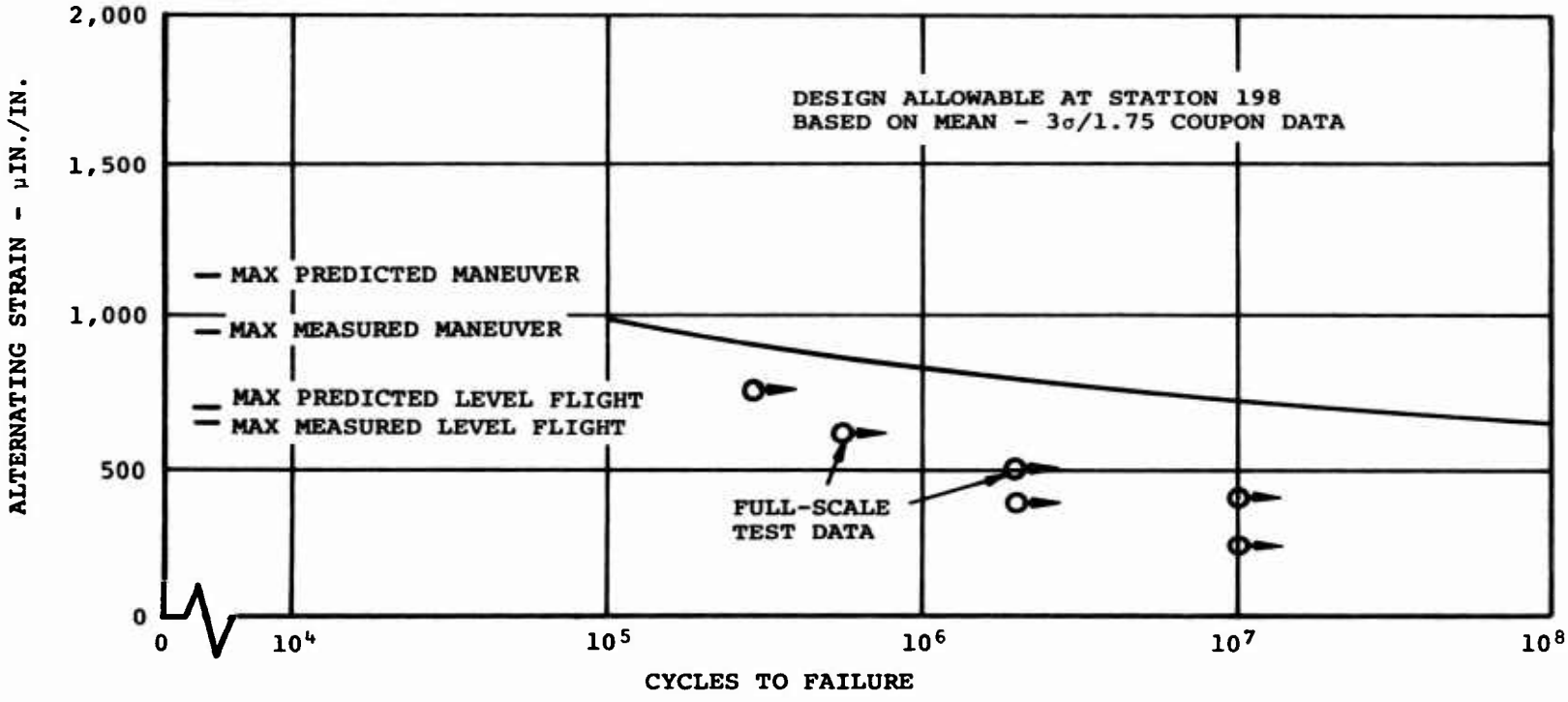

Figure 73. Allowable Fatigue Strain for Chordwise Bending of the Boron Advanced-Geometry Blade at Station 198.

VIBRATION

The purpose of this section is to discuss any significant differences in vibration characteristics as a result of installing the boron advanced-geometry blades on a CH-47 helicopter. Vibration data with boron blades installed on the aft rotor head are compared to data obtained during evaluation of the all-fiberglass advanced-geometry blade in 1969. Most of the data are comprised of 1/rev and 3/rev levels at various gross weights and altitudes as a function of airspeed. Rotor speed effects were examined, but due to the incompatibility of the self-tuning absorbers with the nonproduction cockpit configuration, cockpit vibration is not consistent with normal 3/rev response characteristics throughout the entire CH-47C rotor speed range. Vibration levels were very erratic, indicating deficiencies in absorber tuning. Higher harmonic vibration was given a cursory examination, and no abnormalities were noted at a 235-rotor-rpm, high-speed condition. The standard production cyclic trim schedule for the CH-47C helicopter was used for all flights.

Vibration Test Conditions

Absorber Configuration

Three production CH-47C self-tuning vibration absorbers were employed in the cockpit to reduce 3/rev vibration. The absorbers were tuned for an operating frequency range coincident with a rotor speed range of 232 to 251 rpm. In addition, two fixed-tuned absorbers (tuned for 243 rpm) were employed in the upper aft pylon.

Vibration Flights

A list of those flights used for vibration data and a summary of the various flight conditions are included as Table XII.

Ballast Arrangement

The flight test program used water ballast along the fuselage in conjunction with lead ballast where space permitted. Ballast arrangements are summarized in Figure 74. The configurations differ slightly from the ballast configurations used during evaluation of the fiberglass blades, but total gross weight packages are similar (Table XIII).

TABLE XII. SUMMARY OF VIBRATION DATA FLIGHTS DURING TEST OF THE BORON ADVANCED-GEOMETRY BLADE

Flight	Date (1972)	TOGW (lb) / TOCG	Density Altitude (ft)	Vibration Data: Airspeed Sweeps Rotor Speed (rpm)	Airspeed Sweeps Airspeed (kn)	Airspeed Sweeps Run GW (lb)	RPM Sweeps Airspeed (kn)	RPM Sweeps Rotor Speed (rpm)	RPM Sweeps Run GW (lb)	Maneuvers
328	15 March	35,000 7.0 in. aft	4,200	235	50-159	34,000	-	-	-	hover, hover
			5,000	245	50-149	33,200	-	-	-	turns, l&r max
			4,600	-	-	-	156	230-245	33,500	bank turns, ppd (500 fpm), flare
330	21 March	48,000 4.0 in. aft	4,200	235	51-138	47,000	-	-	-	hover, hover
			2,800	235	49-147	46,200	-	-	-	turns, l&r 30°
			2,300	245	50-151	45,400	-	-	-	turns, mil pwr
			2,400	-	-	-	125	230-245	45,900	climb, flare
333	28 March	52,000 0	2,000	245	52-132	51,000	-	-	-	hover,
			6,000	245	61-106	49,700	-	-	-	10-20-30° turns,
			5,000	245	55-132	48,800	-	-	-	climb, landing
			5,000	235	93-125	48,500	-	-	-	flare
			1,600	235	68-139	48,000	-	-	-	
			1,950	-	-	-	120	230-245	50,500	
336	20 April	48,000 3.0 in. fwd	2,500	245	52-136	47,000	-	-	-	hover, hover
			2,000	245	52-135	46,000	-	-	-	turns, landing
			3,700	-	-	-	47	230-245	45,800	flare
			3,700	-	-	-	89	230-245	45,500	
			3,700	-	-	-	136	230-245	45,000	
340	28 April	51,900 4.4 in. fwd	2,200	245	66-148	51,000	-	-	-	climb to
			3,300	245	69-147	51,000	-	-	-	14,000 ft
			11,200	245	78-137	41,000	-	-	-	
			7,200	245	71-144	41,000	-	-	-	
			6,400	235	88-151	40,000	-	-	-	
			5,200	235	88-148	40,000	-	-	-	

TABLE XIII. COMPARISON OF HELICOPTER WEIGHT AND BALANCE FOR FLIGHT TEST OF FIBERGLASS AND BORON ADVANCED-GEOMETRY BLADES			
Glass Blade Program		Boron Blade Program	
GW (lb)	CG	GW (lb)	CG
34,500	6.1 in. aft	35,000	7 in. aft
41,000	5.6 in. aft	-	-
47,500	3.5 in. aft	48,000	4 in. aft
52,000	0.2 in. aft	52,000	0

Vibration Measurement Locations

The 12 vibration transducers were located as shown in Figure 75. Each of the accelerometers was operational for the five vibration flights.

Test Results

The following data were obtained from harmonic analyses of digitized data converted from analog impulses recorded on magnetic tape. Where no scatter band is plotted, the levels represent top of scatter. For the glass blade and production CH-47C data, 85-percent levels were selected from 20 consecutive rotor cycles of data. Only 10 consecutive rotor cycles were requested for the boron blade data. Data scatter was such that the 85-percent level was not significantly lower than 100 percent of the data.

Basic 3/Rev Vibration

The 3/rev vibration levels for the 35,000-pound configuration are shown in Figures 76 and 77. Cockpit levels begin to deteriorate above 140 knots true airspeed, indicating poor performance of the self-tuning vibration absorbers. Although production absorbers were acquired for this program, the nonproduction configuration of the cockpit windshield post prevented their effective operation. Lateral cockpit vibration was acceptable; and although longitudinal 3/rev levels increased steadily at the high airspeeds, the CH-47C compliance criterion of 0.2g would have been met.

Midcabin vibration shows a distinct valley in the data curve at 120 to 130 knots. Not only are 3/rev levels extremely low, but also the depth of the vibration valley

is accentuated by the high 3/rev response at the low airspeeds (50 knots). The midcabin pickup on the isolated floor (BL 25) shows response characteristics similar to those from the airframe transducers at BL 44. This would indicate that the water ballast tanks and the ballast boxes have reduced the effect of cabin floor isolation in some local areas.

Lateral 3/rev vibration at the middle and aft end of the cabin is low. Aft cabin vertical levels are very high at 160 knots true airspeed and demonstrate the same vibration trends as the midcabin locations.

Basic 1/Rev Vibration

The 1/rev vibration problem associated with blade geometry inconsistencies in the fiberglass advanced-geometry blades was still a factor for the boron blade program. Tower tracking of the boron blades for the aft head was easily accomplished with good results. Attempts to achieve an equally good track for the forward rotor glass blades were less successful. The result, as expected, was an unacceptable cockpit vertical 1/rev vibration environment throughout the program. The data that follow constitute the total of the 1/rev information.

The 1/rev data for the 35,000-pound configuration are shown in Figures 78 and 79. Cockpit levels exceed 0.1g at 160 knots, producing displacements as high as 0.15 inch double amplitude. Figure 80 is a comparison of 1/rev levels from the glass blade program with those recently recorded with boron blades on the aft head. High-speed cockpit vertical 1/rev vibration is comparable for both blade configurations. It is interesting to note, however, that aft cabin 1/rev levels are reduced significantly, indicating the impact of a closely matched blade set. Cockpit lateral 1/rev vibration is also a measure of aft rotor head tracking due to an aft pylon lateral mode which results in lateral cockpit response. The lateral 1/rev levels at station 95 centerline are reduced approximately 40 percent.

Effect of Gross Weight

Figures 81 and 82 compare 3/rev vibration levels for three gross weight configurations evaluated during the boron blade program. As shown, cockpit vertical vibration levels grew worse during the heavy-gross-weight flights. The 245-rpm operating rotor speed and the increased rotor loads have all but eliminated the effectiveness of the cockpit absorbers at airspeeds approaching V_{max}.

Midcabin results were mixed. Left side vertical 3/rev levels increased, especially at 51,000 pounds, but other locations improved with added weight. Reductions in 3/rev levels were most notable at the lower airspeeds. Midcabin and aft cabin lateral vibration increased substantially at the higher gross weights.

Aft cabin vertical levels also show definite increases during the high-gross-weight flights. At 140 knots, 3/rev vibration doubles between the 34,000- and 45,400-pound configurations. At 120 knots, levels again increase by approximately 40 percent as the run gross weight increases to 51,000 pounds.

Figure 83 compares 3/rev vibration data obtained from the harmonic analysis program for a series of maneuvers performed at three gross weights. The gross weight effect is similar to that during level-flight conditions. Aft cabin vibration levels during the turns (nominally, 130 knots) doubled during the flight at 35,000 pounds gross weight.

Effect of Altitude

Figures 84 and 85 compare selected altitudes from three separate flights for each of the pickup locations. As can be seen, the variations in gross weight and the effects of airspeed do not allow a clear interpretation of altitude effects. At some locations the data are bracketed by the 5,000-foot (high data) and 6,500-foot (low data) airspeed sweeps. To better examine the effect of altitude, a climb to altitude is shown in Figure 86. At 90 knots the cockpit absorbers maintain 3/rev levels at a minimum. At midcabin, vertical levels increase by 60 percent as the aircraft climbs from 100 to 11,000 feet density altitude. The aft cabin 3/rev levels increase 2-1/2 times, peaking at 0.44g at 11,000 feet.

Boron Versus Fiberglass and Production Blade Configuration

Figure 87 compares cockpit and cabin 3/rev data obtained during evaluation of the boron and fiberglass advanced-geometry blades and CH-47 compliance data. Cockpit vertical levels were worse than the other two configurations during the boron blade evaluation flight at high airspeeds due to the cockpit absorber problem. Cockpit lateral and longitudinal vibration levels on the helicopter with either advanced-geometry blade configuration were slightly lower than the production CH-47C levels with metal blades.

At midcabin the ballast arrangement (water tanks) on the aircraft reduced the high 3/rev airframe vibration that is normally associated with the CH-47C at BL 44. The aft set of boron blades produced about twice the 3/rev response of the all-glass blade configuration at 160 knots.

The aft cabin levels are higher with the boron blade configuration than with either the glass advanced-geometry blades or the CH-47C production configuration. The stiffer blades on the aft head have, as suspected, created a higher 3/rev environment due to the proximity of the first flap mode to the 3/rev rotor excitation frequency. Flap bending moments on the aft blade are high but not critical at both the low-airspeed and high-airspeed conditions, which accounts for the severity of the valleys in the cabin vibration data curves. Analysis of 3/rev flap bending response during a rotor speed sweep revealed 3/rev bending moments increasing with decreasing rpm, suggesting that the first flap mode of the boron blade is still below the operating rotor speed range of the CH-47C helicopter. This indication is contradictory to predicted first mode rotating natural frequency trends.

The three blade configurations are compared in Figure 88 at gross weights of approximately 48,000 pounds. The boron blade configuration attained an airspeed of 150 knots, while only 130 and 140 knots were flown with the glass and production blades. Cockpit vibration levels are worse for the boron blade flight due to limited effectiveness of the self-tuning vibration absorbers as a result of increased rotor speed and loads and high airspeed. Increases in vibration levels at station 50 at the low airspeeds resemble the cabin trends that resulted from the higher flap bending moments of the boron blades. It is probable that the aft blades are contributing to cockpit 3/rev loads, especially at the higher gross weights.

Cabin vibration levels reflect trends similar to those for the comparisons at lighter weight. Aft cabin levels with the boron blades are nearly twice the level with the glass advanced-geometry blades installed.

Figure 89 compares cockpit vibration levels for a series of maneuvers with the three blade configurations. Cabin levels were not available for all flights and are not shown. The maneuvers produced nearly identical cockpit 3/rev responses at all locations, regardless of rotor blade. The difference in the turn data at station 50 is due to the effect of a large airspeed differential.

Summary

The effect of the advanced-geometry boron blades on aircraft vibration was limited to aft cabin response. The cockpit vibration environment was clouded by high 1/rev levels resulting from dynamic dissimilarities in the fiberglass advanced-geometry blades on the forward rotor hub and the deterioration of 3/rev levels due to ineffectiveness of the self-tuning absorbers at high speeds. In the aft cabin at station 482, 1/rev levels with boron blades were half the value measured during the glass blade program; cockpit lateral 1/rev vibration was reduced 40 percent, indicating that geometric properties of the stiffer blades were more uniform and that blade tracking minimized aerodynamic differences. Aft cabin 3/rev vertical levels were generally higher than either the glass or the production configuration. The data show significant increases at the low-airspeed and high-airspeed conditions. Furthermore, at the higher-gross-weight configurations, there is evidence that the boron blades are contributing to 3/rev loads in the cockpit. The contribution of the third rotor harmonic to aft rotor blade flap bending moment corresponds to the vibration increases. It was forecast that the stiffer boron blades would increase 3/rev vibration due to the proximity of the first flap mode to the n/rev frequency of the CH-47C. It is concluded that, while the elimination of blade geometry inconsistencies is desirable from a 1/rev vibration standpoint, a blade flap mode near n/rev would compound cockpit and cabin vibration problems in a CH-47-type helicopter.

Mechanical Instability

As part of the safety-of-flight review package, an analysis of mechanical instability characteristics was conducted for a nominal 40,000-pound configuration. Blade properties were updated to reflect lag moment and inertia changes between the glass advanced-geometry blades and the boron configurations.

The analytical results and summary are given in Figure 90. The summary shows that the updated blade properties produced no significant changes in mechanical instability characteristics from the glass blade analysis and concludes with a statement that ground testing of the glass blades resulted in stable characteristics for all configurations and conditions. It was concluded that the boron blades would provide the same stability; this was later verified by mechanical instability ground testing on the testbed aircraft.

Compatibility Analysis

Because of dissimilar uncoupled blade lag frequencies between the forward and aft rotors, a check of drive system natural frequencies was performed for the safety-of-flight review of the boron blade flight test program. Figure 91 shows the analytical results with drive system natural frequencies noted where the residual torque goes to zero. Torsional modes are excited by primary rotor harmonics, thereby making the drive system frequencies, close to 3/rev, 6/rev, 9/rev, etc., the most critical.

A list of uncoupled and coupled modes in Figure 92 summarizes the analytical results. A coupled mode of the forward rotor system at 6.07/rev was considered a possible problem due to possible resonance with 6/rev of the rotors. However, as the mode involved blade rigid lag motion out of phase with blade flexible motion, there was a good chance the mode would not be excited. Results during flight testing of the advanced-geometry boron blades did not indicate large 6/rev rotor shaft torque loads.

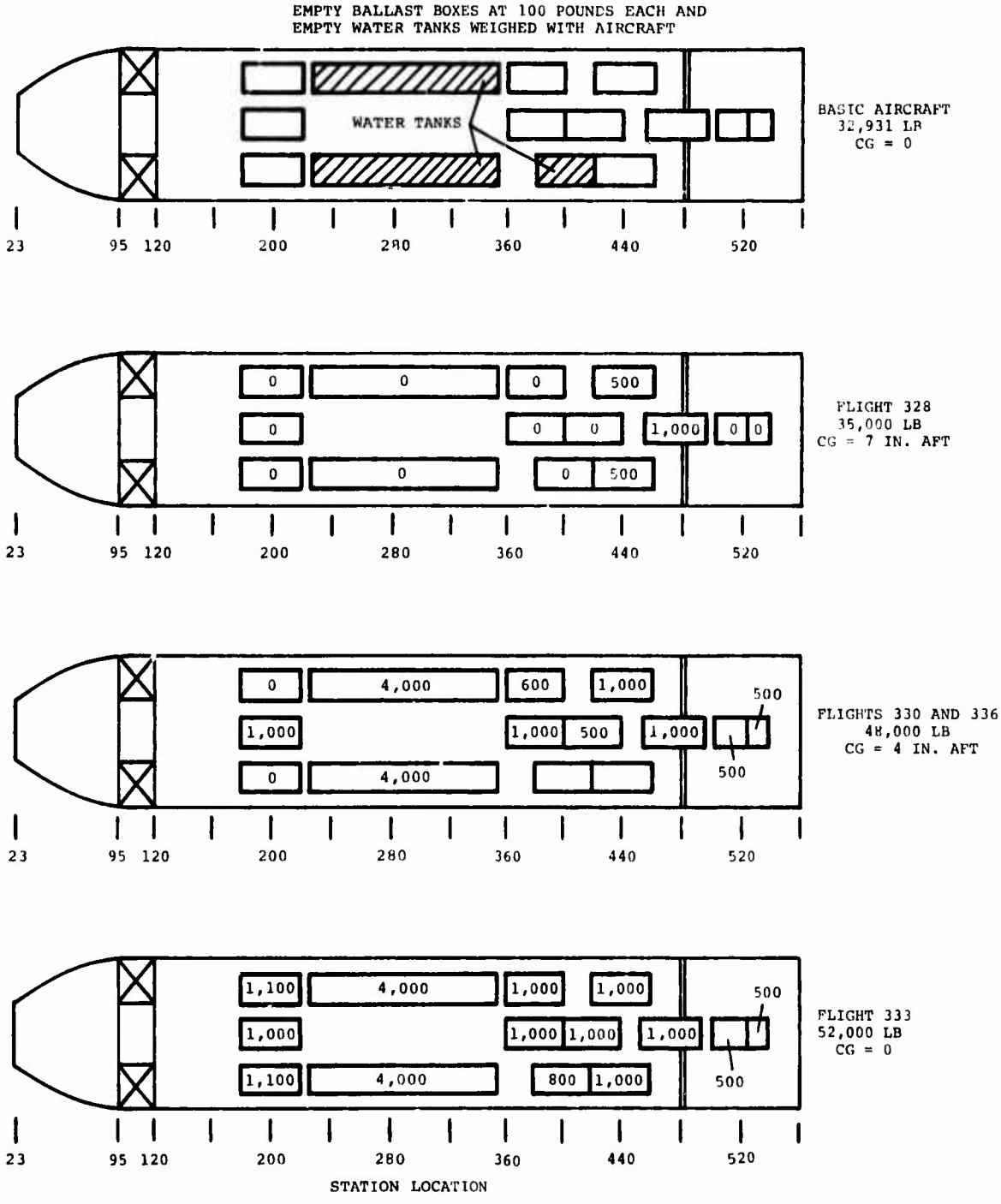

Figure 74. Aircraft Ballast Diagram for Flight Test of Boron Blades.

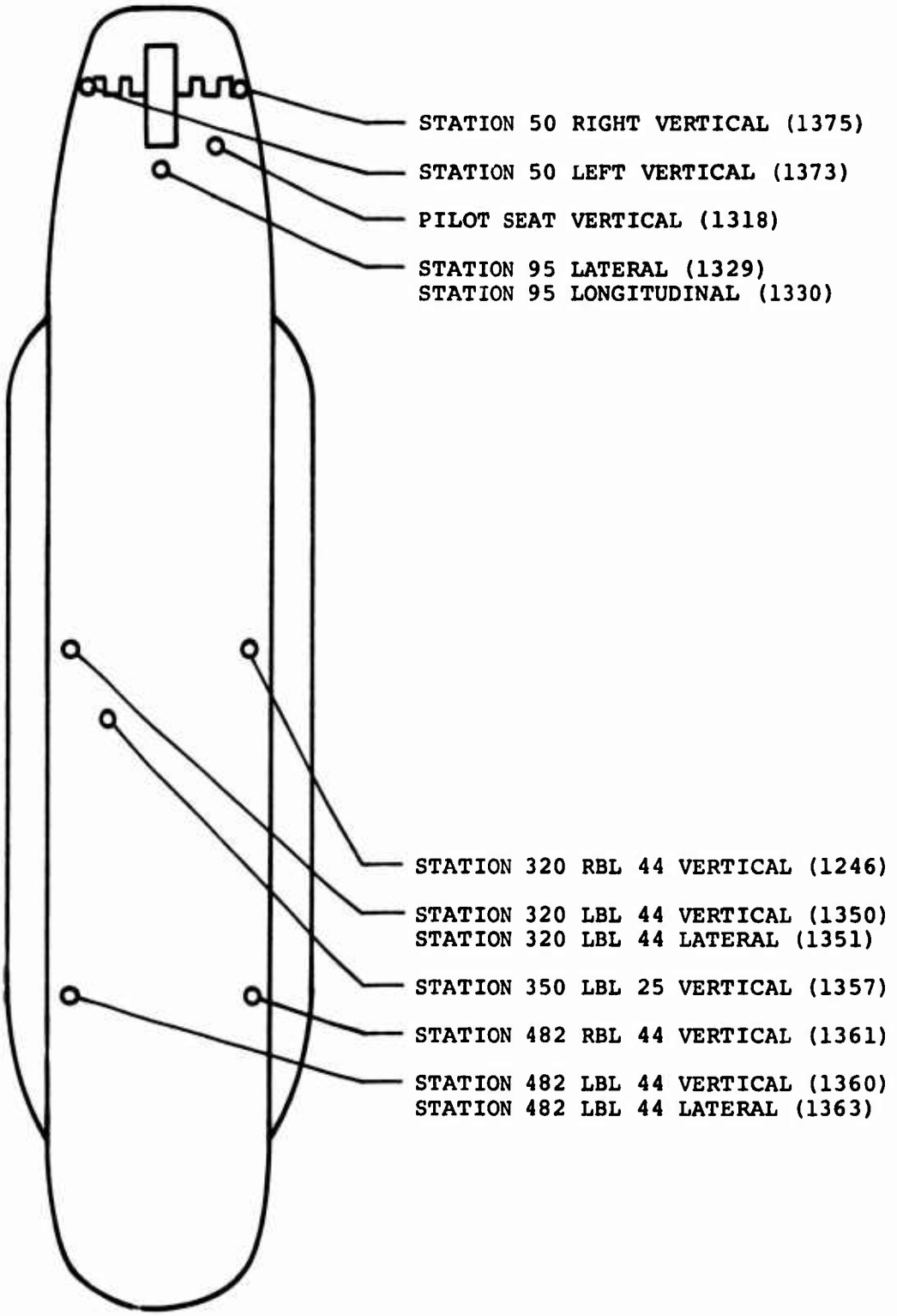

Figure 75. Helicopter Vibration Instrumentation for Flight Test of Boron Blades.

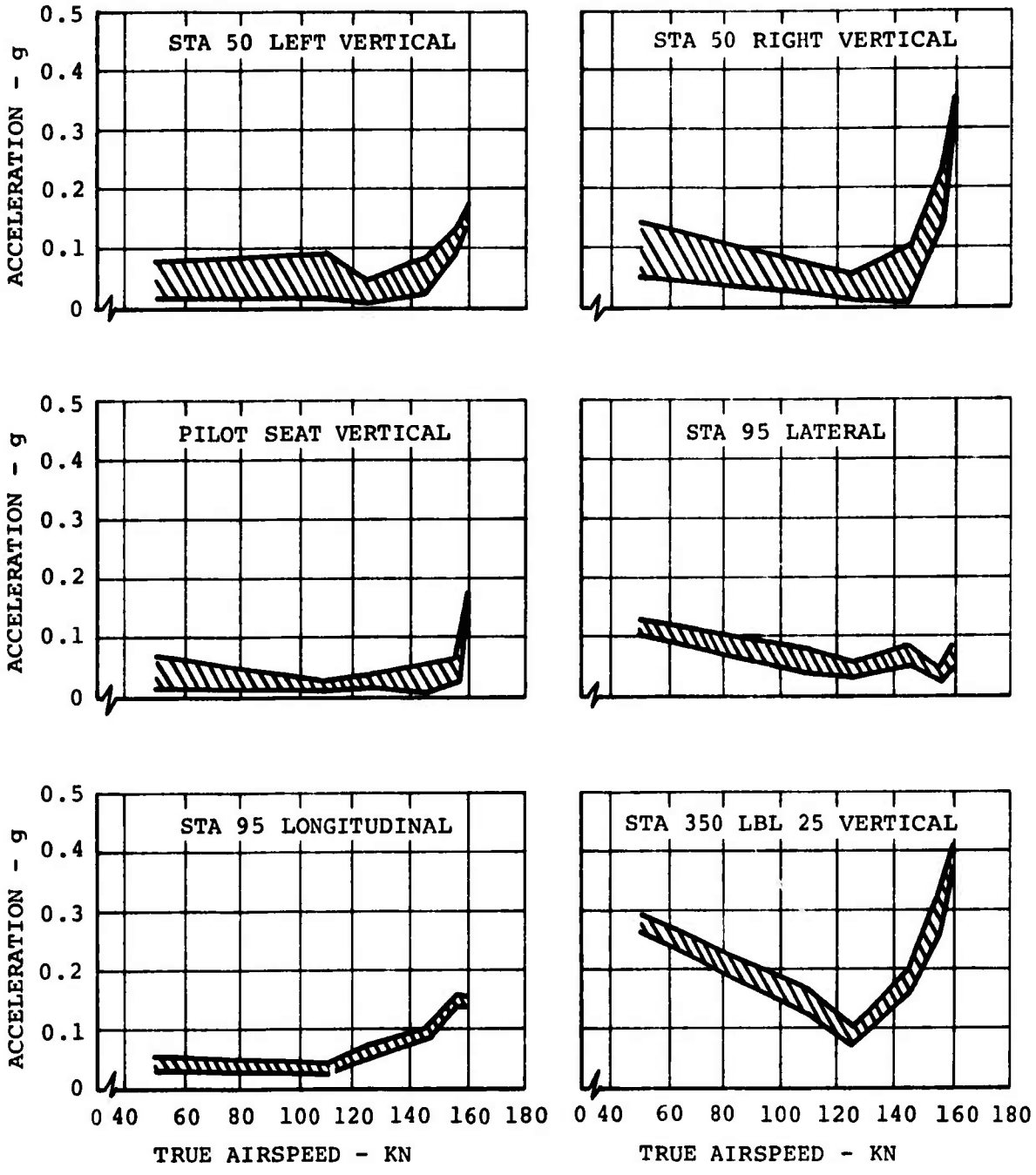

Figure 76. Basic 3/Rev Vibration Levels at Stations 50, 95, and 350 and at Pilot Seat During Flight Test of Boron Blades.

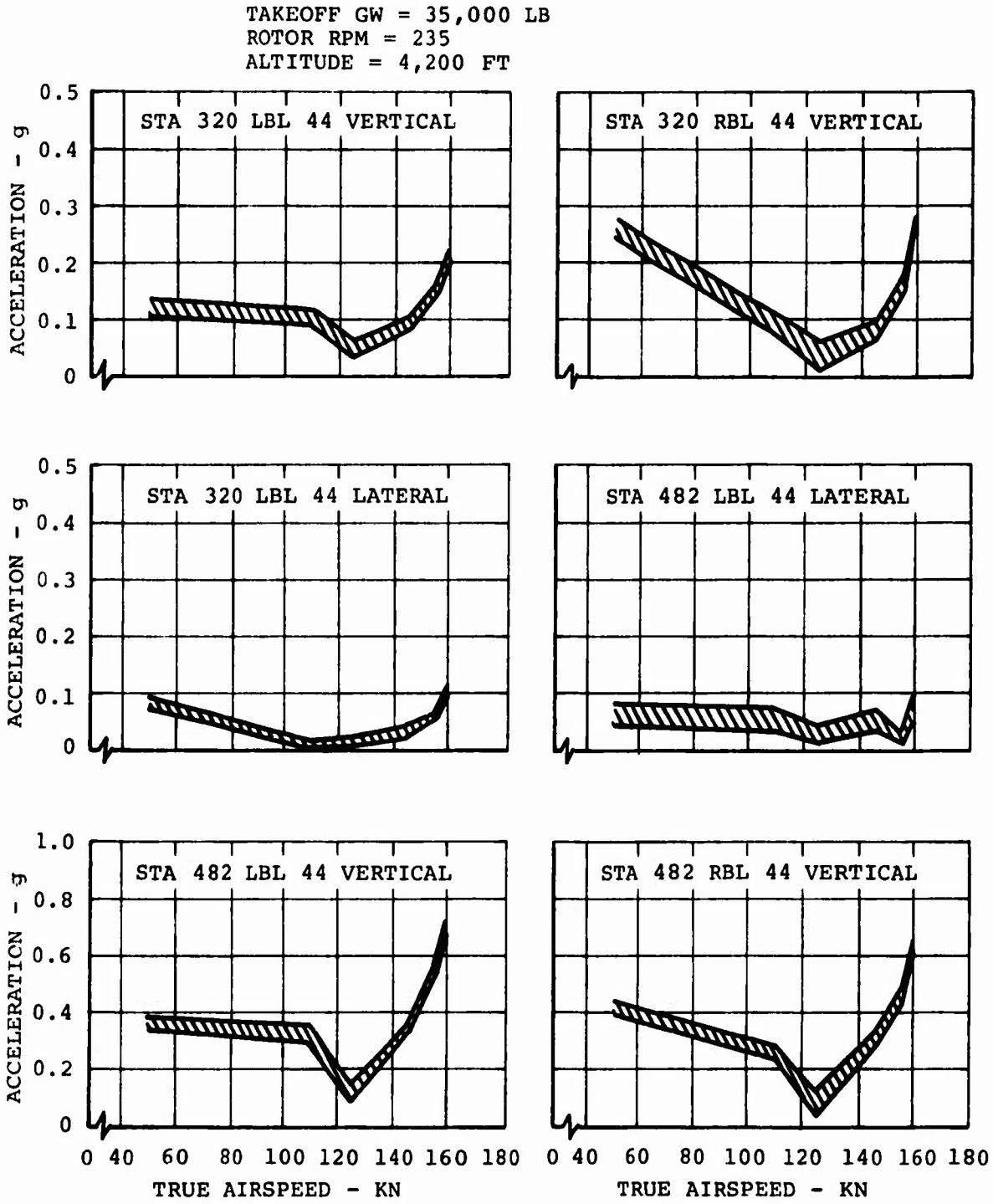

Figure 77. Basic 3/Rev Vibration Levels at Stations 320 and 482 During Flight Test of Boron Blades.

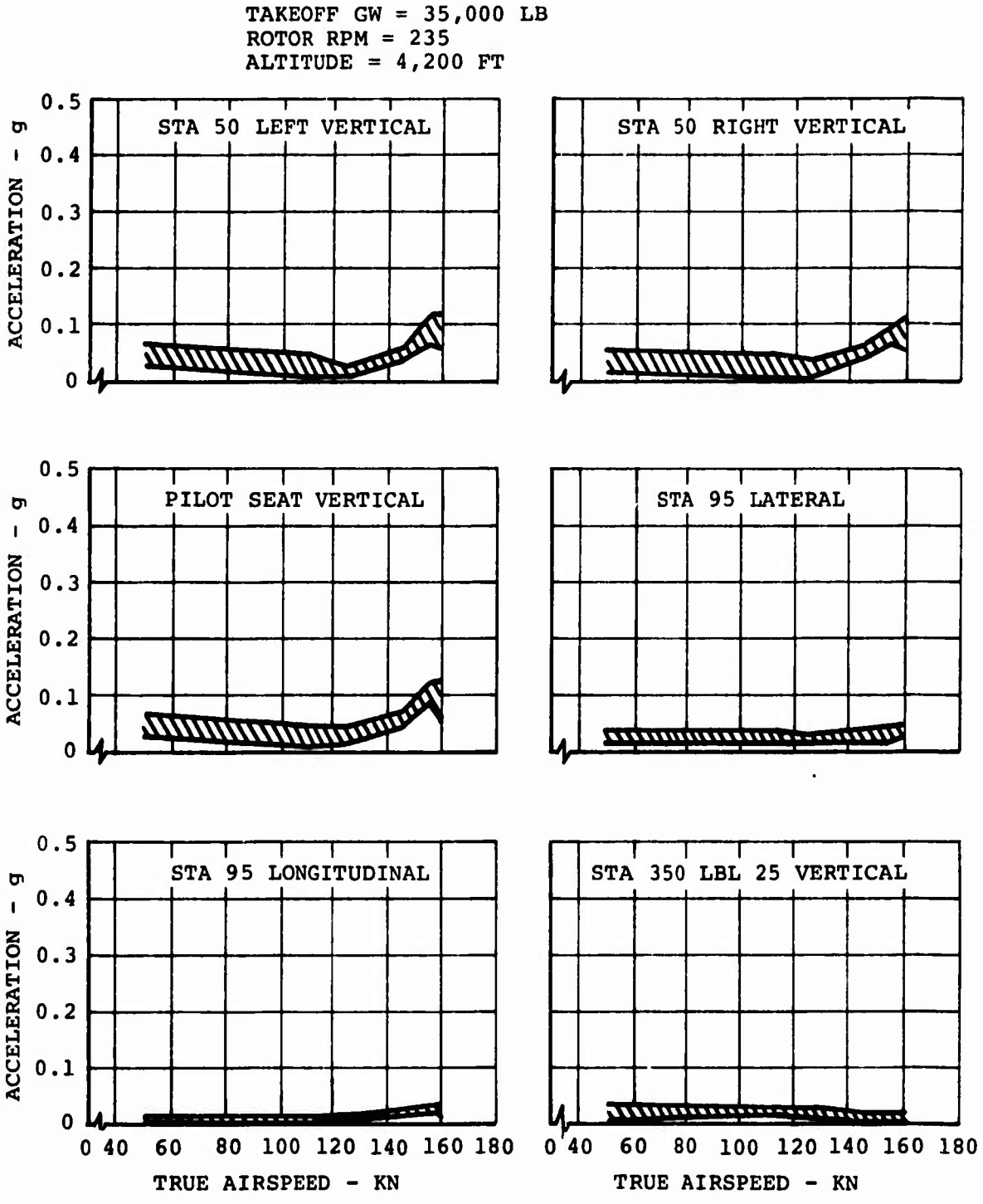

Figure 78. Basic 1/Rev Vibration Levels at Stations 50, 95, and 350 and at Pilot Seat During Flight Test of Boron Blades.

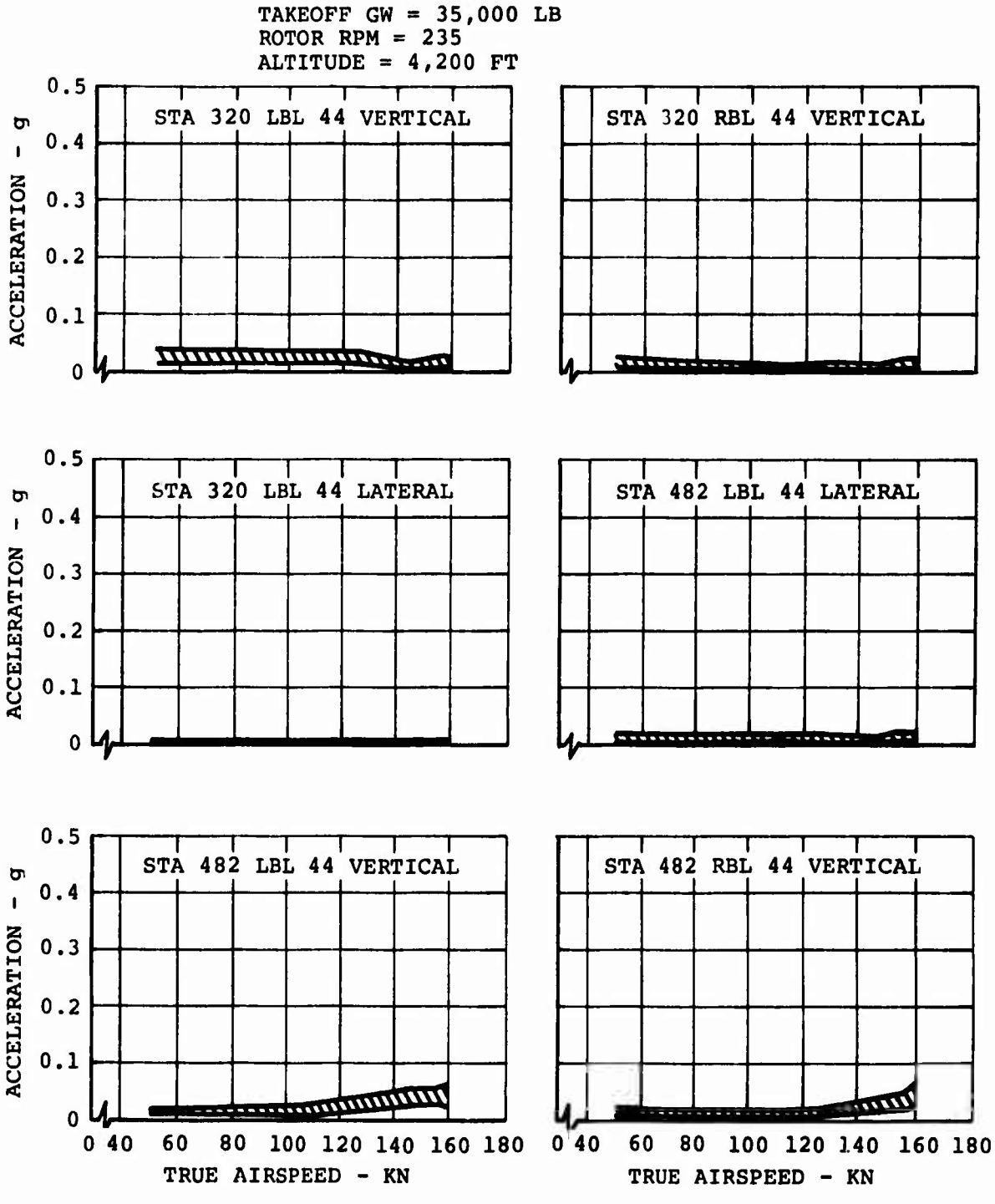

Figure 79. Basic 1/Rev Vibration Levels at Stations 320 and 482 During Flight Test of Boron Blades.

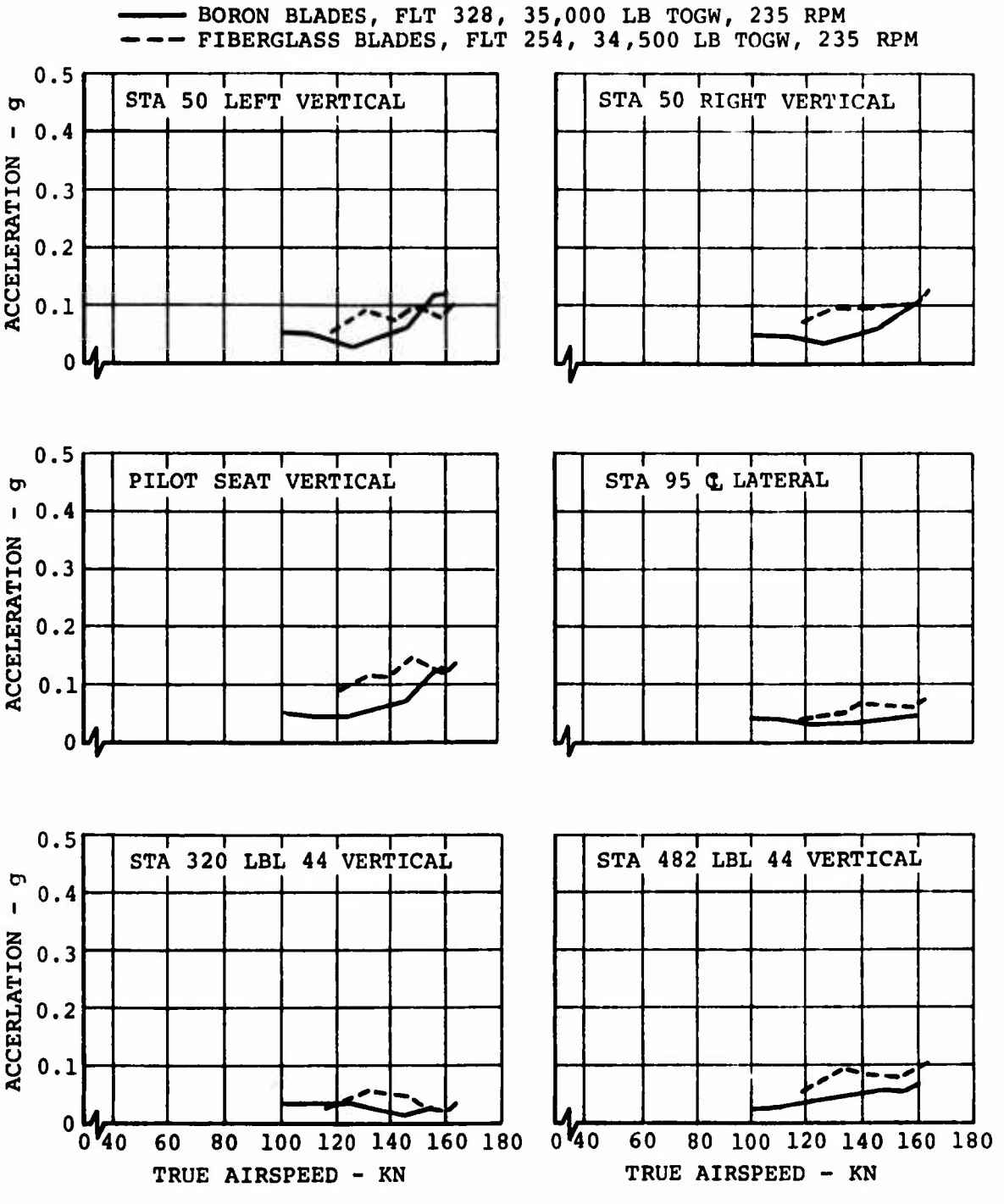

Figure 80. Comparison of 1/Rev Vibration Levels of Fiberglass and Boron Advanced-Geometry Blades.

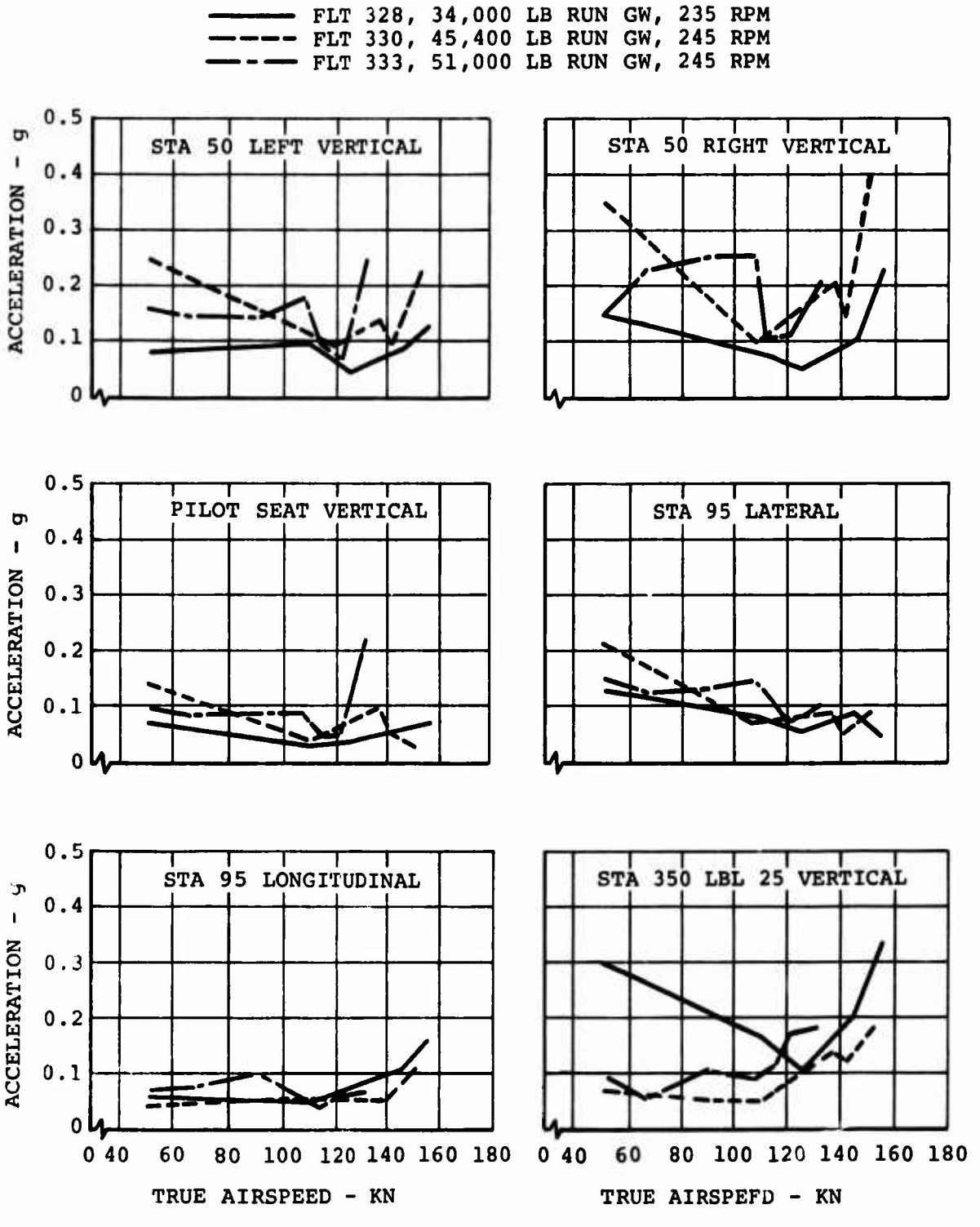

Figure 81. Effect of Gross Weight on 3/Rev Vibration Levels at Stations 50, 95, and 350 and at Pilot Seat During Flight Test of Boron Blades.

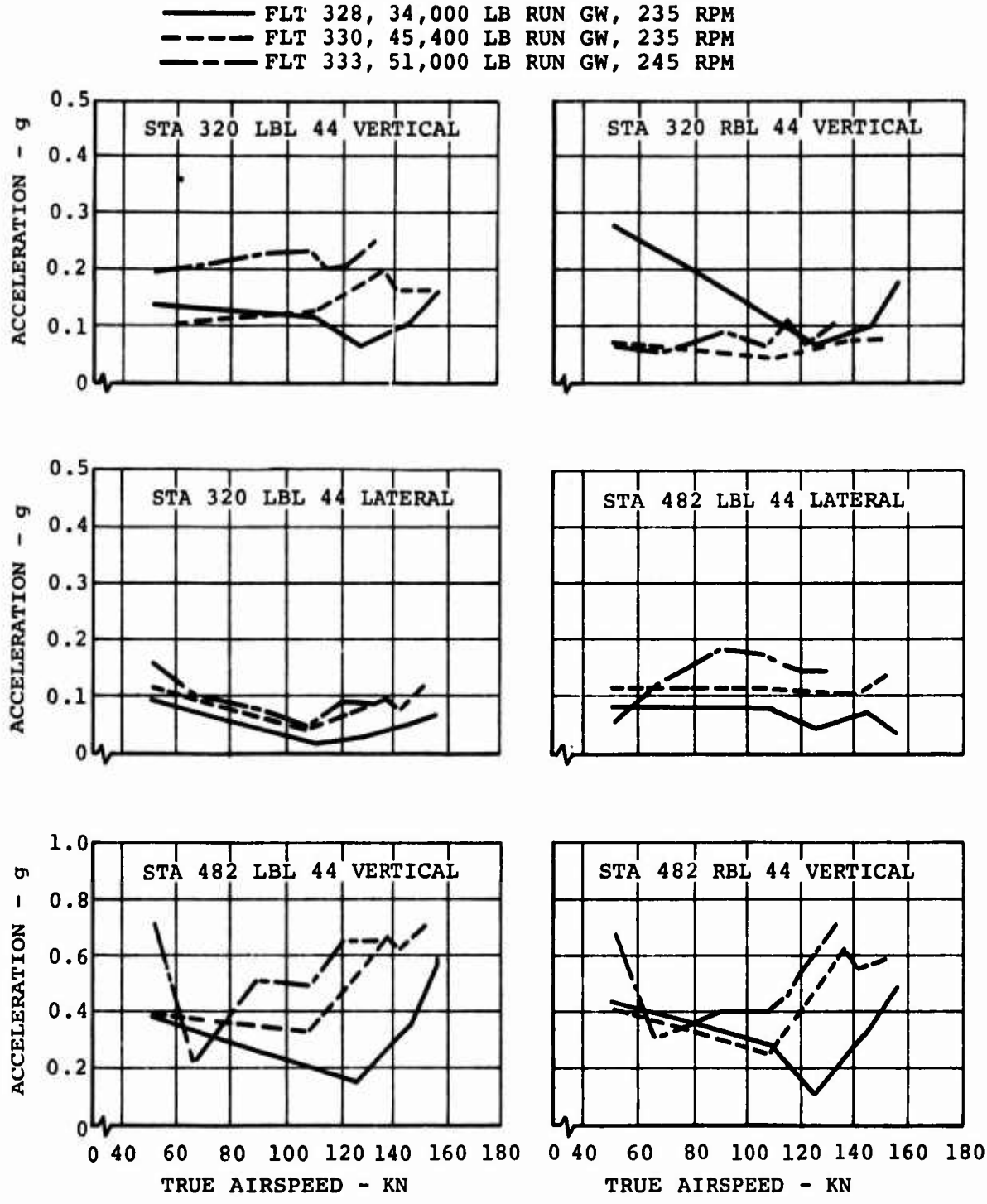

Figure 82. Effect of Gross Weight on 3/Rev Vibration Levels at Stations 320 and 482 During Flight Test of Boron Blades.

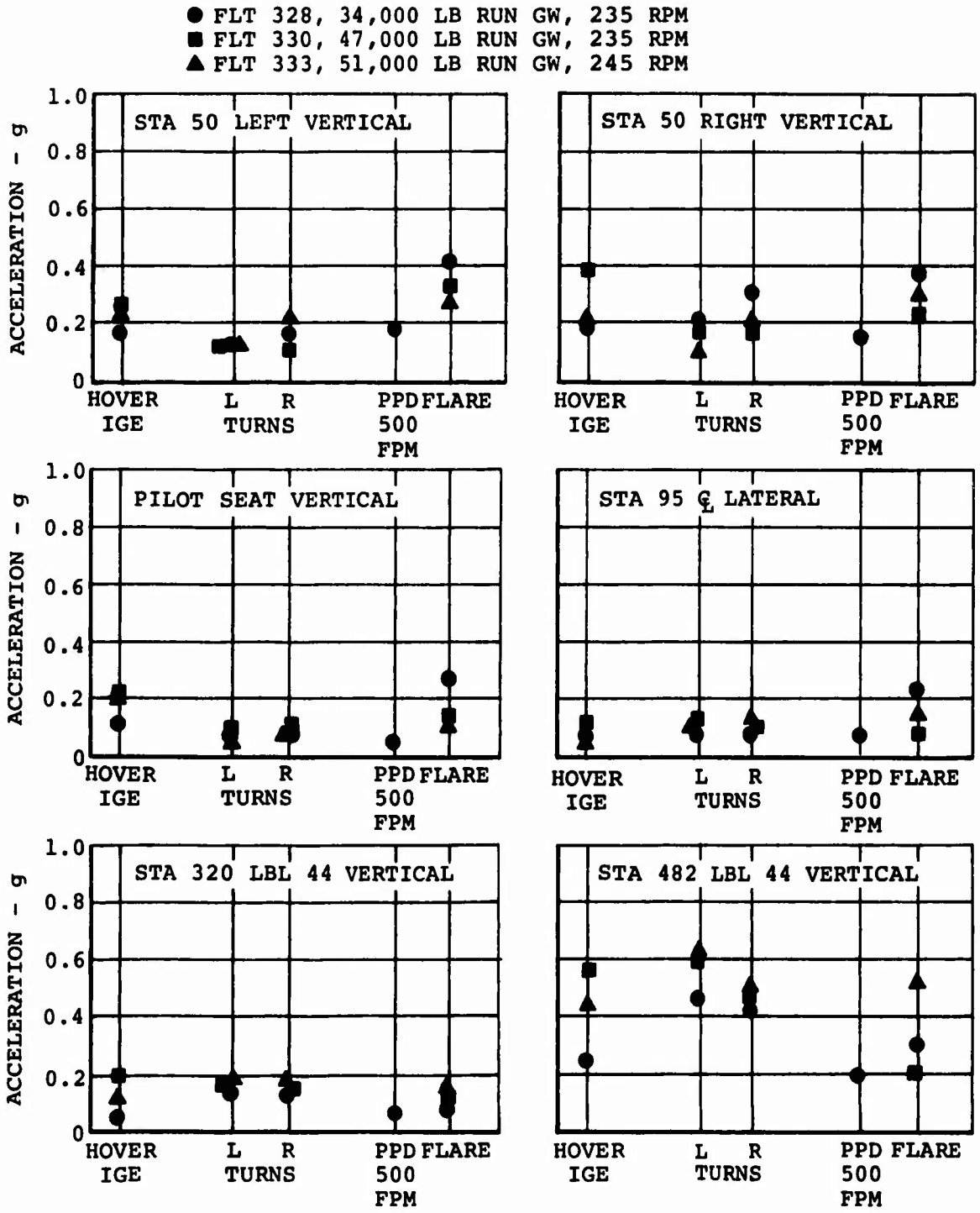

Figure 83. Effect of Gross Weight and Maneuvers on 3/Rev Vibration Levels During Flight Test of Boron Blades.

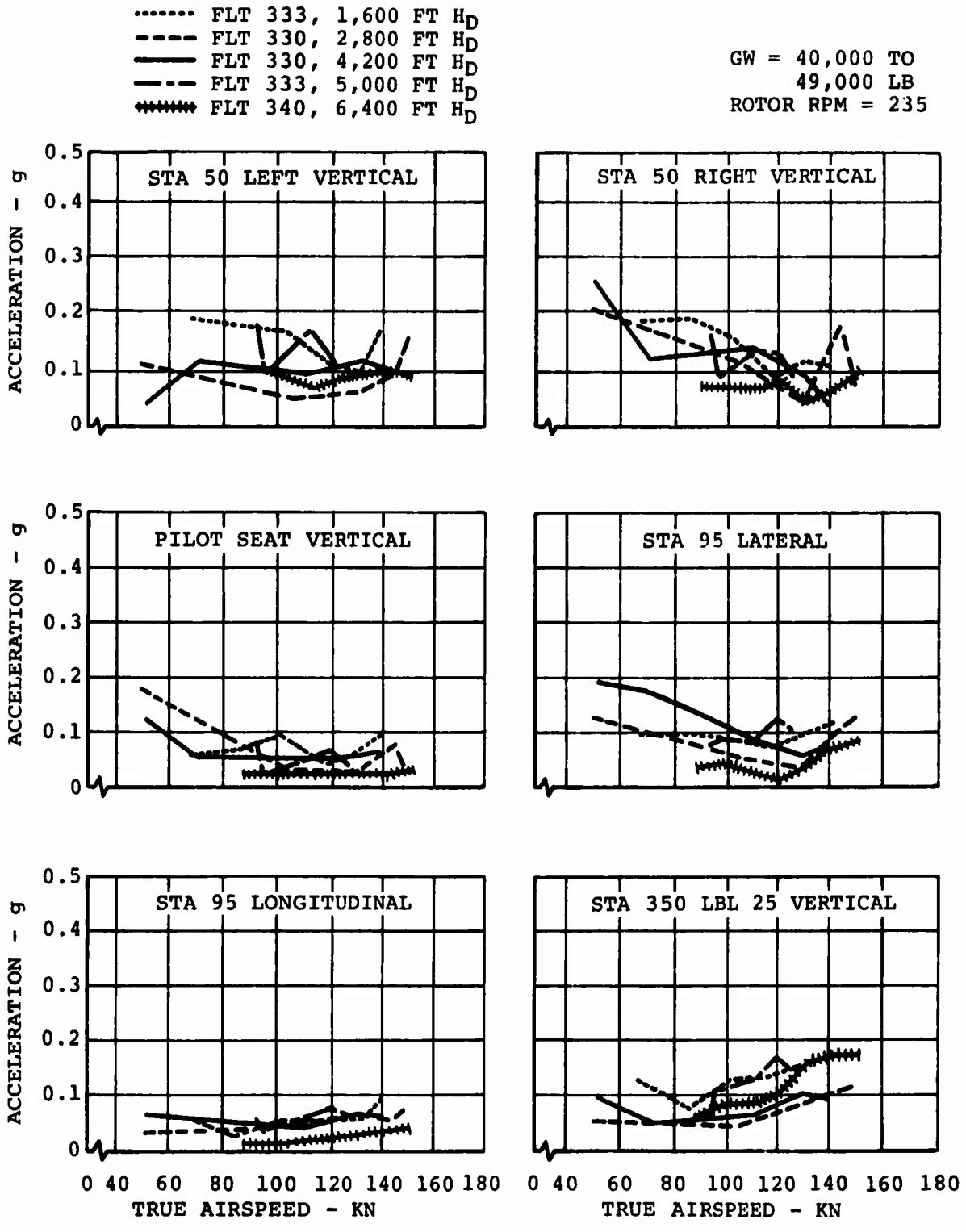

Figure 84. Effect of Altitude on 3/Rev Vibration Levels at Stations 50, 95, and 350 and at Pilot Seat During Flight Test of Boron Blades.

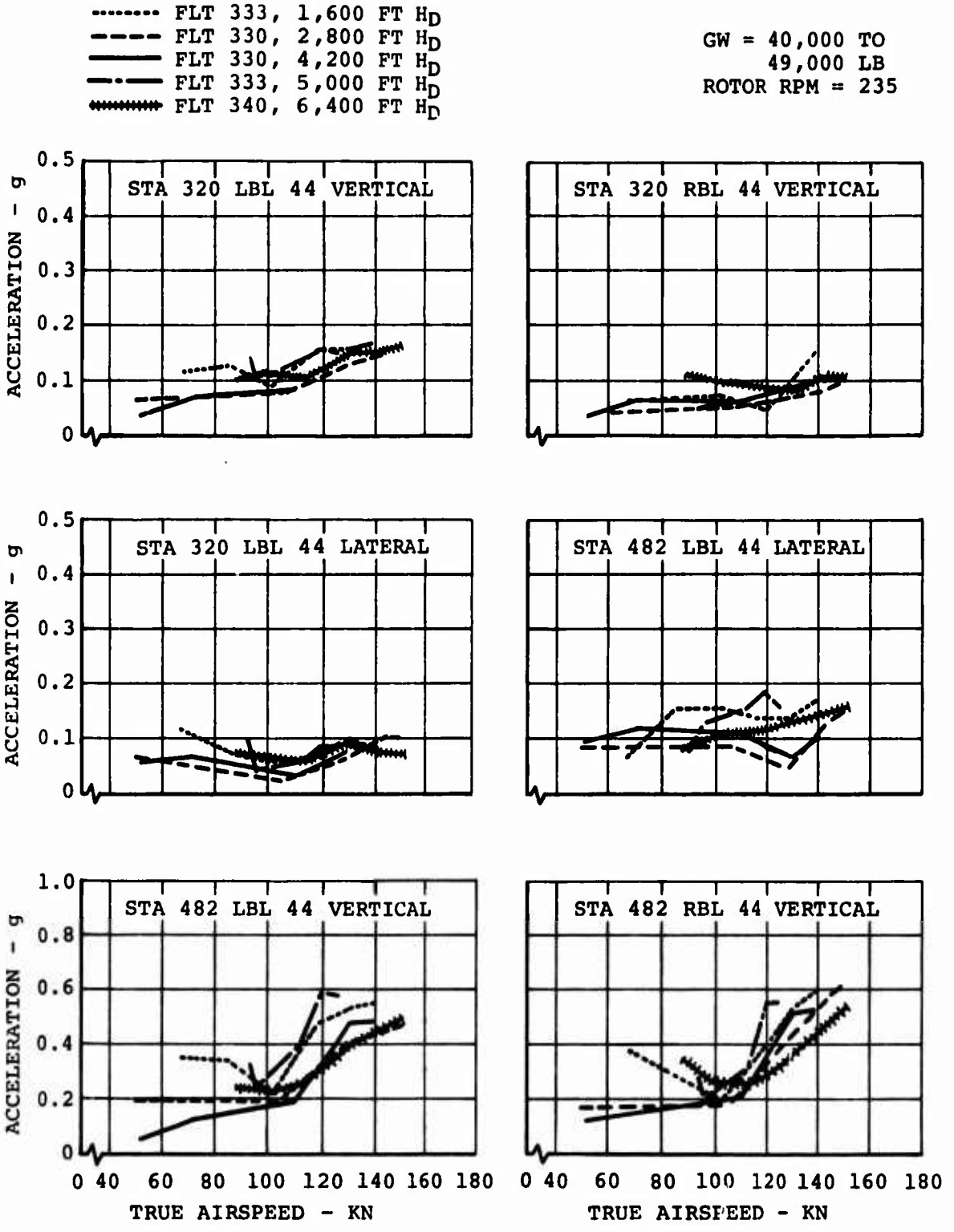

Figure 85. Effect of Altitude on 3/Rev Vibration Levels at Stations 320 and 482 During Flight Test of Boron Blades.

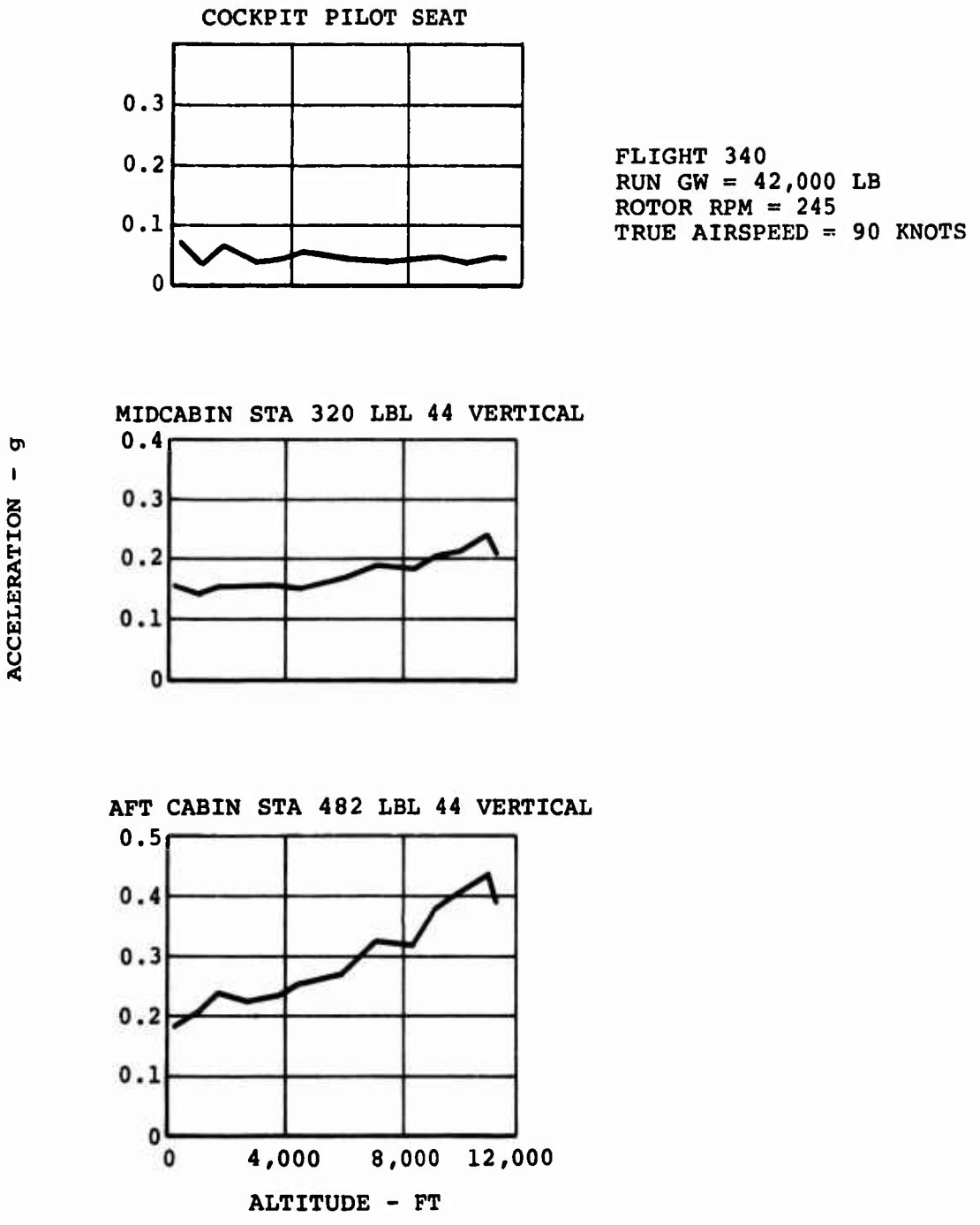

Figure 86. Effect of Altitude on 3/Rev Vibration Levels at Stations 320 and 482 and at Pilot Seat During Flight Test of Boron Blades.

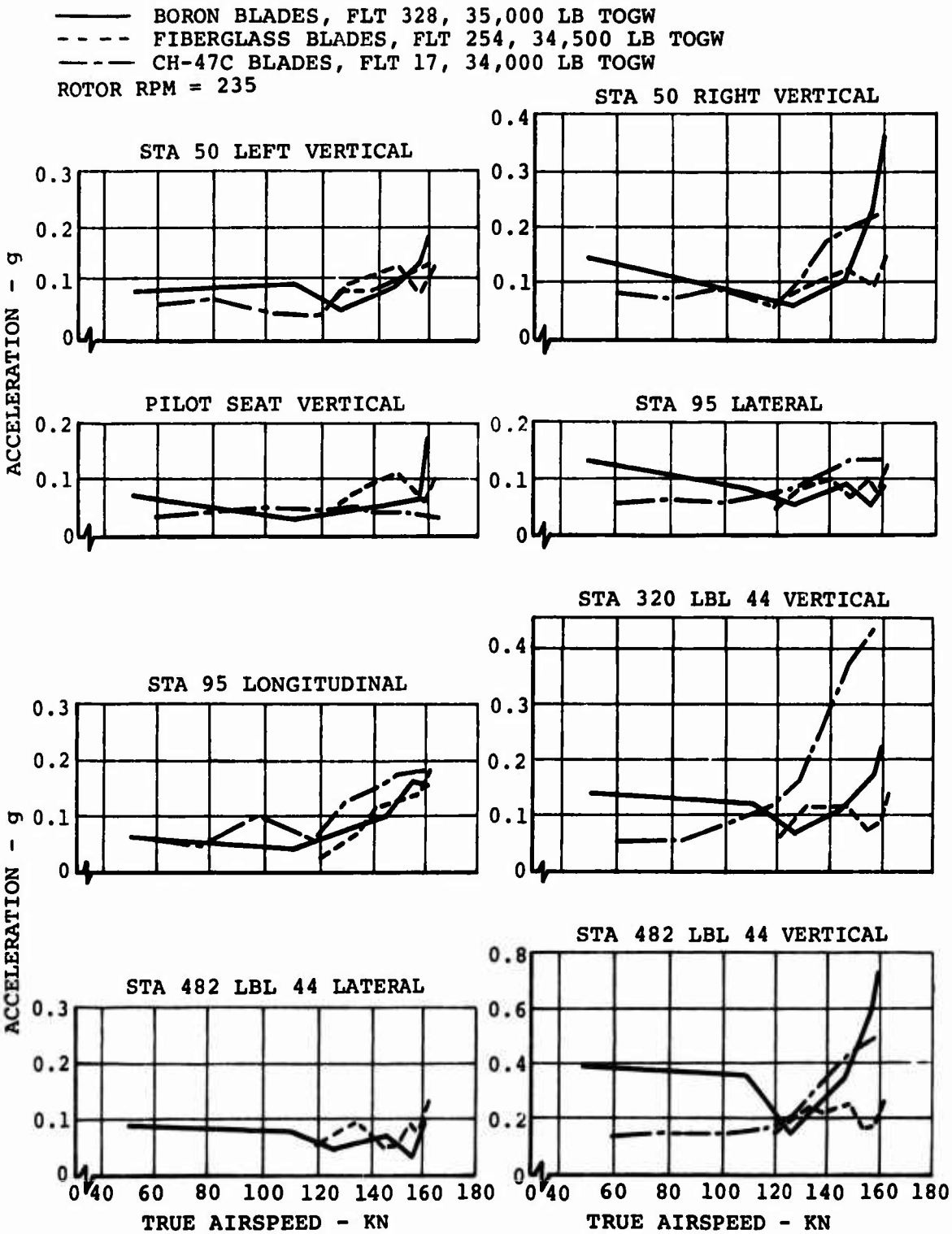

Figure 87. Comparison of 3/Rev Vibration Levels of Fiberglass and Boron Advanced-Geometry Blades and CH-47C Blades at Normal Gross Weight.

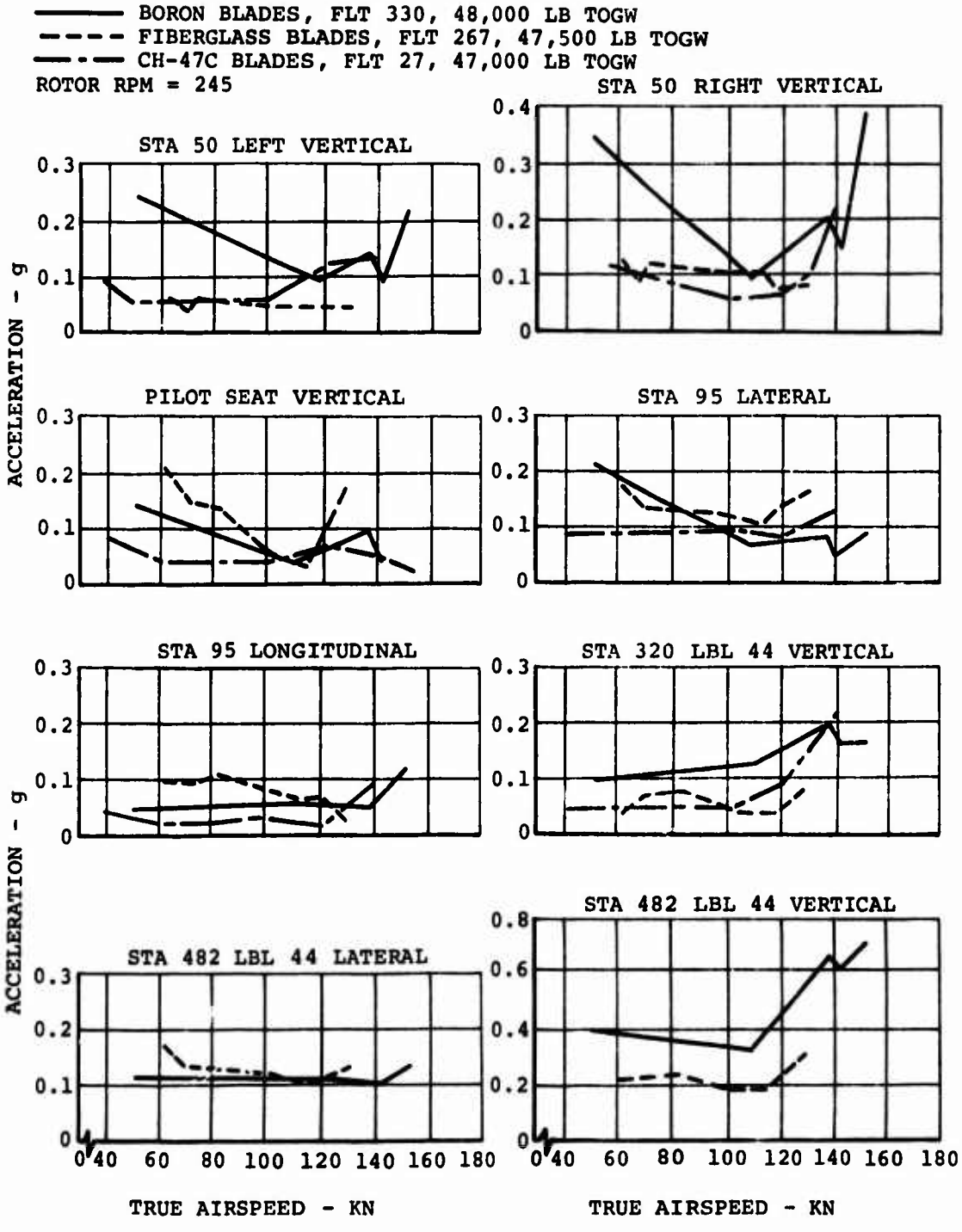

Figure 88. Comparison of 3/Rev Vibration Levels of Fiberglass and Boron Advanced-Geometry Blades and CH-47C Blades at Heavy Gross Weight.

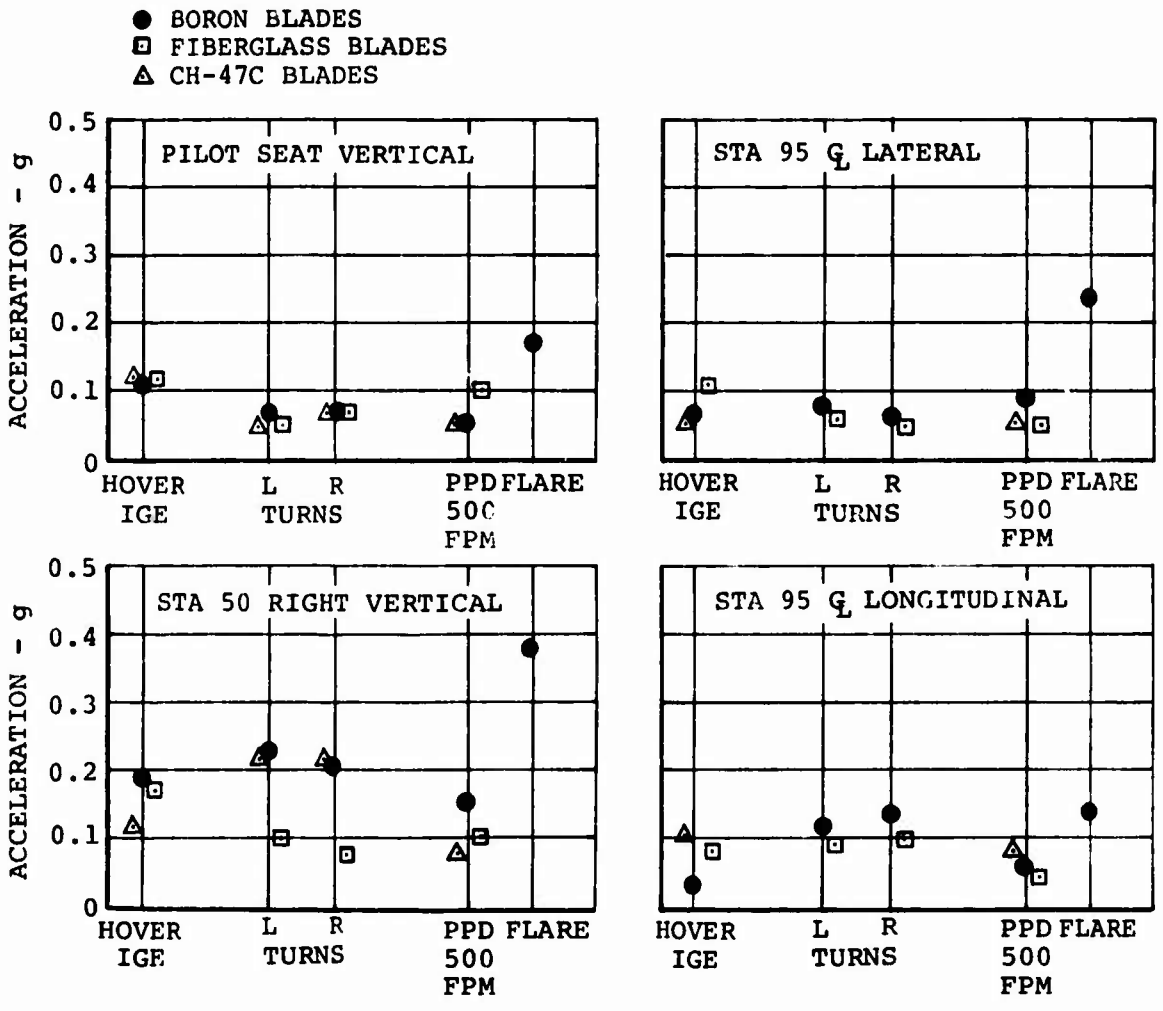

Figure 89. Comparison of Effect of Maneuvers on 3/Rev Vibration Levels of Fiberglass and Boron Advanced-Geometry Blades and CH-47C Blades.

BLADE PROPERTIES AFFECTING MECHANICAL INSTABILITY CHARACTERISTICS	STATIC LAG MOMENT ($LB\text{-}SEC^2$)	BLADE LAG INERTIA ($LB\text{-}SEC^2\text{-}IN.$)
CH-47C BLADES	121.3	26,740
GLASS AGB (ANALYSIS)	134.9	28,700
GLASS AGB (UPDATED)	134.8	28,850
BORON AGB (UPDATED)	143.0	32,720

NOTES:
1. GW = 40,000 LB
2. AFT GEAR SWIVELS LOCKED
3. SMALL INCREASES IN BLADE LAG MOMENT AND INERTIA PROPERTIES DO NOT PRODUCE SIGNIFICANT CHANGES IN MECHANICAL INSTABILITY CHARACTERISTICS.
4. THE MECHANICAL INSTABILITY ANALYSIS CASE RUN WITH UPDATED BORON BLADE PROPERTIES SHOWED NO SIGNIFICANT CHANGE FROM THE COMPARABLE CHARACTERISTICS OF THE FIBERGLASS BLADES.
5. QUALITATIVE PILOT EVALUATION OF THE MECHANICAL INSTABILITY CHARACTERISTICS OF THE FIBERGLASS ADVANCED-GEOMETRY BLADES SHOWED STABILITY FOR ALL CONFIGURATIONS AND CONDITIONS.

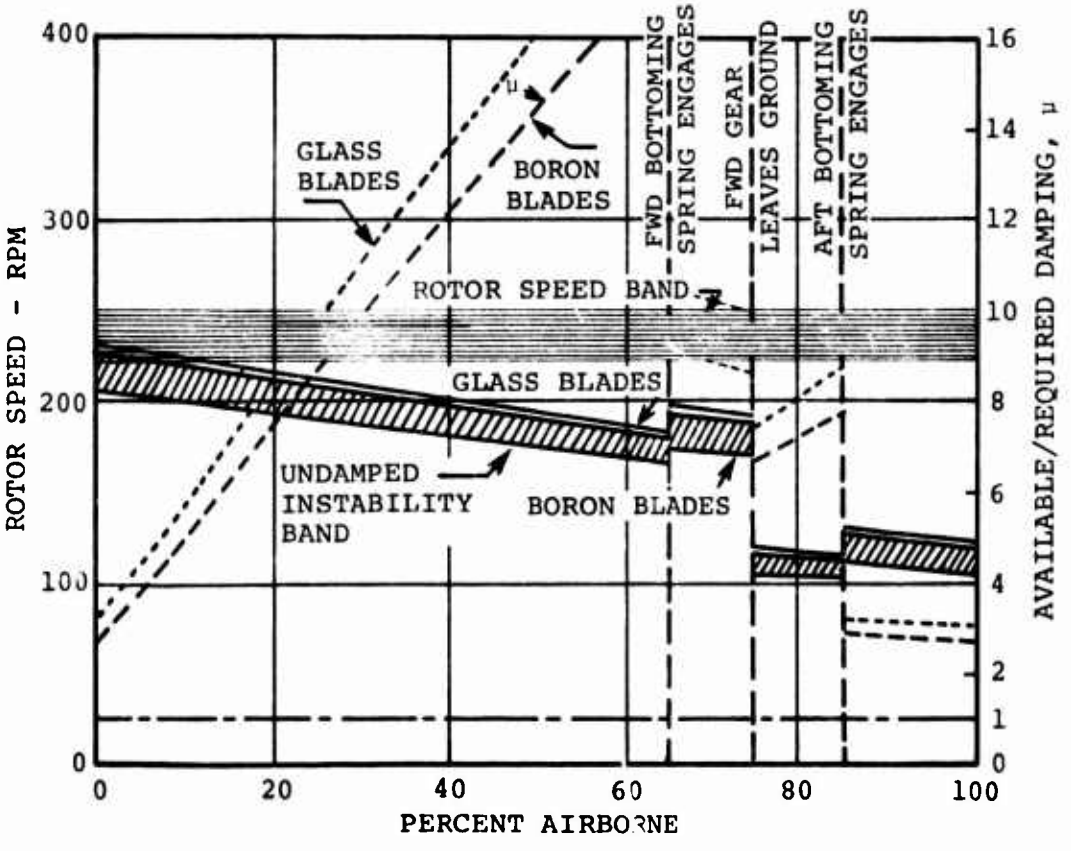

Figure 90. Mechanical Instability Analysis of the Boron Advanced-Geometry Blades.

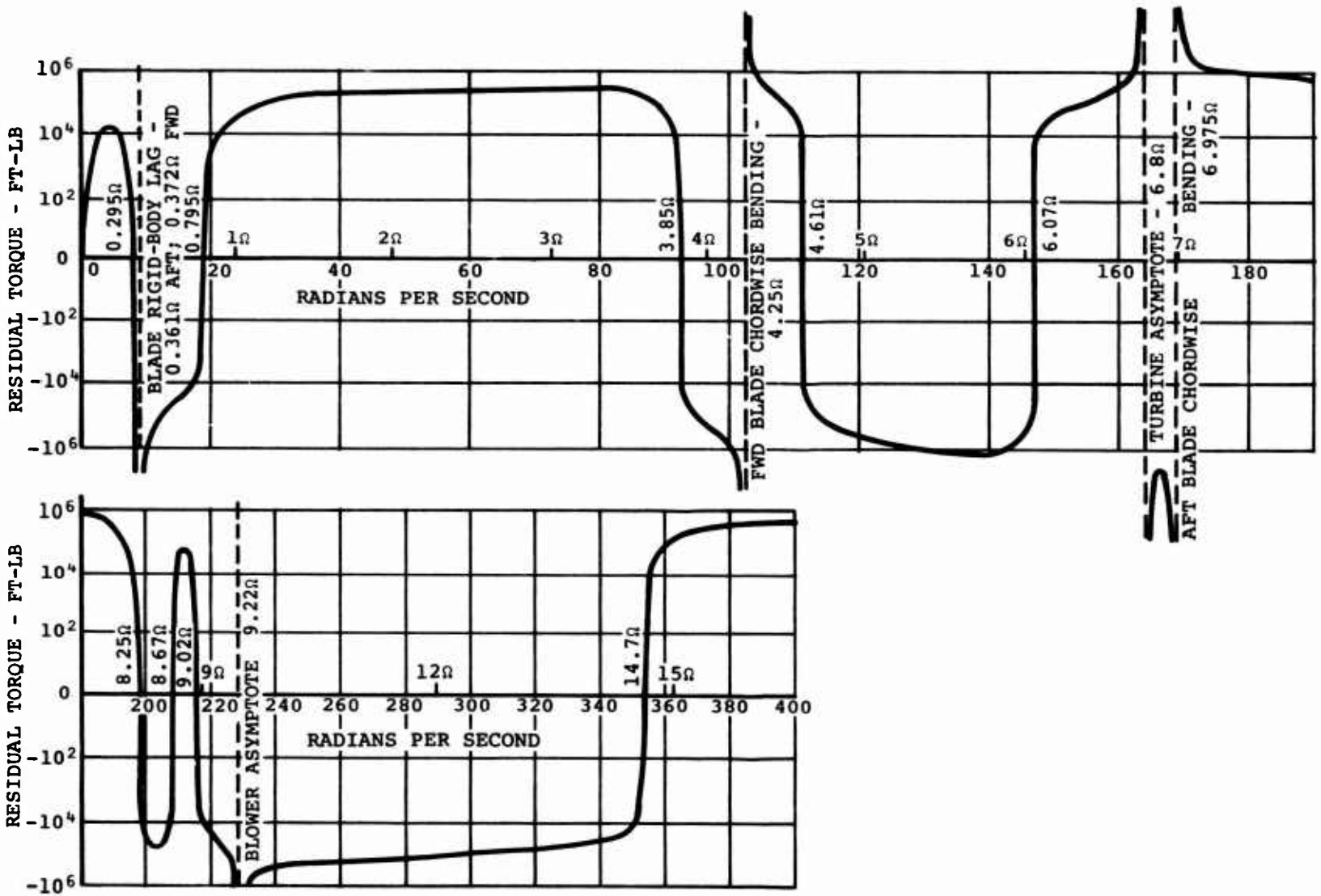

Figure 91. Residual Torque and Input Frequencies of the Forward Fiberglass and Aft Boron Advanced-Geometry Blades.

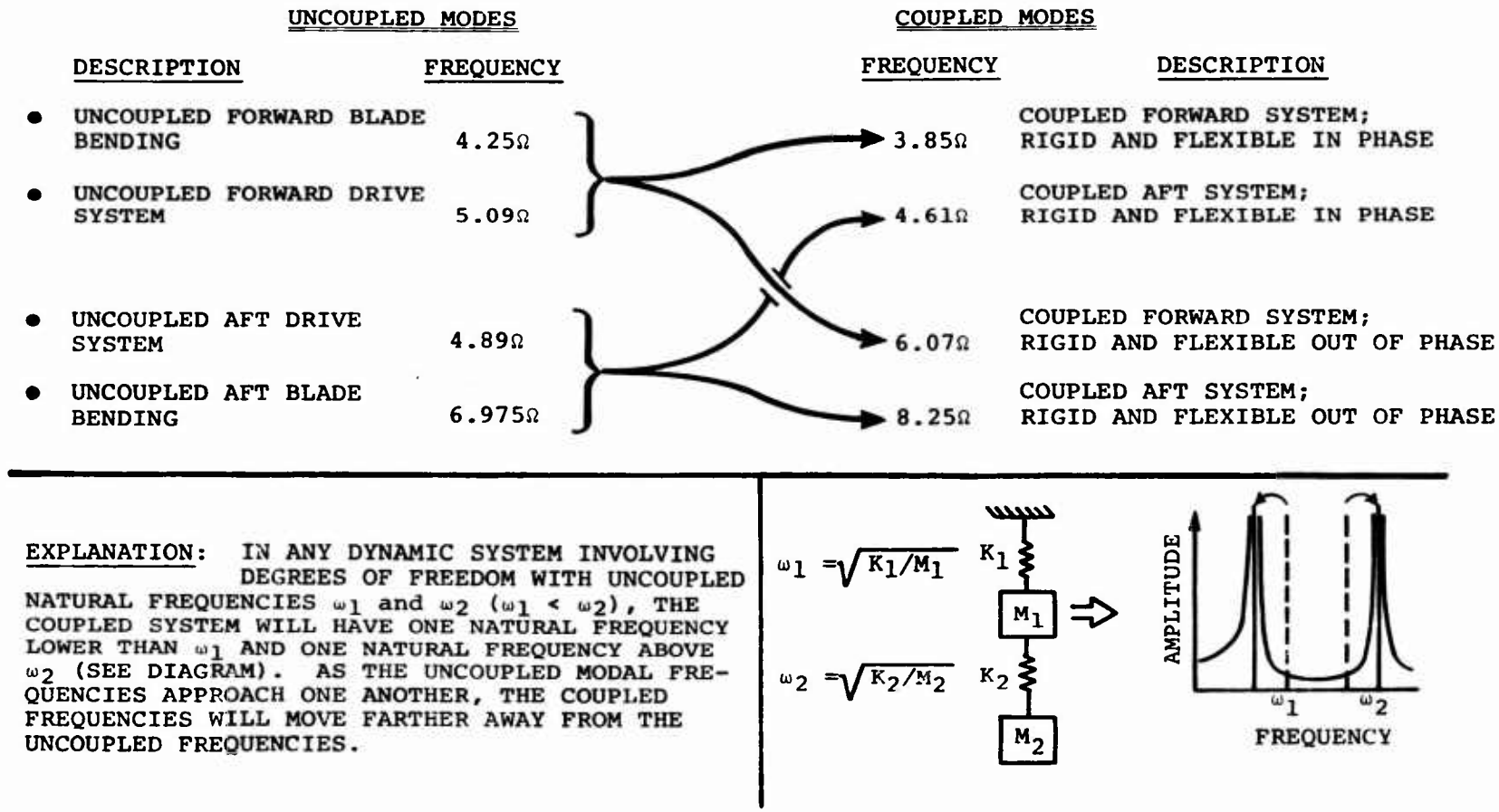

Figure 92. Comparison of Blade and Drive System Natural Frequency Modes.

FLYING QUALITIES

During the course of flight testing of the boron advanced-geometry rotor blades, qualitative pilot reports indicated that increased amounts of longitudinal and lateral trim control were required in level flight relative to that required for a CH-47C aircraft with standard blades. It was also reported that the longitudinal gradient with speed was more negative (i.e., increased aft stick trim with increased forward speed) than the standard CH-47C. Figures 93 through 96 provide the substantiating data for these qualitative reports. The boron blade trim control data reveal maximum lateral displacements of 70 to 78 percent and forward longitudinal displacements of 70 to 75 percent at 40 knots. Standard CH-47C control requirements under comparable flight conditions are 65 to 70 percent lateral stick and 63 to 67 percent longitudinal control.

Subsequent control rigging checks indicated that the lateral control was out of rig, with the stick centered position corresponding to 63.5 percent (RT. stick) on the position indicator. This discrepancy in rigging was corrected.

Data trends indicate that the longitudinal gradient becomes increasingly more negative as rotor speed is increased. Nominally the standard CH-47C gradient is slightly negative, varying from 4.5 to 8.0 percent longitudinal control over a 100-knot speed trim range with no obvious trend as a function of rpm. The negative gradients, as shown by the data, range from 12.5 to 23.5 percent longitudinal control over 100 knots for rotor speeds of 235 and 245 rpm, respectively. The cause for this deterioration in longitudinal stick gradient is not fully understood; however, an explanation has been offered.

The test aircraft was equipped with three fiberglass advanced-geometry blades on the forward rotor and three boron blades on the aft rotor. One significant difference between these two blades is that the torsional stiffness of the fiberglass blade is less than that of the boron blade. The significance attached to this fact is vested in the assumption that the rotor blade tends to wash out (decrease angle of attack) with increased centrifugal force (associated with increased rpm) and as collective pitch is increased. It follows that, as the forward rotor blade angle decreases elastically with increased rpm and collective relative to the aft rotor, the longitudinal stick trim will move aft.

The impact which these facts and assumptions have on the stick gradient characteristics is dependent on the relative difference in magnitude of the torsional stiffness between the fiberglass and boron blades. A detailed rotor system analysis is required to assess this theory and estimate the blade angle twist differences attributable to these flight conditions.

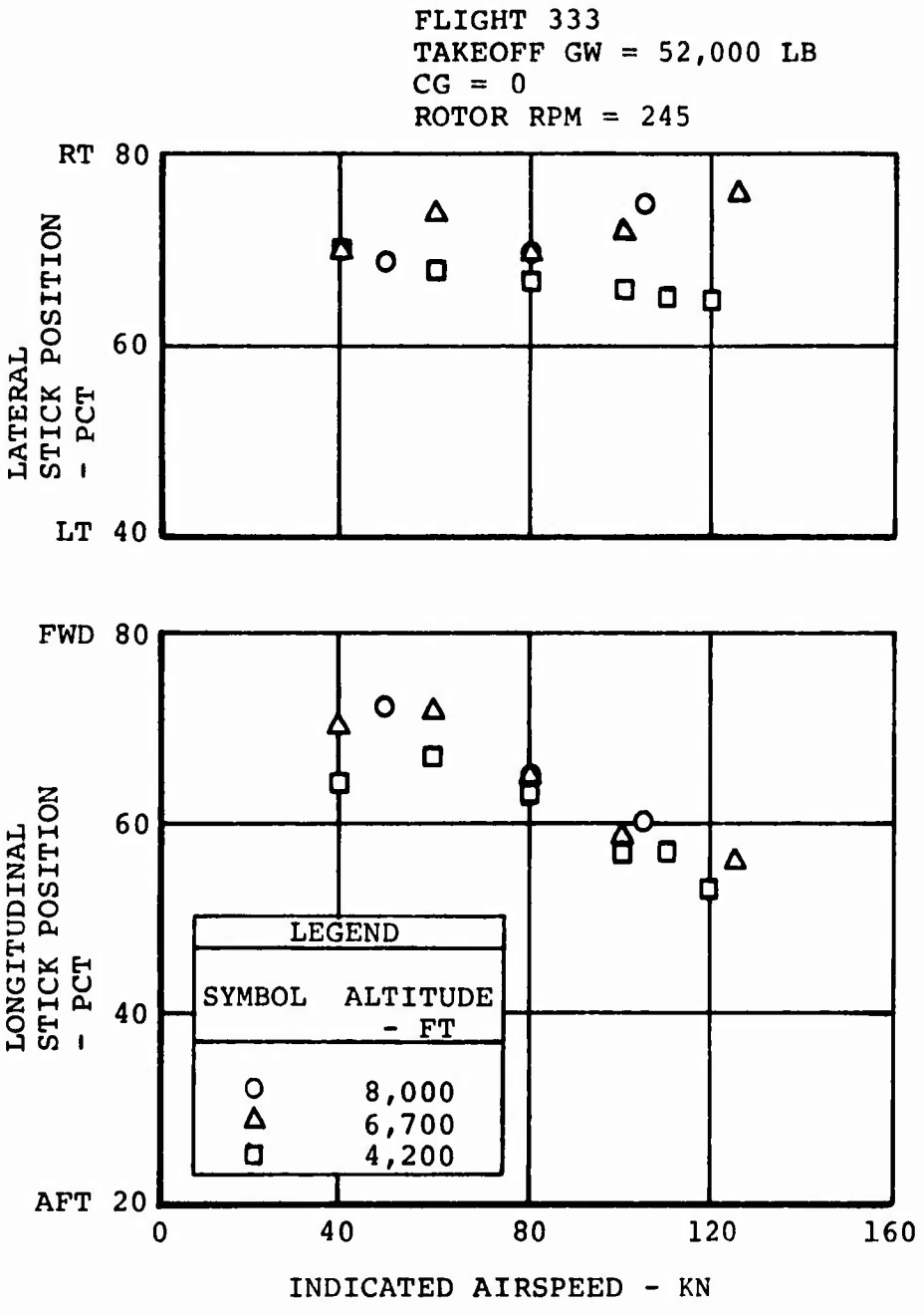

Figure 93. Aircraft Trim Control Positions During Flight Test of the Boron Advanced-Geometry Blades.

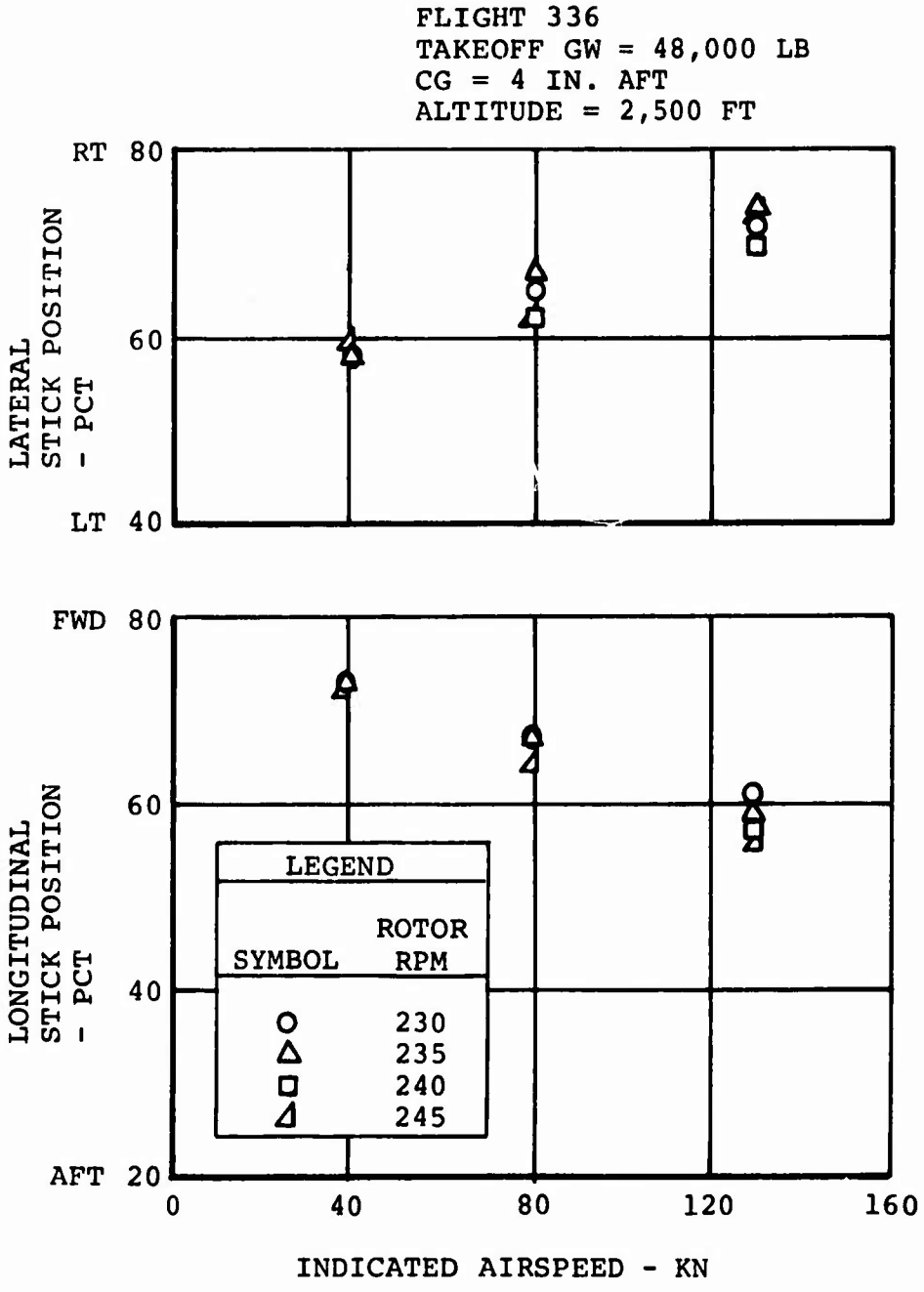

Figure 94. Aircraft Trim Control Positions During Flight Test of the Boron Advanced-Geometry Blades.

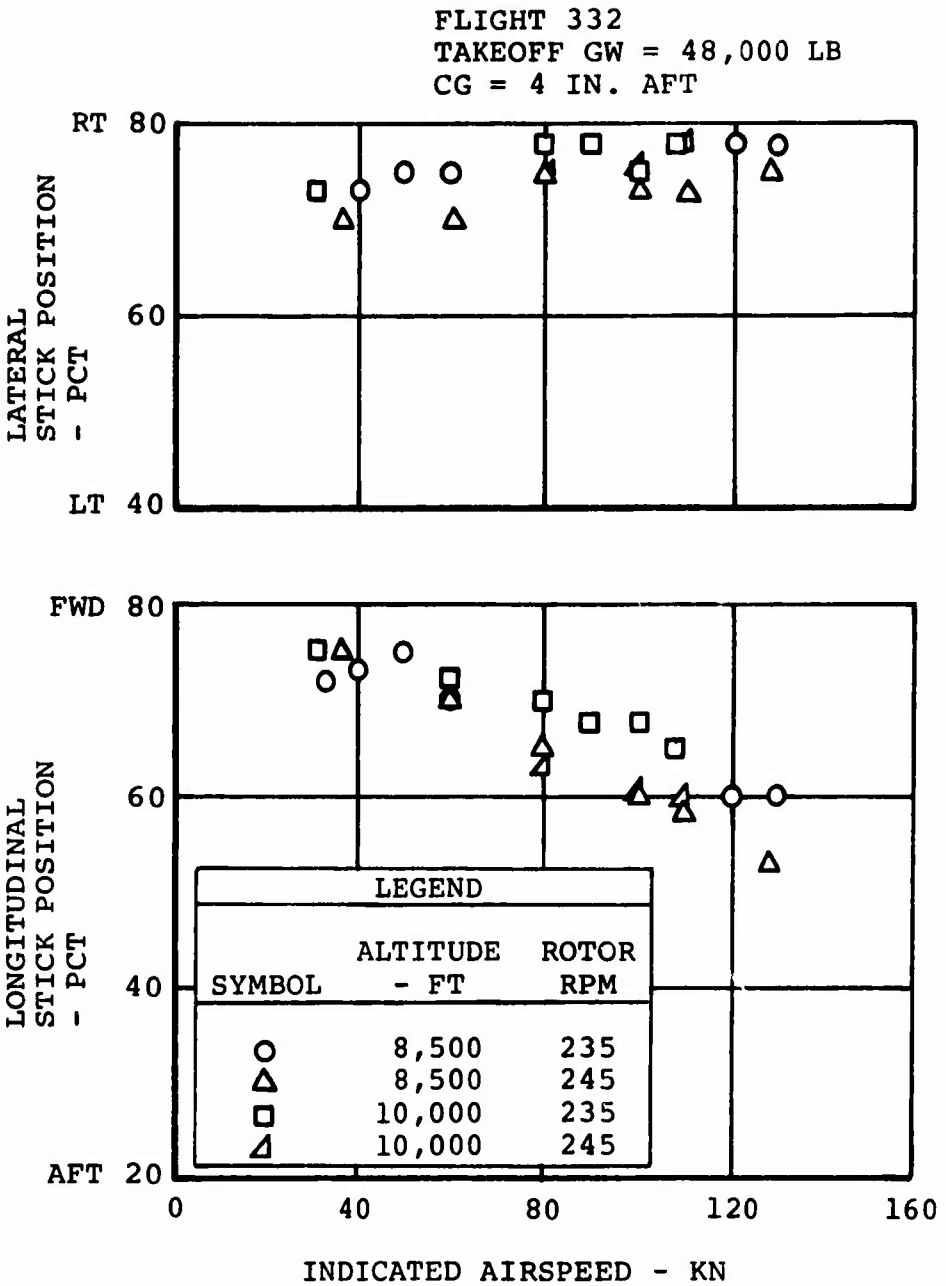

Figure 95. Aircraft Trim Control Positions During Flight Test of the Boron Advanced-Geometry Blades.

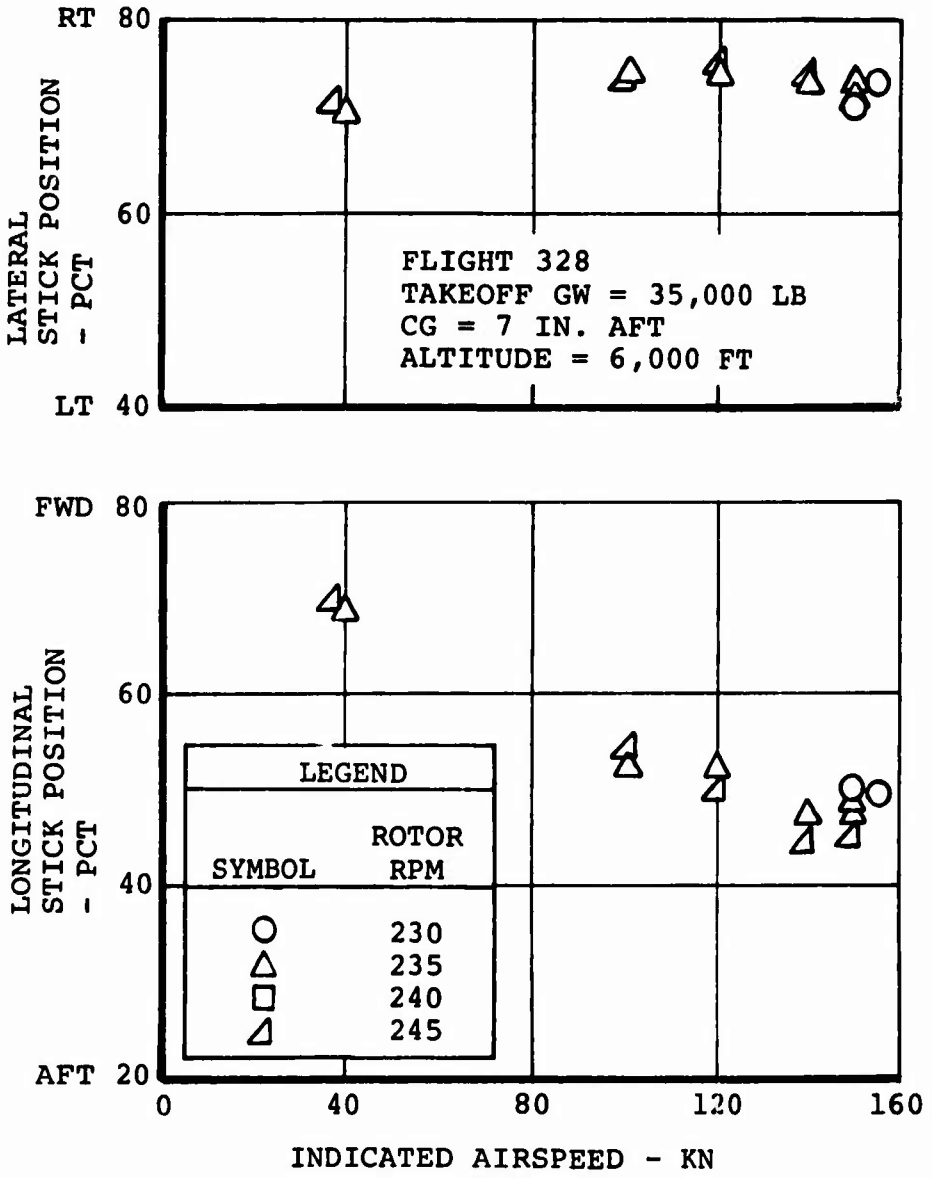

Figure 96. Aircraft Trim Control Positions During Flight Test of the Boron Advanced-Geometry Blades.

QUALITY TECHNOLOGY

The requirements for the manufacture of the fiberglass and boron advanced-geometry rotor blades were established by engineering design drawings and fabrication documents. To provide inspection guidelines for both these blades during manufacturing and after whirl test and flight test, Quality Technology organization prepared detailed nondestructive test plans. These plans, References 6, 7, and 8, identified inspection characteristics and procedures to be used for the inspection of all details, subassemblies, and final assemblies and were supported by the additional process control logs, documentation procedures, and records.

In order to assure the structural integrity of critical components, both penetrating-radiation (x-ray) and ultrasonic techniques were used extensively to determine the presence of voids, delaminations, honeycomb core defects, and unbond areas. Augmenting the penetrating-radiation methods was the incorporation of lead-base glass tracers into the preimpregnated fiberglass material used in the spar molding to determine conformance of the unidirectional fiber orientation.

Nondestructive Inspection (NDI)

During manufacture of both the fiberglass and boron rotor blades, modified immersion (standing-water column and wheel) and contact ultrasonic techniques were used for inspection. The standing-water column and contact methods were used initially on the fiberglass rotor blades; during the boron blade program, the automatic ultrasonic inspection and recording system (Figure 97) was used extensively for the spar-to-core assembly bonds and after the blades were whirl-tested and flight-tested. The automated scanning system was not available during the early inspection phases of the advanced-geometry fiberglass rotor blade program. At that time the glass rotor blade was inspected by using the standing-water column and hand-scanning techniques.

To provide permanent records of the glass blades for comparison with future test results, C-scan records were made of the honeycomb core section and paper overlays (maps) were made of the bonded final assemblies. Typical reduced-scale representations of these maps are shown in the upper parts of Figures 98, 99, and 100. These are composite reproductions of the ultrasonic pulse echo inspection results from both sides of the final assembly after whirl testing. The shaded sections represent those areas on the blade which produced ultrasonic indications. The presentation of the hand-mapped and outlined areas is not as detailed as the full-size C-scan recordings made later with the automatic ultrasonic inspection and recording system, as shown in the lower portions of Figures 98, 99, and 100.

Conclusion

A review of the postwhirl test hand-scan maps and the post-flight test C-scan recordings showed that the areas indicated by pulse-echo ultrasonic techniques and hand scanning are not as extensive as depicted by the through-transmission method. The ultrasonic through-transmission method employed with the automatic ultrasonic inspection and recording system was used throughout the boron rotor blade program, and the C-scan recordings made can be directly compared with subsequent reruns of the records. The upper portions of Figures 101, 102, and 103 show the C-scan results of the initial postwhirl ultrasonic testing. Approximately the same level of sensitivity employed for the postwhirl ultrasonic test was used to make the post-flight records, revealing essentially the same general indications (Figures 101, 102, and 103, bottom). A comparison of these recordings shows that no significant growth of the indications has occurred.

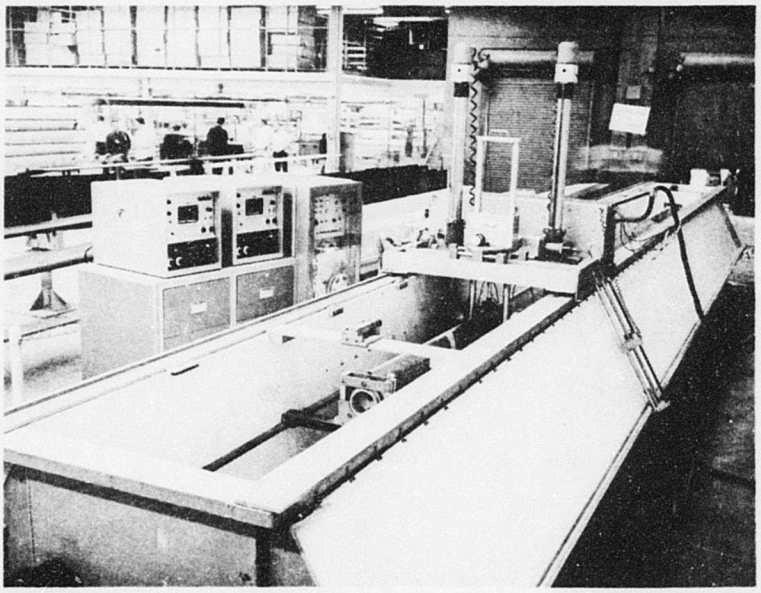

Figure 97. Automatic Ultrasonic Inspection and Recording System.

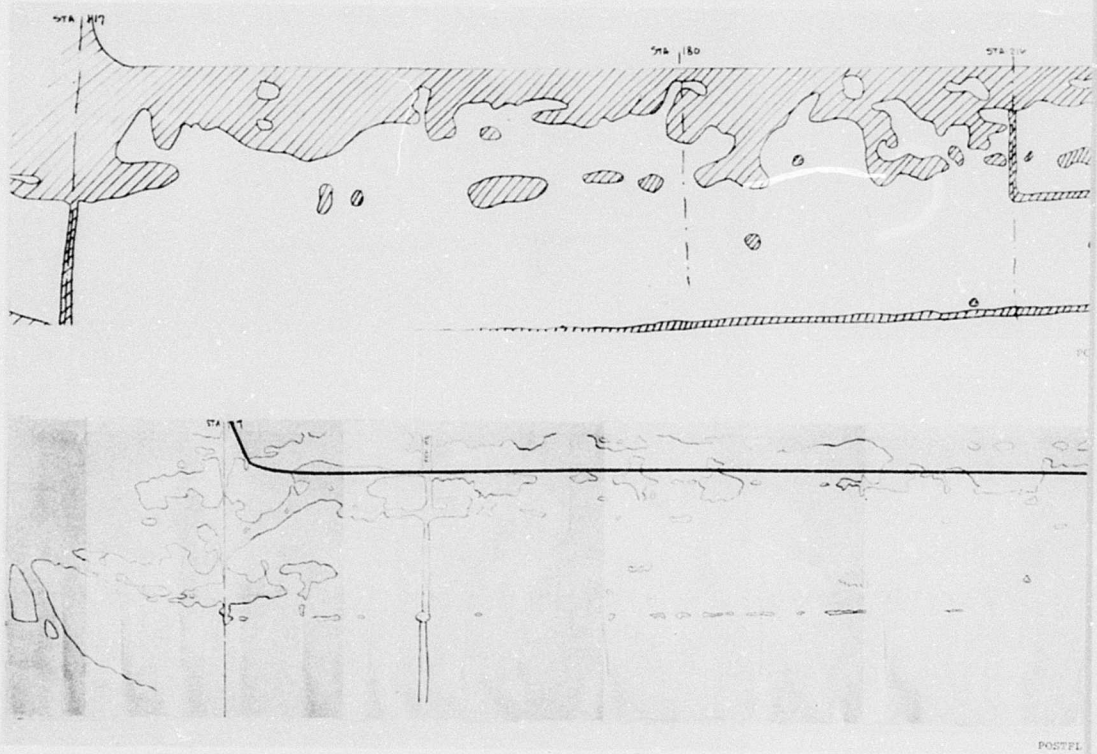

Figure 98. Ultrasonic Inspection Maps of Fiberglass Rotor Blade A-1-104.

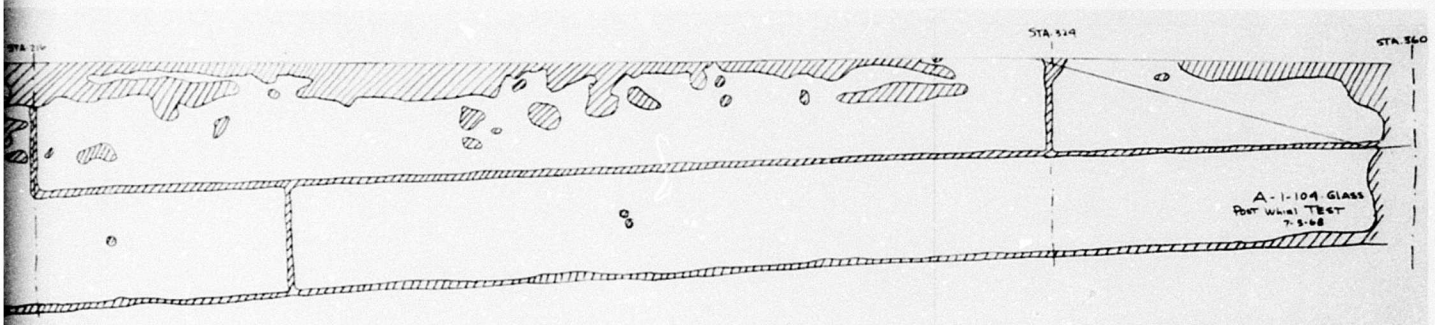

POSTWHIRL COMPOSITE ULTRASONIC MAP

POSTFLIGHT AUTOMATED ULTRASONIC C-SCAN RECORDING

tor

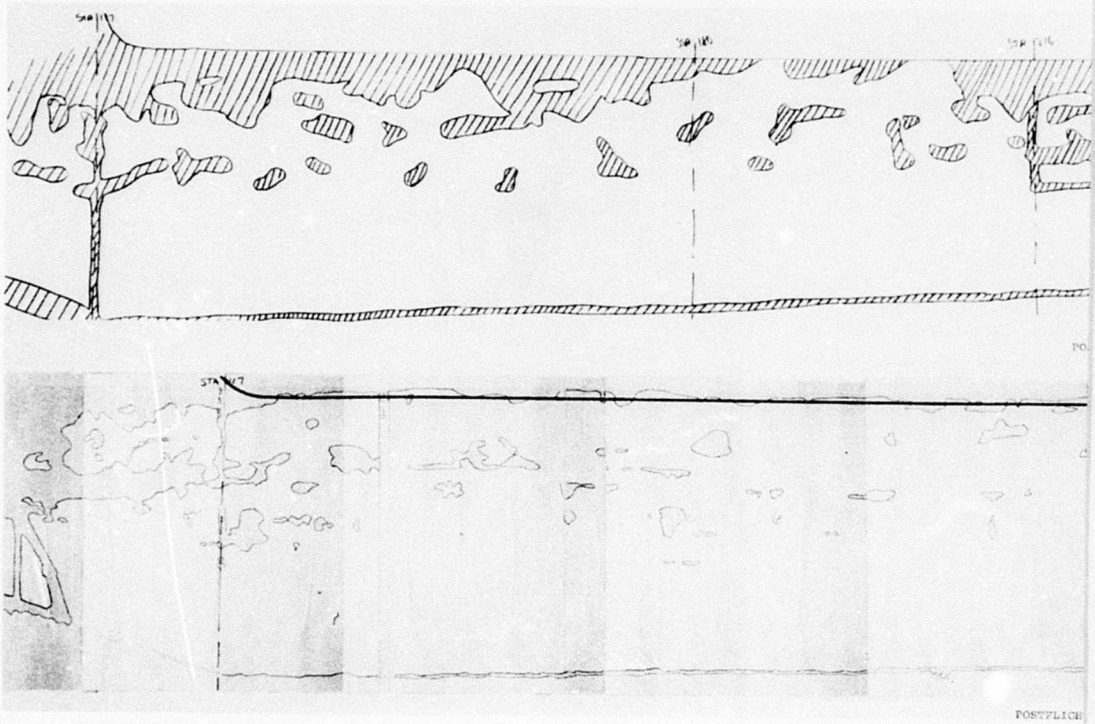

Figure 99. Ultrasonic Inspection Maps of Fiberglass Rotor Blade A-1-105.

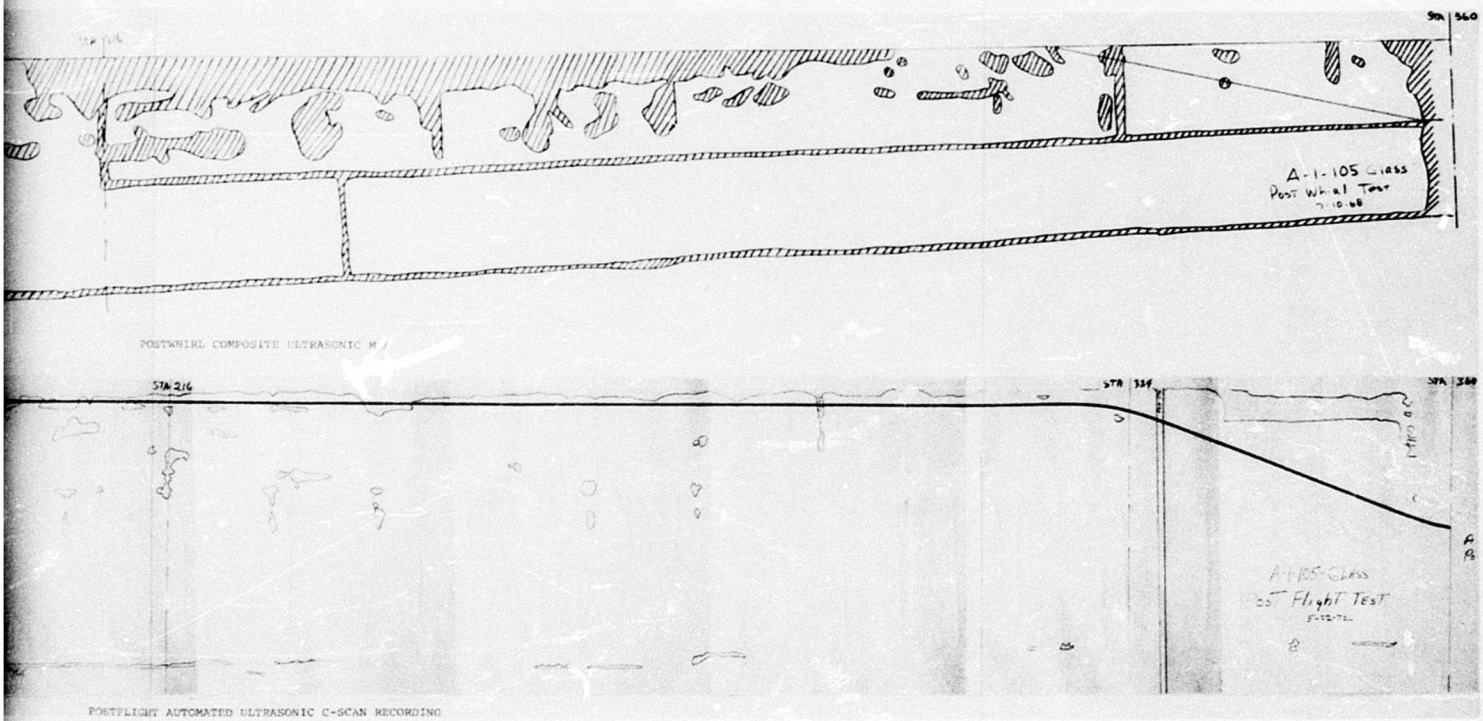

POSTFLIGHT AUTOMATED ULTRASONIC C-SCAN RECORDING

Rotor

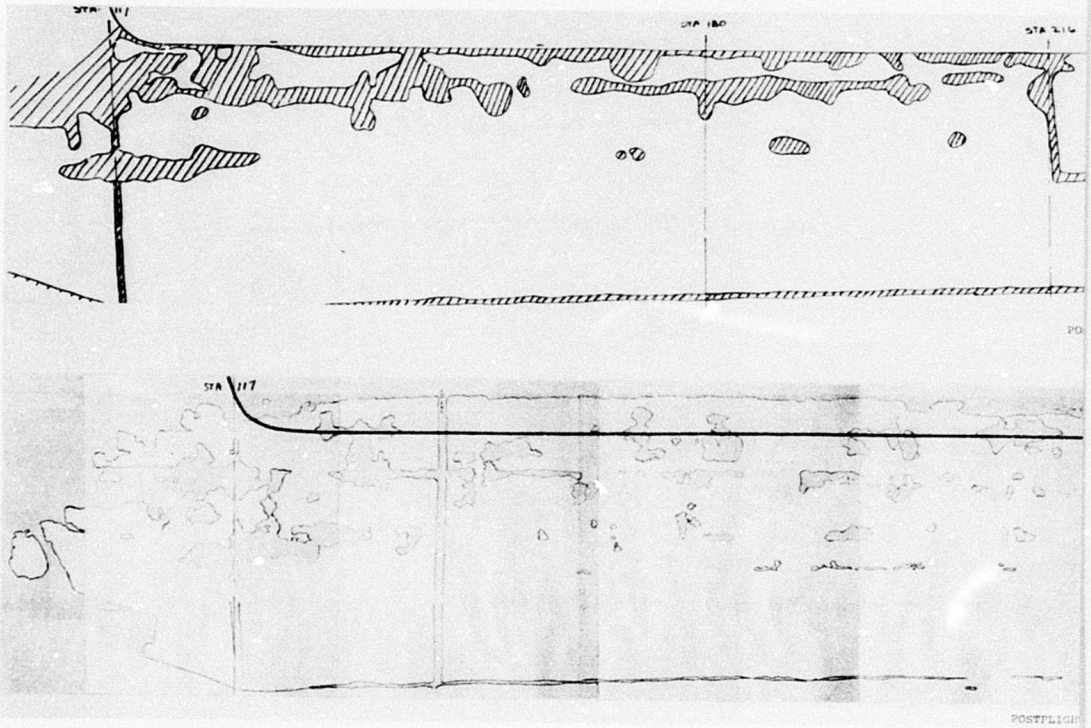

Figure 100. Ultrasonic Inspection Maps of Fiberglass Rotor Blade A-1-106.

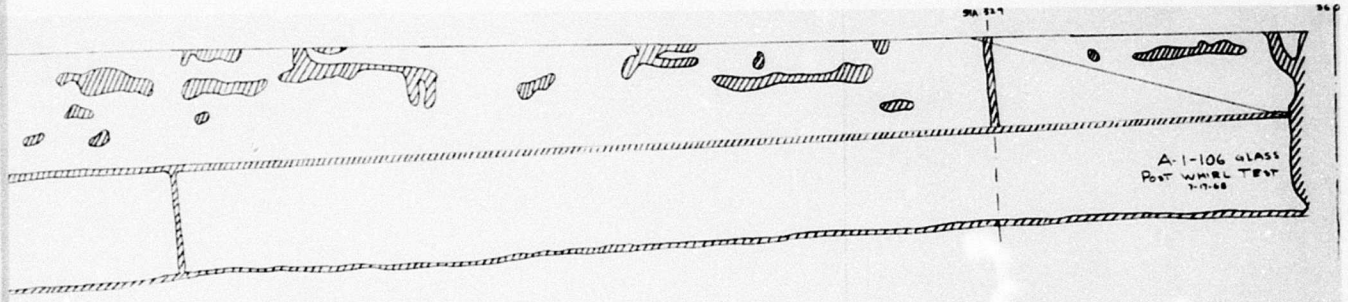

STWHIRL COMPOSITE ULTRASONIC MAP

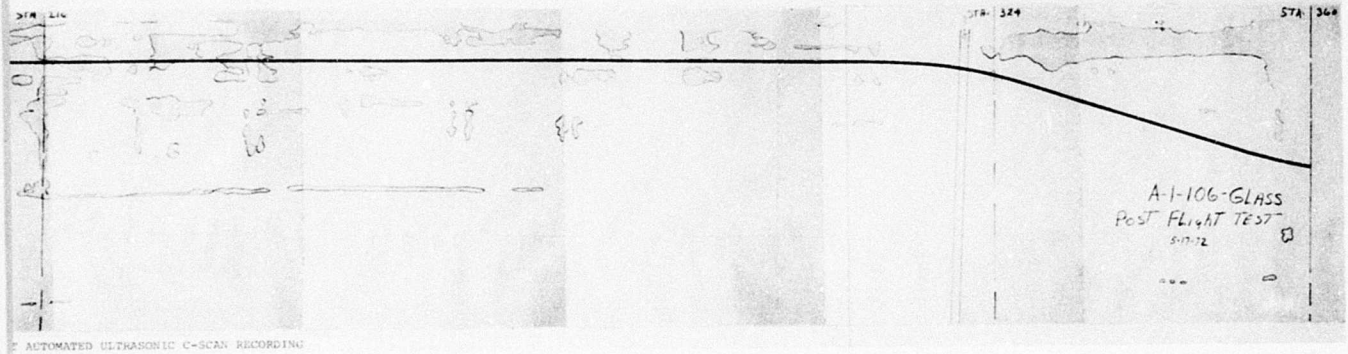

AUTOMATED ULTRASONIC C-SCAN RECORDING

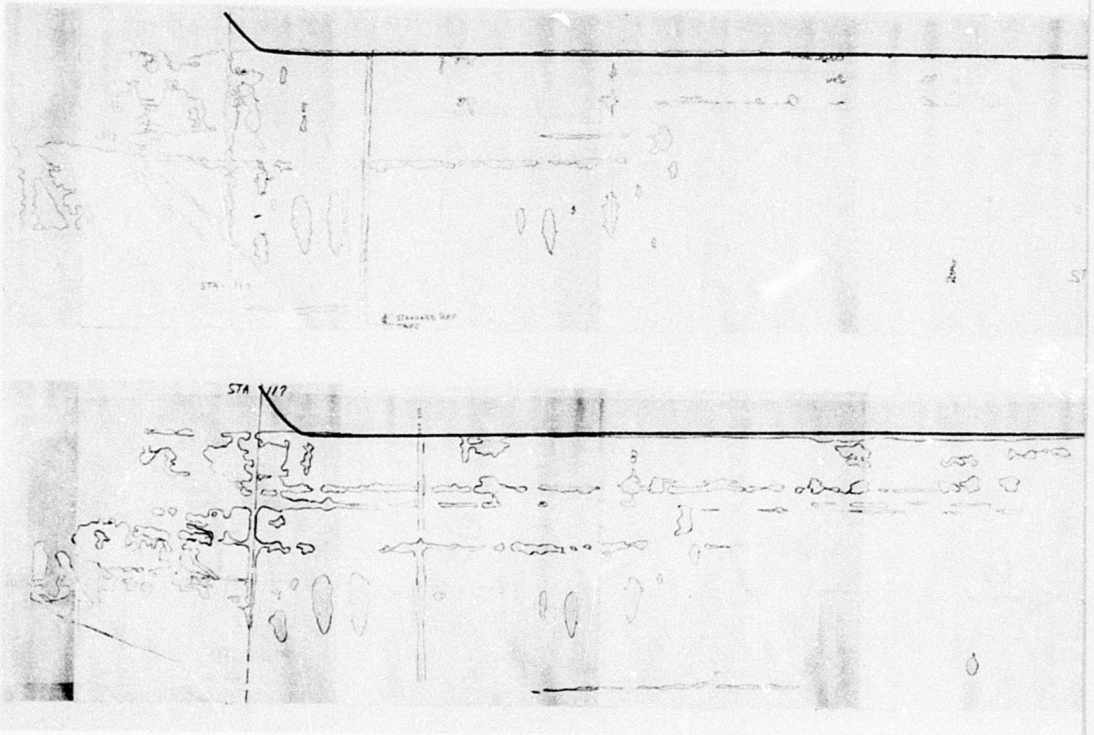

Figure 101. Automated Ultrasonic C-Scan Recording of Boron Rotor Blade A-2-101.

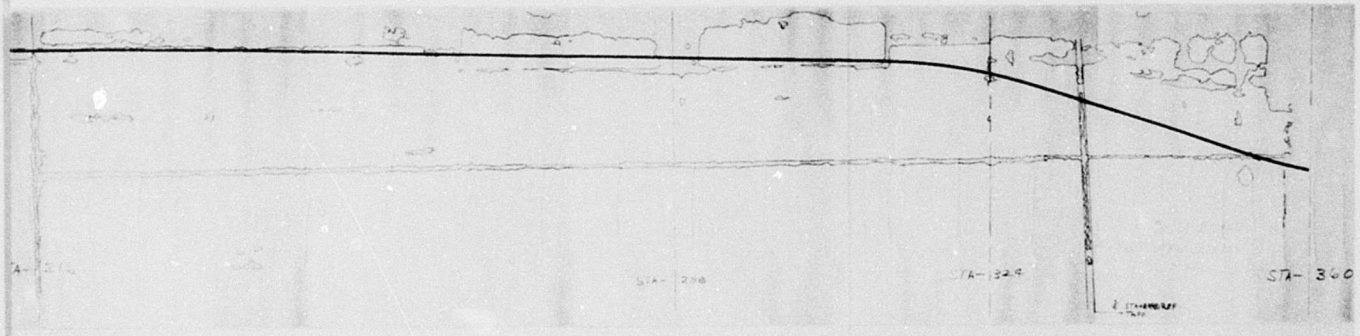

POSTWHIRL

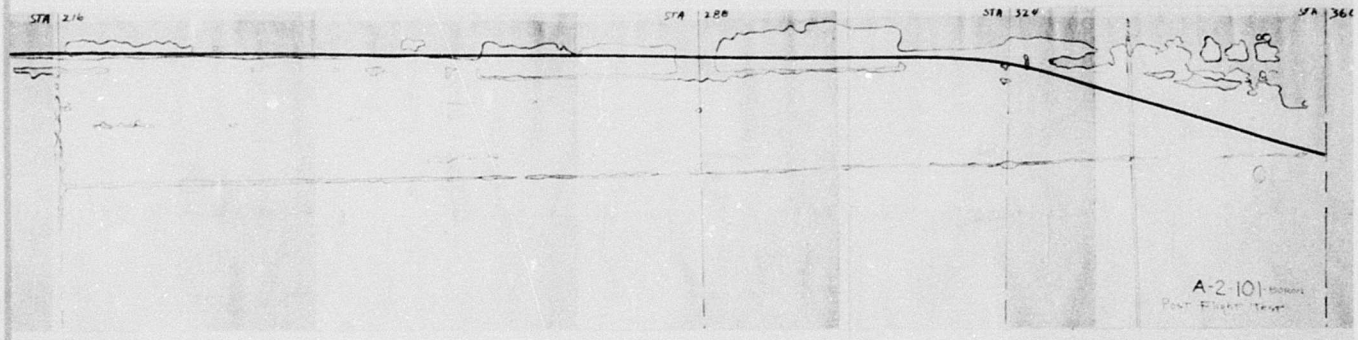

POSTFLIGHT

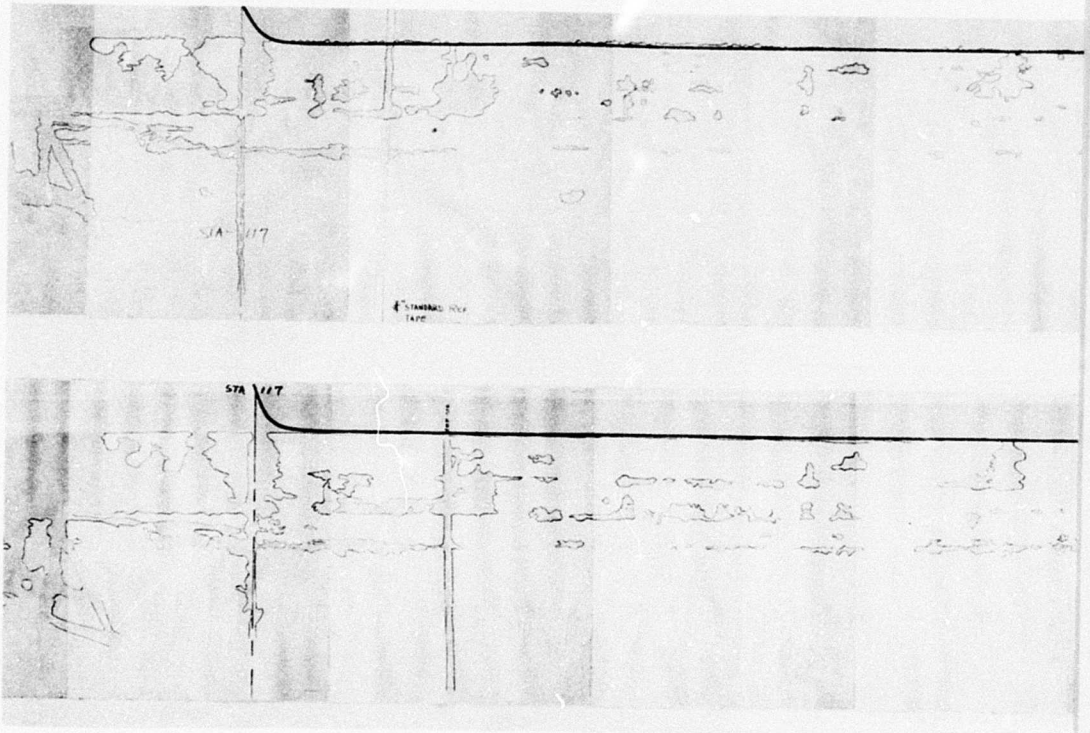

Figure 102. Automated Ultrasonic C-Scan Recording of Boron Rotor Blade A-2-103.

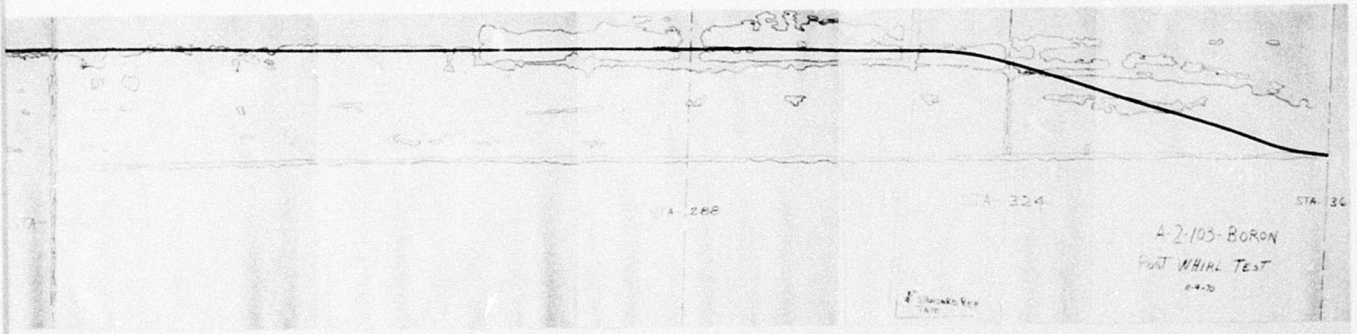

POSTWHIRL

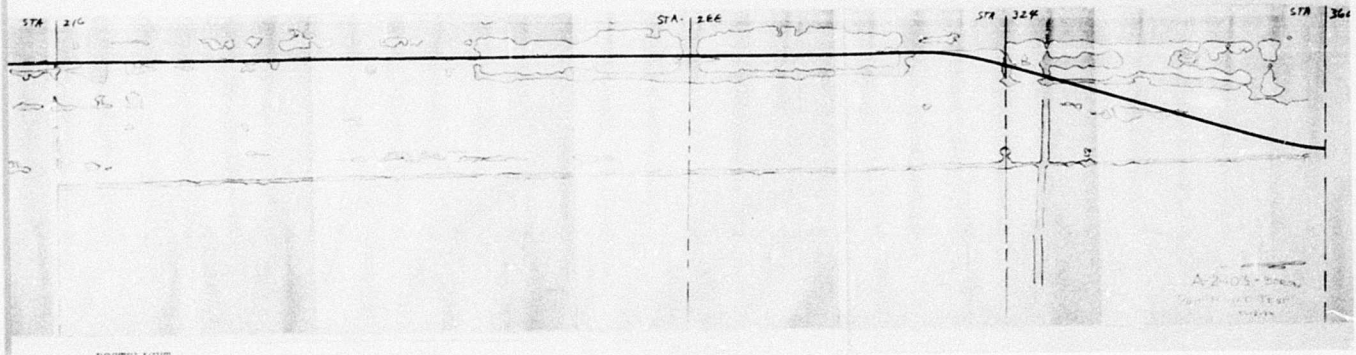

POSTFLIGHT

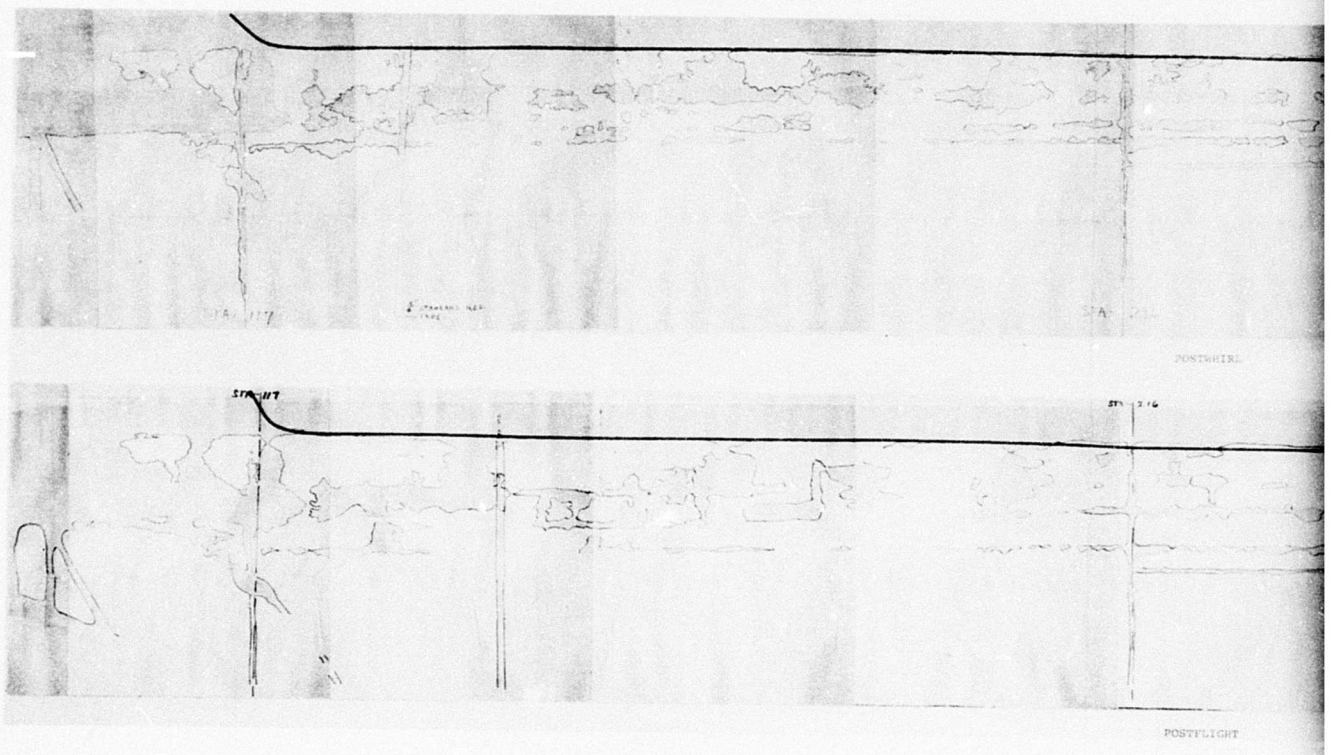

Figure 103. Automated Ultrasonic C-Scan Recording of Boron Rotor Blade A-2-104.

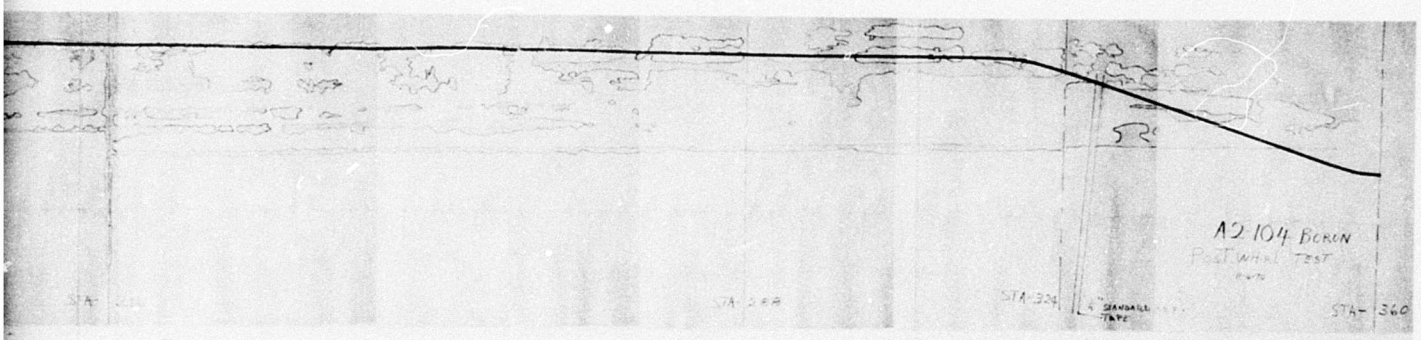

POSTWHIRL

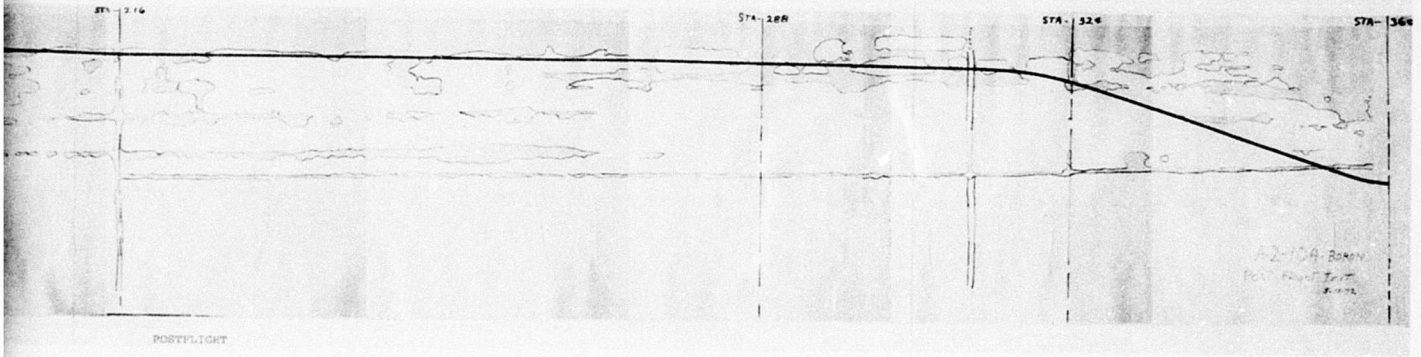

POSTFLIGHT

CONCLUSIONS

Flight evaluation of advanced geometry boron-epoxy rotor blades on an NCH-47C aircraft in March and April of 1972 has demonstrated the flightworthiness of properly designed boron-epoxy main helicopter rotor blades.

The increased solidity of the boron aft rotor, as on the S-glass aft rotor (both average 32 in. chords compared to 25.25 in. on the CH-47C standard metal blades), significantly improves the structural envelope of the CH-47C aircraft.

Comparison of post whirl and post flight C-scan ultrasonic recordings of the full-scale rotor blades showed no significant growth of bonding imperfections throughout the course of the program.

The part-to-part uniformity of the boron-epoxy rotor blades is improved over the S-glass-epoxy prototype configuration. This factor in conjunction with the blades' high flapwise and torsional stiffness resulted in excellent tower and flight tracking characteristics, as well as reduction of 1/rev unbalance vibration in the aft section of the fuselage.

Exceptionally high stiffness contributed by boron in flapwise bending, evidenced by a low cantilever 1g droop and a high first-mode flapwise bending frequency of 3.21 times rotor speed, was evaluated on a fully articulated three-bladed rotor system. The associated aft blade loads and 3/rev vibration transmitted to the structure were greater than those observed on the previously evaluated S-glass blades, but not high enough to impact flight plans. Modifications in the blade/airframe dynamic tuning, or improved 3/rev vibration suppression devices would be required for production utilization.

The increased torsional stiffness of the boron-epoxy blades as compared to S-glass epoxy blades of geometrically identical aerodynamic configuration did not result in the expected delay of moment stall inception as measured by aircraft parameters of rotor rpm, forward speed, density altitude, gross weight and trim conditions. It is theorized that the local angle of attack on the retreating boron reinforced blade is significantly higher than on the S-glass reinforced blade because of reduced "live" or aeroelastic twist. Thus, due to the increased angle of attack, moment stall inception is observed earlier on the boron blade than on the S-glass blade. Local flapping velocity differences due to blade stiffness may also be affecting inception.

The position of the longitudinal stick versus forward speed was observed to move aft with increasing forward speed at a

more rapid rate than on the standard CH-47C helicopter. This gradient deterioration is not fully understood, but it is theorized to be caused by the difference in aeroelastic twist between the forward (S-glass) rotor blades and the aft (boron) rotor blades. Flapwise stiffness differences and the associated change in local flapping velocity outboard must also be considered as contributing to increased aft rotor authority at higher collective pitch.

RECOMMENDATIONS

Boron-epoxy structure should be considered for helicopter rotor blade design applications where stiff, lightweight structure is required.

Selection of materials for fatigue-critical structures other than rotor blades should include boron-epoxy among candidate material systems for stiff, lightweight components.

Additional analysis of the data accumulated in this flight program should be performed to fully explore some of the following areas:

- Effect of flapwise stiffness and aeroelastic twist on moment stall inception, including recommendations on optimum twist schedule to delay stall inception when utilizing high torsional stiffness feature of boron and graphite.

- Effect of flapwise stiffness and aeroelastic twist on longitudinal stick position gradient on tandem helicopters with differing forward and aft rotor blade structural characteristics.

- Scale-model rotor wind tunnel test data comparison with full-scale free-flight data to analyze and resolve differences in test results when comparing S-glass epoxy with graphite/boron-epoxy rotor blades.

- Aeroelastic response differences between the S-glass and boron composite rotor blades based on the flight data available; to include rotating natural frequencies in relation to wave-form harmonics in flap bending and torsion.

Further investigation of structural applications of boron filament orientations in combination with glass filaments in a common matrix should be conducted to permit optimization of strength/stiffness characteristics of epoxy matrix composites.

A comparison should be made of flight test data to theoretical predictions with emphasis on waveform and magnitude correlation of pitch link loads. Further investigation is required to examine airfoil characteristics as they affect blade torsional loads.

LITERATURE CITED

1. RESEARCH AND DEVELOPMENT OF HELICOPTER ROTOR BLADES UTILIZING ADVANCED COMPOSITE MATERIALS, The Boeing Company, Vertol Division, Technical Report AFML-TR-71-125, Air Force Materials Laboratory, Air Force Systems Command, Wright-Patterson Air Force Base, Ohio, October 1971.

2. CH-47 ADVANCED-GEOMETRY BLADE FLIGHT TEST PROCEDURE, The Boeing Company, Vertol Division, Philadelphia, Pennsylvania, 114-FT-039-1, January 1972.

3. FLIGHT TEST SECTION STANDARD PLANS OF TEST, The Boeing Company, Vertol Division, Philadelphia, Pennsylvania, D8-1087, 1966.

4. SAFETY-OF-FLIGHT REVIEW DATA FOR BORON ROTOR BLADE FLIGHT TEST PROGRAM, The Boeing Company, Vertol Division, Philadelphia, Pennsylvania, D210-10401-1, 1972.

5. Hoffstedt, Donald J., ADVANCED-GEOMETRY, GLASS-FIBER-REINFORCED PLASTIC ROTOR BLADE TEST PROGRAM, The Boeing Company, Vertol Division, USAAMRDL Technical Report 71-42, Eustis Directorate, U.S. Army Air Mobility Research and Development Laboratory, Fort Eustis, Virginia, September 1971.

6. NONDESTRUCTIVE TEST PLAN FOR THE ADVANCED-GEOMETRY ROTOR BLADE, The Boeing Company, Vertol Division, Philadelphia, Pennsylvania, D8-0280-1, October 1966.

7. NONDESTRUCTIVE TEST PLAN FOR THE BORON-FILAMENT-REINFORCED COMPOSITE ALUMINUM HONEYCOMB ROTOR BLADE, The Boeing Company, Vertol Division, Philadelphia, Pennsylvania, D8-1009, November 1967.

8. NONDESTRUCTIVE TEST PLAN FOR FLIGHT TEST OF ADVANCED-GEOMETRY BORON ROTOR BLADES, The Boeing Company, Vertol Division, Philadelphia, Pennsylvania, D8-4890.88, January 1972.

APPENDIX I

PITCH LINK LOAD WAVEFORMS

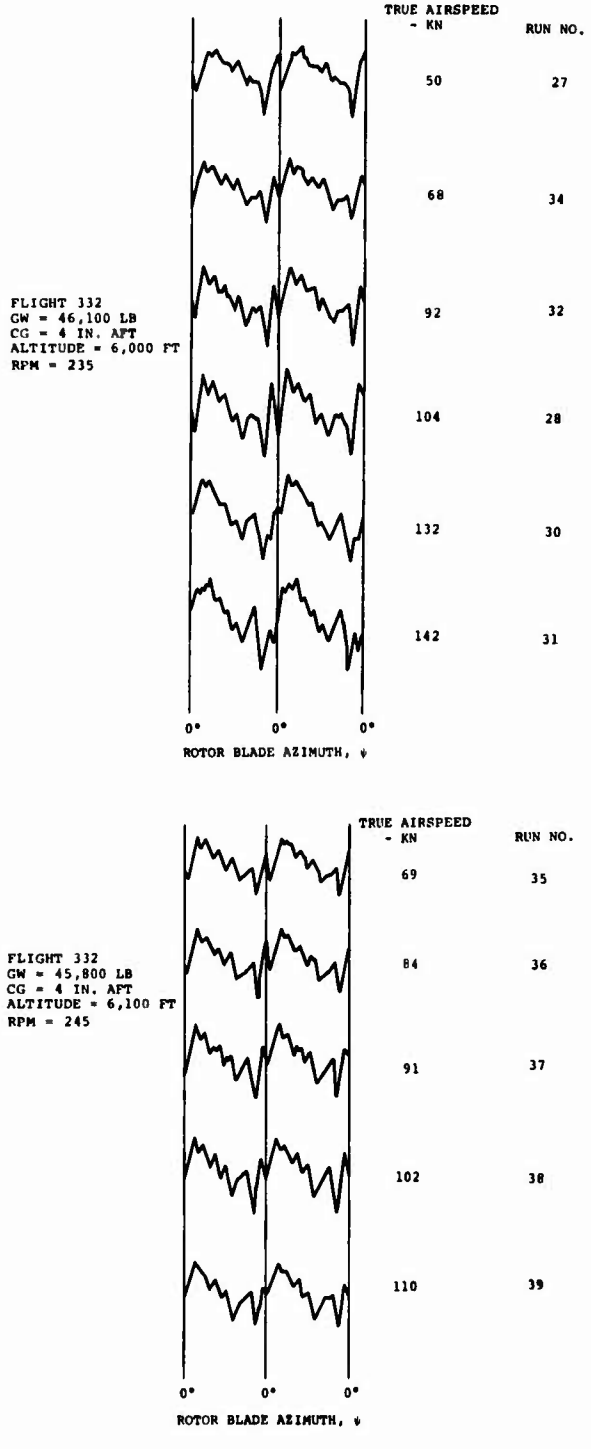

Figure 104. Pitch Link Load Waveforms During Flight Test of the Boron Advanced-Geometry Blades.

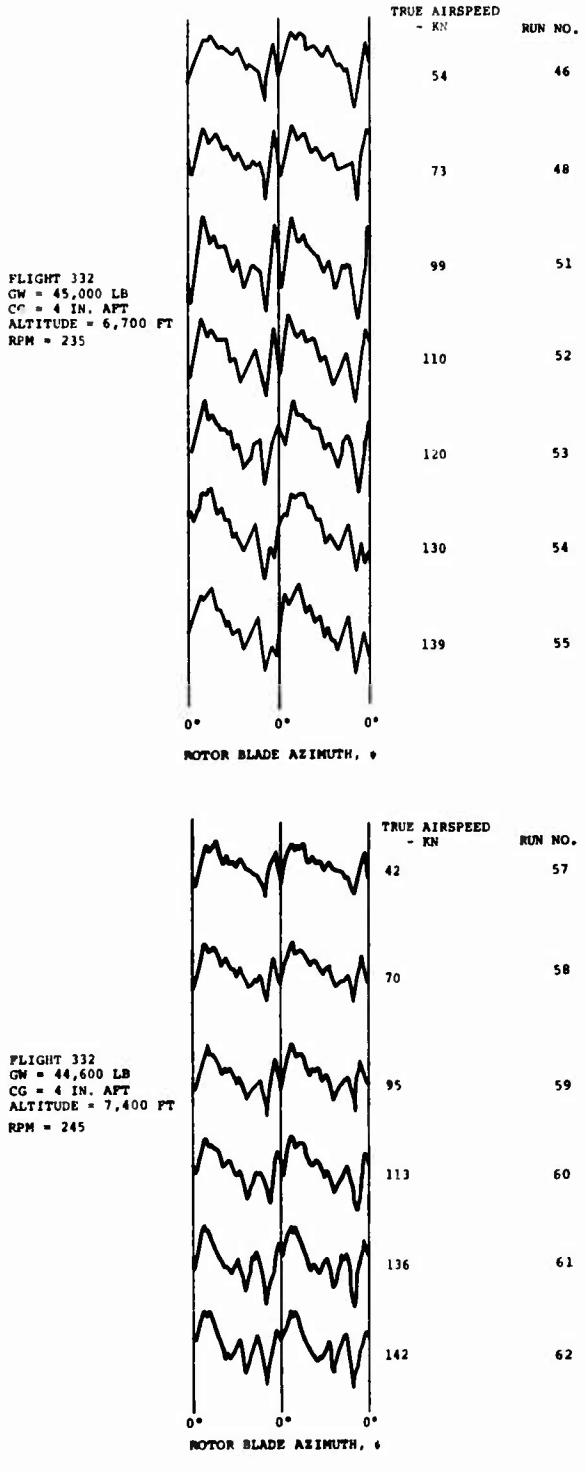

Figure 105. Pitch Link Load Waveforms During Flight Test of the Boron Advanced-Geometry Blades.

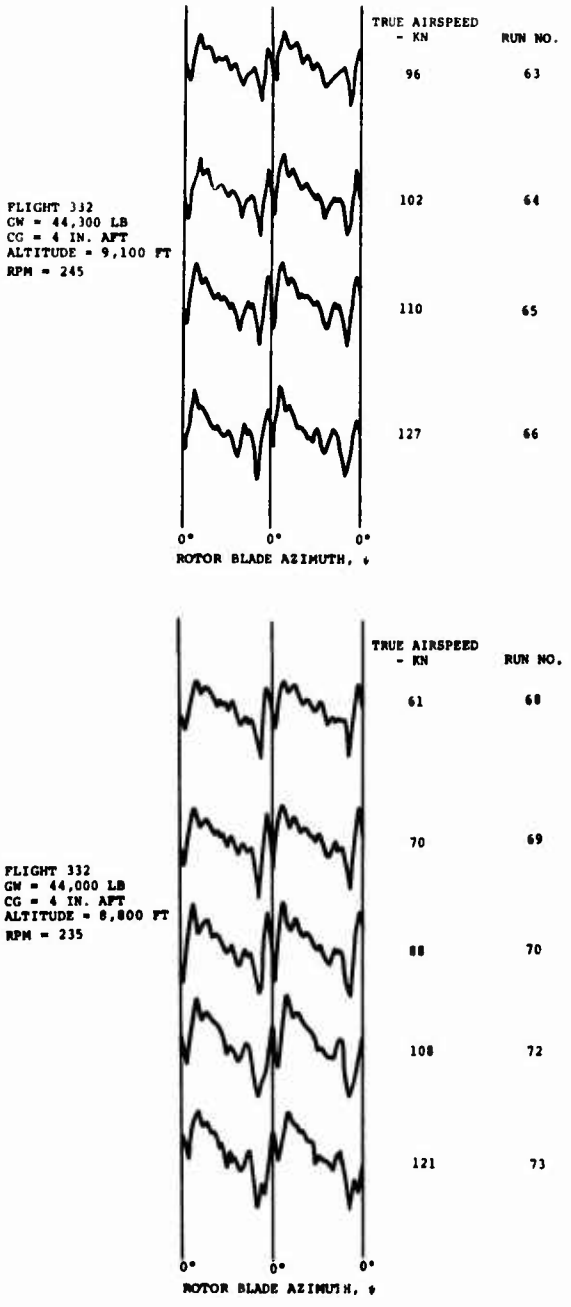

Figure 106. Pitch Link Load Waveforms During Flight Test of the Boron Advanced-Geometry Blades.

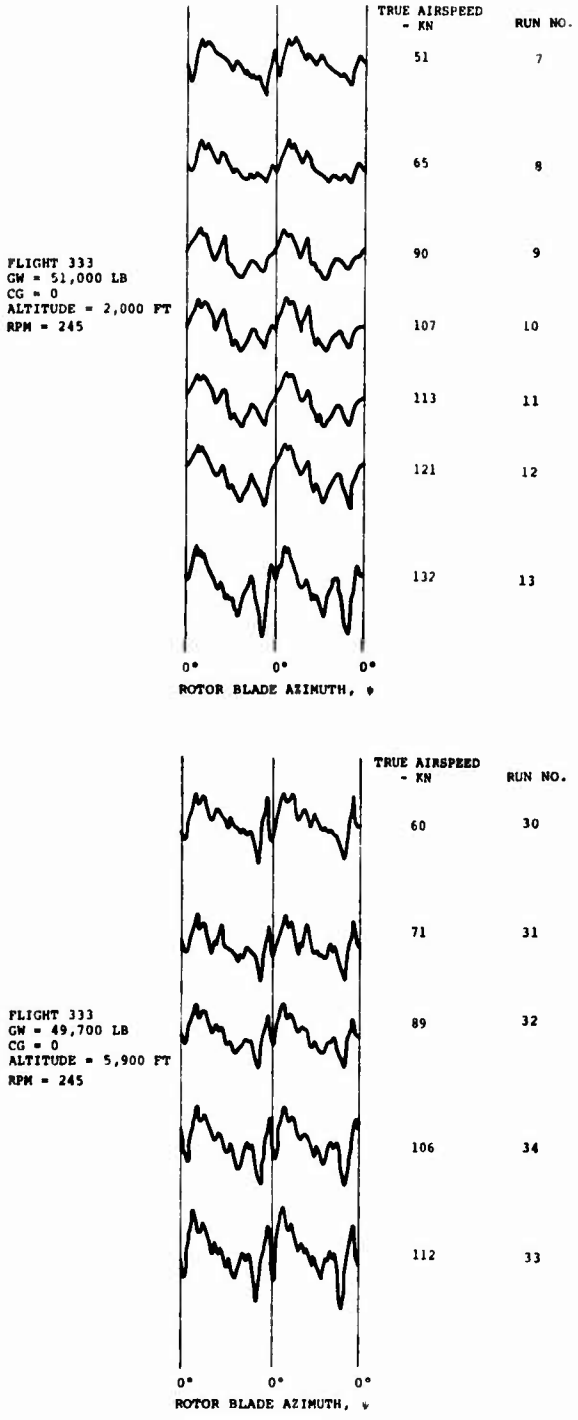

Figure 107. Pitch Link Load Waveforms During Flight Test of the Boron Advanced-Geometry Blades.

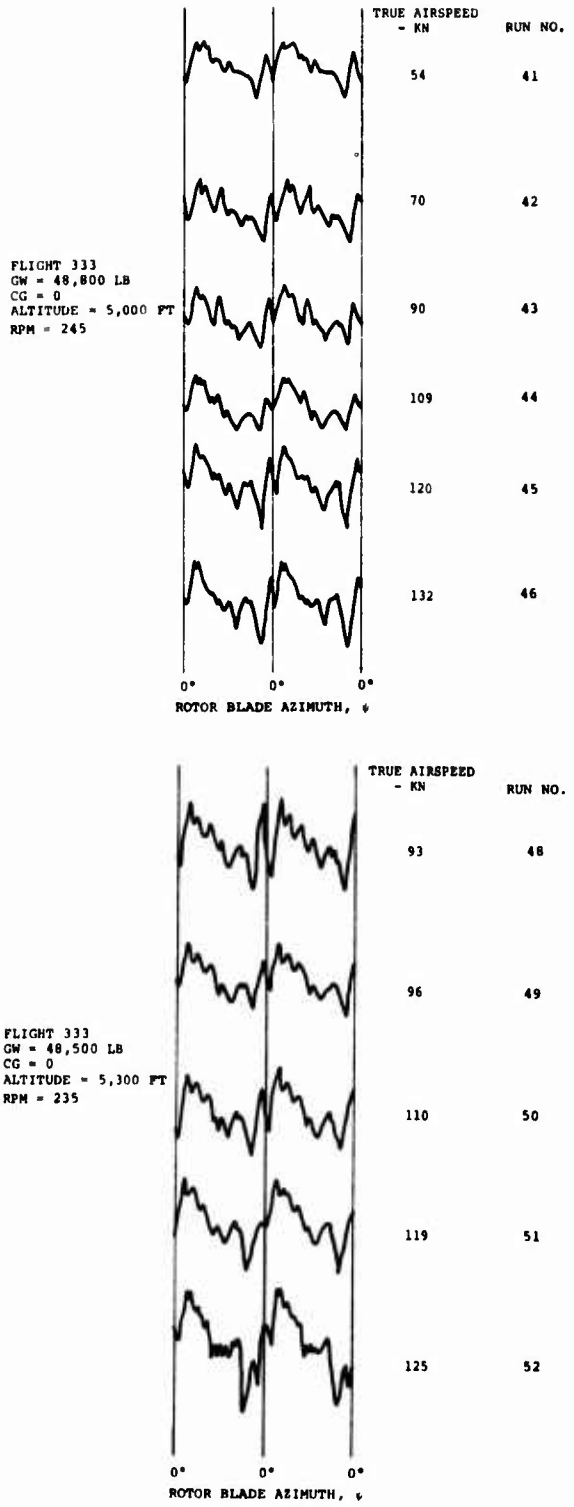

Figure 108. Pitch Link Load Waveforms During Flight Test of the Boron Advanced-Geometry Blades.

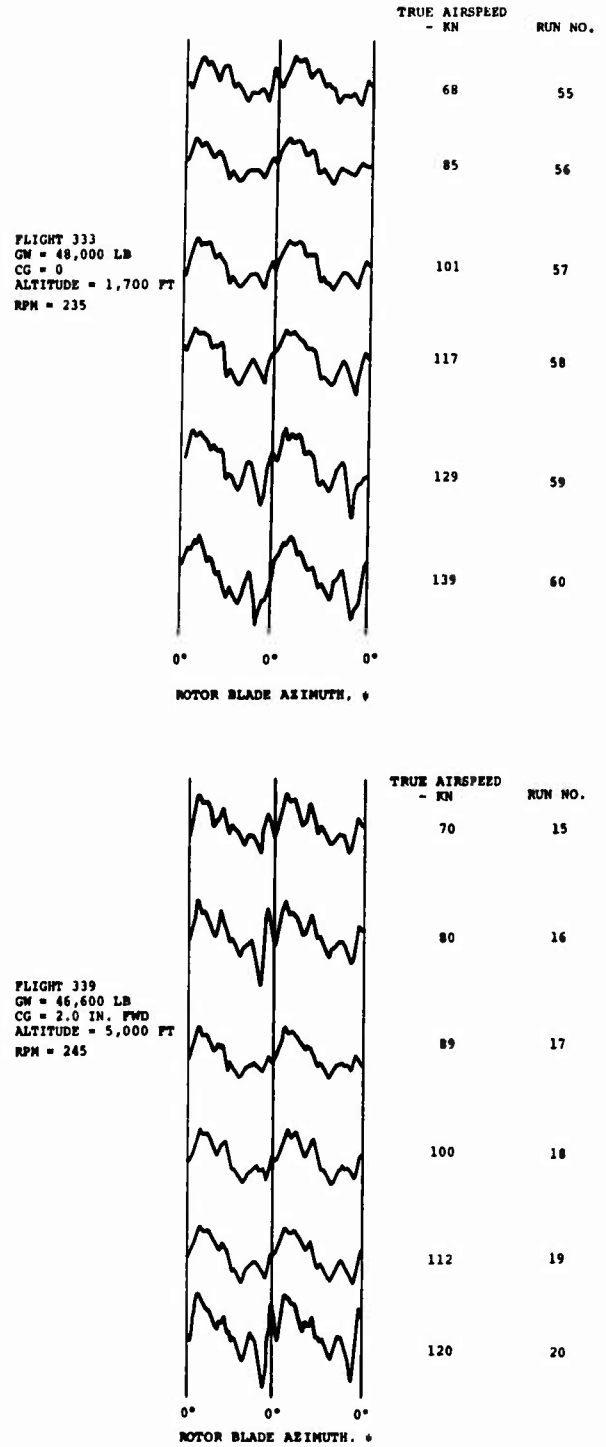

Figure 109. Pitch Link Load Waveforms During Flight Test of the Boron Advanced-Geometry Blades.

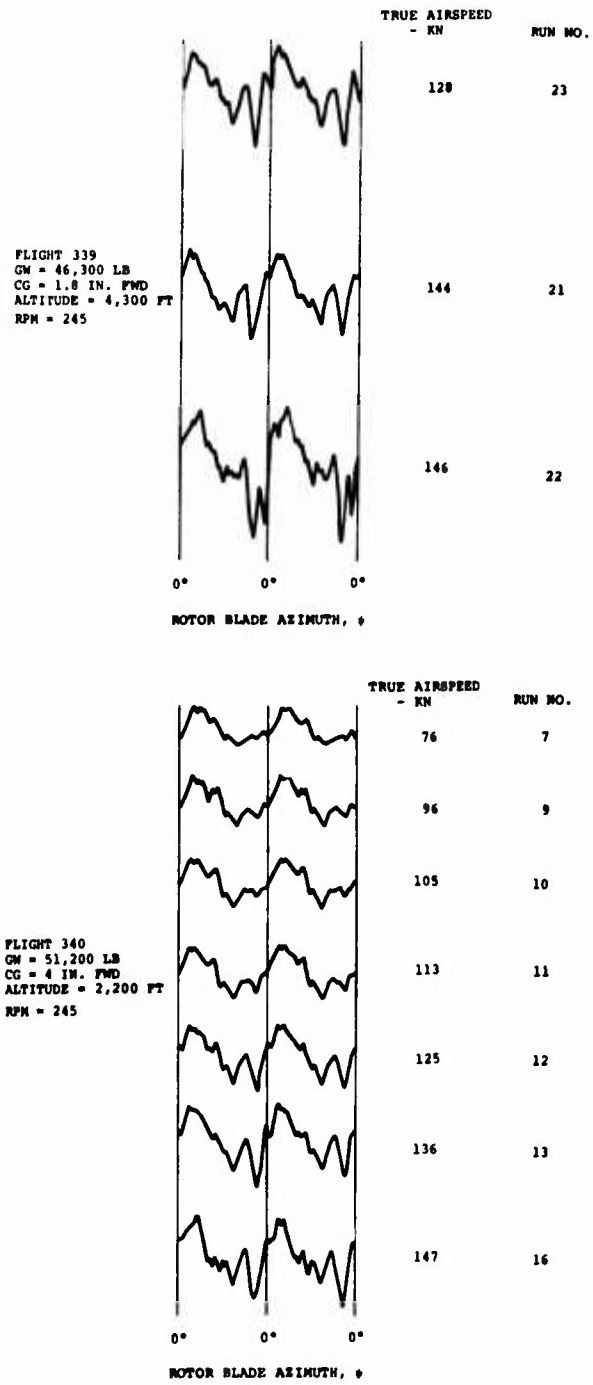

Figure 110. Pitch Link Load Waveforms During Flight Test of the Boron Advanced-Geometry Blades.

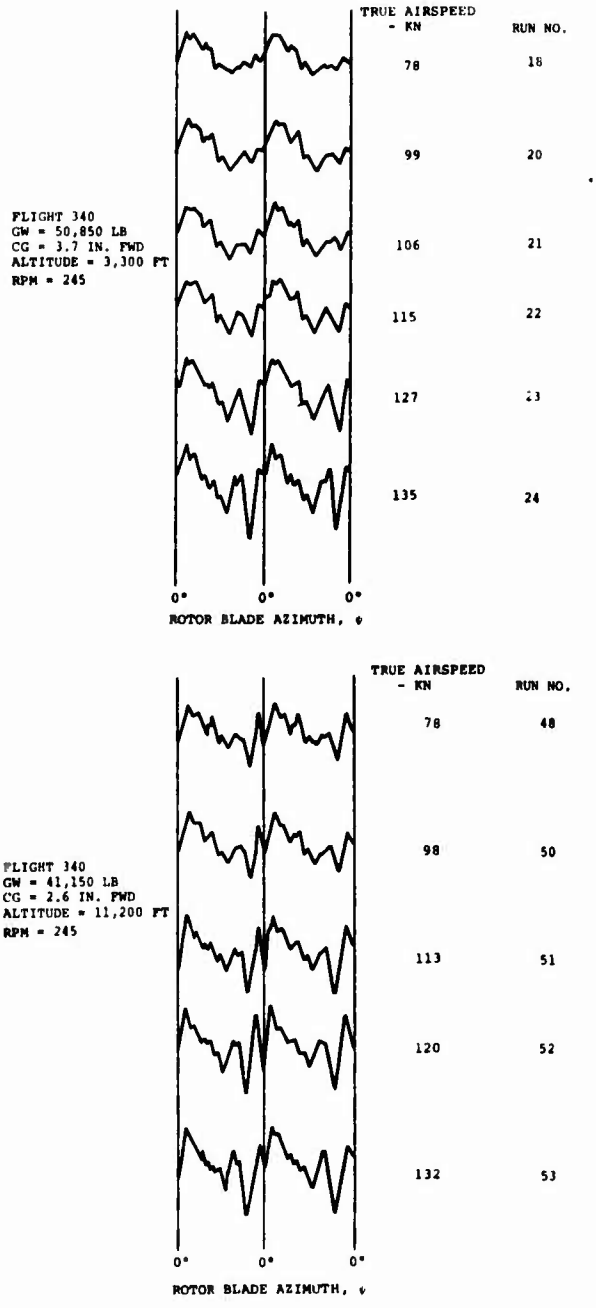

Figure 111. Pitch Link Load Waveforms During Flight Test of the Boron Advanced-Geometry Blades.

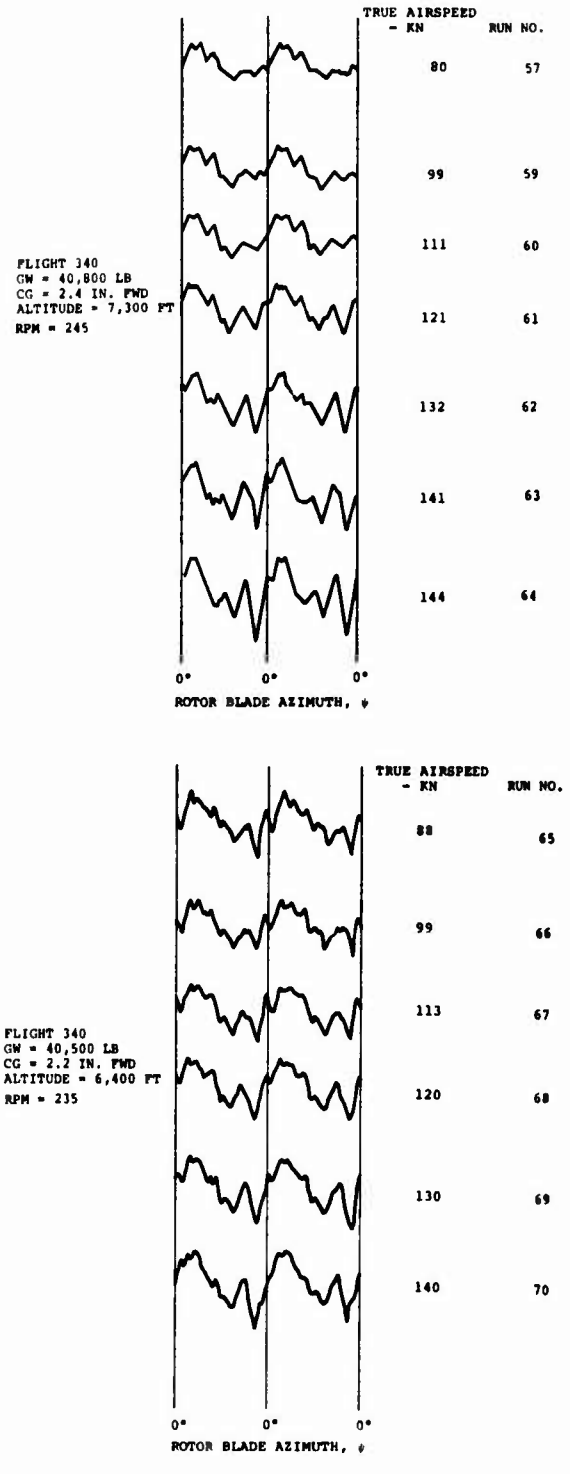

Figure 112. Pitch Link Load Waveforms During Flight Test of the Boron Advanced-Geometry Blades.

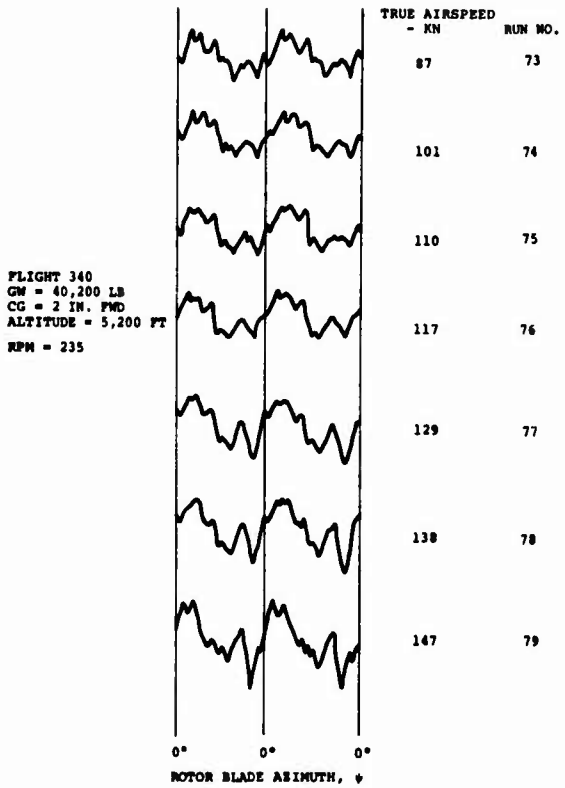

Figure 113. Pitch Link Load Waveforms During Flight Test of the Boron Advanced-Geometry Blades.

APPENDIX II

SCATTERGRAMS OF PITCH LINK LOADS

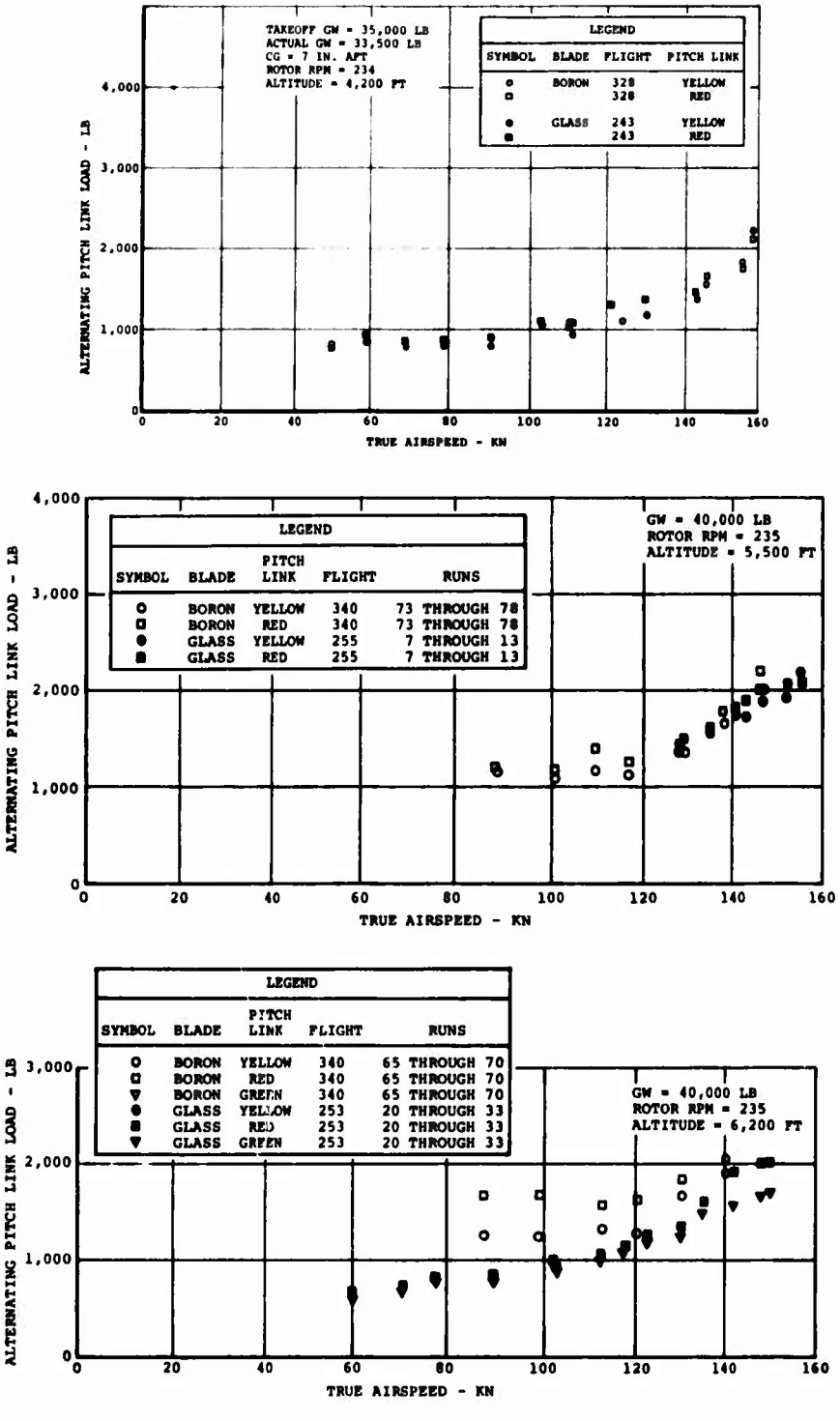

Figure 114. Comparison of Pitch Link Loads With the Fiberglass and Boron Advanced-Geometry Blades.

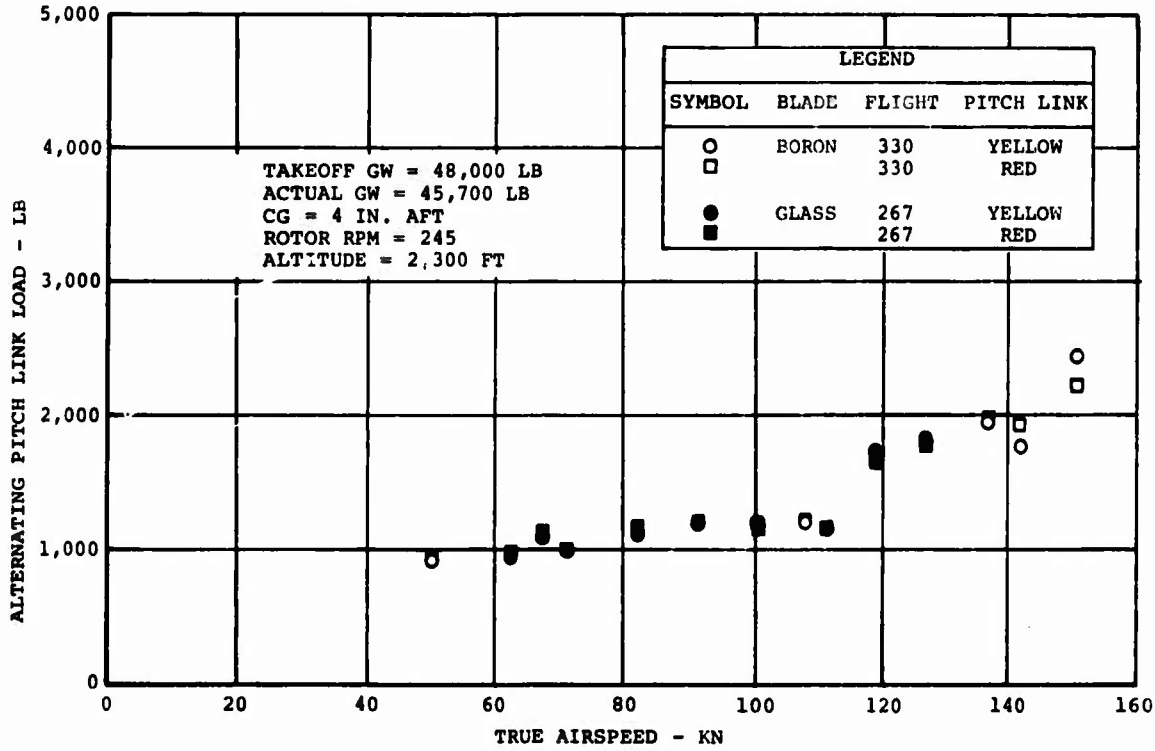

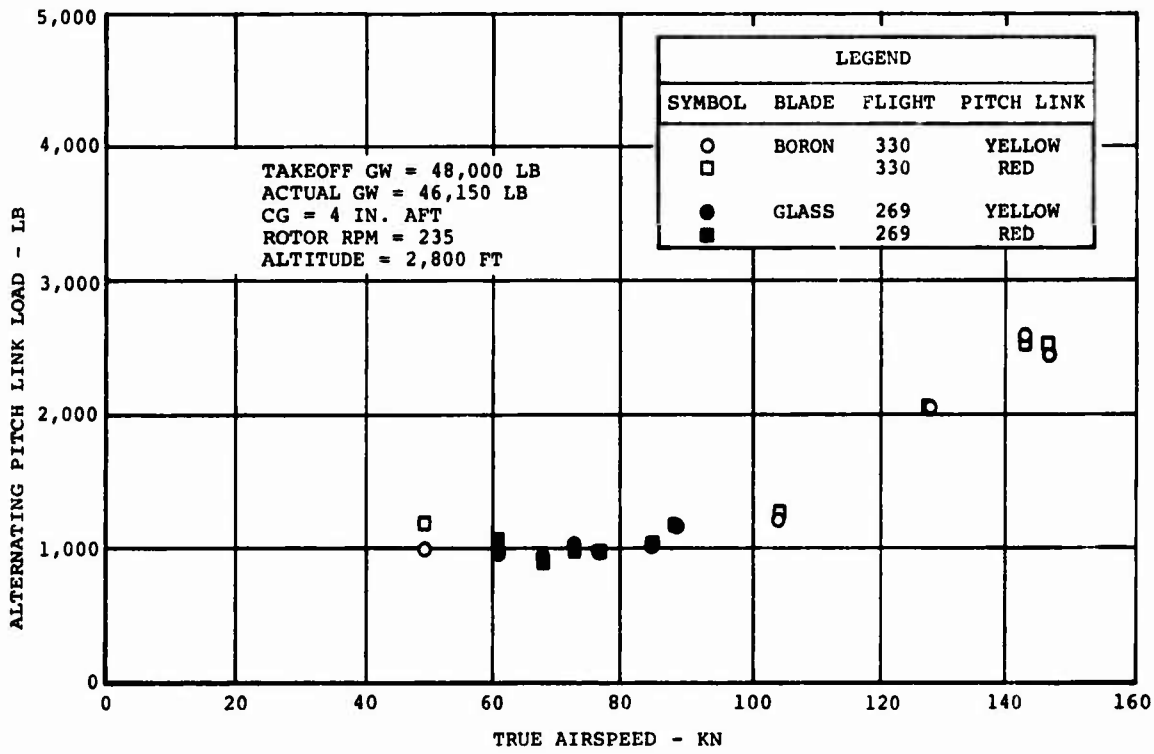

Figure 115. Comparison of Pitch Link Loads With the Fiberglass and Boron Advanced-Geometry Blades.

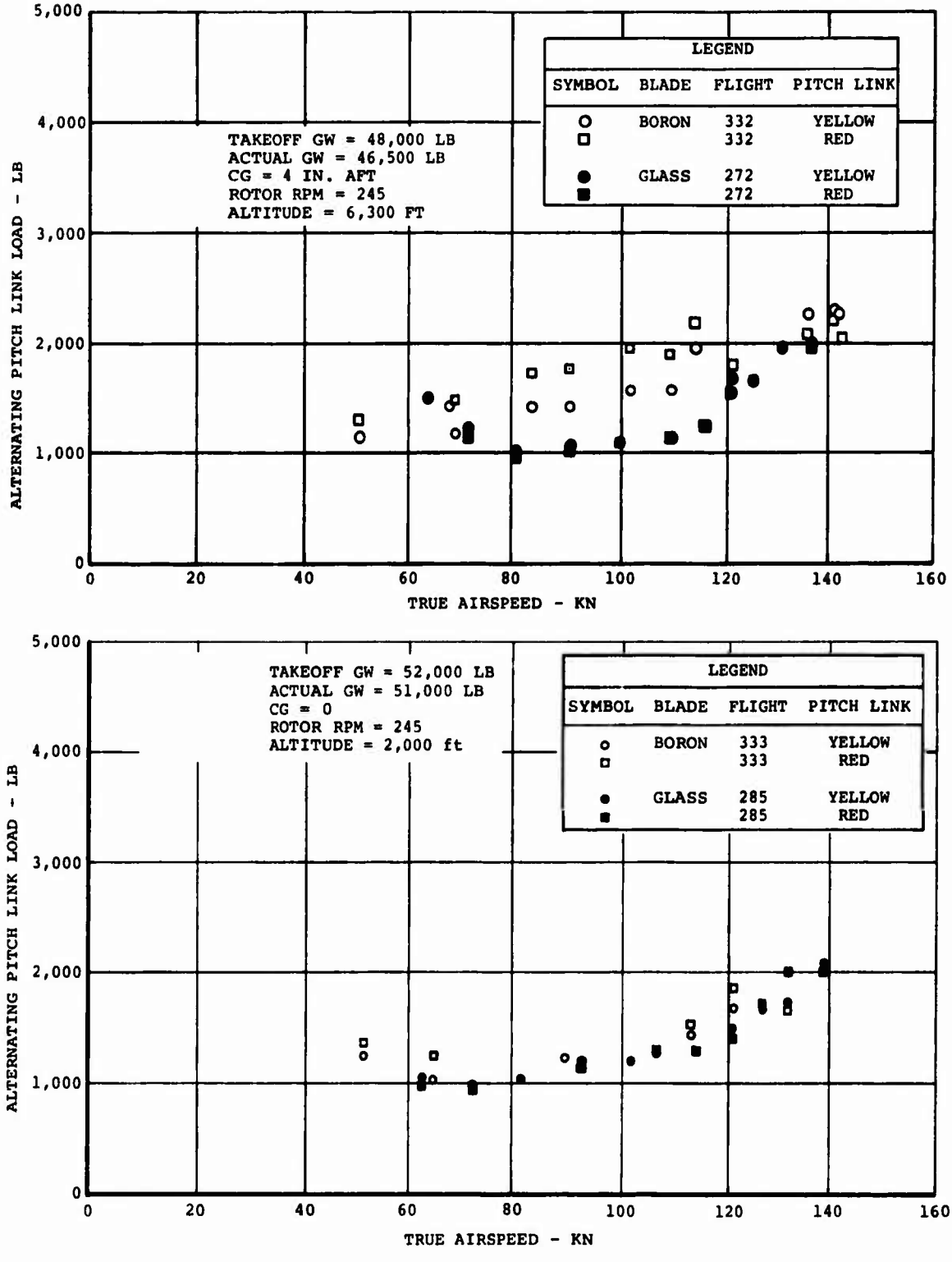

Figure 116. Comparison of Pitch Link Loads With the Fiberglass and Boron Advanced-Geometry Blades.

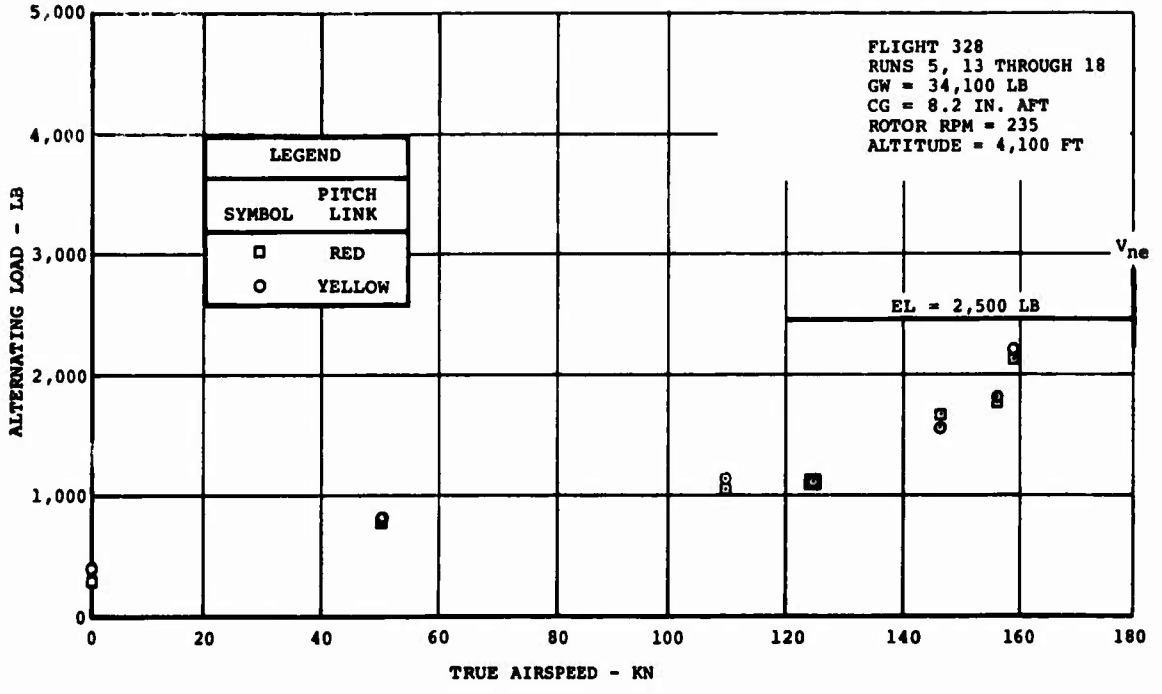

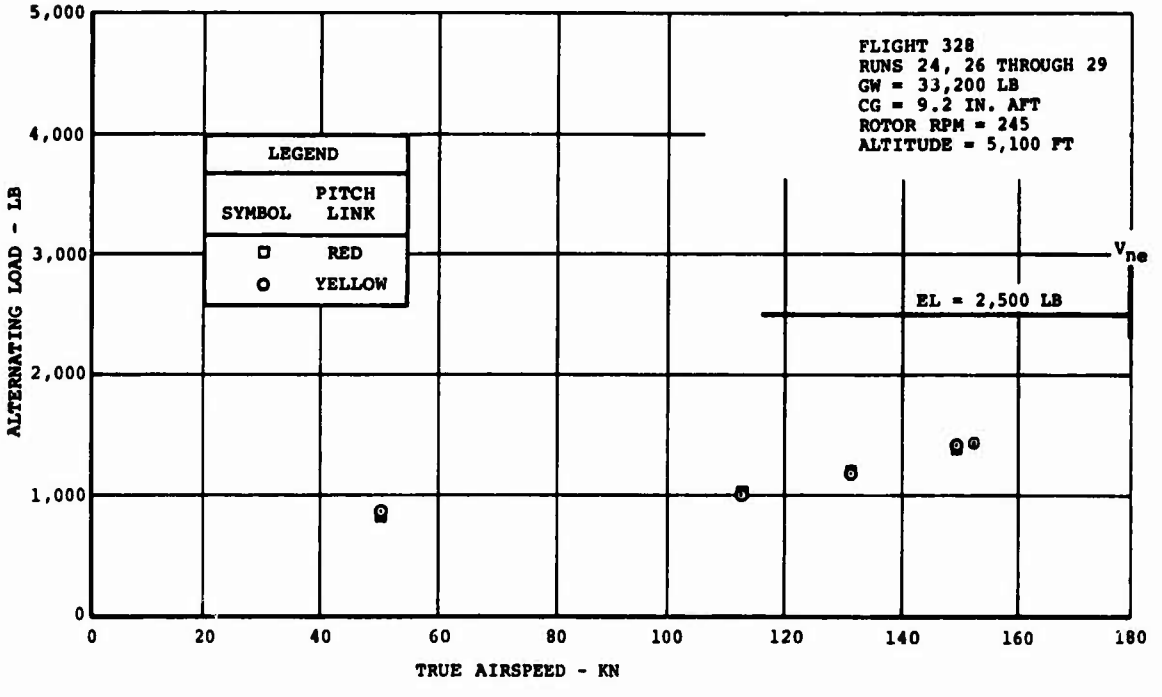

Figure 117. Pitch Link Loads on CH-47C Helicopter Equipped With Boron Advanced-Geometry Blades (V_{ne} for Glass AGB Shown for Reference).

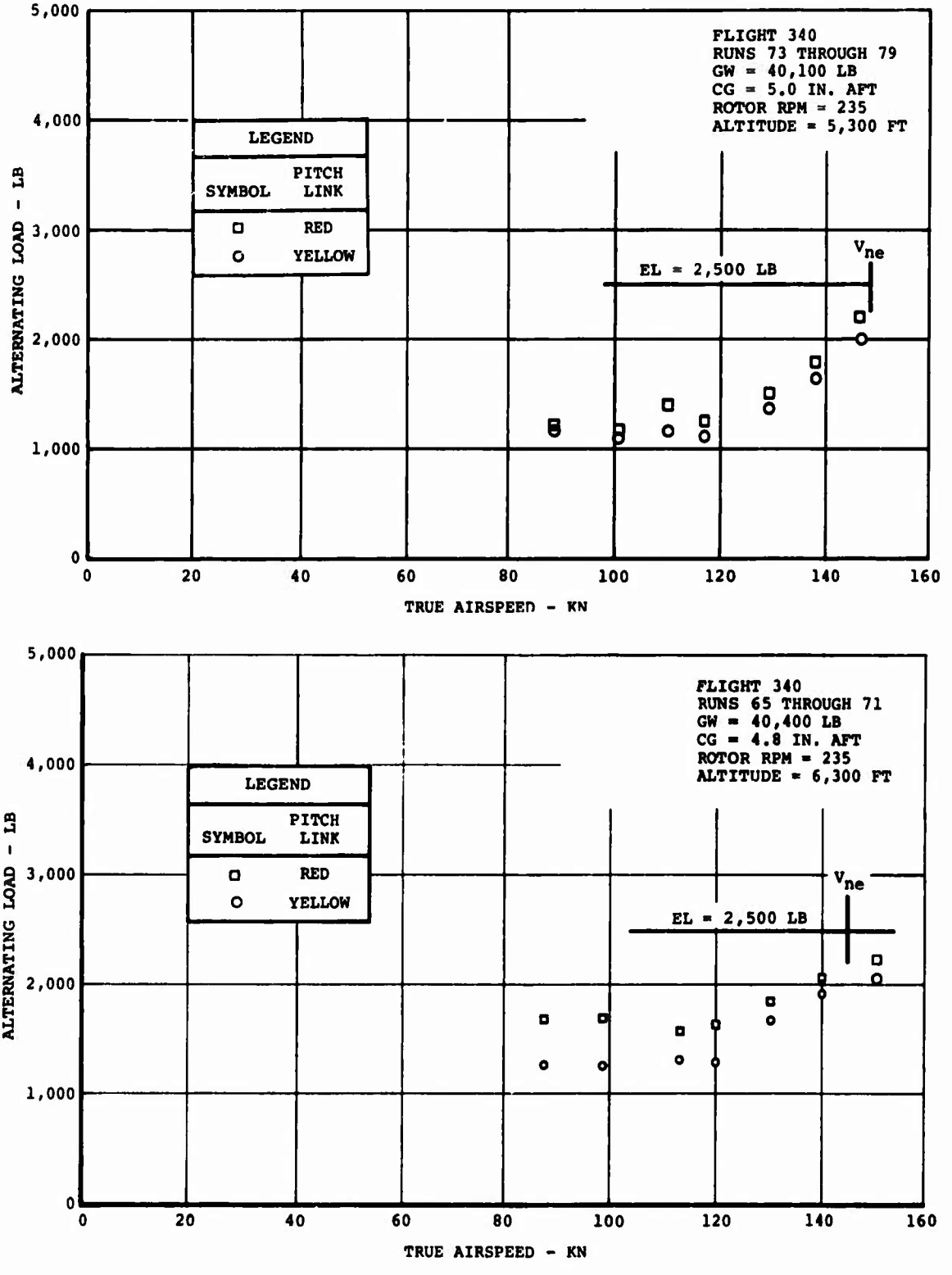

Figure 118. Pitch Link Loads on CH-47C Helicopter Equipped With Boron Advanced-Geometry Blades (V_{ne} for Glass AGB Shown for Reference).

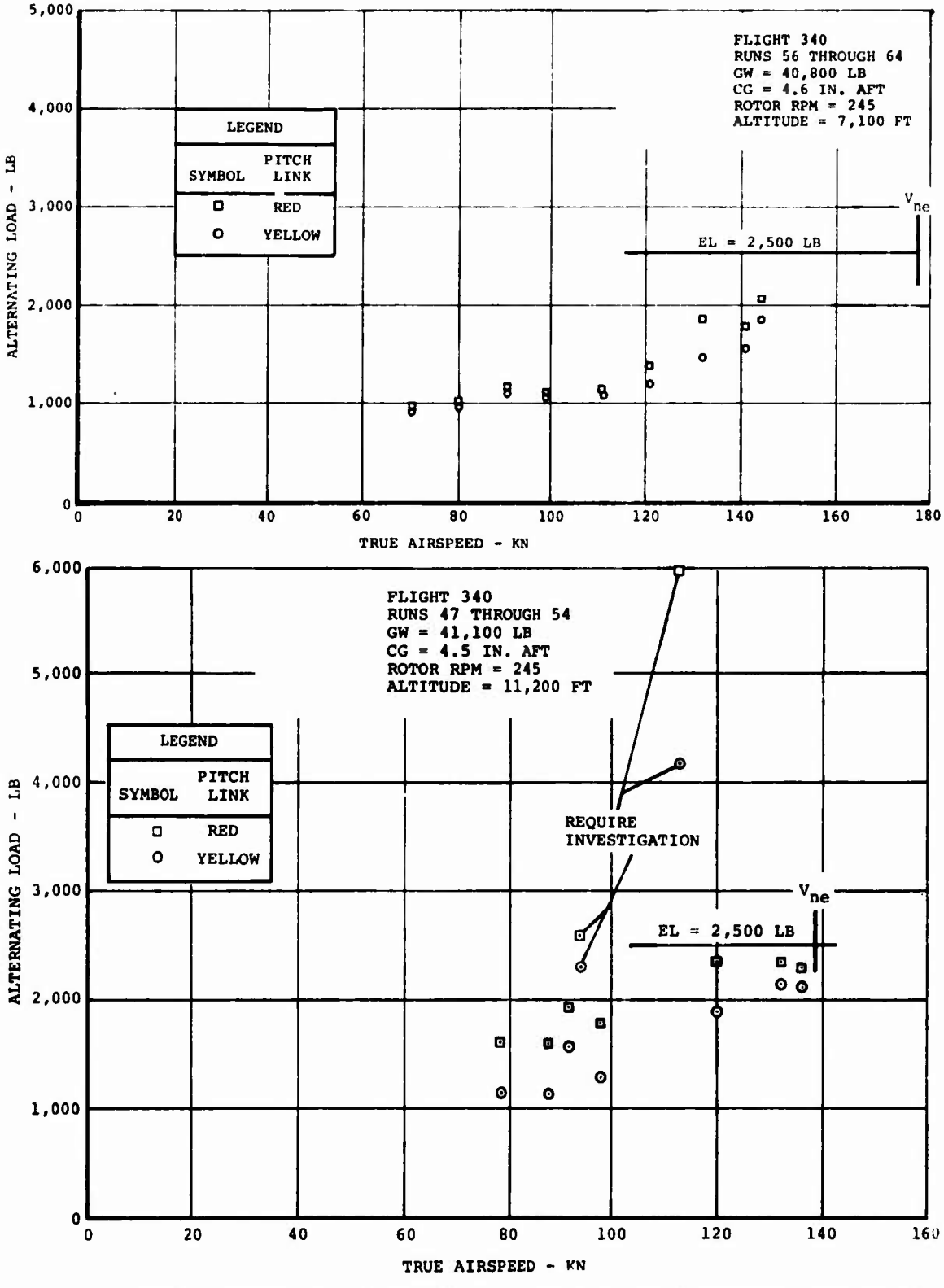

Figure 119. Pitch Link Loads on CH-47C Helicopter Equipped With Boron Advanced-Geometry Blades (V_{ne} for Glass AGB Shown for Reference).

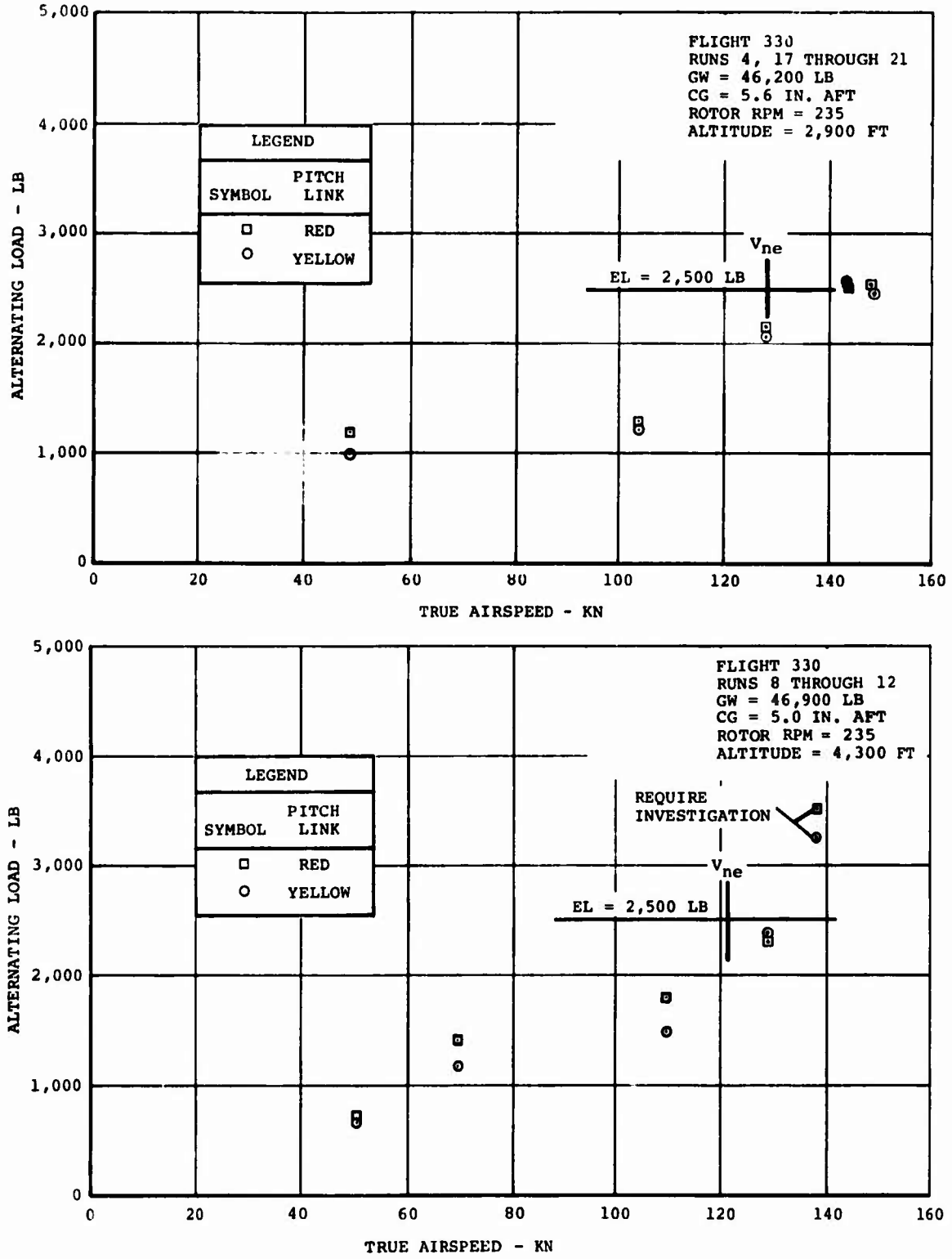

Figure 120. Pitch Link Loads on CH-47C Helicopter Equipped With Boron Advanced-Geometry Blades (V_{ne} for Glass AGB Shown for Reference).

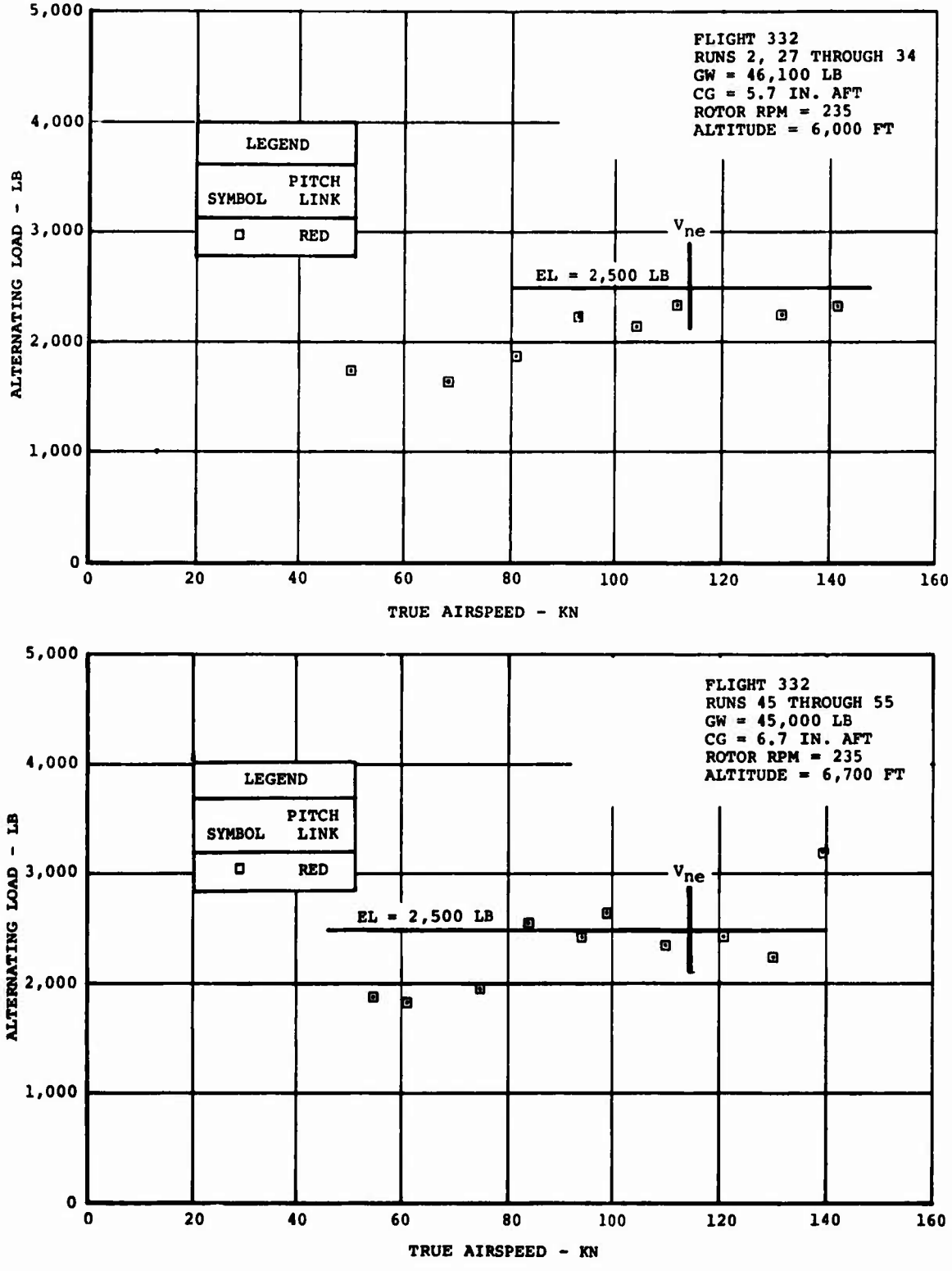

Figure 121. Pitch Link Loads on CH-47C Helicopter Equipped With Boron Advanced-Geometry Blades (V_{ne} for Glass AGB Shown for Reference).

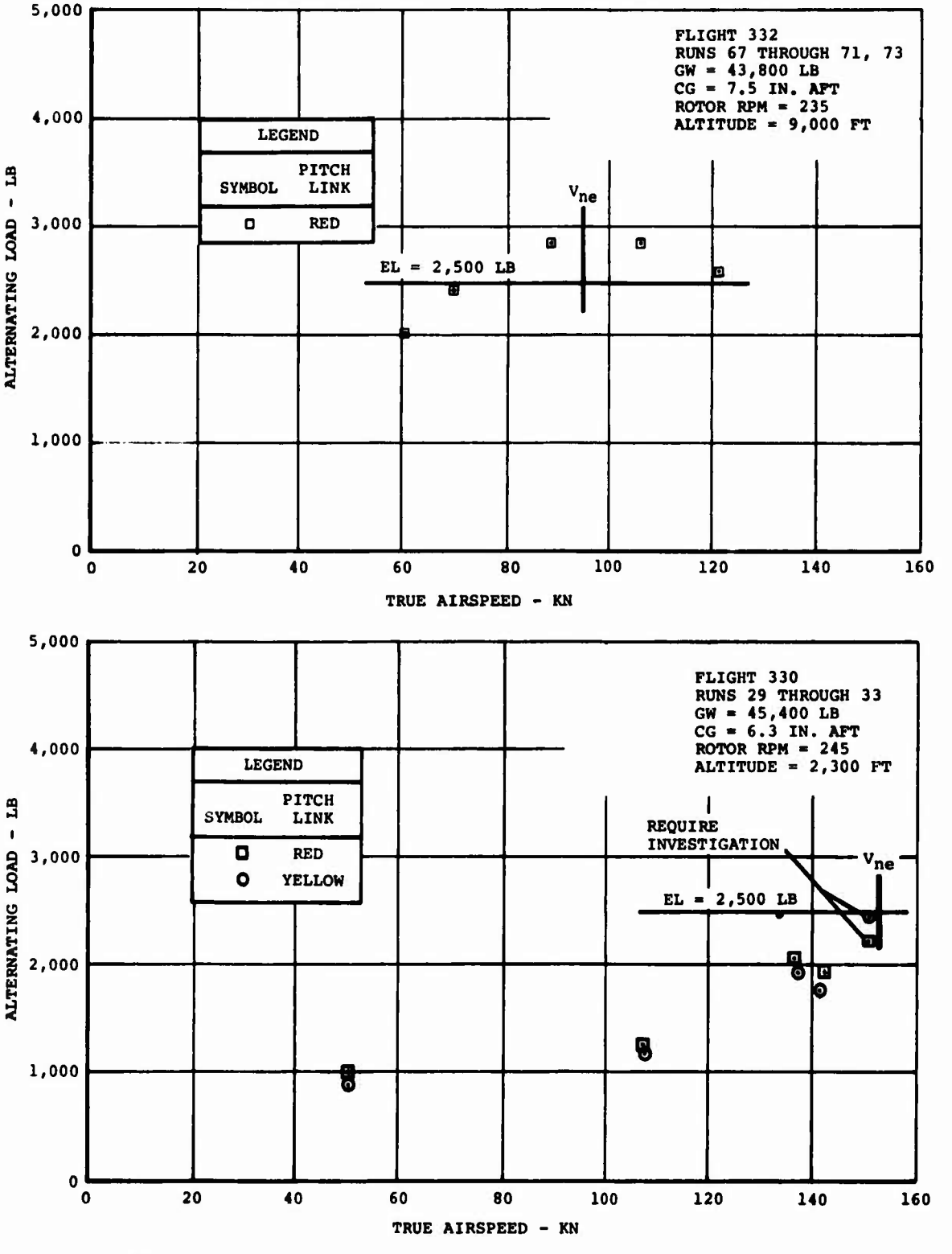

Figure 122. Pitch Link Loads on CH-47C Helicopter Equipped With Boron Advanced-Geometry Blades (V_{ne} for Glass AGB Shown for Reference).

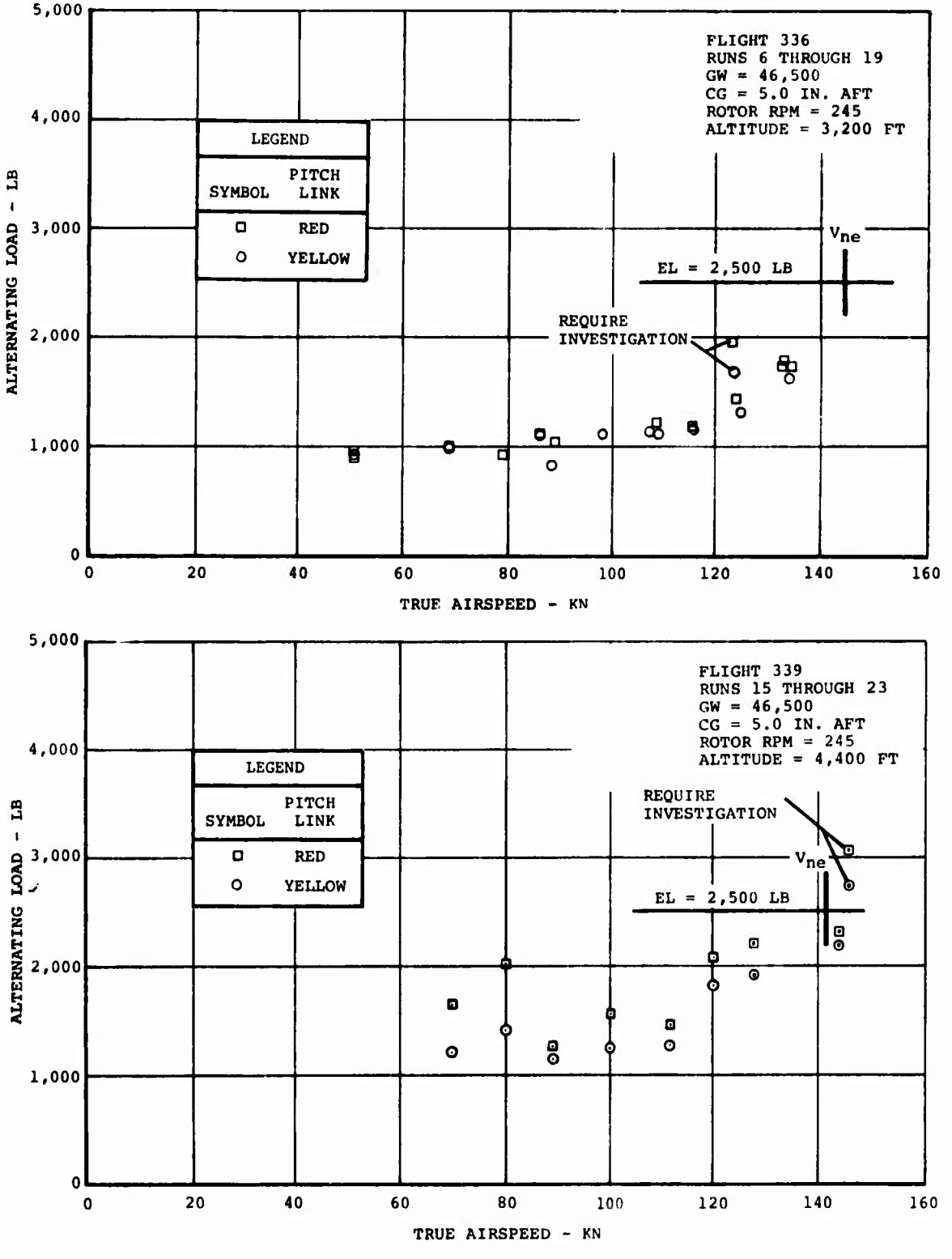

Figure 123. Pitch Link Loads on CH-47C Helicopter Equipped With Boron Advanced-Geometry Blades (V_{ne} for Glass AGB Shown for Reference).

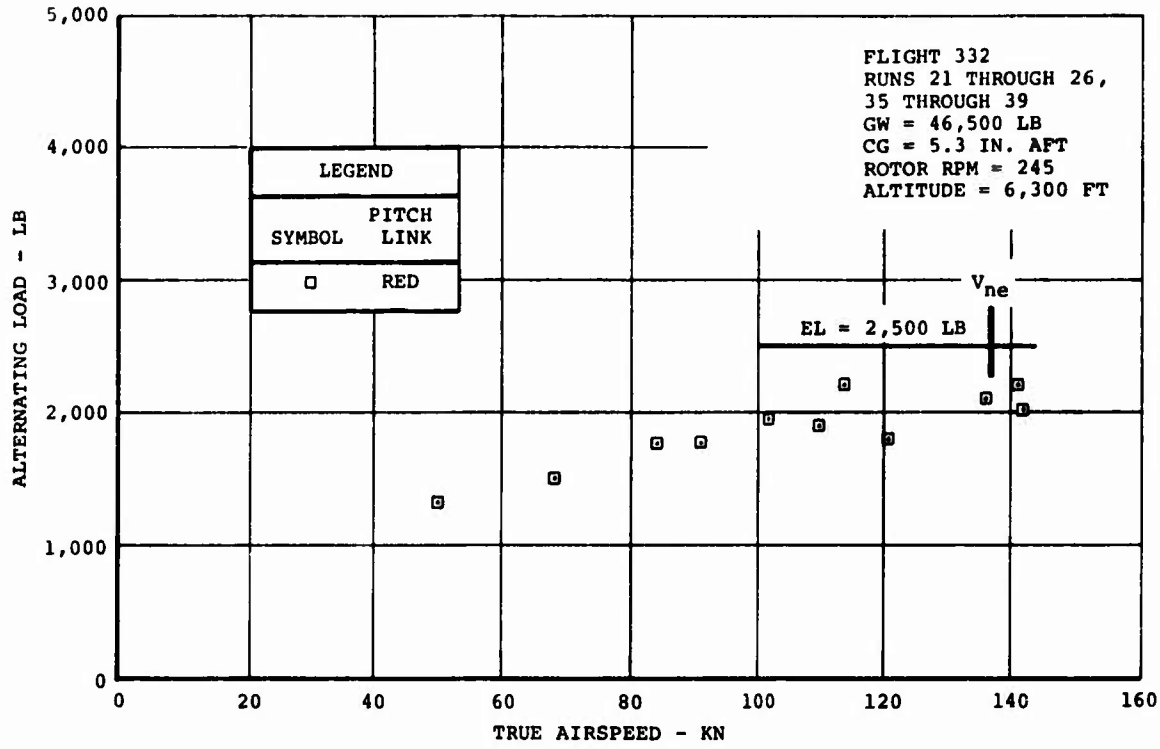

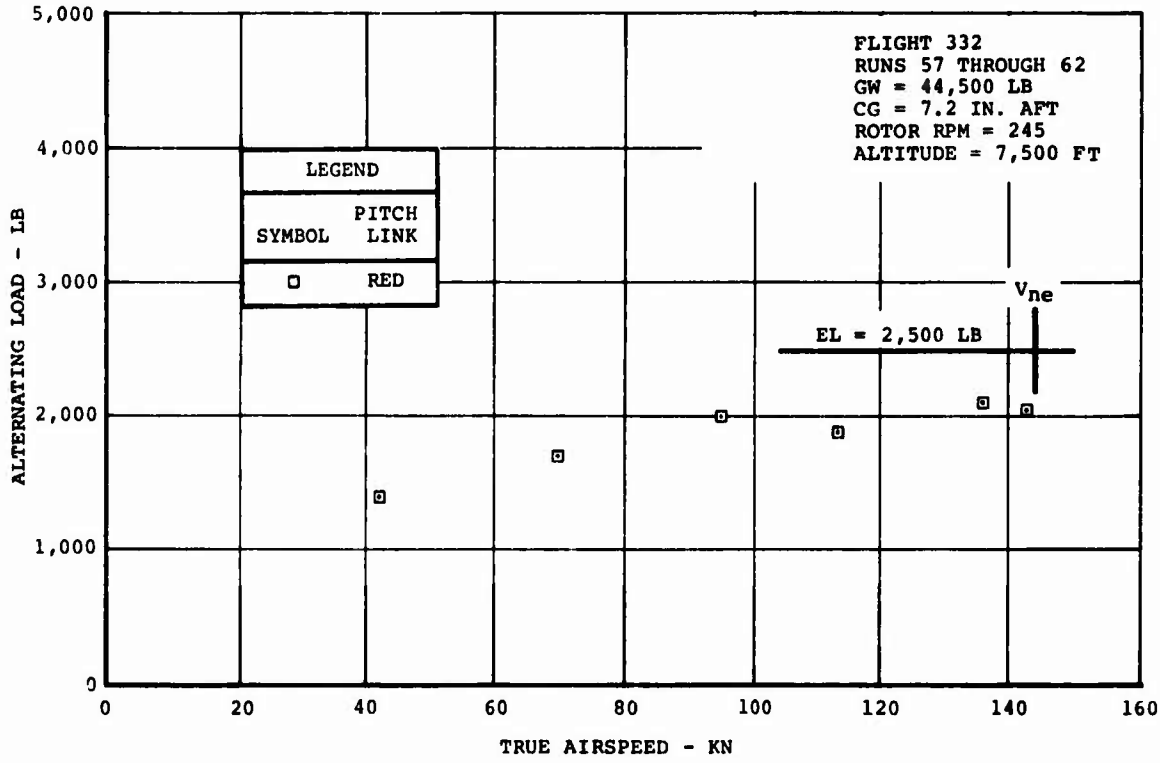

Figure 124. Pitch Link Loads on CH-47C Helicopter Equipped With Boron Advanced-Geometry Blades (V_{ne} for Glass AGB Shown for Reference).

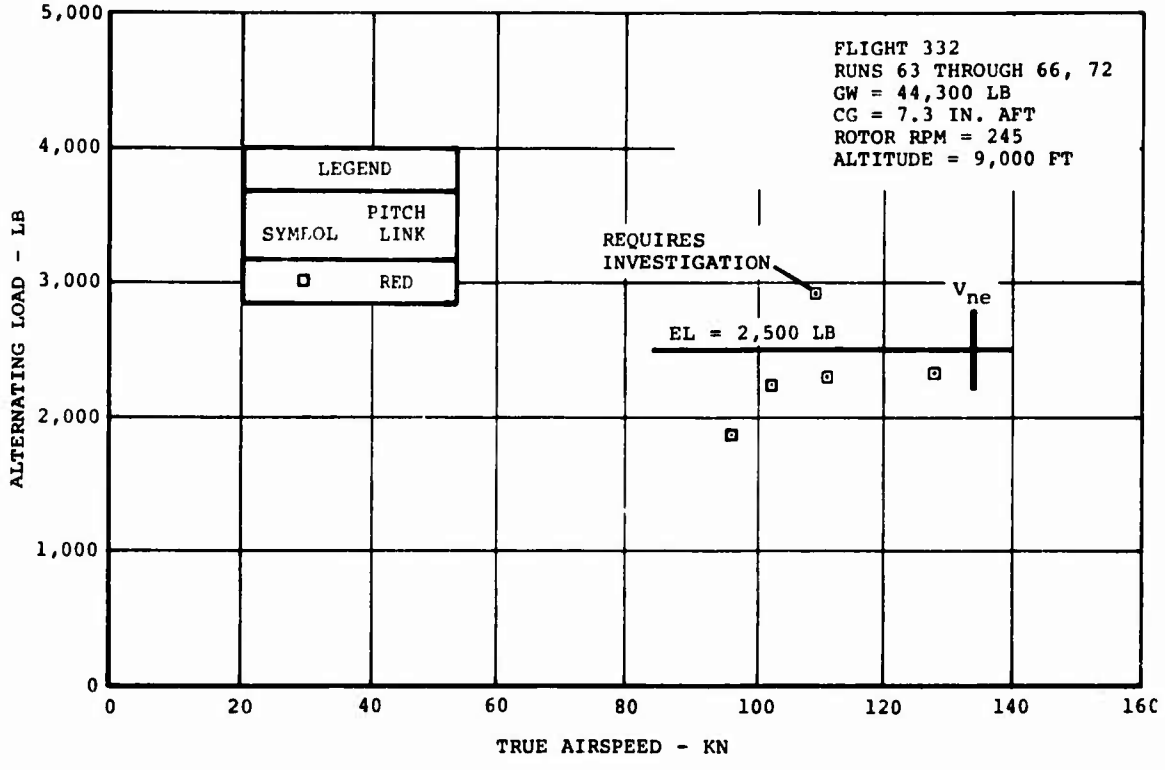

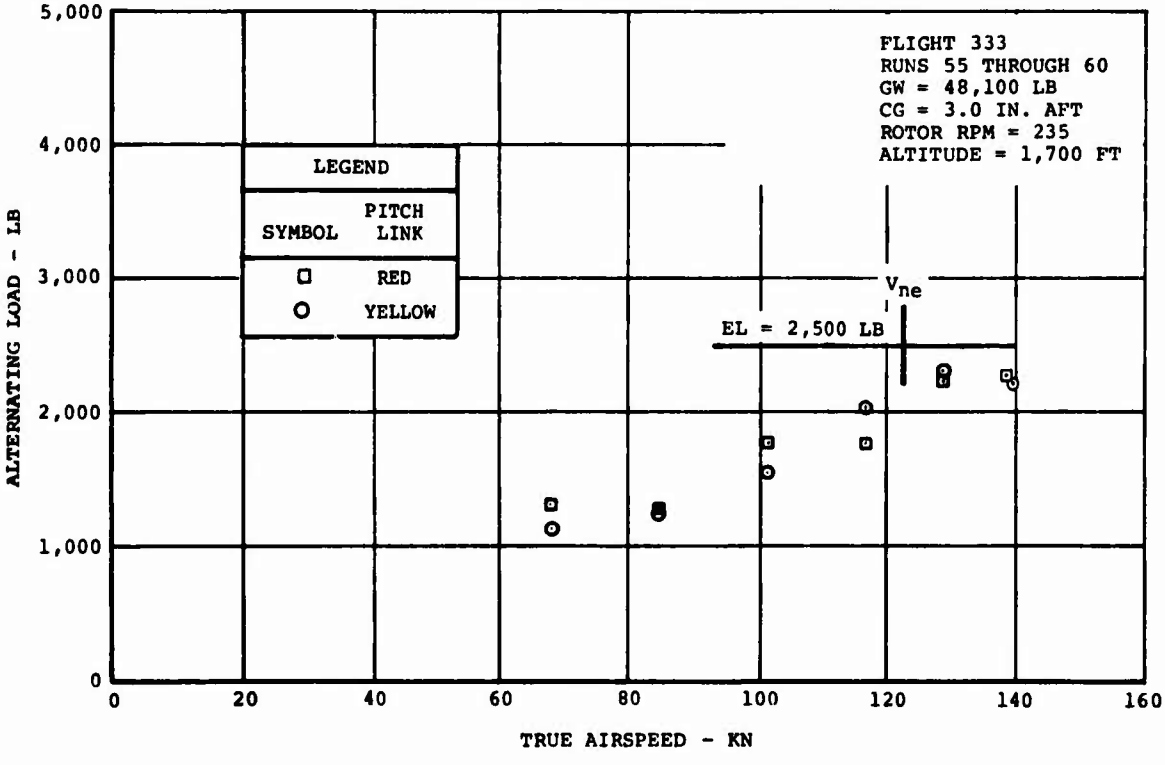

Figure 125. Pitch Link Loads on CH-47C Helicopter Equipped With Boron Advanced-Geometry Blades (V_{ne} for Glass AGB Shown for Reference).

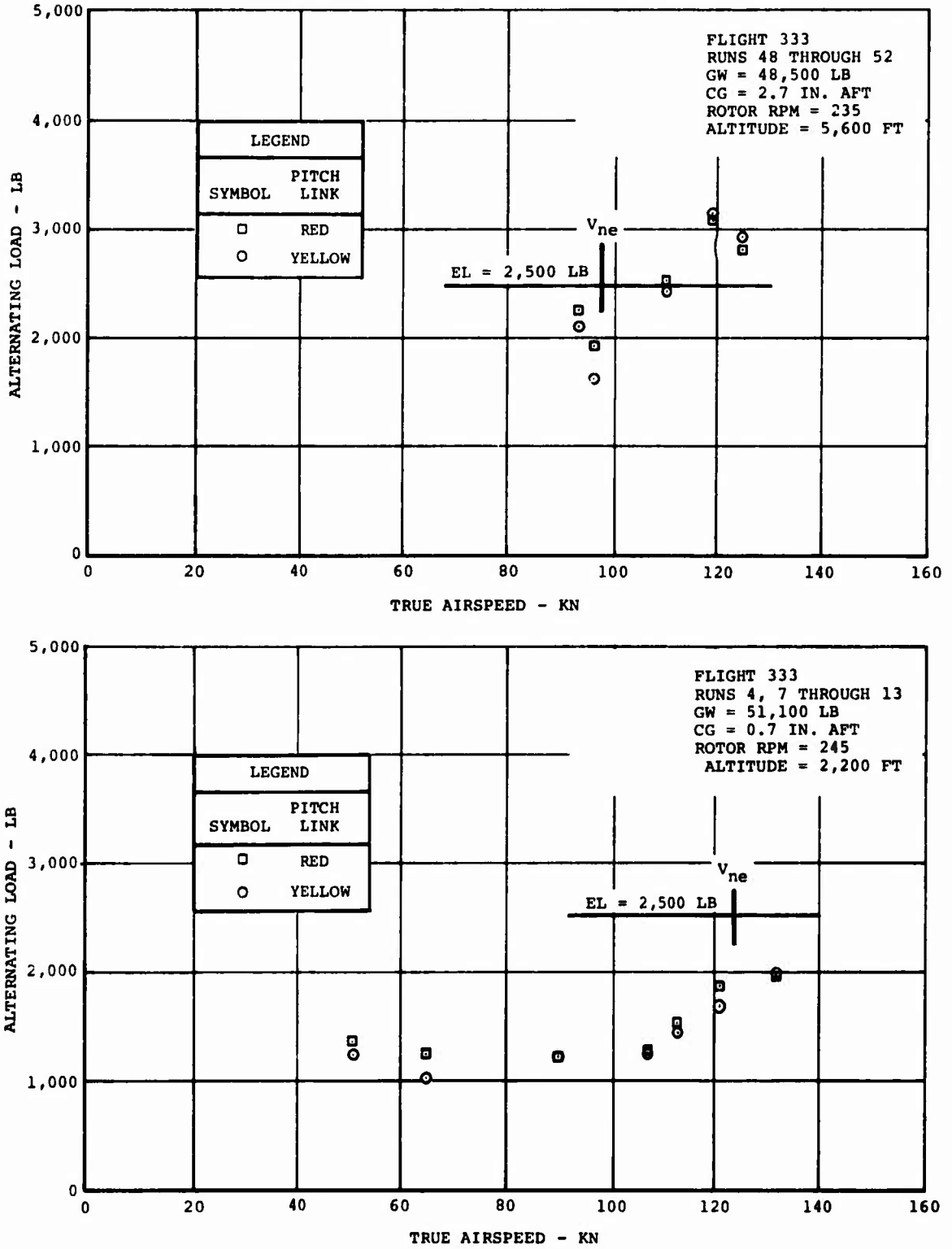

Figure 126. Pitch Link Loads on CH-47C Helicopter Equipped With Boron Advanced-Geometry Blades (V_{ne} for Glass AGB Shown for Reference).

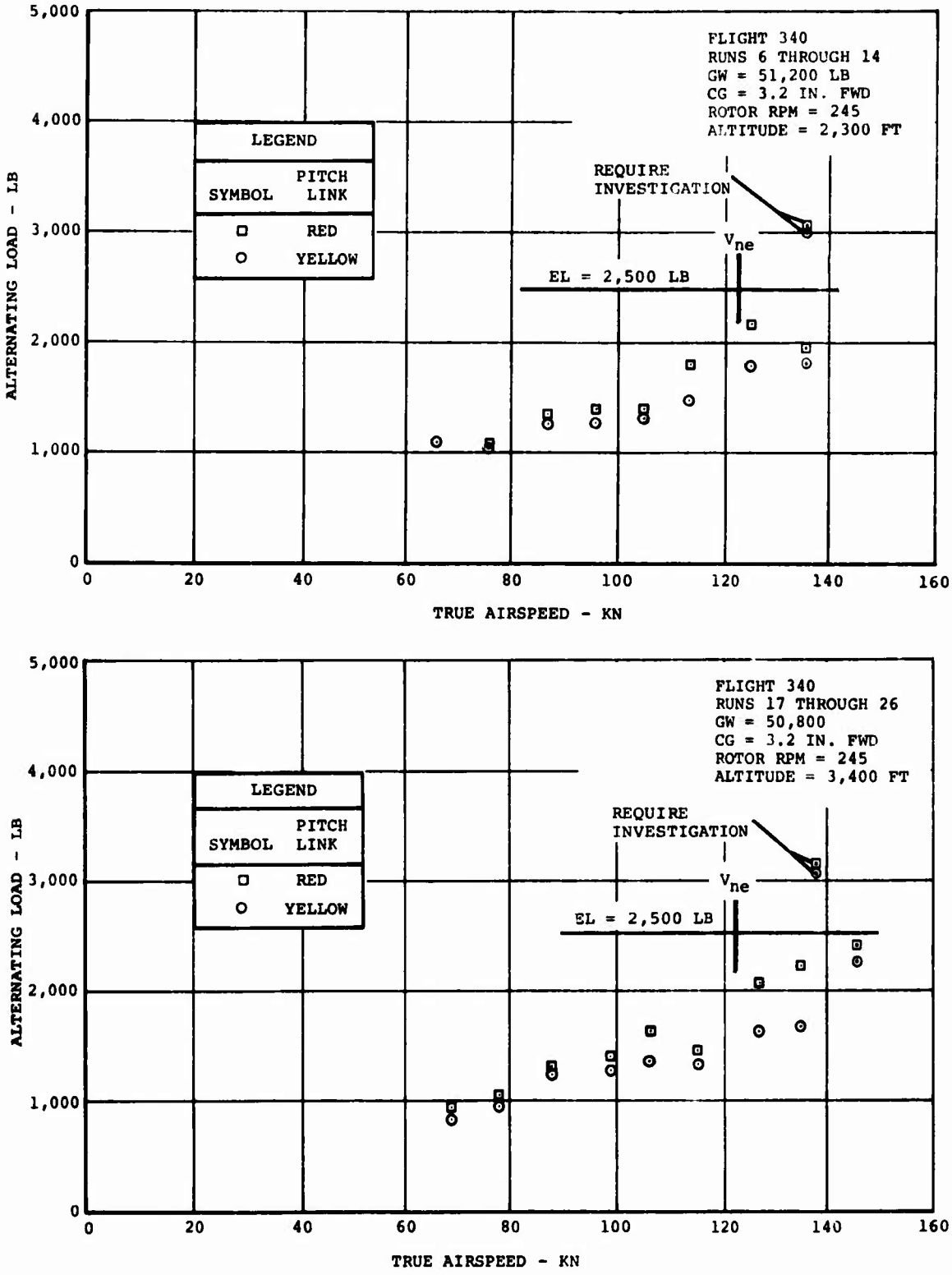

Figure 127. Pitch Link Loads on CH-47C Helicopter Equipped With Boron Advanced-Geometry Blades (V_{ne} for Glass AGB Shown for Reference).

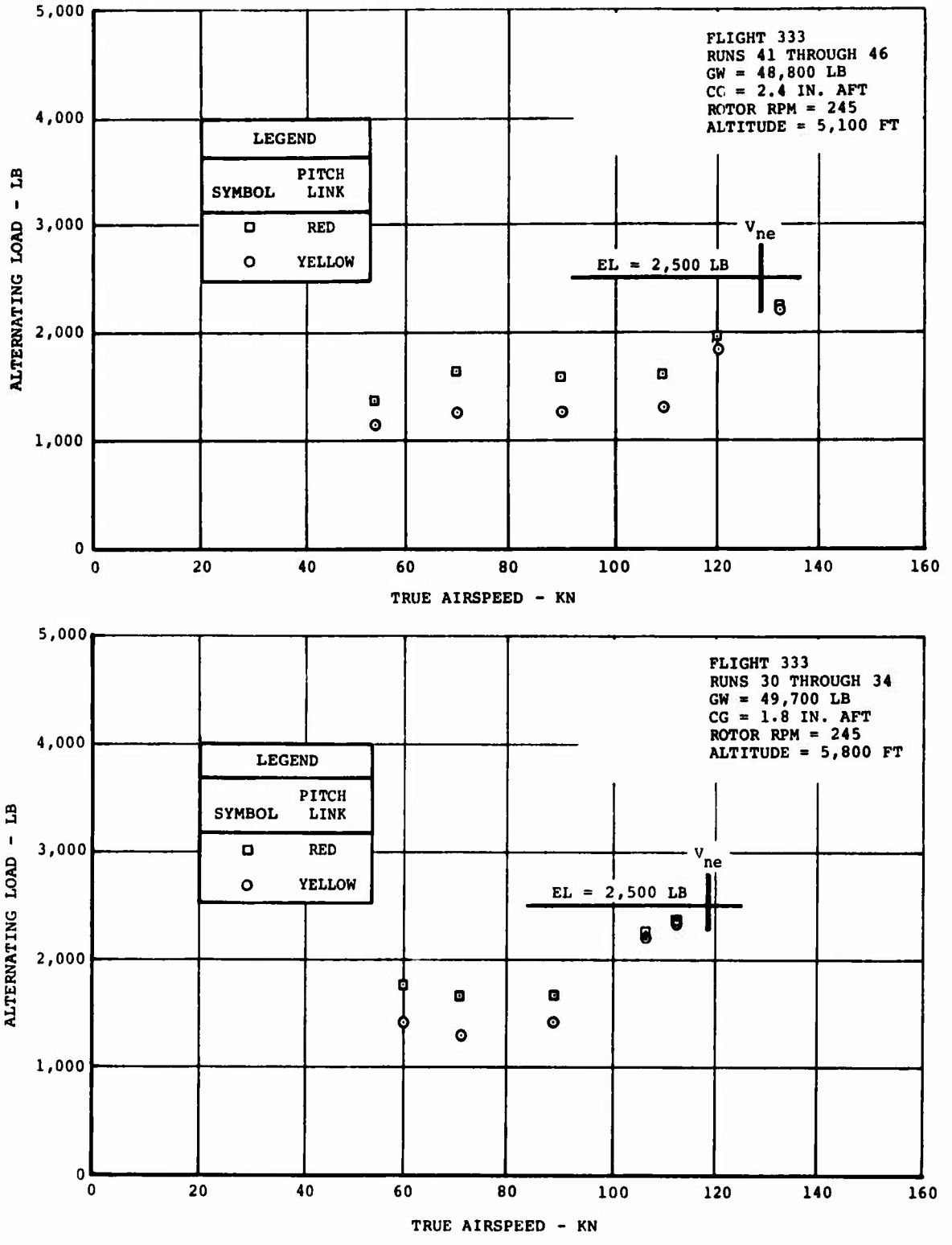

Figure 128. Pitch Link Loads on CH-47C Helicopter Equipped With Boron Advanced-Geometry Blades (V_{ne} for Glass AGB Shown for Reference).

APPENDIX III

SCATTERGRAMS OF FIXED LINK LOADS

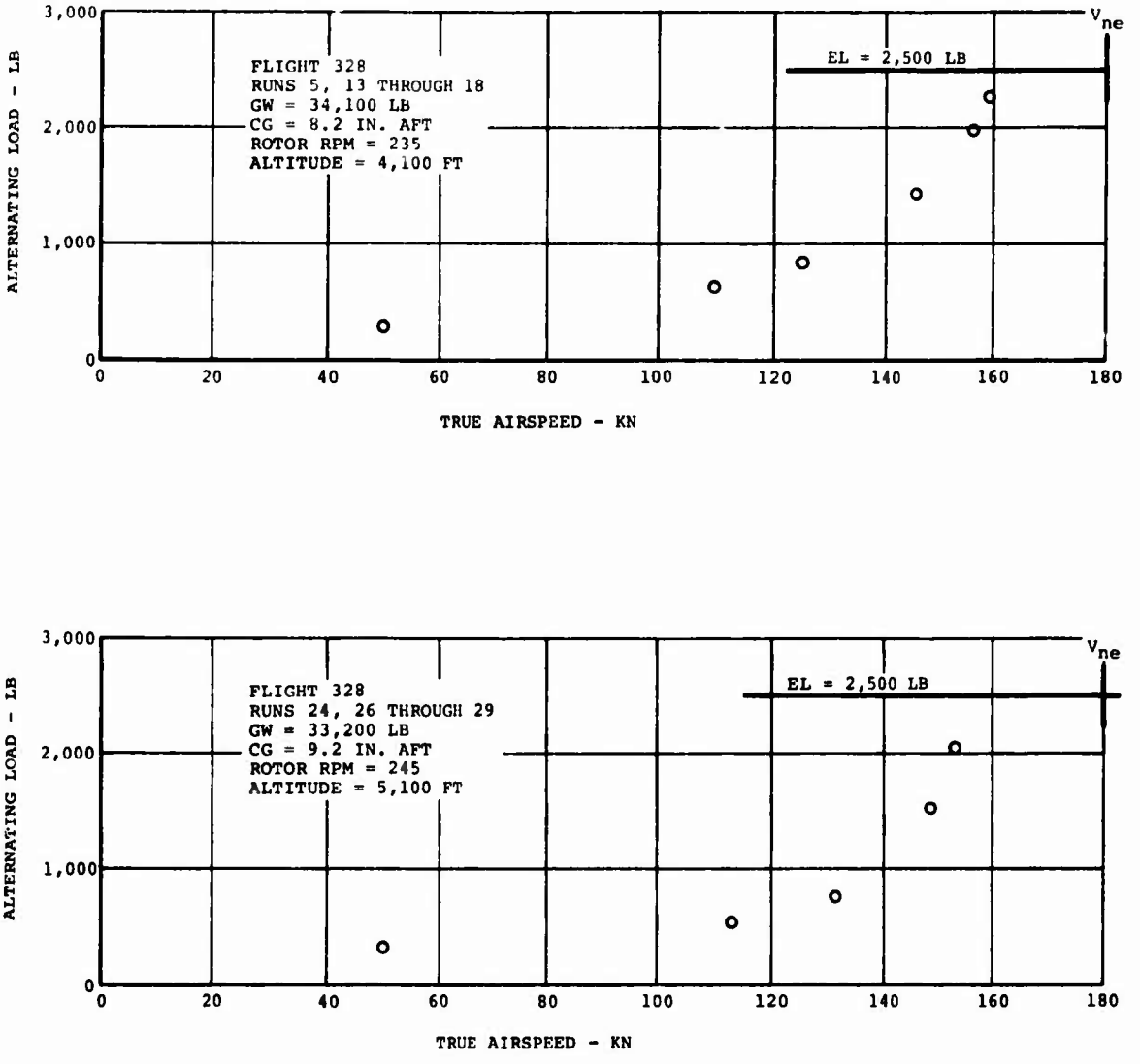

Figure 129. Fixed Link Loads on CH-47C Helicopter Equipped With Boron Advanced-Geometry Blades (V_{ne} for Glass AGB Shown for Reference).

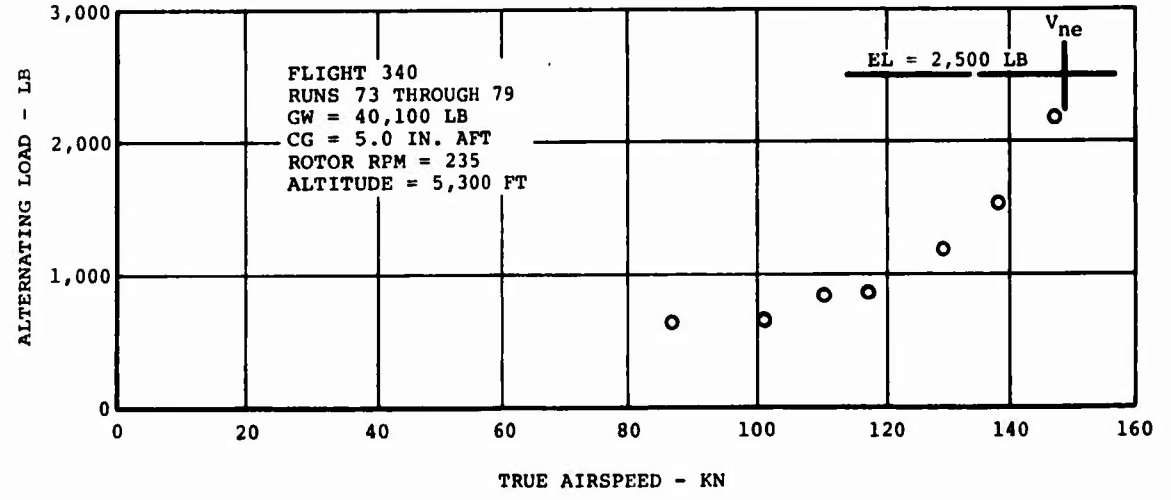

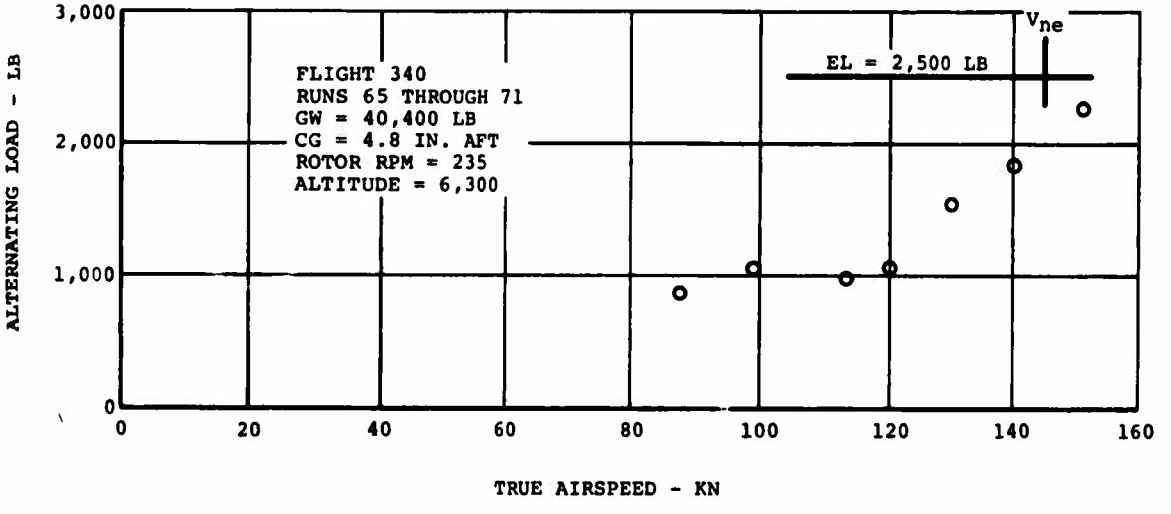

Figure 130. Fixed Link Loads on CH-47C Helicopter Equipped With Boron Advanced-Geometry Blades (V_{ne} for Glass AGB Shown for Reference).

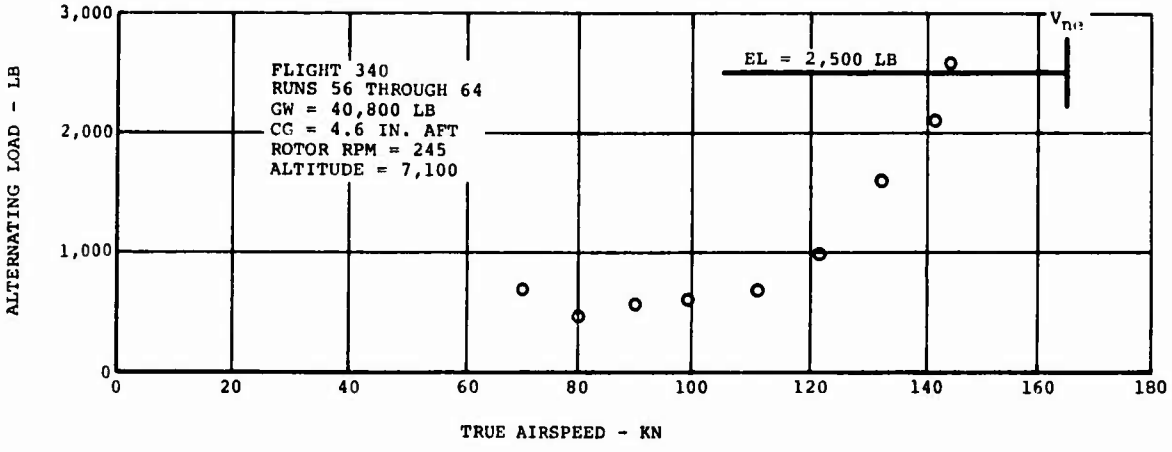

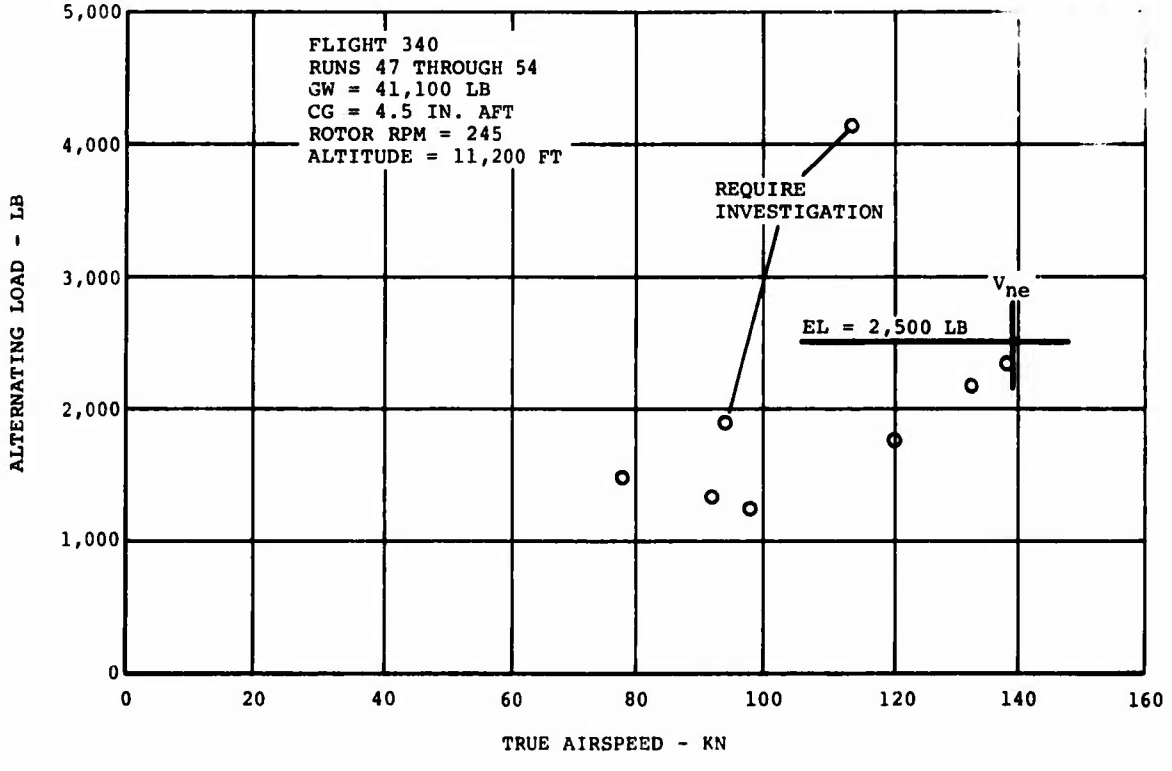

Figure 131. Fixed Link Loads on CH-47C Helicopter Equipped With Boron Advanced-Geometry Blades (V_{ne} for Glass AGB Shown for Reference).

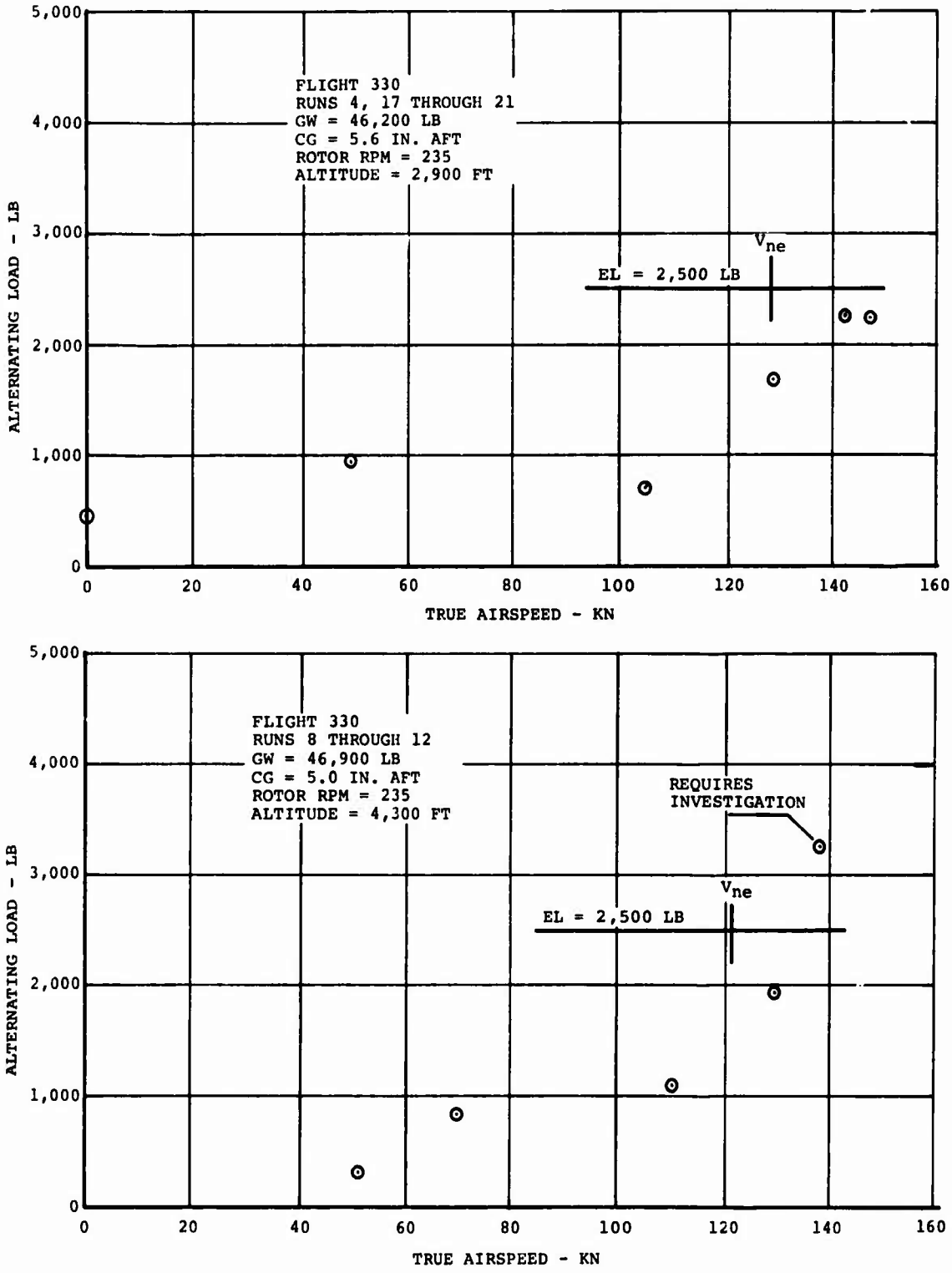

Figure 132. Fixed Link Loads on CH-47C Helicopter Equipped With Boron Advanced-Geometry Blades (V_{ne} for Glass AGB Shown for Reference).

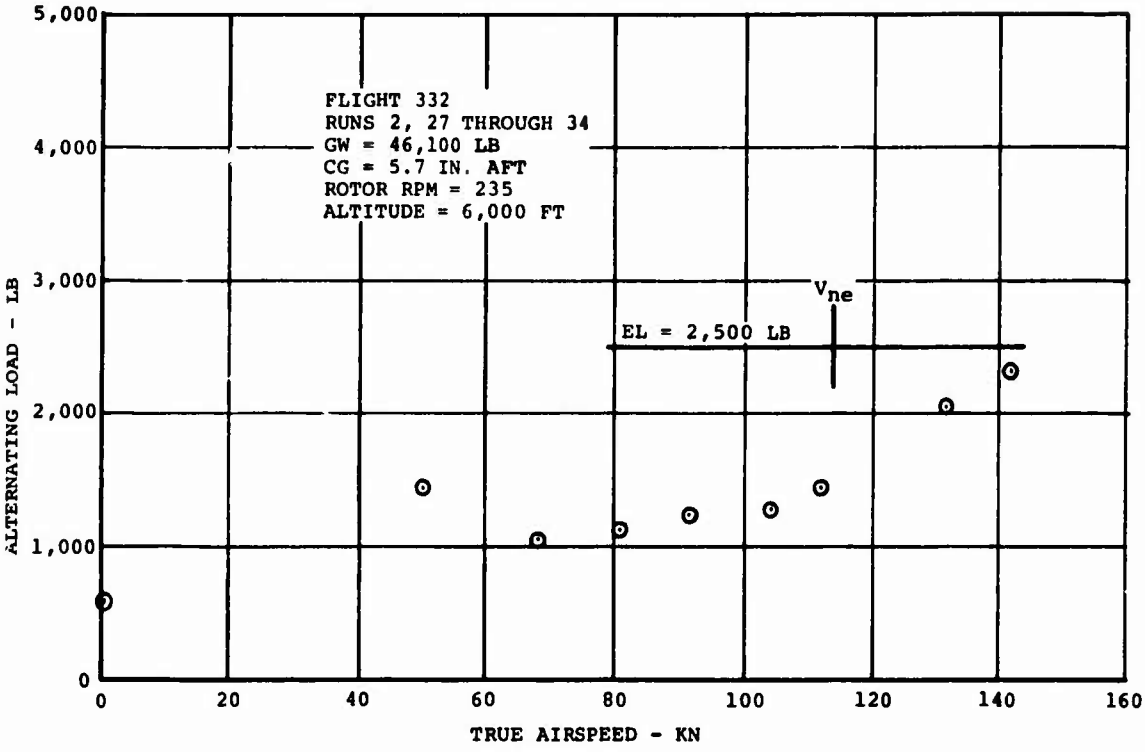

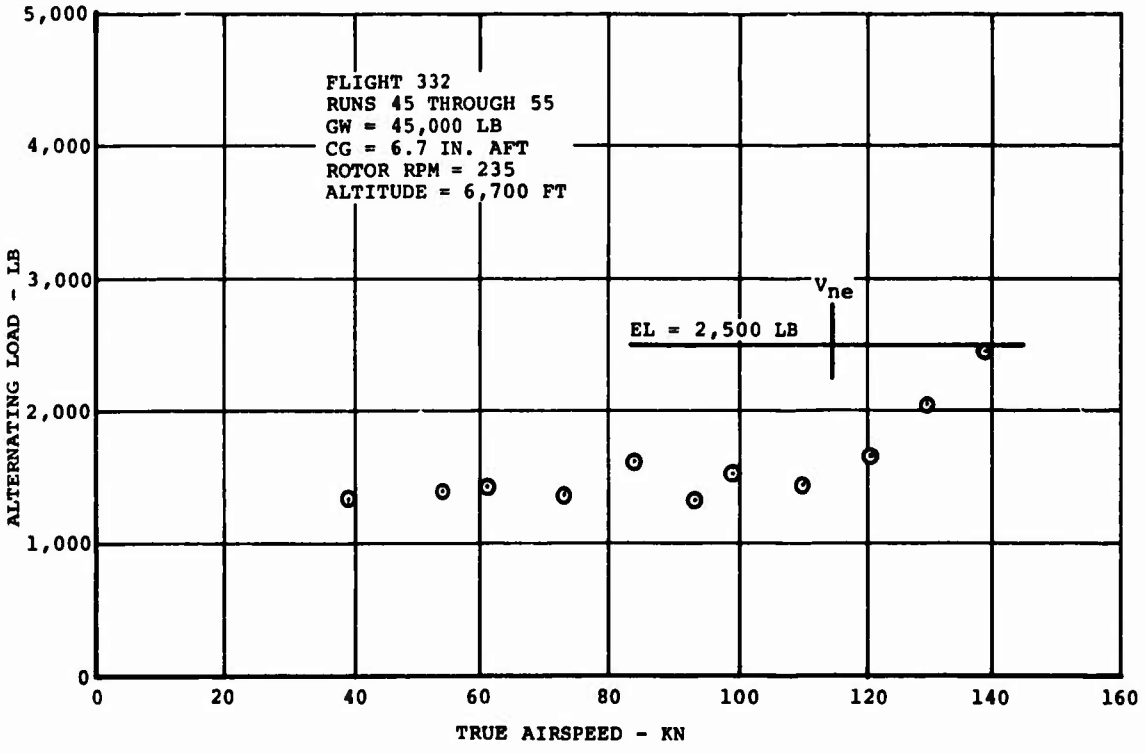

Figure 133. Fixed Link Loads on CH-47C Helicopter Equipped With Boron Advanced-Geometry Blades (V_{ne} for Glass AGB Shown for Reference).

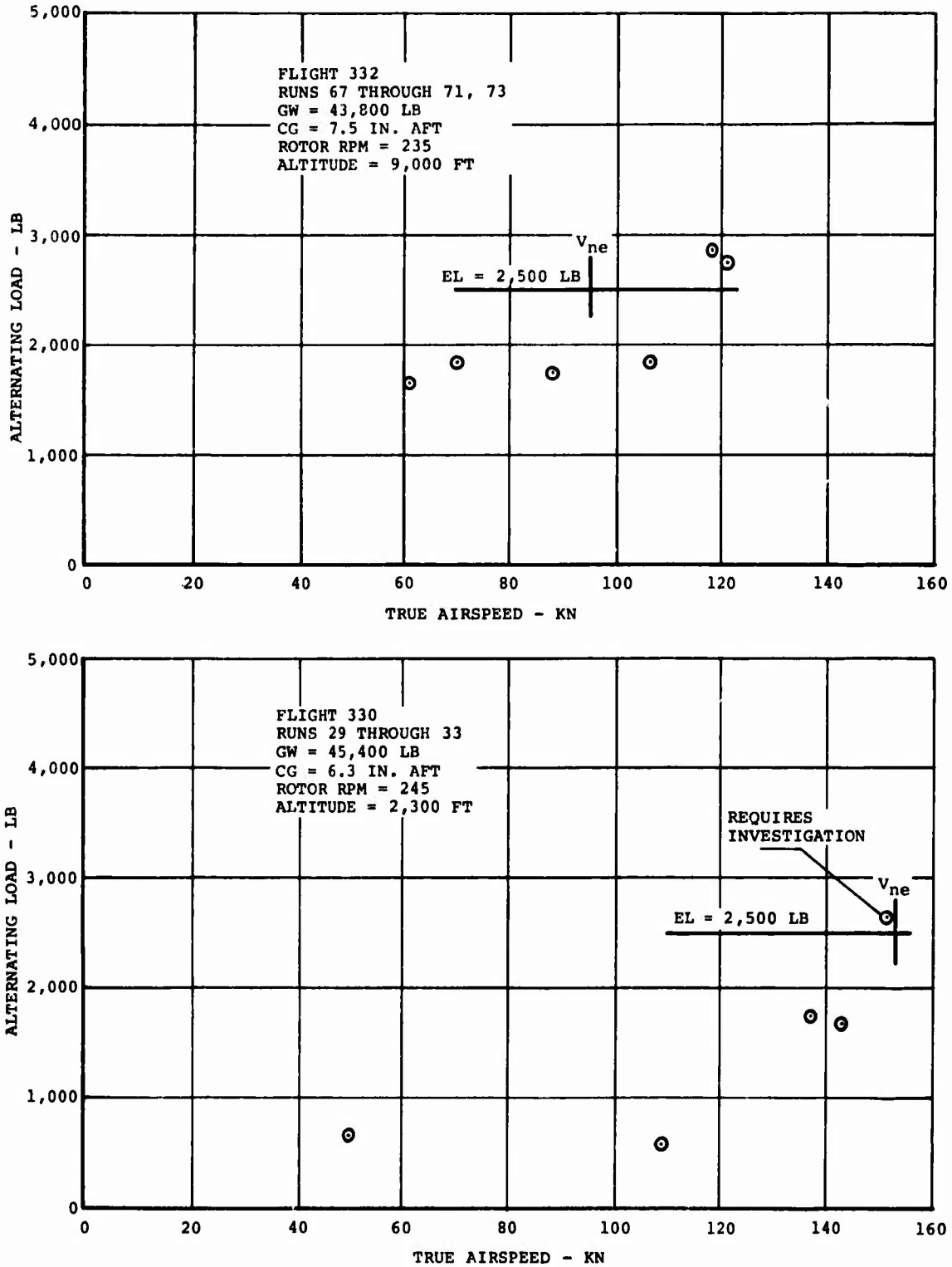

Figure 134. Fixed Link Loads on CH-47C Helicopter Equipped With Boron Advanced-Geometry Blades (V_{ne} for Glass AGB Shown for Reference).

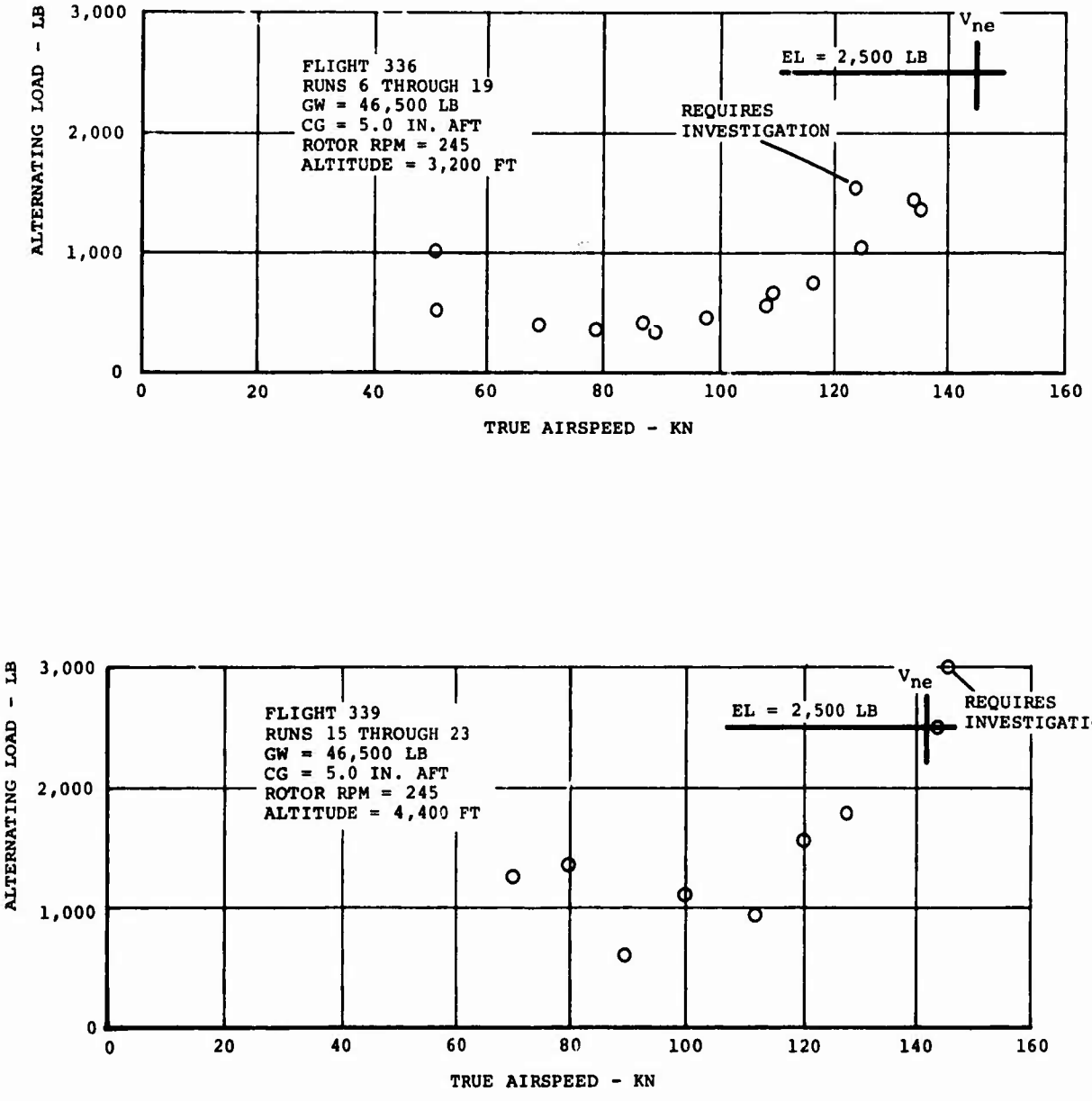

Figure 135. Fixed Link Loads on CH-47C Helicopter Equipped With Boron Advanced-Geometry Blades (V_{ne} for Glass AGB Shown for Reference).

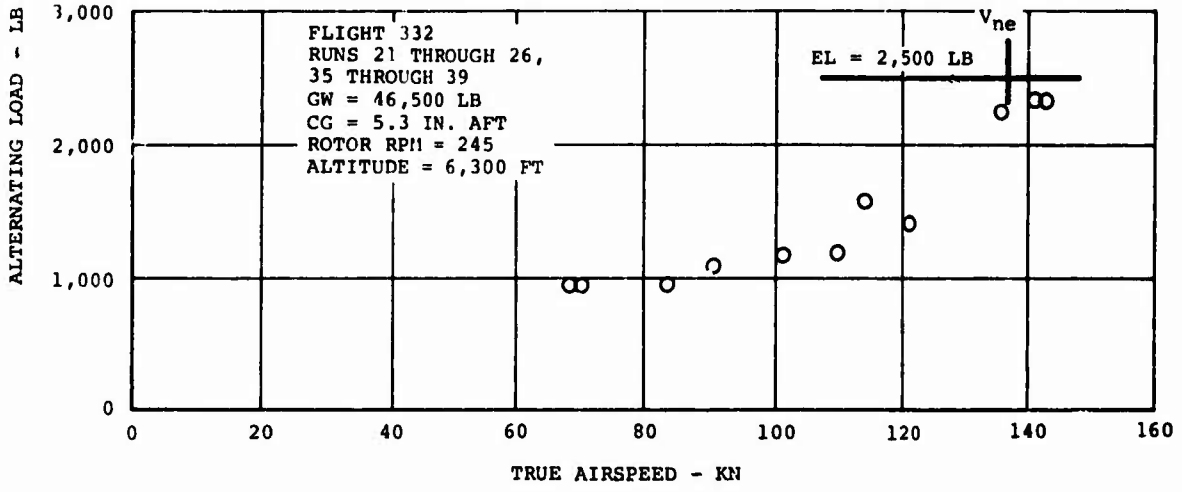

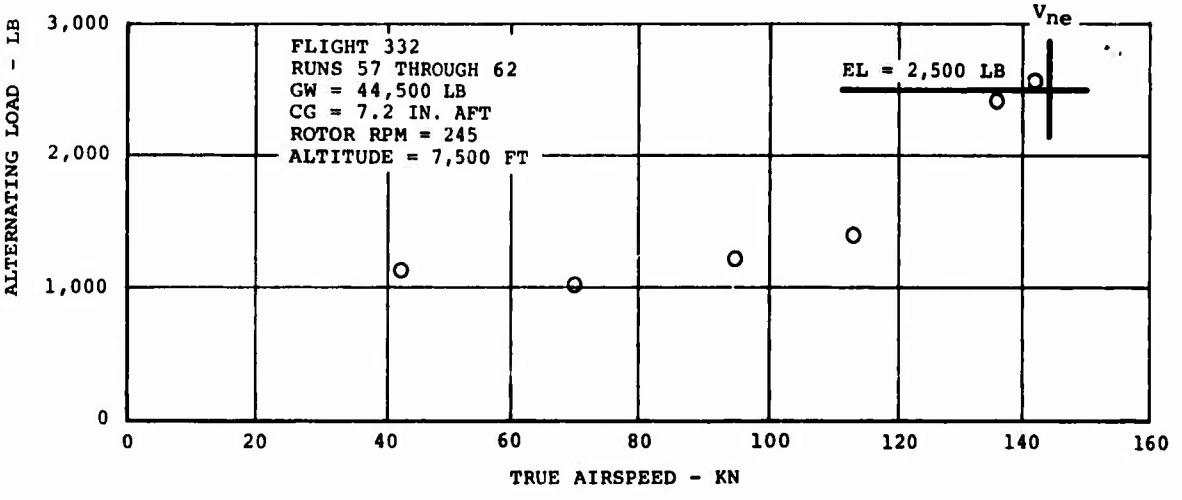

Figure 136. Fixed Link Loads on CH-47C Helicopter Equipped With Boron Advanced-Geometry Blades (V_{ne} for Glass AGB Shown for Reference).

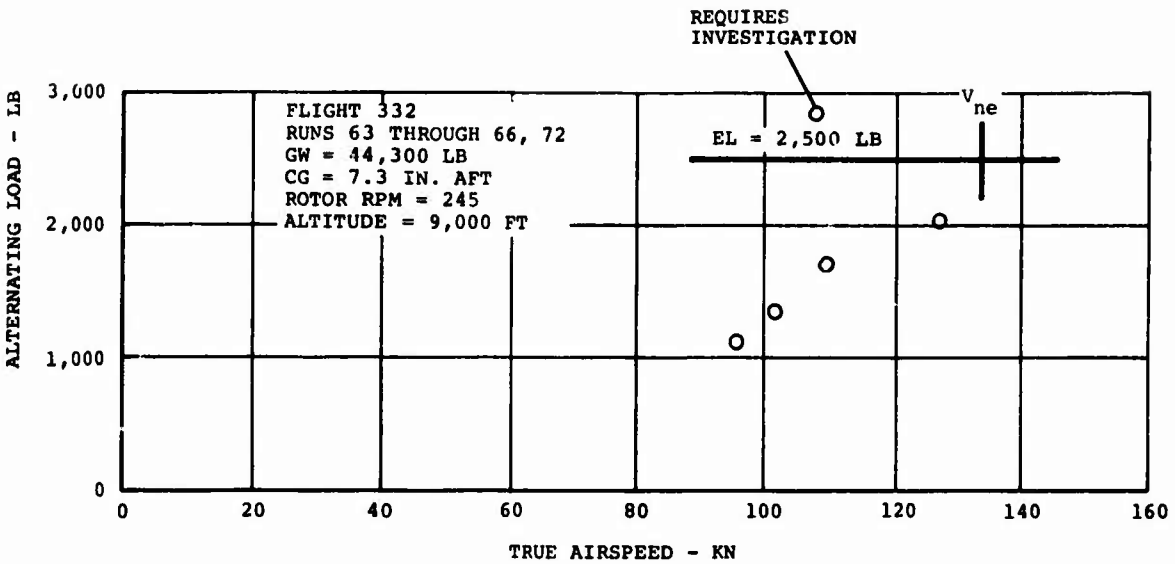

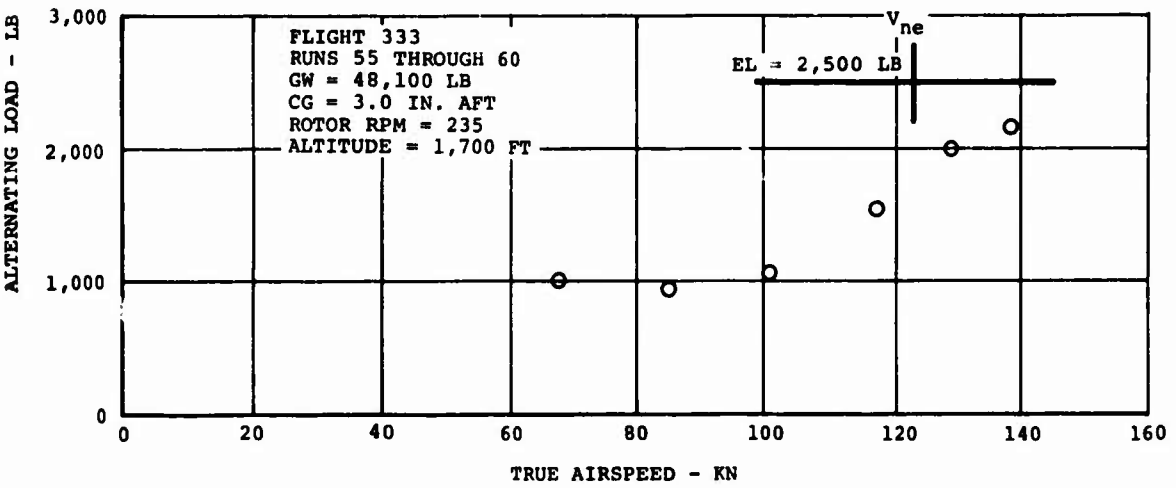

Figure 137. Fixed Link Loads on CH-47C Helicopter Equipped With Boron Advanced-Geometry Blades (V_{ne} for Glass AGB Shown for Reference).

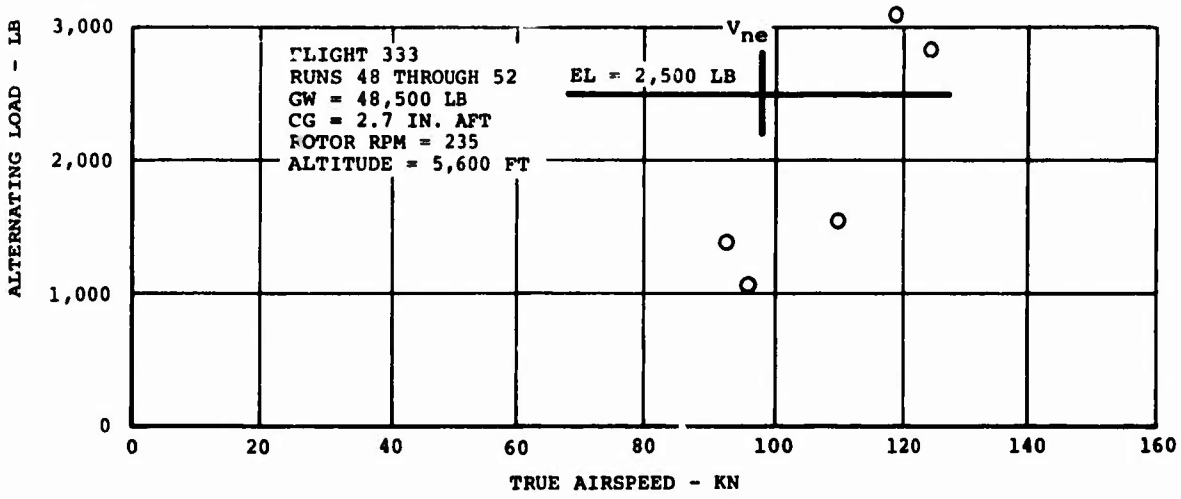

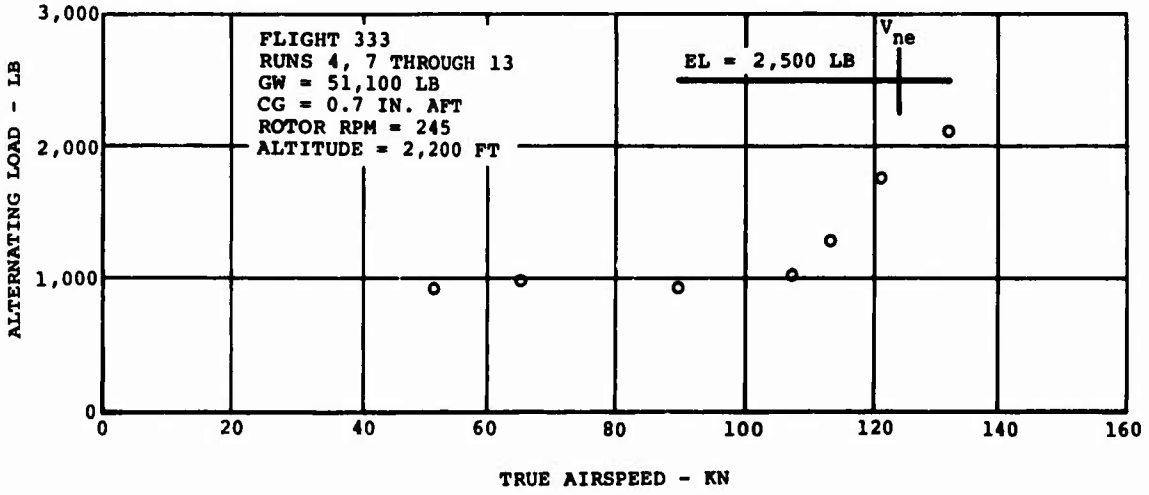

Figure 138. Fixed Link Loads on CH-47C Helicopter Equipped With Boron Advanced-Geometry Blades (V_{ne} for Glass AGB Shown for Reference).

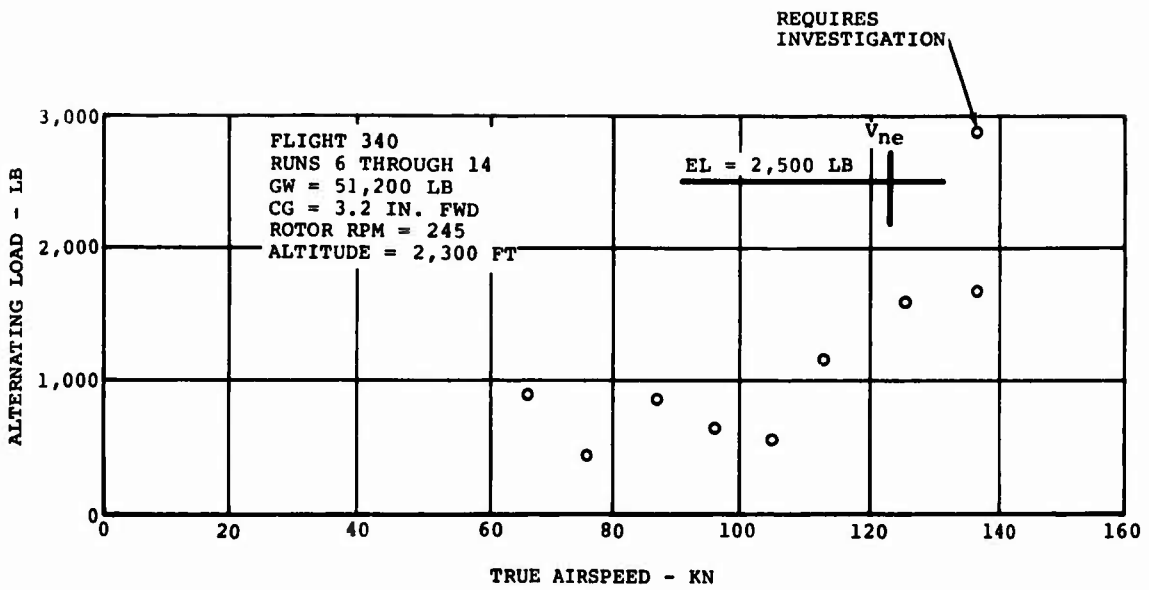

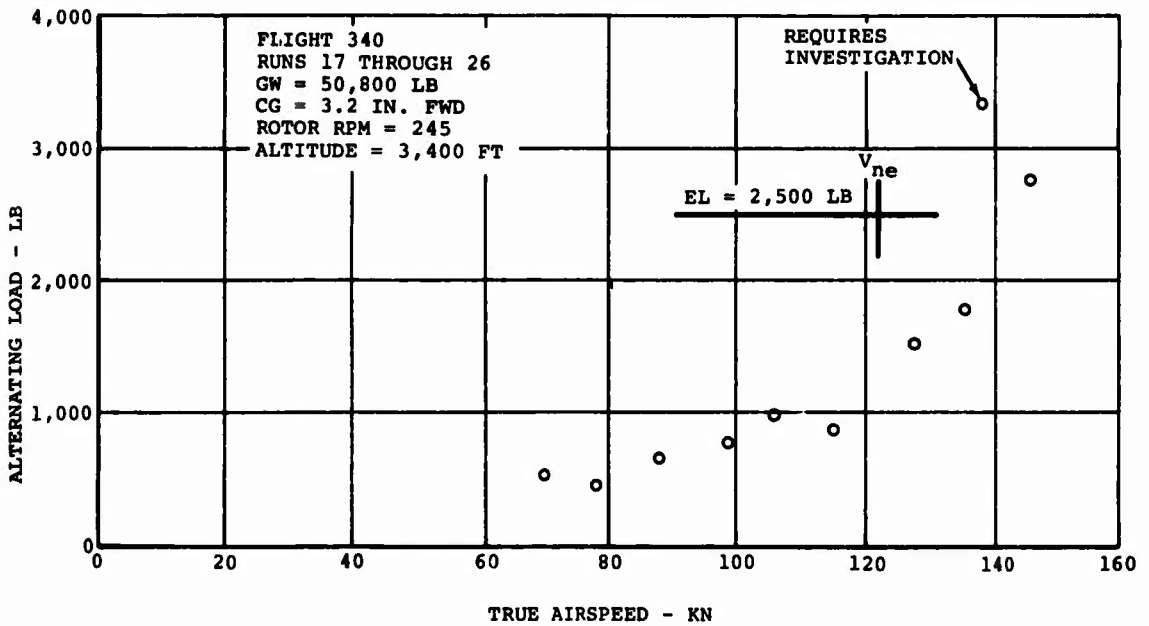

Figure 139. Fixed Link Loads on CH-47C Helicopter Equipped With Boron Advanced-Geometry Blades (V_{ne} for Glass AGB Shown for Reference).

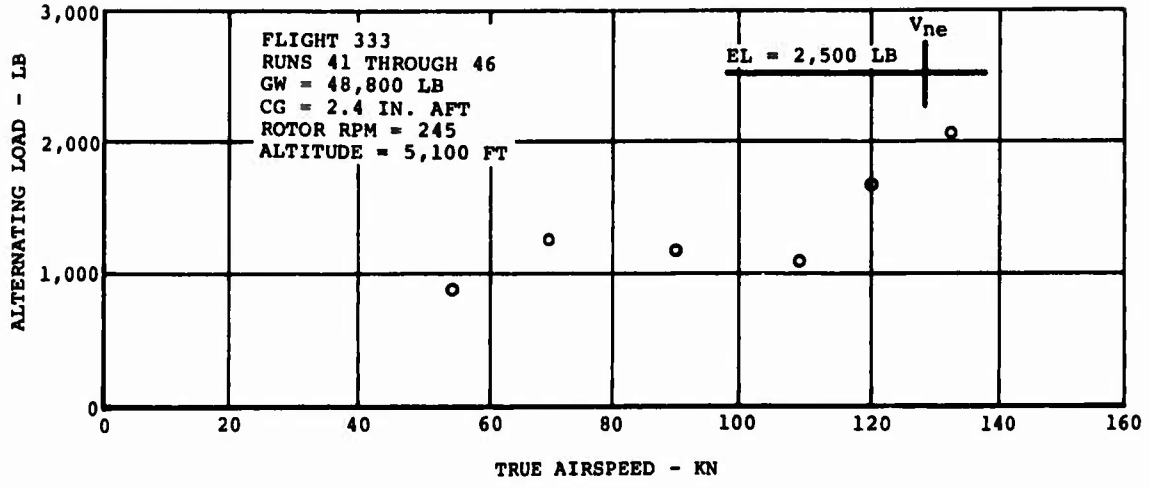

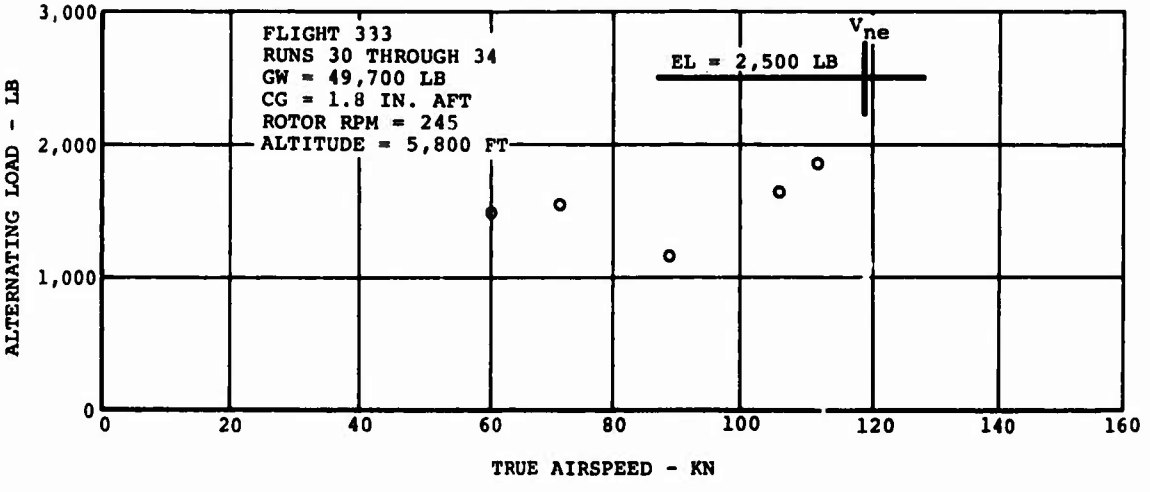

Figure 140. Fixed Link Loads on CH-47C Helicopter Equipped With Boron Advanced-Geometry Blades (V_{ne} for Glass AGB Shown for Reference).

APPENDIX IV

SCATTERGRAMS OF ROTOR SHAFT LOADS

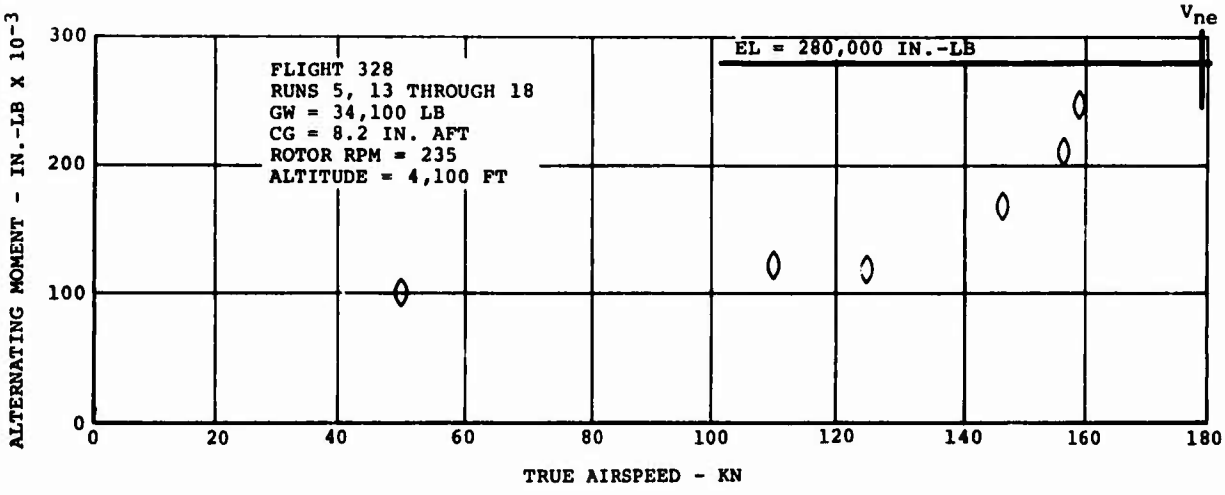

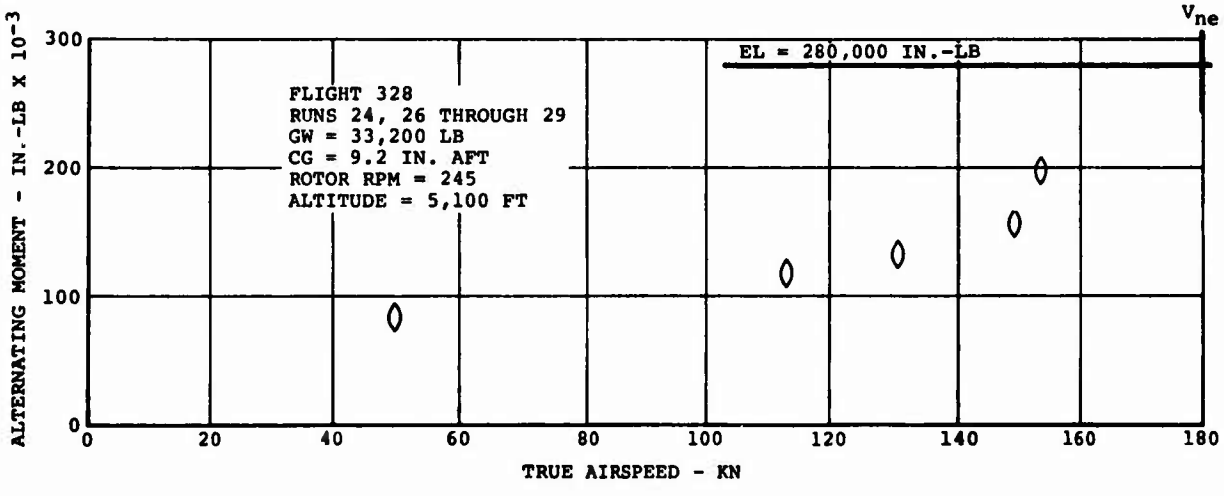

Figure 141. Rotor Shaft Bending (23.1 Inches TOS) on CH-47C Helicopter Equipped With Boron Advanced-Geometry Blades (V_{ne} for Glass AGB Shown in Reference).

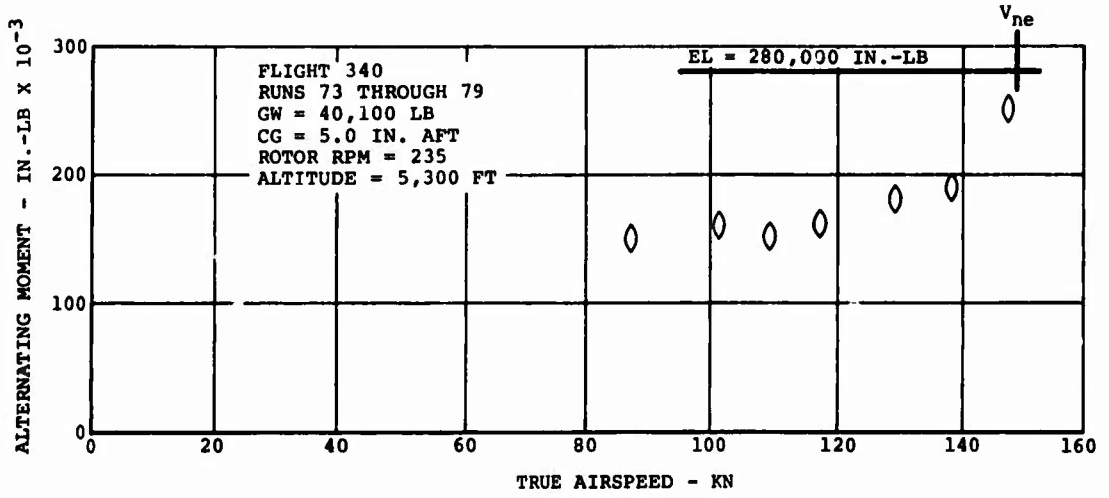

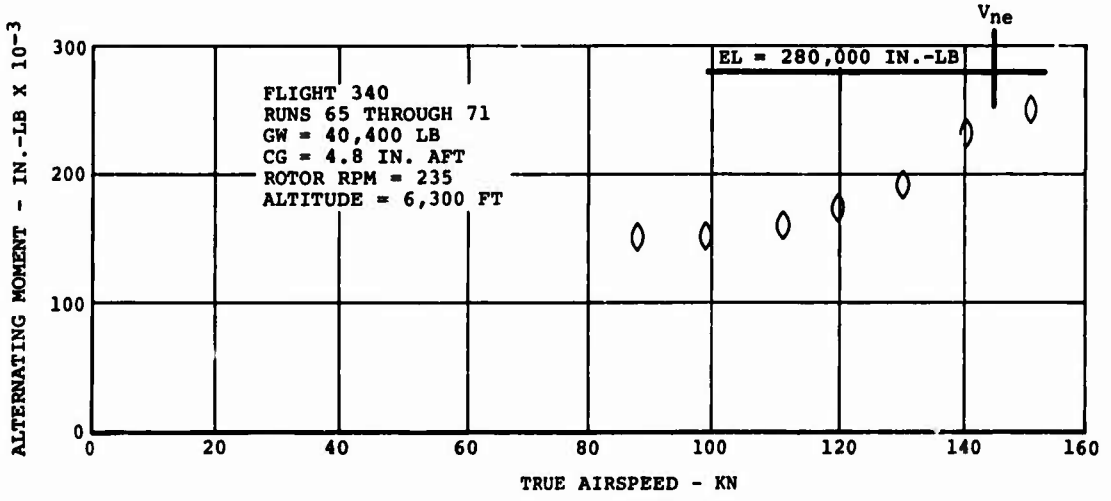

Figure 142. Rotor Shaft Bending (23.1 Inches TOS) on CH-47C Helicopter Equipped With Boron Advanced-Geometry Blades (V_{ne} for Glass AGB Shown in Reference).

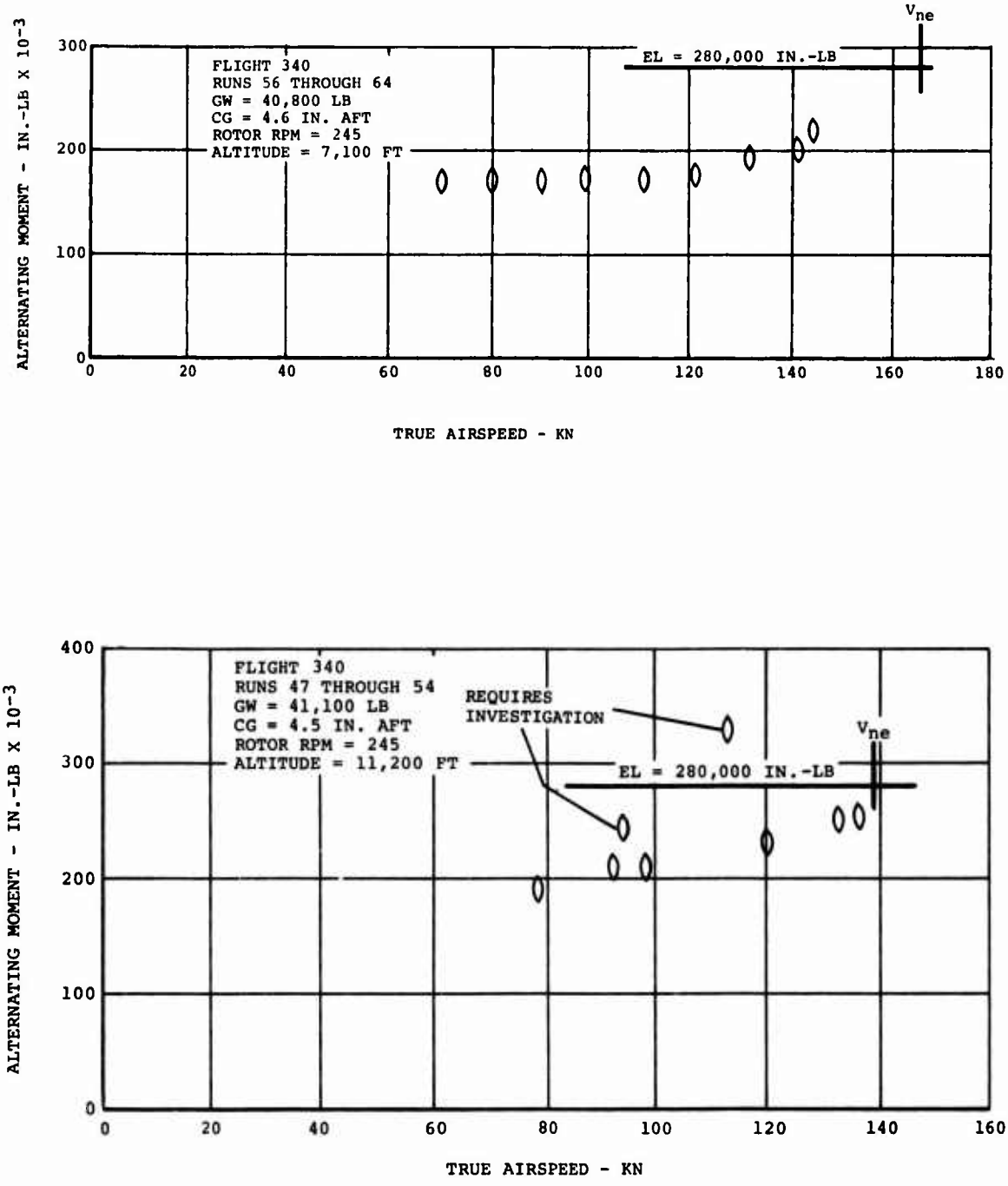

Figure 143. Rotor Shaft Bending (23.1 Inches TOS) on CH-47C Helicopter Equipped With Boron Advanced-Geometry Blades (V_{ne} for Glass AGB Shown for Reference).

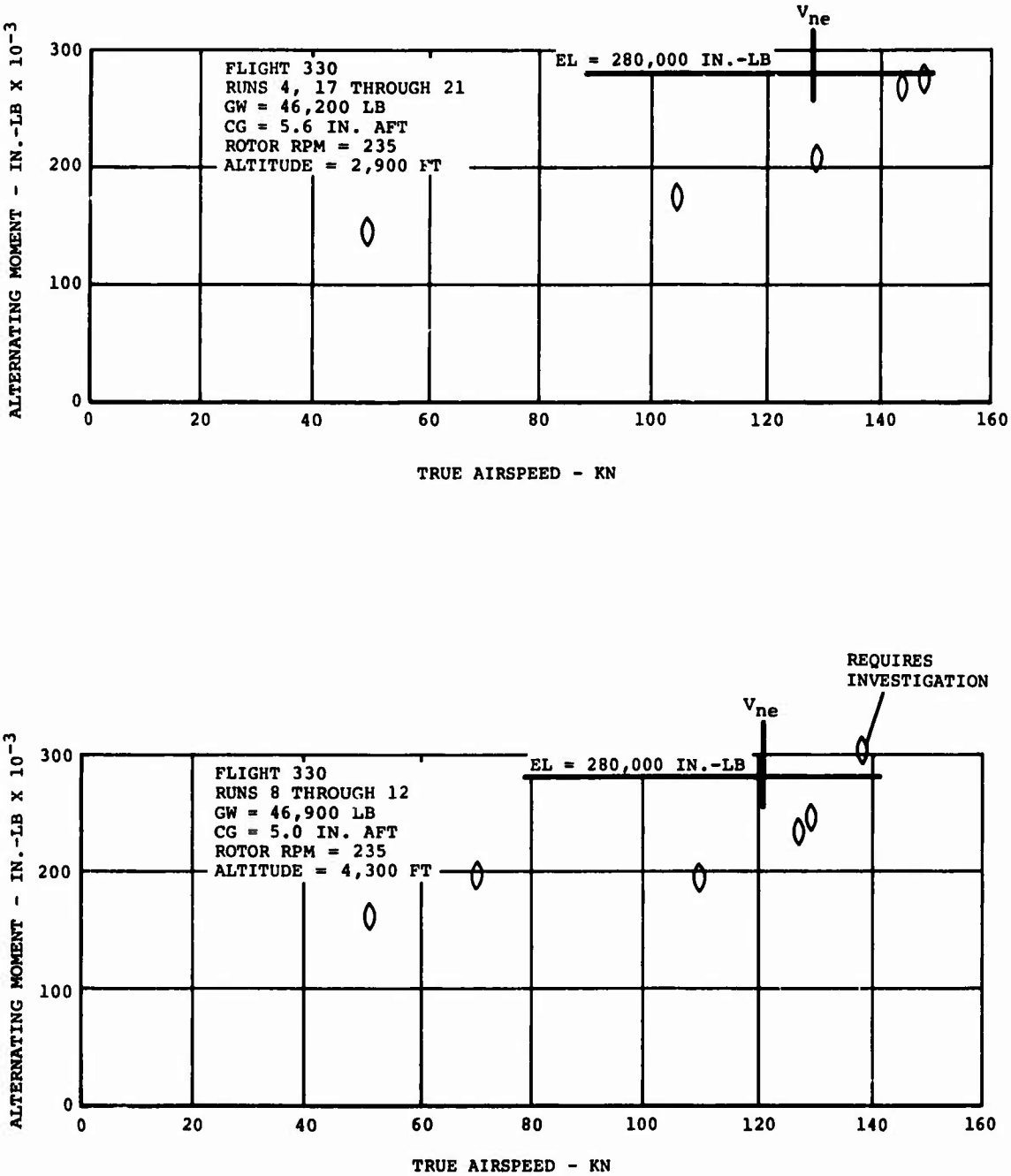

Figure 144. Rotor Shaft Bending (23.1 Inches TOS) on CH-47C Helicopter Equipped With Boron Advanced-Geometry Blades (V_{ne} for Glass AGB Shown for Reference).

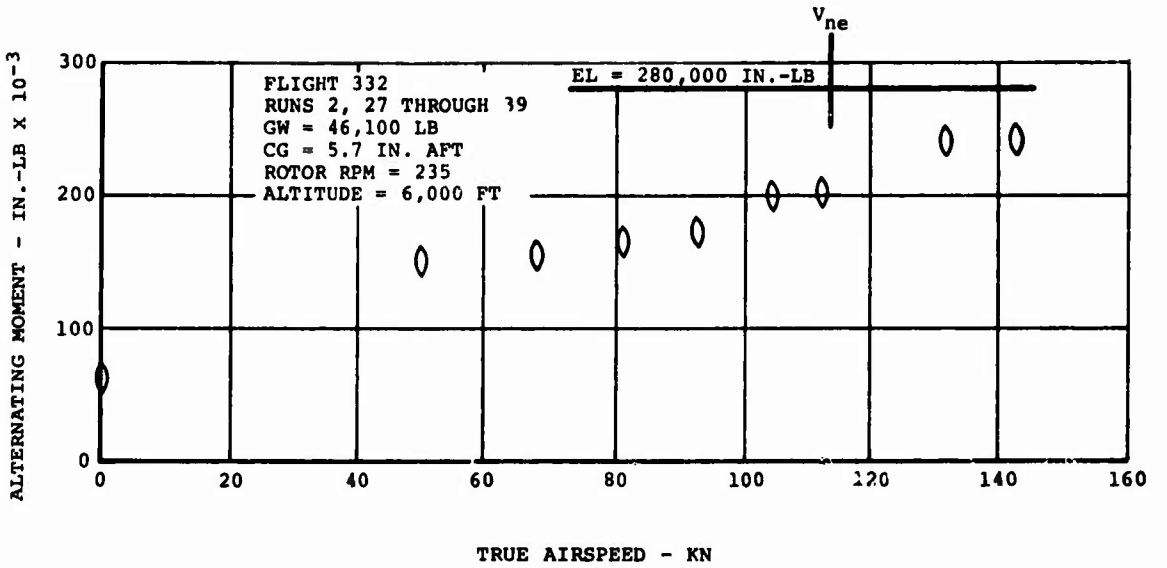

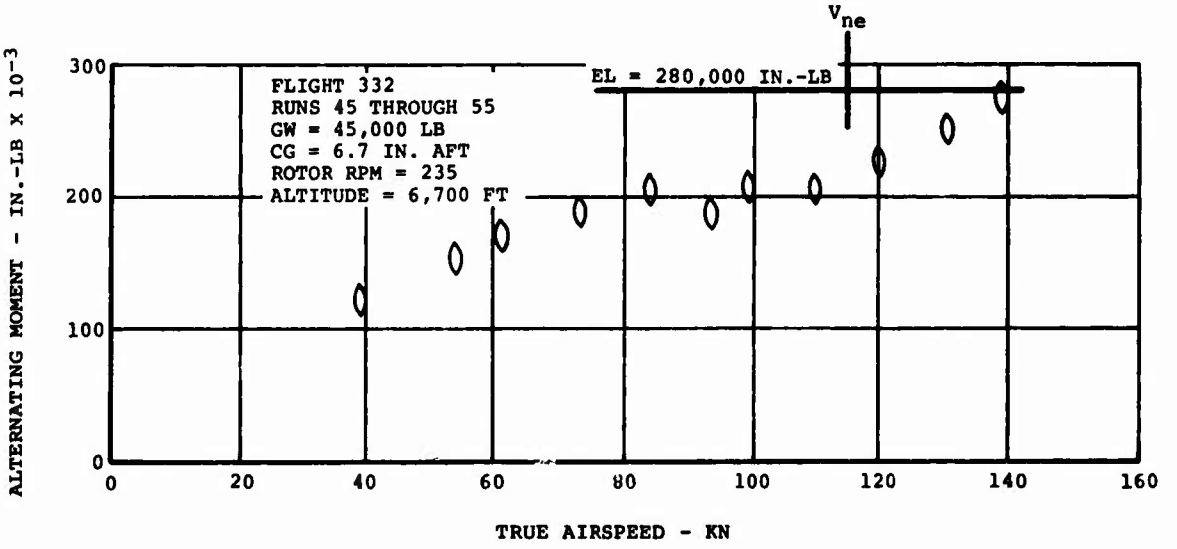

Figure 145. Rotor Shaft Bending (23.1 Inches TOS) on CH-47C Helicopter Equipped With Boron Advanced-Geometry Blades (V_{ne} for Glass AGB Shown for Reference).

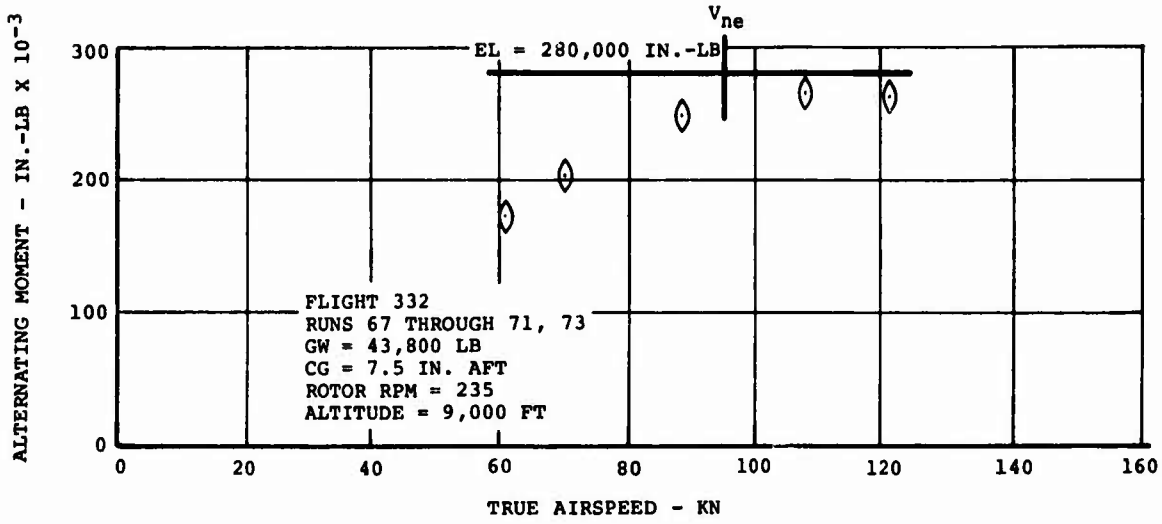

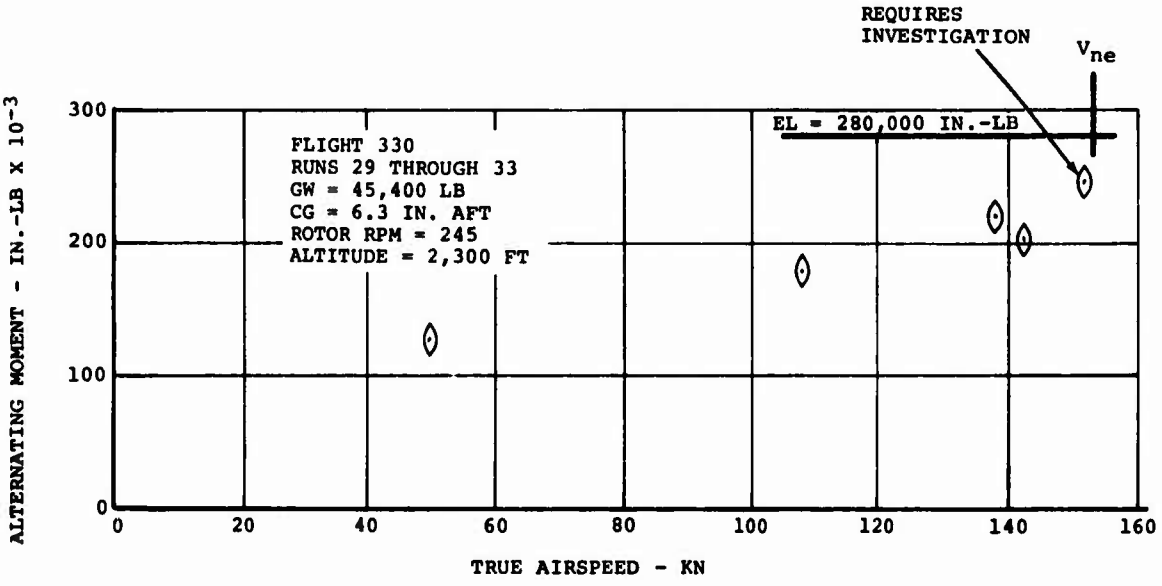

Figure 146. Rotor Shaft Bending (23.1 Inches TOS) on CH-47C Helicopter Equipped With Boron Advanced-Geometry Blades (V_{ne} for Glass AGB Shown for Reference).

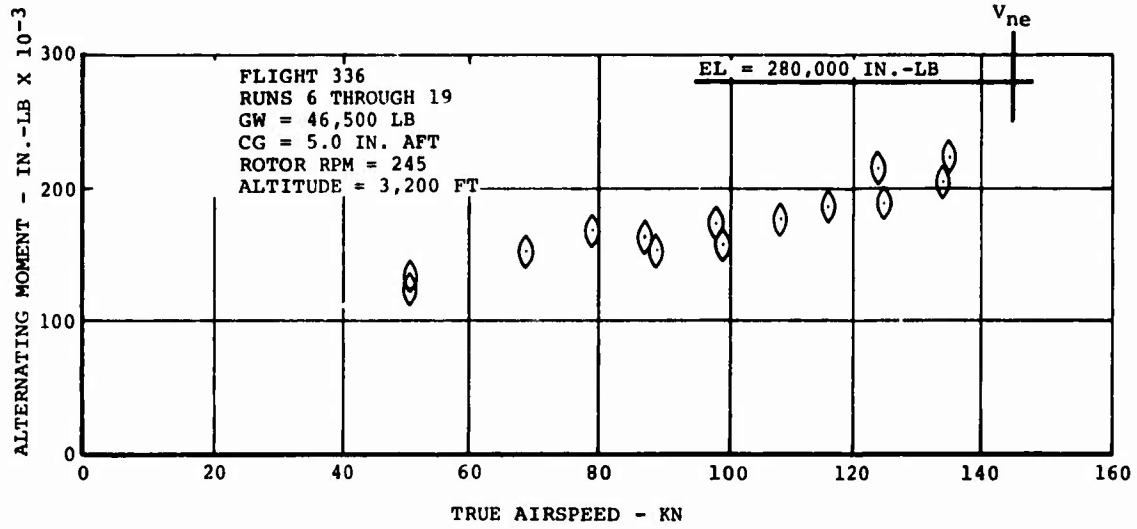

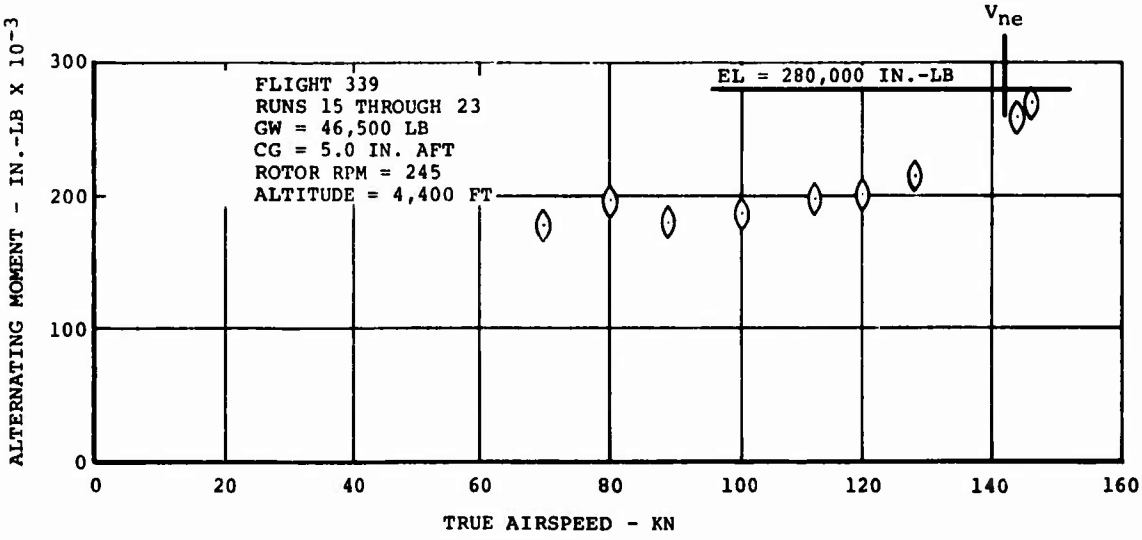

Figure 147. Rotor Shaft Bending (23.1 Inches TOS) on CH-47C Helicopter Equipped With Boron Advanced-Geometry Blades (V_{ne} for Glass AGB Shown in Reference).

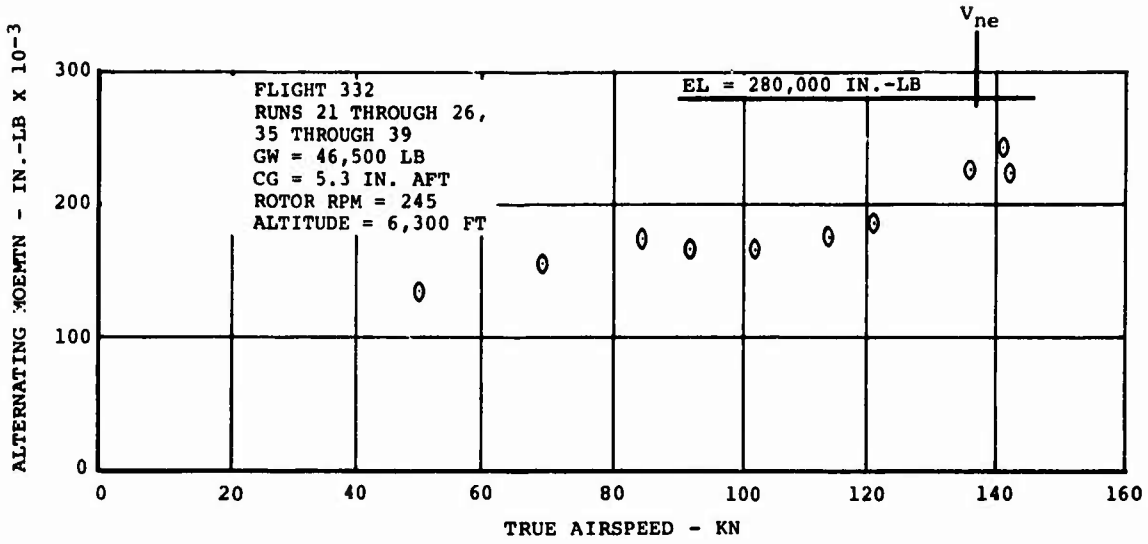

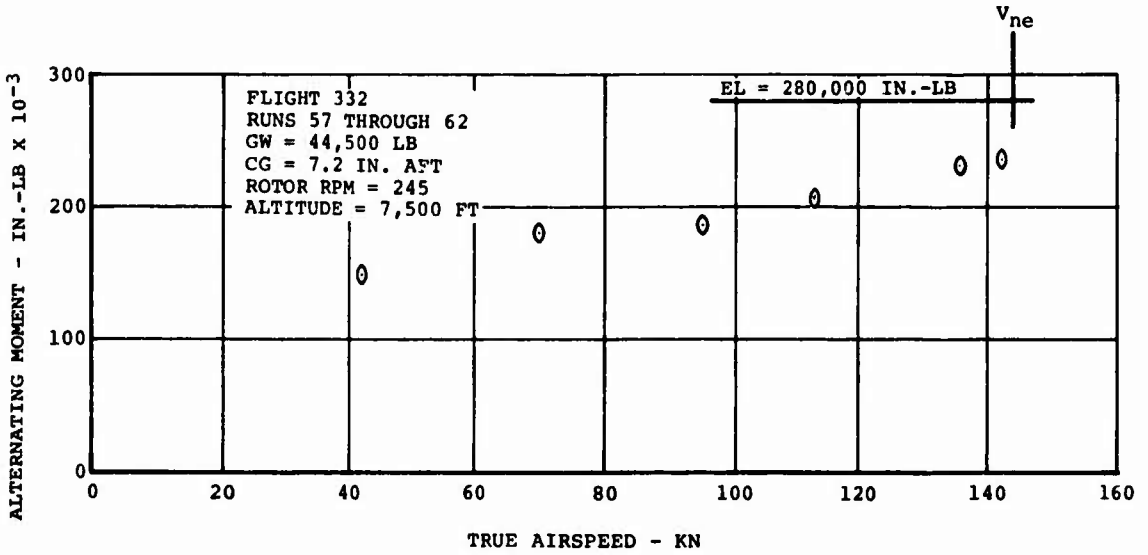

Figure 148. Rotor Shaft Bending (23.1 Inches TOS) on CH-47C Helicopter Equipped With Boron Advanced-Geometry Blades (V_{ne} for Glass AGB Shown in Reference).

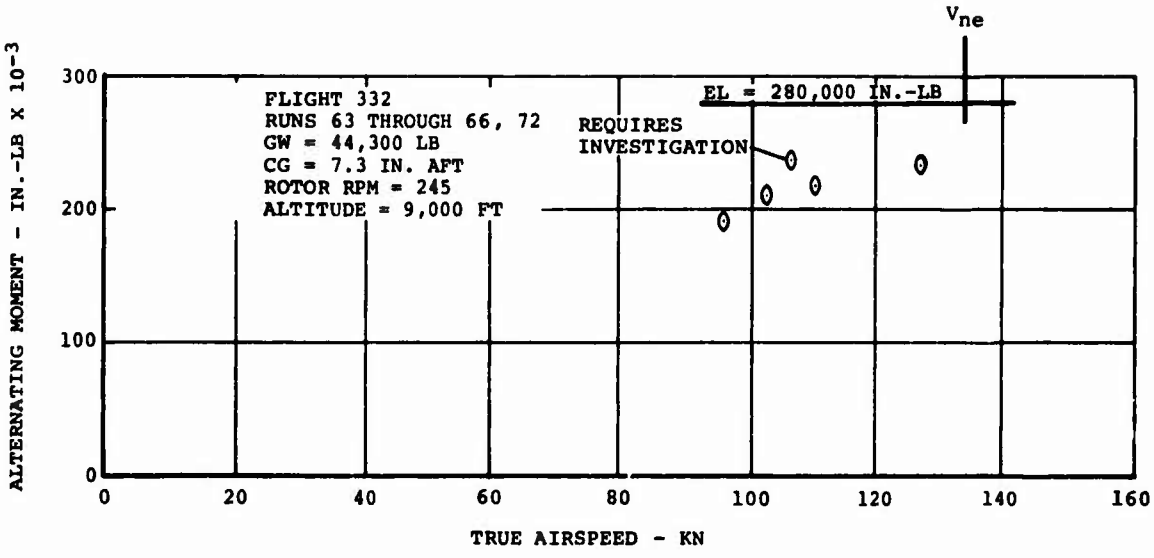

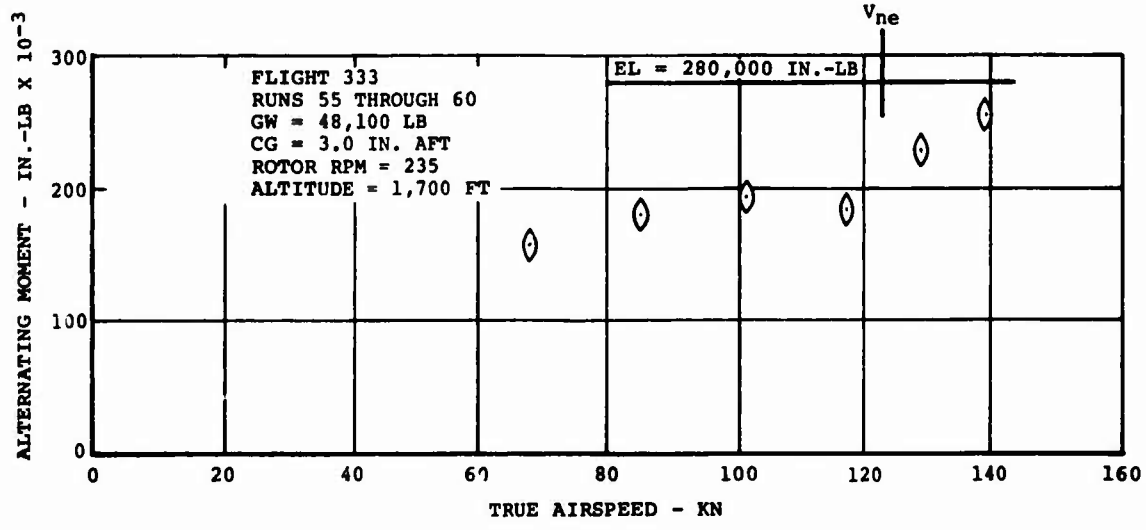

Figure 149. Rotor Shaft Bending (23.1 Inches TOS) on CH-47C Helicopter Equipped With Boron Advanced-Geometry Blades (V_{ne} for Glass AGB Shown in Reference).

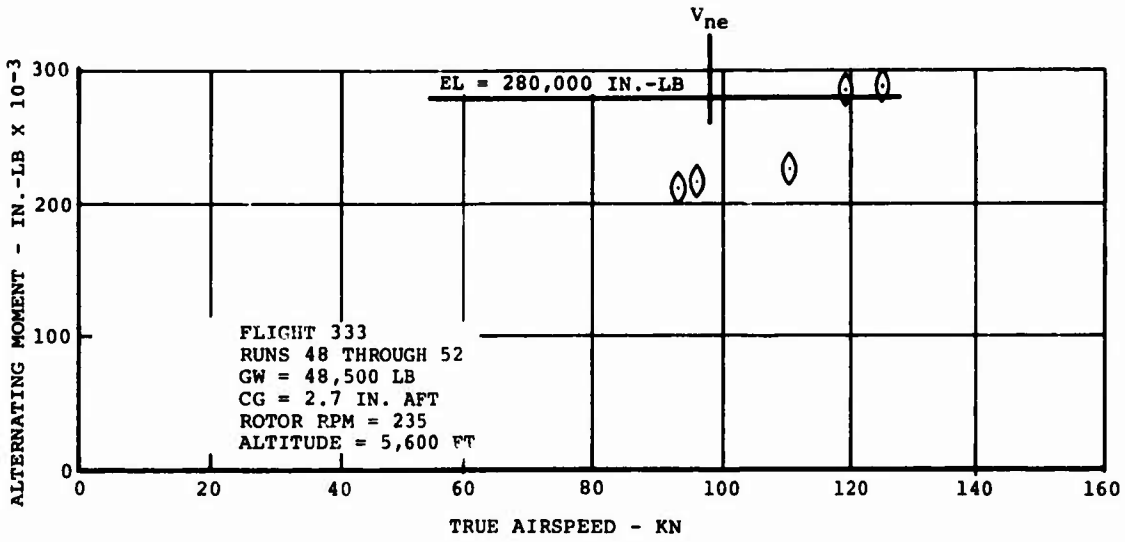

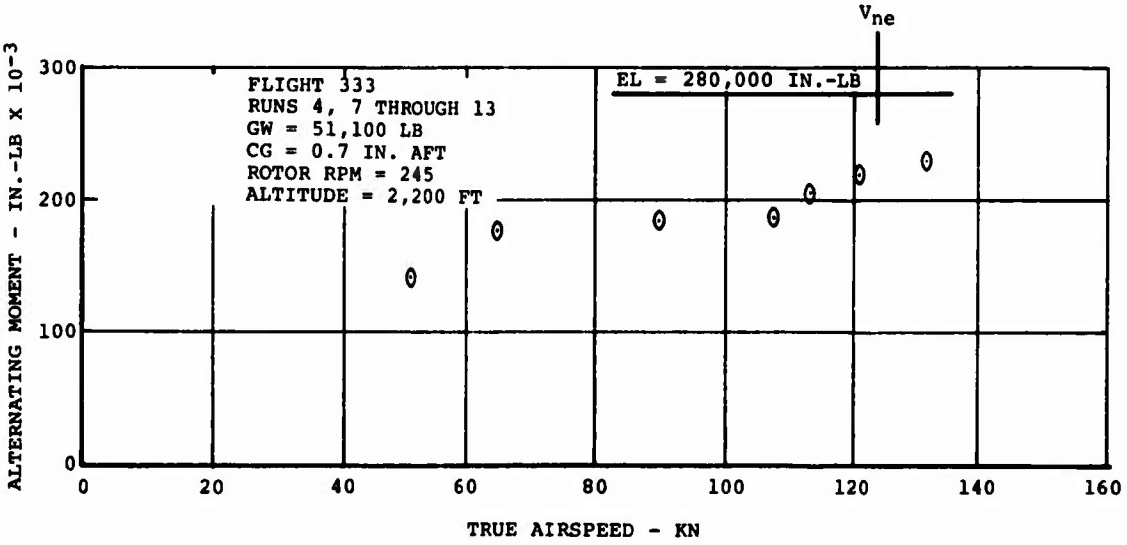

Figure 150. Rotor Shaft Bending (23.1 Inches TOS) on CH-47C Helicopter Equipped With Boron Advanced-Geometry Blades (V_{ne} for Glass AGB Shown in Reference).

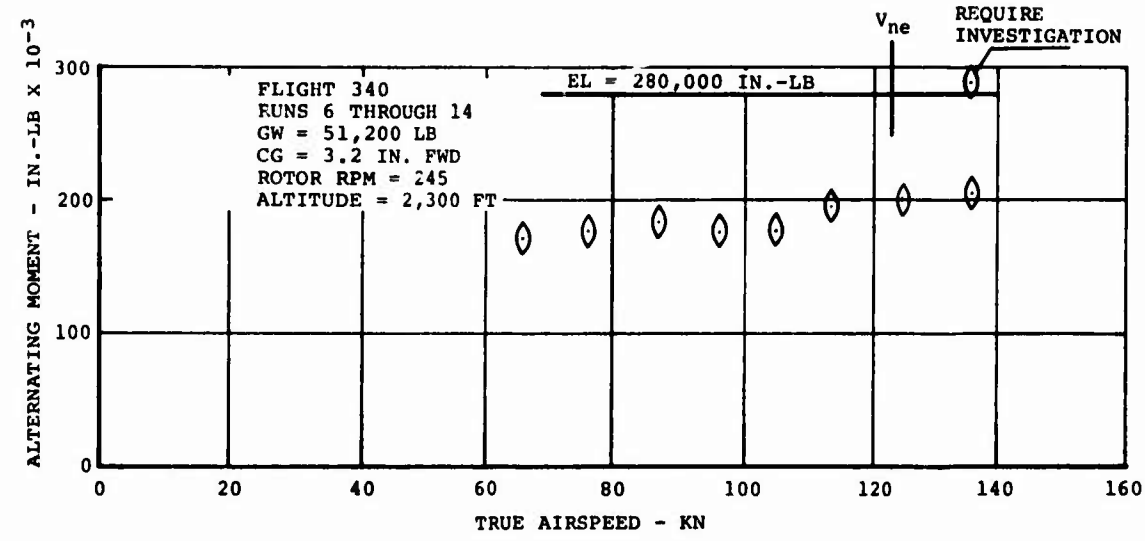

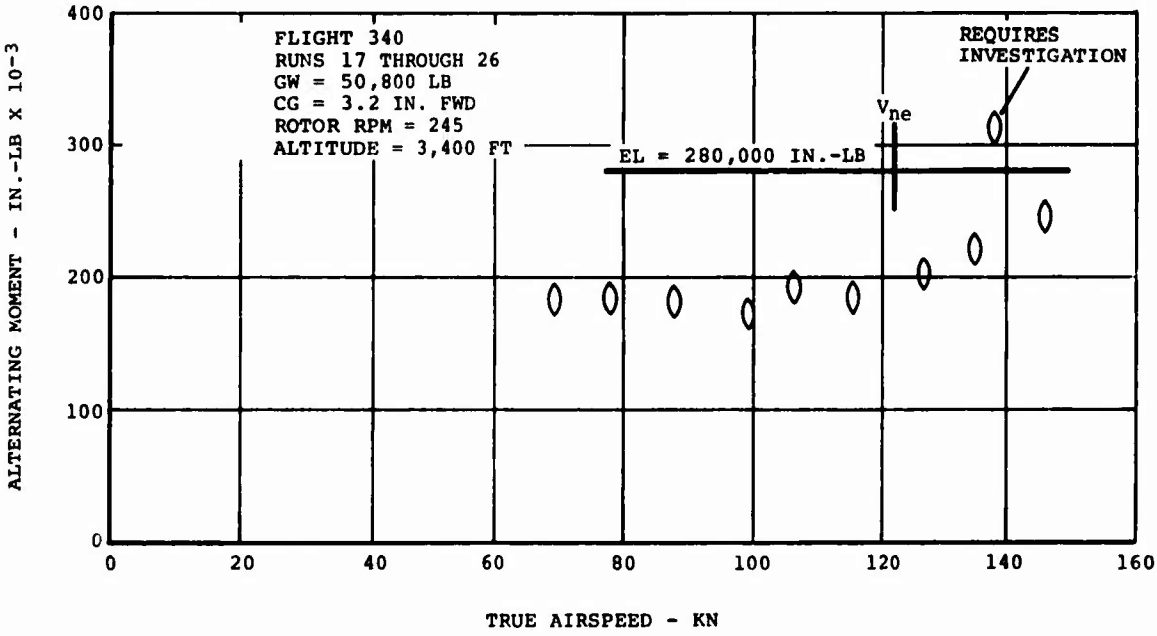

Figure 151. Rotor Shaft Bending (23.1 Inches TOS) on CH-47C Helicopter Equipped With Boron Advanced-Geometry Blades (V_{ne} for Glass AGB Shown in Reference).

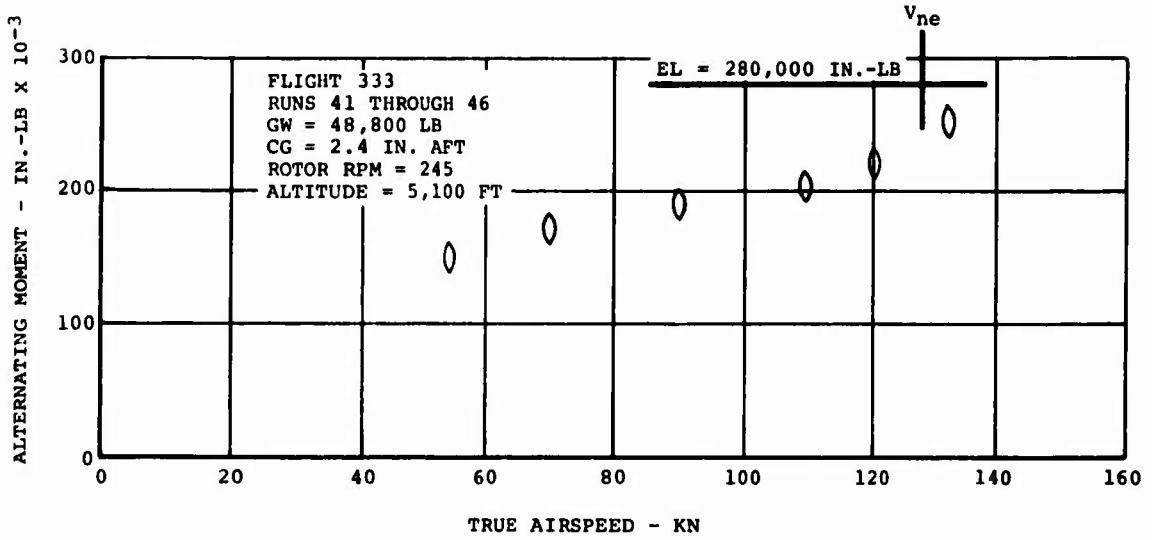

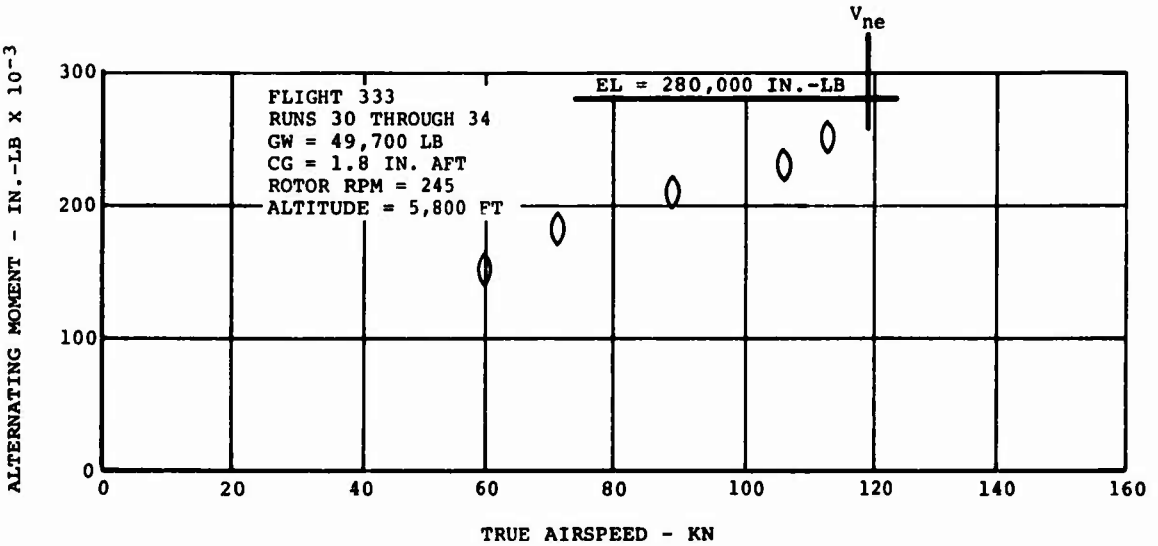

Figure 152. Rotor Shaft Bending (23.1 Inches TOS) on CH-47C Helicopter Equipped With Boron Advanced-Geometry Blades (V_{ne} for Glass AGB Shown in Reference).

DISTRIBUTION

Director of Defense Research & Engineering	1
Assistant Secretary of the Army (R&D)	1
Assistant Chief of Staff for Force Development, DA	1
Deputy Chief of Staff for Logistics, DA	1
Deputy Chief of Staff for Personnel, DA	2
Chief of Research & Development, DA	1
Army Materiel Command	1
Army Aviation Systems Command	2
Hq, Army Air Mobility Research & Development Laboratory	2
Systems Research Integration Office, USAAMRDL	1
Ames Directorate, Army Air Mobility R&D Laboratory	1
Eustis Directorate, Army Air Mobility R&D Laboratory	12
Langley Directorate, Army Air Mobility R&D Laboratory	2
Lewis Directorate, Army Air Mobility R&D Laboratory	2
Army Aviation Systems Test Activity	2
Army R&D Group (Europe)	2
Army Scientific & Technical Information Team (Europe)	1
Army Advanced Materiel Concepts Agency	1
Army Research Office	1
Army Materials & Mechanics Research Center	6
Army Plastics Technical Evaluation Center	1
Army Materiel Systems Analysis Agency	1
USACDC Aviation Agency	2
Edgewood Arsenal	1
Army Aviation Test Board	2
Army Agency for Aviation Safety	1
Army Field Office, AFSC	1
Hq, USAF	1
Air Force Flight Test Center	1
Air Force Materials Laboratory	7
Air Force Flight Dynamics Laboratory	3
Aeronautical Systems Division, AFSC	2
Naval Air Systems Command	10
Chief of Naval Research	3
Naval Research Laboratory	1
Naval Air Rework Facility	1
Naval Air Test Center	1
Naval Air Development Center	3
Naval Ship Research & Development Center	1
Marine Corps Liaison Officer, Army Transportation School	1
U.S. Coast Guard	1
Ames Research Center, NASA	2

Langley Research Center, NASA	2
Lewis Research Center, NASA	1
Manned Spacecraft Center, NASA	1
Scientific & Technical Information Facility, NASA	2
Department of Transportation Library	1
Eastern Region Library, FAA	1
Federal Aviation Administration, Washington	2
Bureau of Aviation Safety, National Transportation Safety Board	1
Government Printing Office	1
Defense Documentation Center	12